Deriving Functional Interfaces from Chemically Reactive and Porous Dip Coating

A Thesis Submitted by

Supriya Das

Roll No. 176122007

To

Indian Institute of Technology Guwahati

For the award of the degree of

Doctor of Philosophy

Department of Chemistry

Indian Institute of Technology Guwahati

North Guwahati,

Assam-781039, India

31st March, 2023

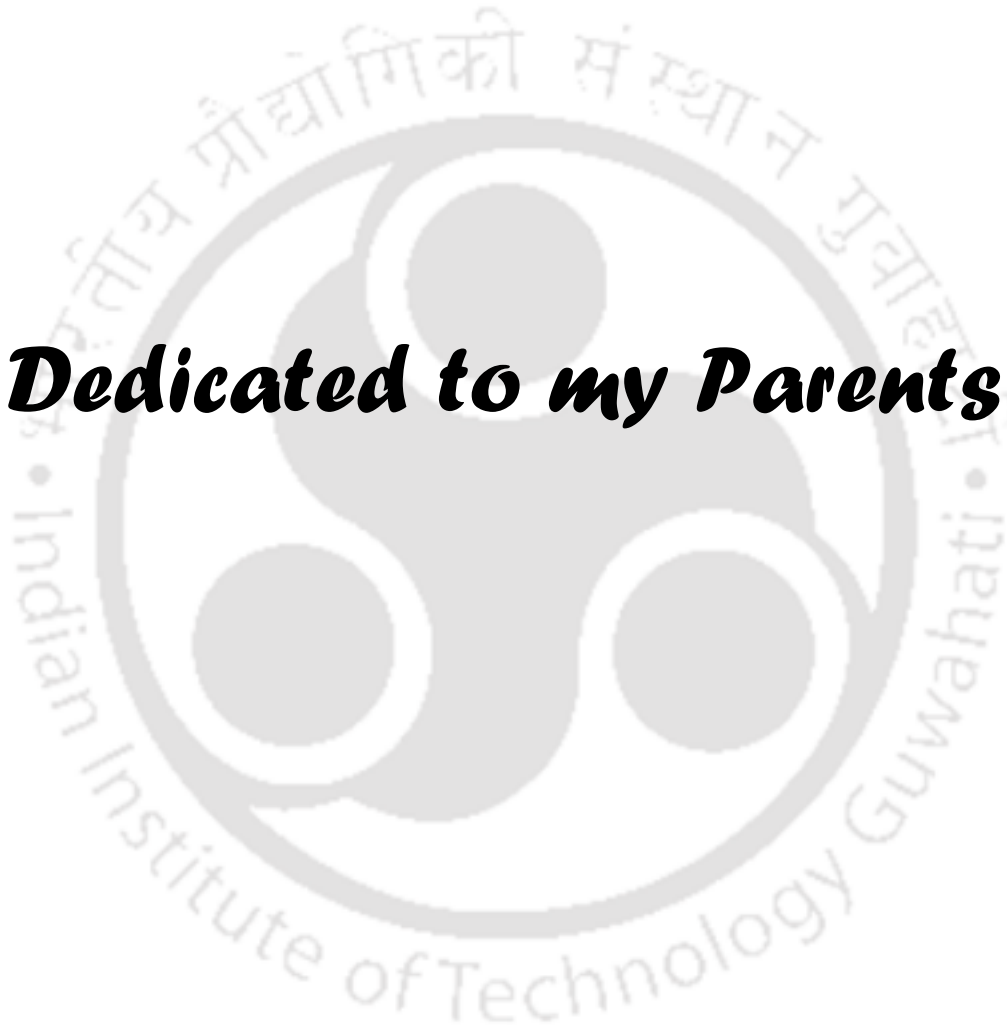

Dedicated to my Parents

Indian Institute of Technology Guwahati

Department of Chemistry

STATEMENT

I hereby declare that the work incorporated in the thesis entitled "**Deriving Functional Interfaces from Chemically Reactive and Porous Dip Coating**" is the result of investigations of research work carried out by me in the Department of Chemistry, under the supervision of Dr. Uttam Manna, Associate Professor, Department of Chemistry, Indian Institute of Technology Guwahati, Assam, India.

Research material used in this thesis from any other source has been fully cited and acknowledged. This work is original and has not been submitted elsewhere for the award of any degree.

Supriya Das

31st March, 2023 **Supriya Das**

IIT Guwahati

Indian Institute of Technology Guwahati

Department of Chemistry

CERTIFICATE

This is to certify that the work presented in this thesis entitled "**Deriving Functional Interfaces from Chemically Reactive and Porous Dip Coating**" by Supriya Das, a Ph.D. student of Department of Chemistry, Indian Institute of Technology Guwahati, for the award of degree of Doctor of Philosophy has been carried out under my supervision and this work has not been submitted elsewhere for the award of any degree.

31st March, 2023

Dr. Uttam Manna
Thesis supervisor
Department of Chemistry
Indian Institute of Technology Guwahati
North Guwahati–781039, Assam, India.

"The key to success is action, and the essential in action is perseverance"

There are no adequate words to express my sincere gratitude and respect for Professor Uttam Manna, PhD supervisor and advisor. He has inspired me to become an independent researcher and helped me realize the power of critical reasoning. He always demonstrated what a brilliant and hard-working scientist can accomplish. I cannot express my gratitude enough, sometimes it had been very tough and stressful situations, still he always believed in me, supported me and paved the way towards success.

My sincere thanks must also go to the members of my doctoral committee: Professors Parameshwar K. Iyer, Debapratim Das and Dipankar Srimani. They patiently provided me with their time and insightful criticism to help me get better at what I do. Their constructive criticism which helped me develop a broader perspective to my thesis.

I am most grateful to the collaborators for lending me their expertise and intuition to my scientific and technical problems: Prof. Dr. Michael Hirtz, Dr. Ravi Kumar from Karlsruhe Institute of Technology, Germany, Prof. Roy P. Paily and Mr. Rajan Singh from Electrical and Electronics Engineering, IIT Guwahati. There is no way to express how much it meant to me to have been a member of "Bio-inspired Polymeric Materials Laboratory". The brilliant labmates inspired me over the many years: Adil Majeed Rather, Dibyangana Parbat, Manideepa Dhar and all the other current and former students and visitors. Further, I would be thankful to the administrative staffs in the office of chemistry department, central instrumental facility and centre for nanotechnology of IITG for their prompt support but also for kind care.

My life in IIT Indore during MSc has changed my life and inspired me towards research that eventually led me to pursue PhD. I thank the great support from Discipline of Chemistry, IIT Indore and my MSc thesis supervisor, Prof. Sampak Samanta.

I cannot forget friends who went through hard times together, cheered me on, and celebrated each accomplishment: Avijit Das, Kousik maji and Akshay Namdeo.

I deeply thank my parents, Mr. Sudhanshu Das and Mrs. Sipra Das for their unconditional trust, timely encouragement, and endless patience. It was their love that raised me up again when I got weary. At the last but not least, I would like to thank all my school teachers and college lecturers, without them I could not achieve any of these in my life.

Abstract

Bioinspired liquid wettability and patterned interfaces remained an inspiration for developing various functional materials/interfaces for relevant and important applications. The essential criteria for contriving bio-inspired extremes of water wettability (either superhydrophobicity or superhydrophilicity) is the co-optimization of hierarchical topography and essential surface chemistry. In general, such optimization is artificially achieved following various top-down and bottom-up approaches, where various hydrophilic building blocks are associated using electrostatic interaction, hydrogen bonding, and other weak bonding (e.g., metal-thiol etc.), for developing the desired hierarchical features and optimizing the appropriate chemistry on top of this featured interface. However, such common and conventional designs are inappropriate for sustaining practically relentlessly harsh settings. So, further development for the synthesis of a durable and substrate-independent superhydrophobic coating is essential for various prospective applications in "real-world" scenarios. In this synopsis report, I have successfully accounted a simple and single-step dip coating process to achieve a substrate-independent, chemically reactive, and porous polymeric coating following a 1,4 conjugate addition reaction at ambient conditions. Such chemically reactive polymeric dip coatings were further exploited for demonstrating pertinent applications, i.e., oil-water separation, self-cleaning, strain sensing, and anti-counterfeiting. The synopsis report entitled as "Deriving Functional Interfaces from Chemically Reactive and Porous Dip Coating" has been codified in six chapters. **Chapter 1** accounts for the introduction of bio-inspired liquid wettability and the discussion on the existing challenges related to durability, scalability and substrate independency. The potential utilization of prospective porous and chemically reactive coatings was also presented in this chapter. In **Chapter 2,** a simplistic approach of single step dip coating technique is introduced to synthesize a substrate-independent and highly abrasion tolerant superhydrophobic coating. Further, the superhydrophobic coating on water soluble (sugar cube) substrate allowed the designing of a highly compressible and durable superhydrophobic sponge for the separation of crude oil-water mixture with an efficiency of > 99%. In **Chapter 3**, I have developed an abrasion tolerant superhydrophobic and conductive patterned interface for real-time and wireless monitoring of slow, fast, weak and strong human motions and expressions as well. The dip coated porous polymeric interfaces were extended in **Chapter 4,** to develop a spatially selective chemically modulated patterned interface, where the strategic association of chemically modulated patterned wettability allowed to achieve a transient, and reversible visualization of hidden information with the naked eye. In **Chapter 5,** I have exploited the dual residual chemical reactivities of the prepared polymeric dip coating for developing an orthogonally readable, abrasion tolerant and miniaturized bulk-patterns through 1,4-conjugate addition reaction. Finally, in **Chapter 6**, summary of my entire thesis work has been elaborated and future prospects of the current design of chemically reactive dip coating are also provided.

Chapter 1: Introduction

The development of artificial bio-inspired wettability is widely recognized due to its diverse and prospective applications in real world scenarios. In nature, we have found various plants and animals associated with asymmetric, adhesive, and non-adhesive extreme water-repellent properties as shown in Figure 1. For example, the lotus-leaf inspired interfaces that displayed an extreme water repellency with high (above 150º) water contact angle and low contact angle hysteresis (below 10º) are widely recognized as non-adhesive superhydrophobic surfaces—and such interfaces were successfully extended to demonstrate self-cleaning, oil/water separation, water harvesting, energy harvesting, etc. Such extreme of water wettability is the result of heterogeneous wetting phenomena–which can be explained by the Cassie-Baxter model.

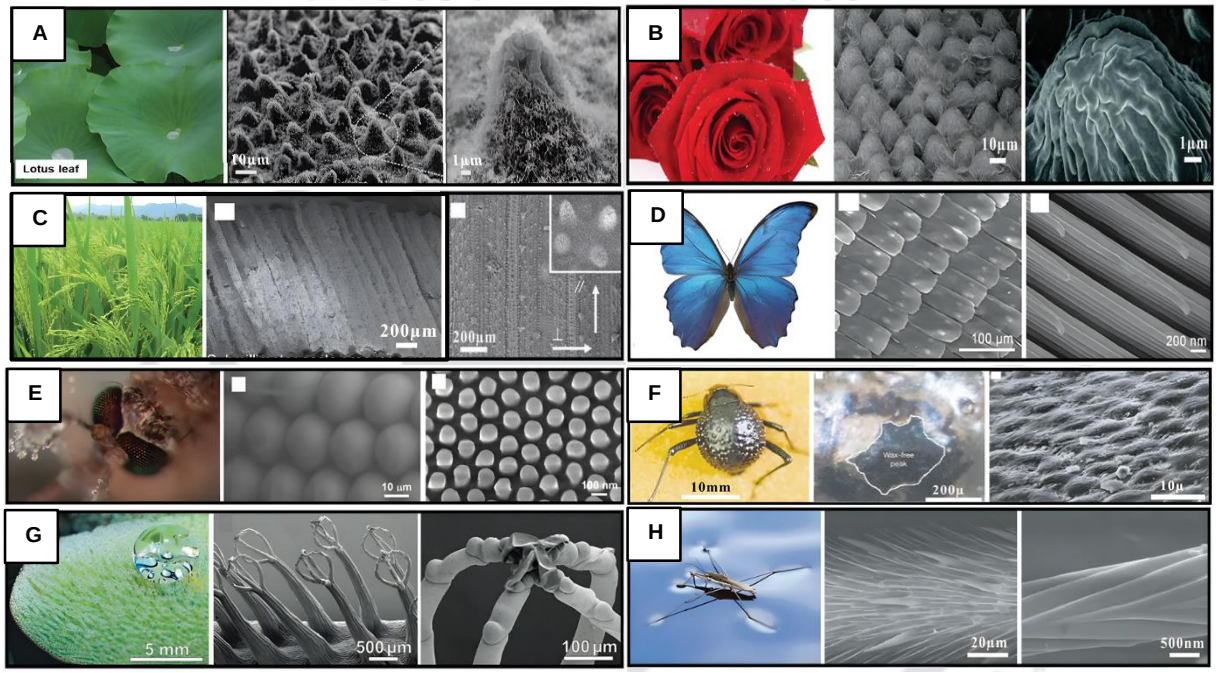

Figure 1. Digital images and scanning electron microscope of various natural animals and plants showing special wettability: (A) lotus leaf, (B) red rose petal, (C) rice leaf, (D) a butterfly wing, (E) mosquito eye, (F) back of a desert beetle, (G) *Salvinia* plant, and (H) leg of a water strider. This figure is adapted from *Chem. Soc. Rev.* **2017**, *46*, 4168—4217. Copyright 2017, The Royal Society of Chemistry.

The detailed microscopic characterizations of naturally existing superhydrophobic interfaces have revealed the presence of two tires (both in micro and nano dimensions) of topography. Later, it has been experimentally validated that the association of two tires of topography (often denoted as hierarchical topography) with essential low surface energy is essential to achieve artificial superhydrophobicity. In the past, various approaches—including self-healable and post-repairable strategies were introduced to achieve superhydrophobic coating—but the development of a scalable, durable, substrate independent and easily functionalizable superhydrophobic coating is rare in the literature. In this context, the design of chemically reactive and porous polymeric bulk coating is promising to attain an abrasion tolerant and readily functionalizable superhydrophobicity. In the past, Levkin et al, embraced Click chemistry and phase separation process to develop a porous polymeric coating that remained capable of displaying

superhydrophobicity and superhydrophobic/superhydrophilic patterned interfaces. Although such a seminal report introduced a bulk superhydrophobic coating that remained tolerant to physical abrasion, such a deposition process is not appropriate to coat various substrates having different chemical compositions and geometry. Later, Lynn et al. successfully applied a tedious layer-by-layer (LbL) deposition process following a mutual reaction between azalactone and amine moieties of two distinct polymers to achieve chemically reactive superhydrophobicity. Recently, Manna et al applied a catalyst free 1,4-conjugate addition reaction at ambient condition to construct multilayer coatings of reactive nanocomplex for controlled modulation of water wettability. However, the design of a substrate independent porous and chemically reactive coating that would be developed following a single step deposition process—and would be capable of associating chemically modulated water wettability is rare in the literature. Recently, Adil et al. introduced superhydrophobic monoliths with tailored physical properties—just by changing the reaction medium (alkyl alcohol) for selected reactants. The higher analogues of ethanol led to an accelerated sol-gel conversation through the formation of chemically reactive polymeric nanocomplex in the reaction mixture. Taking advantage of this reaction solvent-mediated accelerated growth of chemically reactive nanocomplex, I have developed a porous and chemically reactive coating via in-situ deposition of chemically reactive polymeric nanoparticles following a substrate independent dip coating process. This dip coating approach has been successfully applied to achieve durable and substrate-independent superhydrophobic coating, extremely water-repellent conductive pattern interface and abrasion-tolerant patterned interfaces of two distinct wettability and fluorescent molecules.

Chapter 2: Rapid and Facile Synthesis of Substrate Independent "Chemically Reactive" and Porous Polymeric Dip Coating

This Chapter 2 demonstrates the development of a substrate-independent, abrasion-tolerant, chemically reactive porous polymeric coating following a single-step dip coating process (Figure 2A-B). The 1,4-conjugate addition reaction between the selected reactants, i.e., di-pentaerythritol pentaacrylate (5-Acl) and branched polyethylene imine (BPEI) provided a rapid growing dispersion of chemically reactive polymeric nanocomplex in 1-heptanol. The in-situ and rapid deposition of the chemically reactive nano-complex allowed to decorate wide range of substrates, including water-soluble, water-sensitive, highly flexible, rigid, and fibrous substrates with a porous and chemically reactive coating (Figure 2C-F). Furthermore, the choice of small alkylamines for post-covalent modifications of the "chemically reactive" dip coating provided superhydrophobicity with a tailored water adhesion. The FTIR analysis in Figure 2F revealed the successful post covalent modification of the coating with octadecylamine (ODA), where the IR peak intensity at 1409 cm^{-1} corresponding to the symmetric deformation of the C−H bond for the β carbon of the vinyl group depleted significantly due to the mutual reaction between residual acrylate groups and primary amine of ODA. Such modification resulted in associating superhydrophobicity with an advancing water contact angle (WCA) of ~161º as shown in Figure 2D. A

gradual increase in both roll-off angles, and the contact angle hysteresis (from 5° to 30°) was noted with a decrease in the hydrocarbon tail of selected alkylamines. Such coating approach was successfully extended to coat even water sensitive substrates having complex geometry. Therefore, litmus paper and

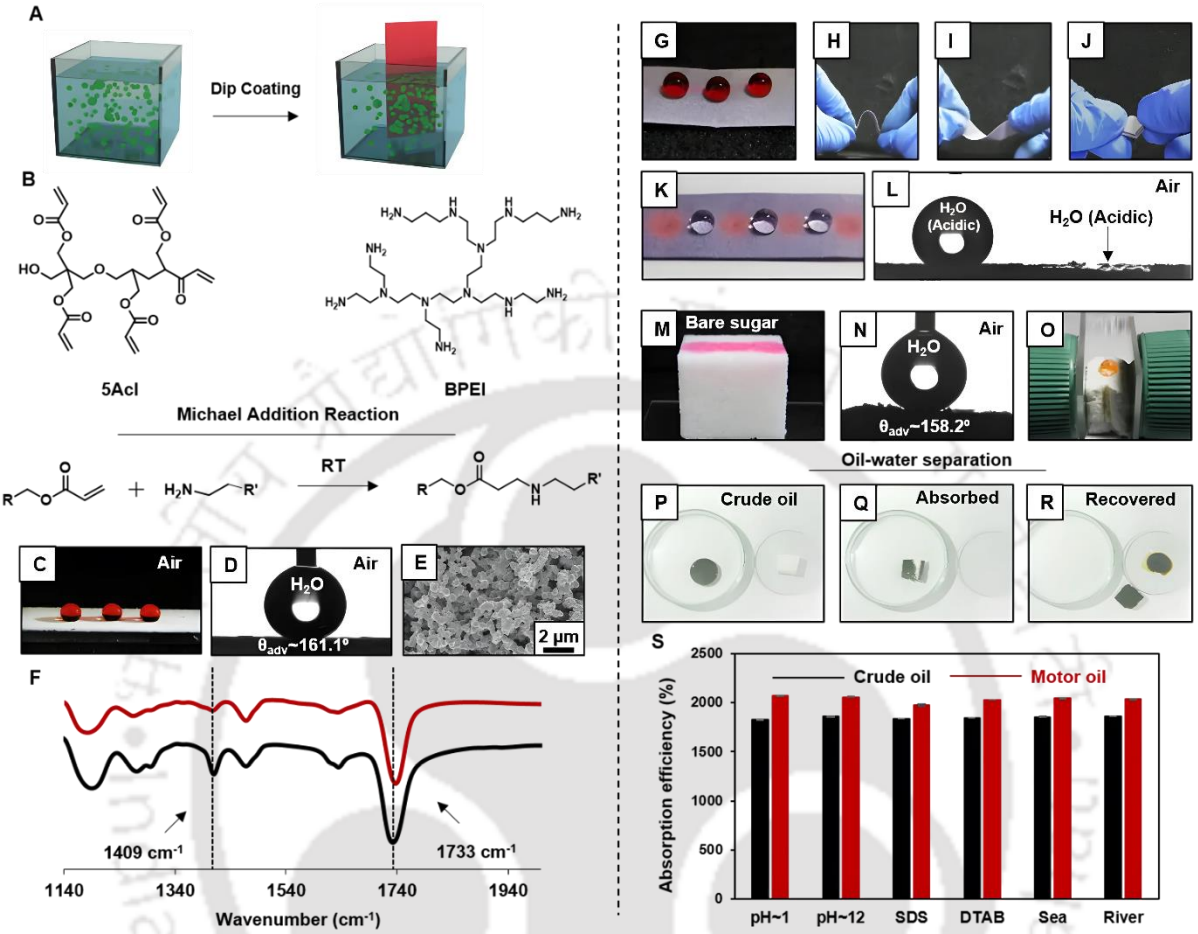

Figure 2. (A-B) Schematic representation of one step dip coating approach and structural representation of the reactants, i.e., pentacrylate and polyethylene imine. Reaction between acrylate and amine was demonstrated by the scheme of Michael addition reaction. (C-F) Digital image (C) and advancing water contact angle image (D) of beaded red colored (dyed with rhodamine-B) water droplets. The Field emission scanning electron microscope (FESEM) images representing the micro/nano-random features of the porous polymeric coating prepared by one-step dip coating approach (E). FTIR spectra of the chemically reactive polymeric coating with the characteristic vinyl C-H deformations at 1409 cm^{-1} normalized with respect to the carbonyl (C=O) at 1733 cm^{-1} has shown using the black bold line. Followed by that, octadecyl amine treated polymeric coating which has diminished peak at 1409 cm^{-1} demonstrated covalent interaction between acrylate and amine (F). (G-J) Digital images of the beaded water droplets on the coated superhydrophobic blue litmus paper, superhydrophobicity remained intact after bending and creasing of the flexible substrate. (K) Digital image and (L) contact angle image describing the beading/wetting of acidic (pH~1) water droplets on superhydrophilic/superhydrophobic patterned interface of the dip coated litmus paper, where the superhydrophilic domain is incurred through introducing of manual holes, and rest of the area remained superhydrophobic. These holes soaked the acidic water and immediately the color of litmus paper changed from blue to red around each hole. (M-R) Uncoated hydrophilic sugar cube readily soaked the dyed water droplets on it (M). Coated superhydrophobic sugar cube repelled the beaded water droplet with advancing WCA of ~ 158º. (J) Digital image of the beaded water droplet on the compressed spongy material; the superhydrophobic sugar cube became a spongy polymeric material after sacrificing the water-soluble sugar substrate. (P−R) Digital images demonstrating successful separation of the floating (P-Q) crude oil from the aqueous phase using a sugar cube-derived spongy superhydrophobic material, and (R) application of a compressive strain allowed to recollect the absorbed crude oil from the material. (S) Illustration of the selective oil-absorption capacity of the superhydrophobic sponge under different harsh chemical environments (Published in *ACS Appl. Mater. Interfaces* **2019**, *11*, 34316-34329).

sugar cubes have been selected as model representing water sensitive and soluble substrates for an efficient illustration of superhydrophobic coating without altering the property of the substrates underneath. The dip coated superhydrophobic litmus paper with WCA ~ 159º (Figure 2G), was exposed to several pertinent deformations, i.e., bending, twisting, and creasing manually (Figure 2H-J). However, the water-repellent property remained unaffected even after the application of these physical manipulations. The acidic water droplet beaded on the coated litmus paper with high WCA (~155°), and no change in color on the coated litmus paper on the area of beading was noted, likely due to the restricted ingression of the acidic aqueous phase to the pH-responsive water-soluble litmus dye.

Next, a few holes were manually introduced to the superhydrophobic litmus paper to expose the underneath hydrophilic substrate that was loaded with water-soluble litmus dye, and acidic water droplets were placed both on the physically damaged interface (manual holes) and the unaffected area of the coating, as shown in Figure 2K. The acidic water droplets, which were placed in the holes are immediately soaked in the litmus paper and turned the color of litmus dye from blue to red. The instant change in the color of the litmus dye revealed that the process of the superhydrophobic coating did not alter the pH-responsive property of the litmus dye. This simple study also provided a basis for developing the physical damage-guided superhydrophobic/superhydrophilic-patterned interface (Figure 2L). Furthermore, such an interface would be useful in the physical defect-triggered release of bioactive small molecules, where physical defects would control the rate of infiltration of the aqueous phase in the material and eventually control the release of the loaded cargo. Thereafter, a highly water soluble substrate, i.e. sugar cube (Figure 2M) was successfully coated to embed superhydrophobicity with WCA ~ 158º (Figure 2N). Here, the selective dissolution of the underlying water soluble substrate at a specific condition allowed us to derive a spongy and compressible superhydrophobic material (Figure 2O). Next, this spongy superhydrophobic material was deformed for 100 cycles to assess the durability and observed no change in its water repellent property. Such highly compressible and porous superhydrophobic material is further employed for environment friendly recovery of oil spillage from the aqueous phase through selective and spontaneous absorption process (Figure 2P-Q) with an absorption efficiency of 1850 weight%. However, the absorbed oil was further recovered by manual squeezing and collected in a separate container (Figure 2R). This oil-absorption capacity remained unaffected in various practically relevant and severe chemical settings including extremes of pH, surfactants (DTAB, SDS) contaminated water, river water, and artificial sea water, as shown in Figure 2S. Thus, the embedded superhydrophobic coating can be performed under various severe chemically challenging settings. Further, the self-cleaning performance was successfully demonstrated with arbitrarily physically abraded superhydrophobic coating.

Chapter 3: Water Repellent Conductive Pattern Interface for Monitoring Human Motions and Expressions

In the past, various approaches were introduced to achieve strain sensor with high gauge factor—mainly associated with a large tensile deformation. But, in reality, a flexible strain sensor displaying a high gauge factor at low applied strain that remains efficient under practically relevant diverse and challenging conditions would be more appropriate for unambiguous and effective monitoring of human motions and other relevant applications. But, the report of a low-strain sensor with high sensitivity and durability is rare in the literature. In Chapter 3, I have introduced a durable, highly flexible, water repellent wearable strain sensor with a high sensitivity. In my design, a readily amine reactive conductive ink developed following 1,4-conjugate addition reaction between amine and acrylate functional groups under ambient conditions is strategically extended for designing a conductive and chemically reactive pattern interface—which became extremely water repellent after an appropriate post-covalent modification with ODA. On the other side, the spatially selective deposition of the prepared ink provided a facile basis for achieving ultrahigh sensitivity as shown in Figure 3A-B. A readily reactive and conductive ink was prepared by mutually reacting amine functionalized graphene oxide (AGO), di-pentaerythritol pentaacrylate (5-Acl) and 3-amino propyltrimethoxysilane (APTMS) through 1,4-cojugate addition reaction. Then, the ink was filled in a calligraphic pen to write various complex and desirable patterns on a chemically reactive coating on paper substrate. The chemically reactive coating was achieved following the same process as mentioned in Chapter 2. The post-covalent modification of the deposited ink on the chemically reactive coated paper with ODA altered the WCA from ~99º to ~155º as shown in Figure 3C-D. Such association of extreme of water wettability protected the conductive interface from aqueous exposure as demonstrated in Figure 3E-G. Even, a bending assisted a change in resistance of the superhydrophobic conductive interface is noted—in the presence of continuous exposure to the tap water. Eventually, the light intensity of the LED that was connected with this sensor significantly depleted on the application of the manual bending to the flexible sensor; however, after releasing the applied strain, the light intensity of the LED recovered back. On bending the ink-deposited flexible substrate, some micro cracks appeared in the same interface (Figure 3H-I), however, on releasing the applied strain, the micro-cracks disappeared (Figure 3J). This reversible appearance of cracks supports the switchable change in the resistance of the interface. The external low-strain induced cracks on the flexible and durable superhydrophobic conductive patterned interface provided a facile basis for real-time and wireless monitoring of slow, fast, weak, and strong human motions as well as expressions as shown in Figure 3K.

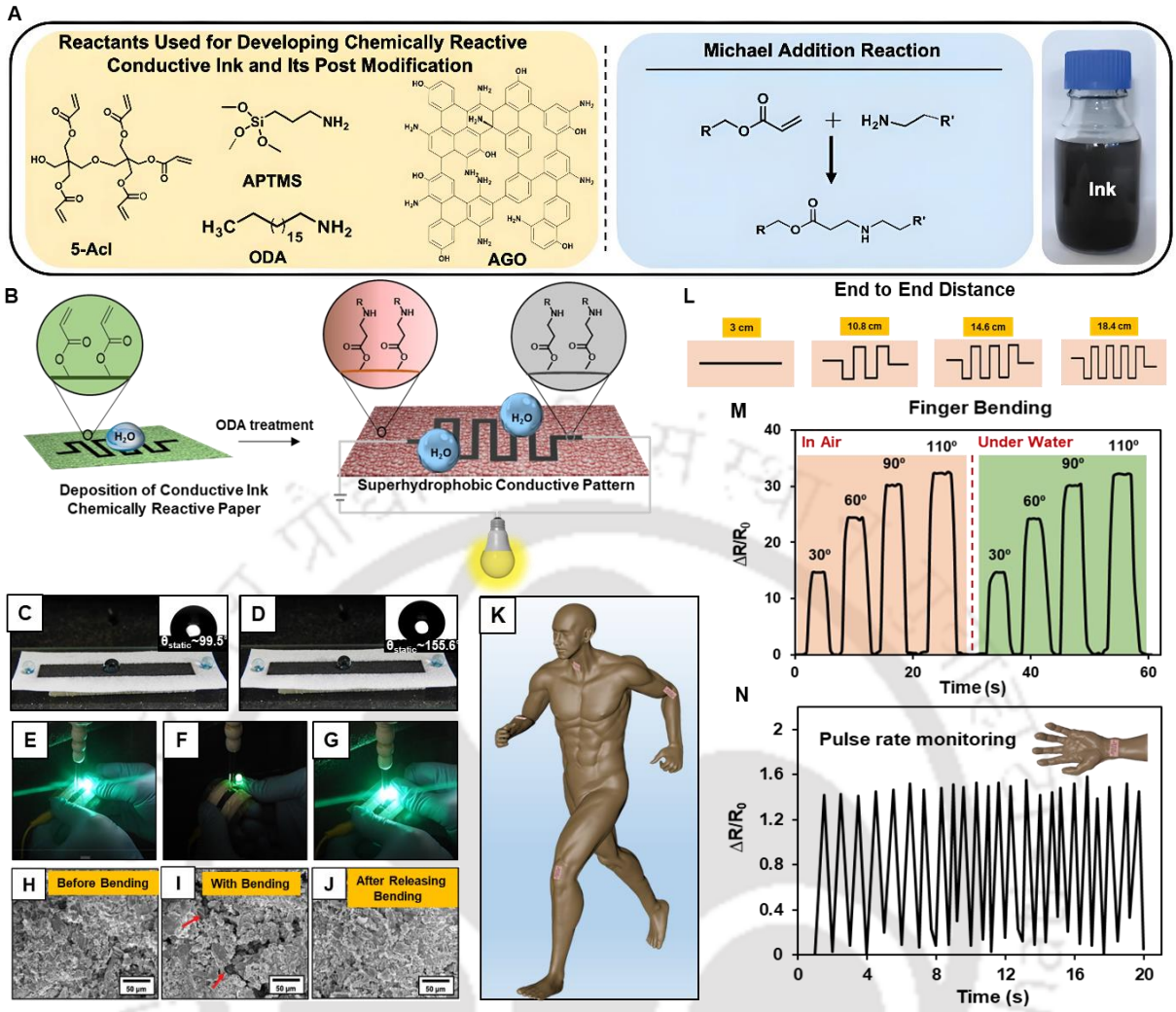

Figure 3. (A) Chemical structures of reactants used for the preparation of a chemically reactive & conductive ink, i.e., dipentaerythritol pentaacrylate (5-Acl), 3-aminopropyltrimethoxysilane (APTMS), octadecylamine (ODA) and aminographeneoxide (AGO); schematic of 1,4-conjugate addition reaction between the acrylate and primary amine groups of the reactants under ambient conditions, without any aid of catalyst. (B) Schematic depicting the fabrication of an extremely water repellent & conductive pattern interface, where the chemically reactive conductive ink was deposited spatially selectively on the dip coated chemically reactive paper, prior to post-modifying with octadecyl amine (ODA). (C-D) Digital images and static contact angle images of the beaded water droplets on the chemically reactive & conductive interface before (C) and after (D) ODA treatment. (E-G) Demonstrating the reversible change in the resistance under continuous exposure of aqueous phase, where the brightness of the LED light varied with bending the conductive and superhydrophobic interface under the continuous exposure of an aqueous phase. (H-J) FESEM images revealed the existence of reversible cracks during the bending of the conductive and superhydrophobic interface. (K) Illustrating wireless detection of different motions of humans. (L) Depicting optimization of the dimension of sensitive pattern interface. (M) The plot accounting the gradual change in resistance of the pattern interface that attached to a finger of a volunteer on bending the finger at different angles (from 30º to 110º) both in air (left side) and under water (right side). (N) A localized pressure sensing mechanism was used to monitor the human heart rate. (Published in *Mater. Horiz.* **2021**, *8*, 2851-2858).

The spatially selective deposition of chemically reactive conductive ink on a chemically reactive paper allowed the preparation of patterned interfaces (Figure 3L) with variable end-to-end distances (3 cm to 20.6 cm) of the conductive region—keeping the overall dimension of all the patterns identical, i.e., 3 cm. With increasing the end-to-end distance (from 3 cm to 20.6 cm) of the deposited conductive ink, the absolute resistance of the patterned interfaces gradually enhanced from 3.2 KΩ to 578.3 KΩ.

As a proof-of-concept demonstration of wireless detection of different soft and strong human motions, the optimized patterned interface was first attached to a finger prior to bending at different angles, and the change in the resistance was noted to be gradually elevated with increasing the bending angle—from 30º to 110º in air as depicted in Figure 3M. A real-time and wireless change in the resistance during the bending of the prepared patterned interface in air was demonstrated with the help of the display of a smartphone. Next, the same pattern interface was gradually bent underwater—and a very similar change in resistance was noted as shown in Figure 3E (right side: green shaded area). As expected, the embedded superhydrophobicity allowed the successful underwater performance of the conductive pattern interface. In order to monitor patients during the rehabilitation process and research the relationship between humans and machines, such devices could be helpful. Furthermore, it could function underwater and in a variety of practically important extreme situations due to the integrated water repellence. Therefore, there is a lot of potential for new and more practical uses for the existing and basic superhydrophobic and conductive pattern interface design. Moreover, the currently developed pattern interface was extended to monitor the pulse rate that is associated with a weak and localized muscle movement as shown in Figure 3N.

Chapter 4: Covalently Modulated and Transiently Visible Writing: Rational Association of Two Extremes of Water Wettabilities

Here, in this Chapter 4, I have utilized the residual reactive acrylate functionality of the synthesized polymeric dip coating which is discussed in the Chapter 2. Such coatings allowed a spatially selective post-covalent modification with glucamine directly from aqueous medium. The inherent hydrophobicity of the chemically reactive polymeric dip coating allowed to achieve spatially selective chemical patterning with glucamine—without having any arbitrary spillage of aqueous solution of glucamine. Further, the post-chemical modification of such spatially glucamine modified interfaces with long chain hydrocarbon amines, i.e., octadecyl amine yielded a superhydrophilic-superhydrophobic pattern as shown in Figure 4A-B. Such nature-inspired pattern wettability is rationally exploited for developing an unprecedented anti-counterfeiting method, where the hidden information can be only identified under direct exposures to an aqueous phase or mist and disappears again on air-drying the interface. The chemically reactive dip coating having residual acrylate groups was separately modified with glucamine and ODA to demonstrate the association of two extremes of water wettability—i.e., superhydrophobicity (WCA of ~156º; Figure 4C-D) and superhydrophilicity (WCA ~ 0º; Figure 4E-F), respectively. The successful post-covalent modification of the chemically reactive dip coating was characterized with FTIR analysis as shown in Figure 4G. Thus, the inherently hydrophobic and chemically reactive dip coating, capable of providing both superhydrophobicity and superhydrophilicity depending on the selection of appropriate chemical modifications, was further exploited in fabricating spatially selective and chemically controlled pattern.

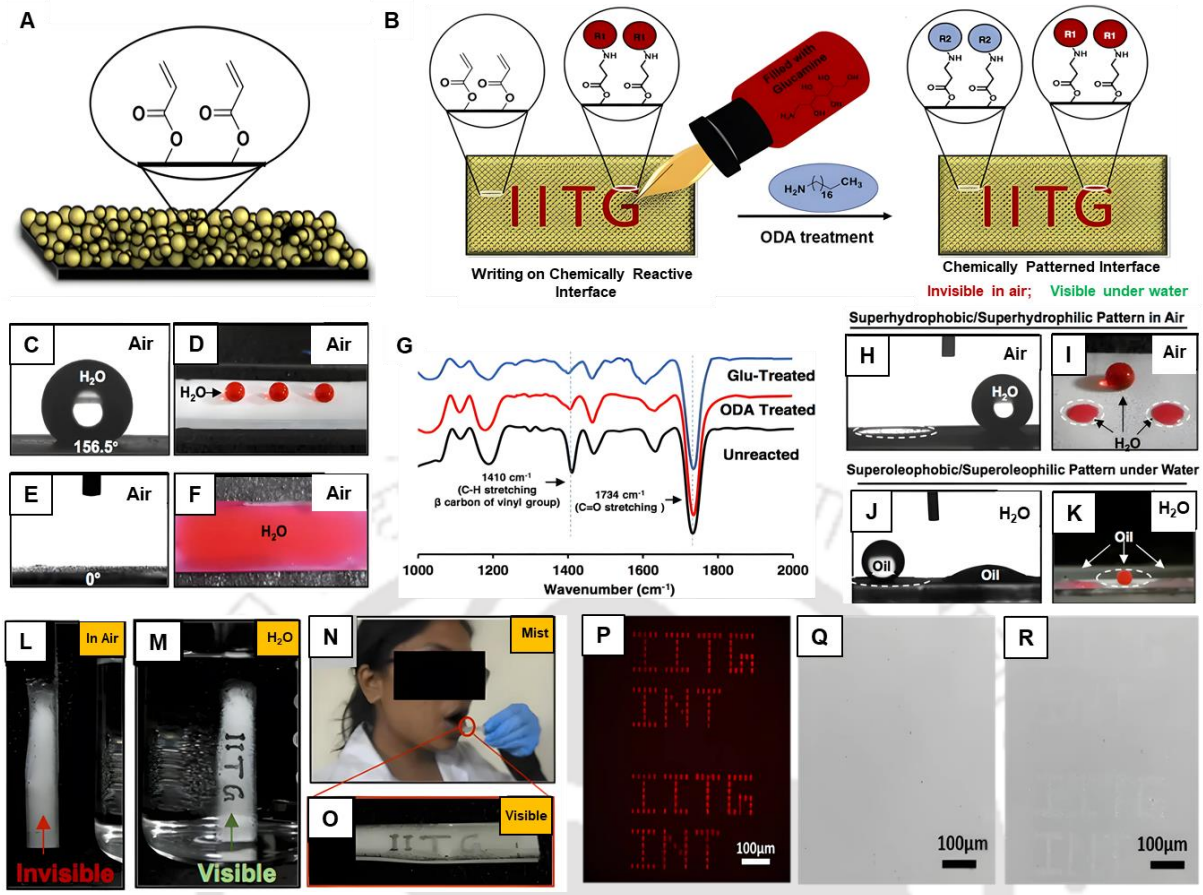

Figure 4. (A-B) Schematic presentation of chemically reactive polymeric dip coating that was directly prepared from the reaction mixture of BPEI/5Acl. Spatially selective chemical modulation of the amine-reactive polymeric dip coating with aqueous ink of glucamine, followed by octadecylamine for the synthesis of invisible patterns. (C-F) Contact angle (C, E) and digital (D, F) images of beaded water (dyed for visual inspection) droplets on the chemically reactive polymeric dip coating after treatments with octadecylamine (C-D) and glucamine (E−F). (G) FTIR spectra showing the successful post covalent modification of chemically reactive polymeric surfaces (Black line, 1410 cm^{-1}) and the ODA molecules (Red line, IR peak decreased at 1410 cm^{-1}) as well as the glucamine (Blue line, IR peak depleted at 1410 cm^{-1}). (H-K) Contact angles (H, J) and digital (I, K) images of location-specific chemically modulated patterned interface that display superhydrophobic/superhydrophilicity (H, I; in air) and superoleophobicity/superoleophilicity (J-K; under water), where the bedding/spreading of water (in air) and oil (underwater) on glucamine and ODA treated area is demonstrated. The glucamine treated area in the patterned interfaces is indicated with the dotted white circles and the rest of the region is treated with ODA. (L, M) Digital images of hand-written (with glucamine-loaded fountain pen) chemical pattern on the polymeric dip coating in air and under water; the hand-written pattern is only visible under water, and the same pattern is invisible after air drying. (N, O) Digital image illustrating the effect of blowing moist air on the patterned interfaces; the hidden text is revealed after exposure to mouth mist (O). (P) Scheme of µCS for IITG and INT microscale logos, spotted with a fluorescently labelled protein. (Q-R) Bright-field images of a wettability pattern before (Q) and during (R) exposure to humid air by breathing over the pattern (Published in *ACS Appl. Mater. Interfaces* **2020**, *12*, 2935-2943).

Here, one type of chemical functionality was selectively applied in the desired location of the reactive dip coating before quenching the rest of the chemical functionality with another type of primary amine containing small molecules through a 1,4-conjugate addition reaction. This covalent bonding-based backfilling approach allows us to fabricate arbitrary permanent patterns of two extreme and opposite liquid wettabilities, depending on the appropriate modification of the reactive dip coating with selected primary amine containing small molecules (glucamine and octadecylamine).This strategy yielded a

superhydrophobic and superoleophobic patterned interface, where the glucamine treated regions were superhydrophilic, while the rest of the area was superhydrophobic, as shown in Figure 4H-I. Furthermore, oil wettability was examined on such chemically modulated patterned interfaces. Oil droplets instantly spread on ODA treated interfaces with a contact angle of 0°, while glucamine treated circular areas on the patterned interface repel oil underwater extremely with a static oil contact angle of above 160°, as shown in Figure 4J-K. Thus, the described chemical modulation approach provides a single basis to create interfaces with patterned wettability with the in air (superhydrophobicity/superhydrophilicity) and underwater (superoleophilicity/superoleophobicity). This approach was extended further to develop covalently modulated apparently invisible handwriting with contrast liquid wettability for the first time, where the spatially selective displacement of trapped air allowed to control the transparency of the chemically modulated patterned interface depending on dry and wet conditions as depicted in Figure 4L-O. To elucidate the feasibility of miniaturizing such patterns on the coating and to show the effect of superhydrophobicity on the microscale, the microchannel-cantilever spotting (μCS) technique was used to pattern dot microarrays under controlled environment and parameters as shown in Figure 4P-R. Such a simple and covalent modulation approach would be of potential interest for addressing issues related to anti-counterfeiting and many other relevant challenges.

Chapter 5: Multiplexed Covalent Patterns on Double-Reactive Porous Dip Coating

During the course of the reaction, it was noticed that the porous polymeric coating discussed in the Chapter 2 is loaded with two distinct residual reactive groups—i.e., acrylate and amine, as shown in Figure 5A. Here, I have conceptualized and demonstrated an approach based on the combination of hydrophobicity, a substrate-independent dip coating as porous material with double residual chemical reactivities for implementing multiplexed, miniaturized and unclonable bulk-infused patterns of different fluorophores following distinct reaction pathways Figure 5B. The embedded hydrophobicity (~102°) of the dip coating (dipping time ~ 1 min) restricted the unwanted spreading of beaded aqueous ink on the coating. The existence of dual (acrylate and amine) chemical reactivity of the porous polymeric coating is validated with FTIR analysis (Figure 5C) and other fluorescence imaging experiments. Thereafter, I have spatially selectively modified the same coating with two distinct fluorescent molecules (tetramethylrhodamine cadaverine (TMRC) and fluorescein isothiocyanate (FITC)) following two independent chemical modulation processes as shown in Figure 5D-E. The confocal microscopy images in Figure 5D confirmed the bulk immobilization of both TMRC and FITC on the chemically reactive dip coating. The merged (both green and red channel) confocal image in Figure 5E (left-side panel) revealed the existence of a common section (indicated by yellow color) that is modified with both, TMRC and FITC. Such strategic dual modifications of the chemically reactive interface with two distinct representative fluorophores following two independent reaction pathways allowed to develop a complex luminescent pattern.

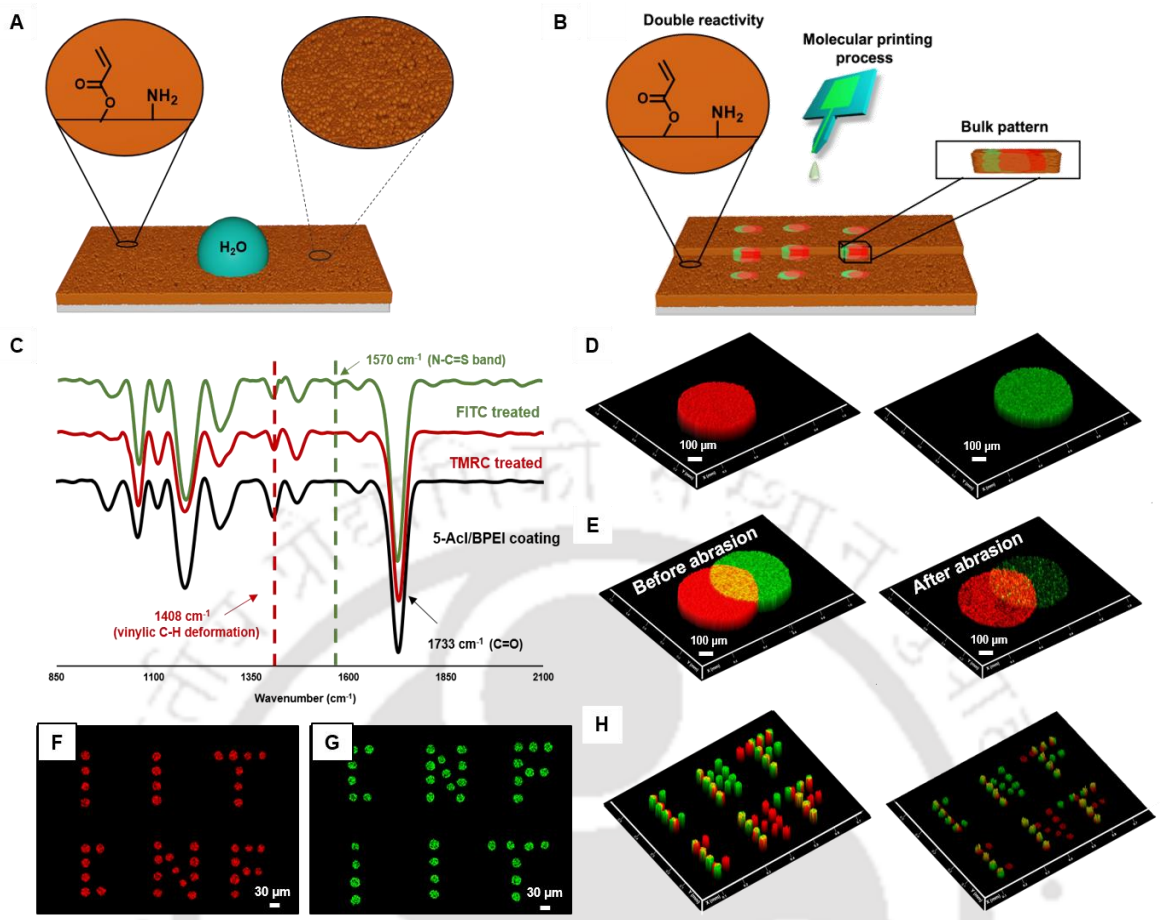

Figure 5. (A) Schematic illustration of porous polymeric coating loaded with dual chemical functionality. (B) Depicting a spatially selective and bulk orthogonal-covalent-modification through molecular printing process. (C) ATR-FTIR spectra accounting the dual chemical modification of dip coating with TMRC and FITC. (D) The confocal microscopic images revealed the presence of bulk patterns of TMRC (red) and FITC (green), respectively. (E) Merged confocal images of the patterned interface before (left-side) and after (right-side) physical abrasion. (F-G) Functional and abrasive resistant micropatterns. Confocal microscopy images (scale bar 100 µm) of (A) TMRC and (B) FITC fluorescence channel of µCS spotted letters. (H) A combined image of the fluorescence channels in (F-G) shows the overlap between the patterns before and after abrasion (Published at *Chem. Asian J.* **2022**, *17*, e202200157).

On the other side, the bulk chemical modifications of the dip coating with selective fluorophores provided an abrasion-tolerant patterned interface as shown in Figure 5E (right-side panel), where the same patterned interface continued to display the desired fluorescence signal-even after the physical abrasion. Encouraged by the multi-functional and abrasive resistant chemical modifications established, trials for miniaturized and functional patterns were implemented. For this task, inkjet printing and microchannel cantilever spotting (µCS) were employed. In µCS, inks are spotted in atomic force microscopy (AFM) by a cantilever with a microchannel connected to an on-chip reservoir for µL volumes of ink, allowing for chemical reactions in such "micro-reactors". When the cantilever is brought into contact with a surface, ink can transfer by capillary force from the reservoir to the surface. On porous and moderately hydrophobic substrates, this allows for delivery of sufficient volume of ink for imbibition and bulk functionalization of the substrate interior. With the highly precise and reproducible position control over the cantilever, arbitrary patterns can be formed and even subsequent

deposition of different inks onto the same spot can be achieved. First, as example of arbitrary micropatterns, the letters "IIT" and "CNF" were spotted with TMRC and FITC inks via μCS (Figure 5F-G). Figure 5F and G show the single channel fluorescence microscopy images for each ink, which when combined reveal an overlap of both patterns demonstrating the dual functionalization of the surface also on the micro/nano-scale (Figure 5H). This multiplexing of inks also allows for selective readout of information by selection of the matching filter channel to reveal different information from the same pattern. Importantly, the micro-patterns even stay legible after abrasion (Figure 5H), enabling a robust information storage. Further, the strategic post covalent modification with various types of selected and appropriate molecules, proteins, DNA or nanoparticles would allow to develop a different functional material for practically relevant applications including sensing, anti-counterfeiting etc.

Chapter 6: Conclusions & Future Directions

In conclusion, I have developed a substrate-independent and chemically reactive porous polymeric coating through in-situ deposition of chemically reactive nanoparticles, adopting a catalyst free 1,4-conjugate addition reaction between selected reactants following the dip coating method. The post covalent modification of such coating allowed to tailor water wettability. Apart from chemical modification, the selection of reaction solvent and deposition time also played an important role in achieving bio-inspired extreme wettability. Such substrate independent chemically reactive coating that remained capable of sustaining physical abrasion allowed to derive various functional materials. For example, the coated water soluble substrate, i.e. sugar cube provided a spongy superhydrophobic material for crude oil separation from aqueous phase. The self-cleaning preformation was demonstrated with physically abraded interface. Further, association of such chemically reactive coating with amine-reactive conductive ink allowed to develop extremely water repellent conductive pattern interface for strain sensing applications. Such interface remained efficient to perform even after aqueous exposure. Even, I have extended this chemically reactive coating to develop chemically modulated transiently visible pattern interface consists of contrast of water wettability. The dual residual reactivity is rationally exploited to develop multiplexed covalent patterns of fluorophores—adopting orthogonal chemical modification process.

In future, such strategy can be applied to develop physically unclonable and self-cleanable anti-counterfeiting interface through strategic association of water wettability, water adhesion and fluorescence molecules. Even, selective modification of such chemically reactive interfaces with protein and aptamers likely to provide biologically relevant functional interfaces. Moreover, spatially selective association of chemically modulated two extremes of wettability can be effectively applied for open microfluidic application. Further, the strategic association of water wettability, conductivity and other functional moieties would likely to provide functional interfaces for sensing toxic volatile gas and other relevant chemicals.

Table of Contents

1. Nature as a Source of Inspiration for Innovation

Nature has always been the motivation for researchers to acknowledge about innumerable phenomena prevailing in it, different materials involved, their properties, textures and designs which resulted in revolutionary technologies while mimicking it.[1] For instance, wettability is a characteristic property of material interfaces which leads to various outstanding applicability of such materials, i.e., self-cleaning, drag reduction etc.[2-7] A very straightforward quantitative expression of surface wettability is the measurement of contact angle of a liquid droplet under consideration on the solid surface. Considering water as the liquid phase in contact with the solid surface, various wetting phenomena has been observed and categorized by the extent of favourable interactions, such as superhydrophilic ($\theta < 0^o$), hydrophilic ($\theta < 90^o$) and hydrophobic ($\theta > 90^o$) interfaces.[8] However, surfaces with very high water contact angles (WCA) especially higher than 150º are known as superhydrophobic surfaces. These surfaces are fascinating because of properties such as anti-sticking, anti-fogging, contamination free surfaces etc.[9-15] These properties are worthwhile for numerous industrial and biological applications such as anti-biofouling paints for boats,[16-17] anti-sticking of snow for antennas and windows,[18-19] self-cleaning windshields for automobiles,[20] oil-water separation,[21-23] metal refining, stain resistant textiles[24] and considerably more. There are various examples of such surfaces with wettability extremes are found in nature, living organisms such as lotus, rice and taro leaves, desert beetle and water strider etc.[25,26] Since 1960, as the evolution of Scanning electron microscopy, plants surfaces have been analysed in detail. The naturally existing surfaces with special wettability property has been investigated carefully and concluded with the fact that they all have unique hierarchical topography consisting of both micro and nano domains as shown in Scheme 1.1.[27] Mostly, the special wettability ascribed to the co-optimization of both the surface topography and chemical functionality exposed.[28-37] To explain such super water repellence existing in nature, water contact angle exclusively not sufficient, along with that contact angle hysteresis (CAH) and sliding angle (SA) played a pivotal role for their comprehensive characterization. While non-adhesive superhydrophobicity was explicated as WCA > 150º and CAH and SA < 10º, the adhesive superhydrophobicity refereed to the interface that displayed WCA > 150º and CAH & SA > 10º. On the other side, superhydrophilicity was interpreted as WCA<5º.[38-45] In the past, researchers have excavated the theories appropriate to explain these phenomena. As a consequence, few theoretical models emerged after hundreds years of research, i.e., Young's model, Wenzel model and Cassie-Baxter's equation.[46-48] Improvement and development of such models helped people understand the nature and life surrounding in a finer way. It would assist in designing more facile, ecological and smart materials to ameliorate our life.

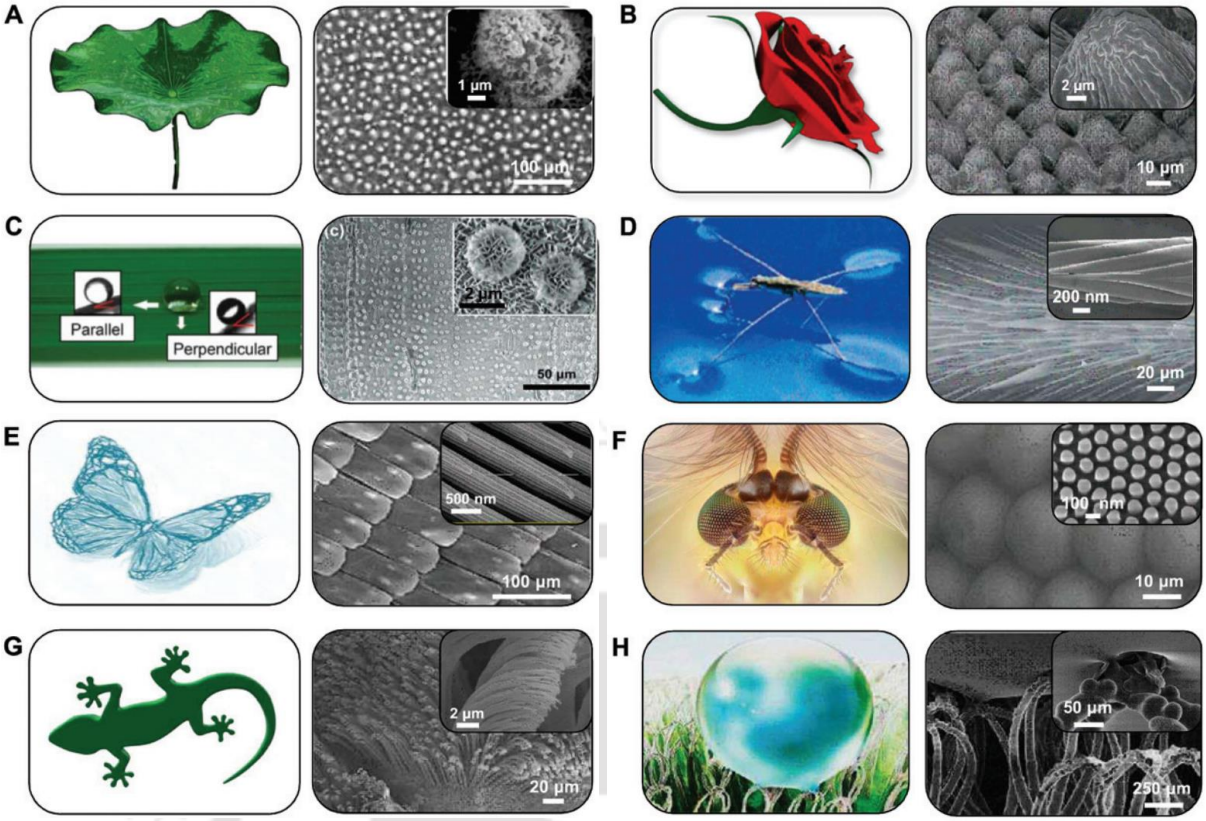

Scheme 1.1. (A) Lotus leaf exhibits non-adhesive superhydrophobicity due to its randomly distributed micropapillae covered by nanotopography. (B) Red rose petals comprising of periodic arrays of micropapillae topped with nanofolds demonstrate highly adhesive superhydrophobicity. (C) The one-dimensionally arranged micropapillae covered with nanofeatures in rice leaf aids in exhibiting anisotropic superhydrophobicity. (D) The legs of the water strider comprise of microsetae topped with fine nanogrooves that aids in displaying robust superhydrophobicity. (E) Butterfly wings exhibit anisotropic superhydrophobicity that is attributed to the presence of multiscale structures. (F) The transparent compound eyes of the mosquito display superhydrophobicity due to the presence of microommatidia topped with nanonipples. (G) Gecko feet possess microscale keratinous setae split into nanoscale spatulae that display adhesive superhydrophobicity. (H) Salvinia molesta exhibit superhydrophobicity arising from their hair-like structures on the surface covered with nanowax crystals. Reprinted with permission from *Chem. Soc. Rev*. **2022**, *51*, 5452–5497.[49] Copyright 2022, The Royal Society of Chemistry.

1.1. Theoretical Models and Mechanism of Liquid Wettability on Solid Surface

Based on the literature reports, wetting phenomena and surface wettability property are meticulously related to surface morphology. Therefore, surface roughness is considered to be very crucial. When a liquid droplet is placed on a smooth surface and it is not outspread, affirms that it is balanced itself on the surface. Three phase interfaces originate when a liquid droplet is settled on any solid surface and the shape of this droplet will be determined by the size of included angle among the tangent of gas-liquid interface, droplet and solid-liquid interface. This angle is known as contact angle or wetting angle, represented by θ as shown in Figure 1.1.[1] Contact angles can be categorized as static contact angle and dynamic contact angles. Static contact angles are obtained when a beaded liquid droplet reaches a steady state on the solid interface. Dynamic contact angles are further classified into advancing and receding contact angles. Advancing contact angle (θ_{adv}) is measured during the growth of a liquid droplet i.e.,

when the liquid droplet wets the solid interface, whereas receding contact angle (θ_{rec}) is measured during the shrinkage of the droplet i.e., when the droplet de-wets the surface.

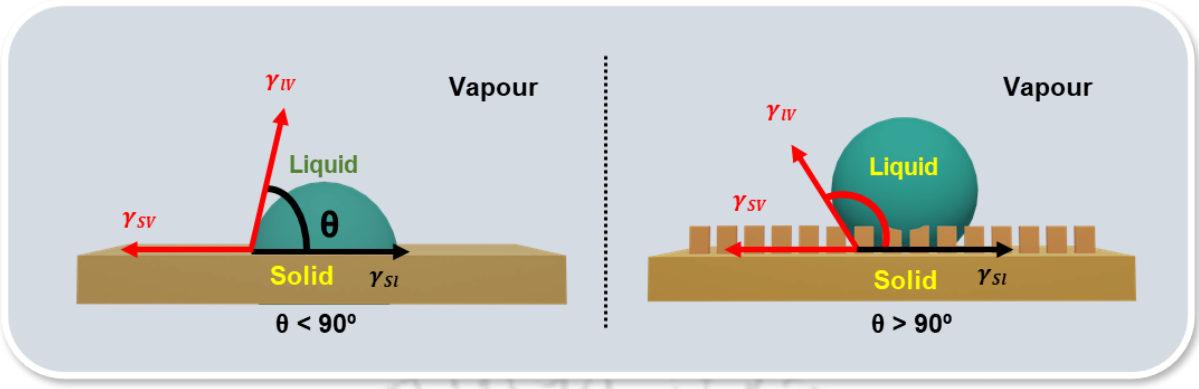

Figure 1.1. The scheme depicting the contact angle on both hydrophilic and hydrophobic interfaces.

Earlier this angle was generally used as a standard to estimate the liquid wettability of solid surfaces. It has been proved that contact angle solitarily was insufficient as it was unable to elucidate the rolling off of liquid on the surface. When a droplet starts sliding off an inclined surface, the corresponding angle (sliding angle) originated between the inclined surface and the horizontal plane is represented by **α** as shown in Figure 1.2. The well-established quantitative relation between sliding angle (SA), advancing contact angle (θ_{adv}) and receding contact angle (θ_{rec}) is as presented in 1962 by Furmidge.

$$mg(\sin\alpha)/\omega = \gamma(\cos\theta_{adv} - \cos\theta_{rec}) \quad (1)$$

where m is the droplet mass, g is the acceleration of gravity, ω is the diameter of the droplet, γ is the surface tension of droplet.

Thus, $\theta_{adv} > \theta_{rec}$, the smaller the value of contact angle hysteresis, the lower will be the adhesive force of liquid droplet on a solid surface. The hierarchical features affected in decreasing sliding angle and lowering contact angle hysteresis in combination with appropriate chemical modulation.[50-57]

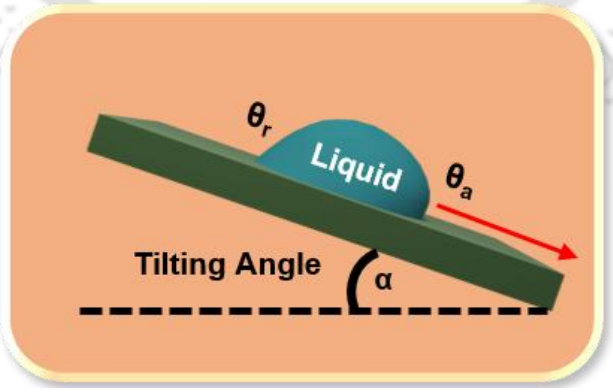

Figure 1.2. Schematic representation of beaded droplet on inclined surface.

There are specific theoretical models to explain distinct wettability properties along with the variation of SA and WCA with each wetting phenomena. Three well established classic models, i.e., Young's

model, Wenzel's model and Cassie-Baxter model, are evolved consecutively and provided basis to understand the different wetting behaviour observed in nature.

1.1.1. Young's Model

This model proposed in 1805, was the elementary model to elucidate the wetting event. When a droplet placed on a homogeneous, smooth and perfectly flat solid surface and immediately stabilized by balancing the surface tension among the interfaces of solid, liquid and gas.[52]

The Young's droplet balanced equation in the horizontal direction is shown as follows, established by the mechanical equilibrium conditions.

$$cos\theta_Y = \frac{(\gamma_{sv}-\gamma_{sl})}{\gamma_{lv}} \quad (3)$$

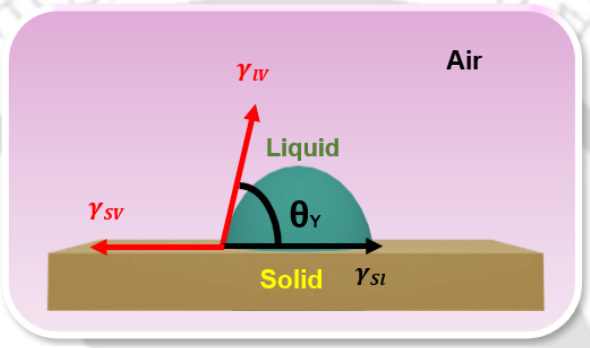

Figure 1.3. A beaded droplet of liquid stabilized on a homogeneous, flat and ideally smooth solid surface.

When, θ_Y is the balanced contact angle in Young's model, and γ_{sv}, γ_{sl} and γ_{lv} are the interfacial surface tension of solid-gas, solid-liquid and liquid-gas respectively, as represented by Figure 1.3.

As it is established that Young's equation is developed based on the flat and highly smooth surfaces, which is practically rare to perceive. However, if this model is considered then the effect of surface topography on wettability ought to be removed, which in fact one of the essential criteria of superhydrophobicity observed in nature. Therefore, except the surface topography only chemical modification can be performed on such smooth surface, and even if the lowest surface energy chemical was used for this purpose, the highest WCA possible to be accomplished was almost up to 120º. Although the WCA on Lotus leaves and various other living organisms are approximately 160º, much higher than the limitations of this model. That means, Young's model and equation is only valid for ideally smooth solid surfaces, and unable to explain the rough surfaces relevant to real life.

1.1.2. Wenzel Model

As per the fact, all naturally existing surfaces have certain extent of roughness and Young's contact angle is different than the true apparent contact angle of the same surface. Therefore, developing a mechanism to demonstrate the high contact angle on superhydrophobic surfaces, effect of surface roughness must be considered to analyse the apparent contact angle.

Then, the concept of introducing "roughness factor" in Young's equation was recommended by Wenzel in 1936 and the revised equation is as follows: [58]

$$cos\theta_W = rcos\theta_Y \quad (4)$$

Where, r is the roughness factor, θ_W is the Wenzel apparent contact angle on the solid surface. r is the ratio of actual area on rough surface and the apparent geometric area (Figure 1.4).

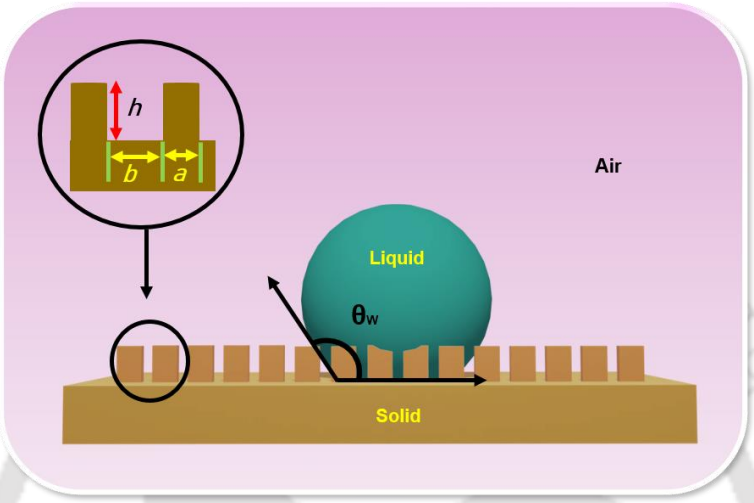

Figure 1.4. Schematic representation of homogenous wetting of liquid droplet on rough solid surface.

According to Wenzel, the real exposed surface area of solid was increased because of the rough features. As a consequence, the actual solid-liquid contact area was larger than the apparent geometric contact area, prevailing the surface increase the hydrophobicity or hydrophilicity based on geometry and chemical modifications. As per the equation, the basis and effects of solid-gas interfacial tension, solid-liquid interfacial tension on system energy were altered by surface roughness. Eventually this became the principal reason of difference between the contact angle on rough surface and contact angle on ideally smooth surface. However, while a water droplet is placed on such rough surfaces, it penetrates the micro-grooves and the homogeneous wetting state is generated. The actual solid-liquid contact area is always higher than the apparent geometric contact area, that provides the value of roughness factor, $r > 1$, therefore when $\theta_Y > 90^o$, the roughness factor r will enhance the hydrophobicity of that surface. Further, if the surface is hydrophilic, $\theta_Y < 90^o$, r will increase the hydrophilicity. However, such homogeneous wettability model also fails to explain super wettability of beaded liquid droplet.

1.1.3. Cassie-Baxter Model

Following the constraints with the Wenzel model, in 1944, Cassie and Baxter heterogeneous wettability model which demonstrates that grooves of the rough features are entrapped with external third phase, i.e., air for superhydrophobicity. Therefore, when a liquid droplet is placed on that surface it does not permeate the grooves as shown here in Figure 1.5. Here, the solid-liquid droplet contact composed of solid-gas and solid-liquid because the air was preserved under the droplet.[59]

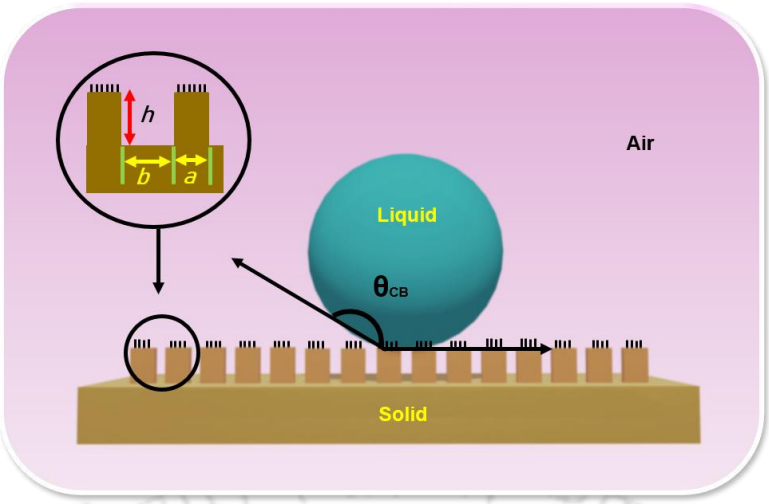

Figure 1.5. Schematic representation of heterogeneous wetting of liquid droplet on third-phase entrapped hierarchically featured solid surface.

According to Young's equation, relationship between the Cassie contact angle and apparent contact angle can be expressed as the following equation (5), where f_1 and f_2 are geometrical fraction of contact area for solid-liquid and liquid-air interfaces respectively.

$$cos\theta_{CB} = f_1 \, cos\theta_1 + f_2 \, cos\, \theta_2 \quad (5)$$

Where, θ_1 and θ_2 are contact angles of beaded liquid on solid and air phase.

Theoretically, $f_1 + f_2 = 1$, as contact angle of liquid in air is 180°. Therefore, the equation (5) can be converted to,

$$cos\theta_{CB} = f_1 \, (cos\theta_1 + 1) - 1 \quad (6)$$

When f_1 tends to zero, the beaded water droplet will be in contact with the trapped air mostly. Hence, the highest Cassie contact angle will be attained, i.e., 180°. From physical point of view, the droplet will be completely spherical in shape.

It is analysed that natural superhydrophobic surfaces consists of hierarchical features, so this Cassie-Baxter equation and model is suitable to defend the actual mechanisms occurring in living organisms. However, under few conditions, such as at high pressure and low temperature, high humidity heterogeneous model to homogeneous wettability transition happens, also known as Cassie-Wenzel transition.[60-64]

1.2. Distinct Wettability of Surfaces in Nature

Living organisms with uttermost anti-wetting characteristics has recognized effectively for domestication of the surface characteristics to fabricate artificial anti-wetting surfaces.

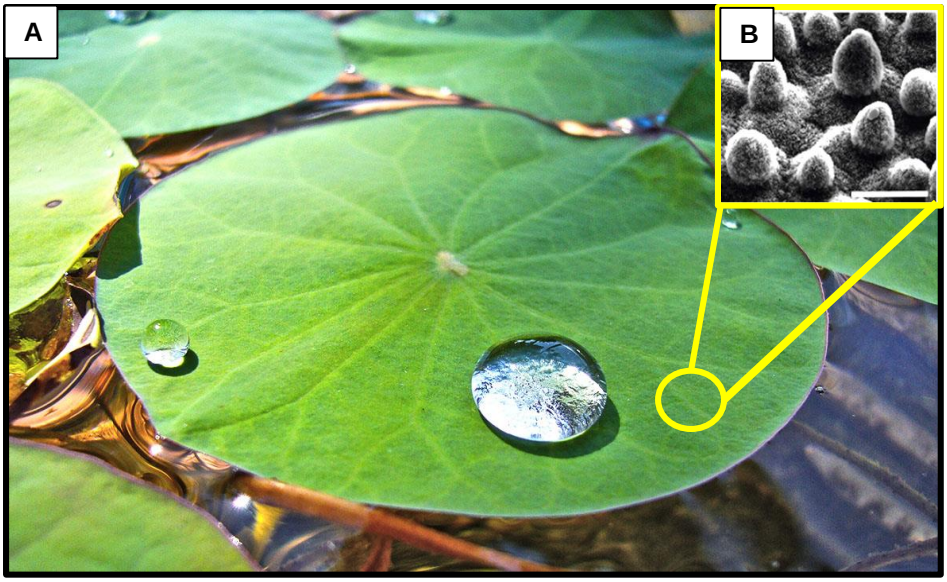

Figure 1.6. (A) Digital image of lotus leaf with beaded droplets of water and (B) SEM analysis of micro/nano-features lying at the leaf interface. Figure A and B are adapted from futurity.org (Credit: Josep M[a]/Flickr, **2015**) and *Chem. Soc. Rev.* **2014**, *43*, 2784-2798. Copyright 2014, The Royal Society of Chemistry.

There are numerous existing natural models that motivated scientists and amongst them few plant leaves have self-cleaning characteristics that helped them sustaining in the dirty environment. Lotus leaf is one of the most popular natural anti-wetting model that remains unstained even growing in muddy water as depicted in Figure 1.6.[65] Barthlott and Neinhius instigated the Lotus leaf inspired superhydrophobicity and perceived that the although the surface of the lotus leaf seemed to be smooth, it consists of micro-scaled roughness with protrusions and valleys of 3-10 µm, with outer surface area covered with 70-100 nm of epicuticular wax like materials consists of a combination of long chain hydrocarbons. Therefore, the reason behind such extreme water repellent behaviour of lotus leaf is the co-existence of hierarchical surface features along with the hydrophobic wax like material. On such surfaces water droplet rolls off easily on crest of the nanofeatures due to the presence of entrapped air in the grooves under the droplets. While a water droplet falls on such hierarchically featured surfaces, they took a spherical shape and fetched the dirt particle with them during rolling off of the surface, this phenomenon well recognized as “self-cleaning” or “Lotus effect” (Schematic representation in Figure 1.7).[66] After that, the extreme de-wetting nature of rice leaf was revealed, where the arrangement of micro papillae was observed and analysed as a reason of superhydrophobicity. Next, in 2008, rose petals with highly adhesive superhydrophobicity was reported where the heterogeneity of micro papillae in combination with nano structural features were noticed as shown in Figure 1.8.[67]

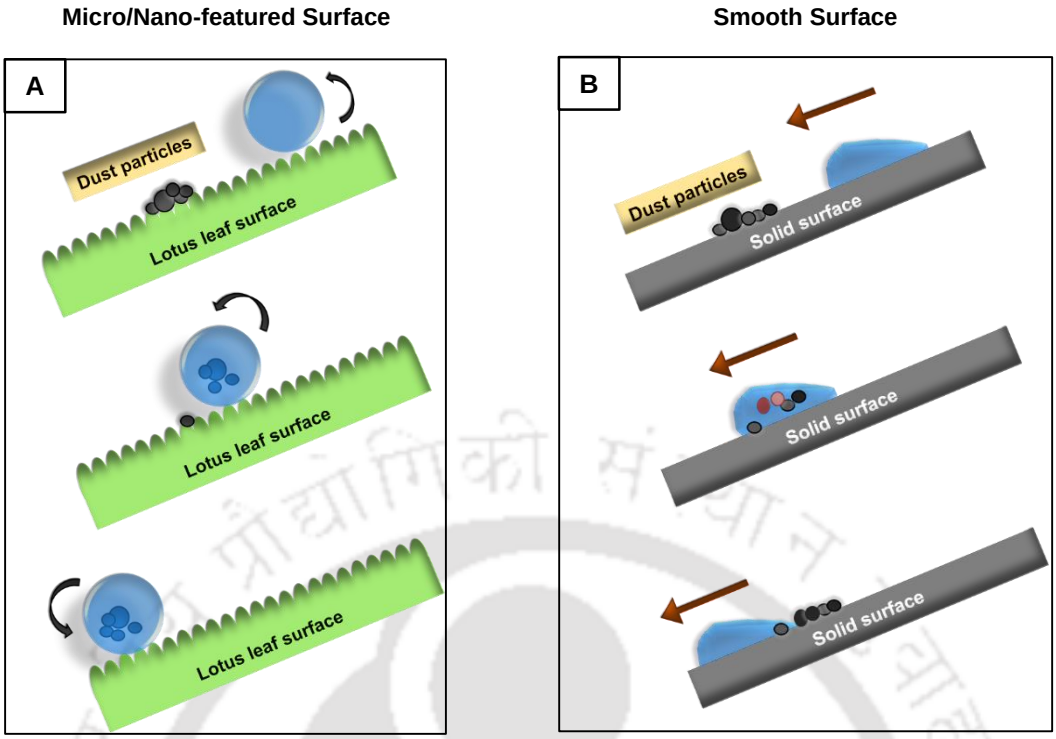

Figure 1.7. (A) Schematic of self-cleaning mechanism on hierarchically featured lotus leaf surfaces, whereas (B) the smooth solid surfaces exhibiting adherence to the dust particles. Reprinted with permission from *J. Mater. Chem. A* **2019**, *7*, 16643-16670. Copyright 2019, The Royal Society of Chemistry.

This type of hierarchical features provided the superhydrophobicity with contact angles ~ 152.4º along with adhesiveness, where water droplets remained in spherical shape but adhered to the petal surface even with the inverted leaf. Such surface characteristics and water repellent properties are replicated by template based method on polystyrene film and achieved the water contact angle ~154º.[68]

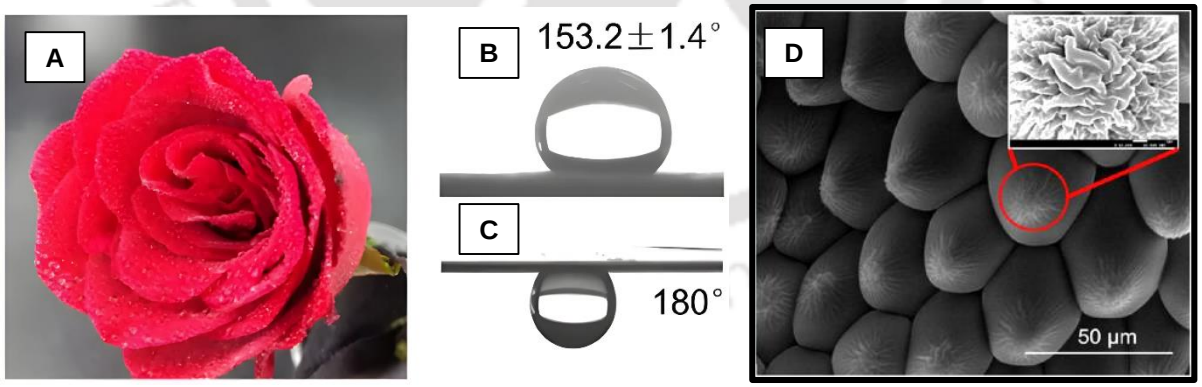

Figure 1.8. (A-D) Superhydrophobicity and natural hierarchical structure of rose petal. Digital (A) and SEM images (D) of rose petals demonstrating embedded micro structures at the interfaces. (B-C) The static water contact angle images showing highly adhesive superhydrophobicity. Reprinted with permission from *Ind. Eng. Chem. Res.* **2017**, *56*, 907–919. Copyright 2017, American Chemical Society.

Natural living organisms holding such interesting extreme wettability properties are not only limited to plants, various insects also exhibit such unique features. In 2001, it has been observed that Stenocara Beetle is capable of harvesting water from atmosphere under extremely dry condition as Namib desert (Figure 1.9A).[69]

It has been investigated that the insect's elytra consist of small, wax free hydrophilic bumps diffused on superhydrophobic waxy background. During morning fog, microscopic droplets deposited and condensed on hydrophilic bumps, and once the critical size of the droplet reached it immediately rolls towards the mouthpart of the beetle (Figure 1.9B). Water harvested by this process is the only source of water for the species in that extremely arid environment.[70]

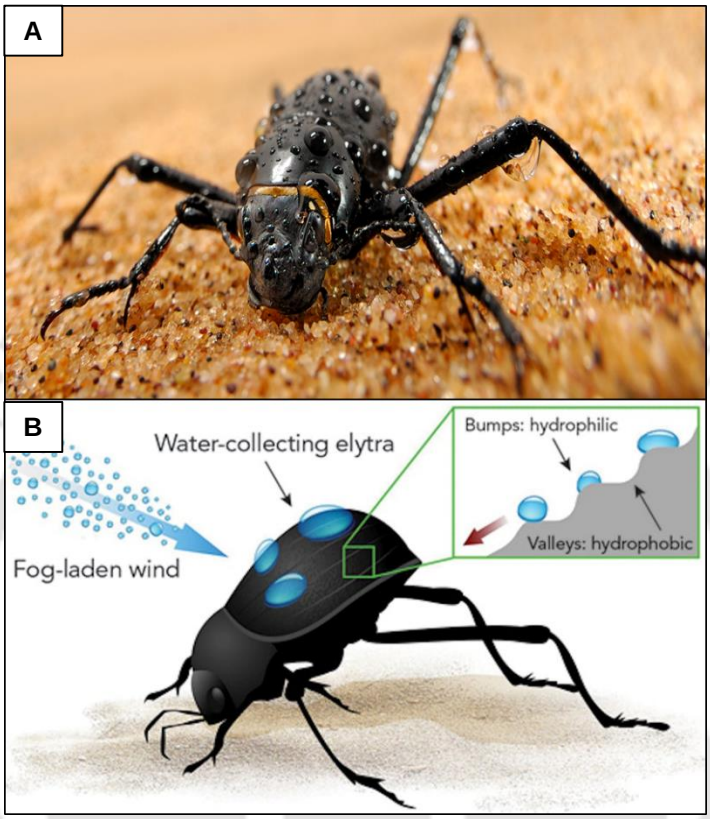

Figure 1.9. (A) Namib desert beetle and the schematic representation of existing wettability pattern on its back. Reprinted with permission from *Science News* **2019**; (B) The Namib Desert beetle's fog-collecting strategy is as follows: as the wind carrying the fog builds up on the hydrophilic peaks, the droplets grow to a critical size followed by rolling down the hydrophobic valleys into the beetle's mouth. Adapted from *Langmuir* **2018**, *34*, 2933–2941. Copyright 2018, American Chemical Society.

Inspired by this phenomena, several researchers have replicated this natural living system by generating hydrophilic bumps on superhydrophobic waxy films, plasma polymers or polyelectrolyte multilayers to demonstrate water harvesting, e.g., removal of drops from industrial exhaust gasses, directional transport of liquids in microfluidic systems and so on.[71,72]

1.3. Existing Approaches for Bio-inspired Superhydrophobic Surfaces

Essential criteria for achieving superhydrophobicity is the combined effect of surface topography and suitable surface chemistry. Nature mimicked artificial superhydrophobic interfaces have been widely investigated for practical applications in environment, energy and health sectors.[73-82] Earlier various approaches such as top down and bottom up approaches have been extensively acquired to evolve artificial superhydrophobic interfaces via quite general synthetic approaches, where substantially hydrophilic components have used to fabricate the hierarchically featured interfaces that post-chemically modified with low surface energy materials, by associating frail chemistry-including silane chemistry, metal-thiol bonds, metal ion interactions. All of such chemical bonding interactions are susceptible under harsh environmental and practical conditions.[83-91] The top interface of the coating after removal under practical abrasive situations, hydrophilic interior of the surface was exposed, and the anti-wetting property of the coating was compromised.[92-93] There are various methods have been adapted and utilized to overcome such durability issues, such as the regeneration of hierarchical topographies and low surface energy coating on the abraded surfaces for the retention of its anti-wetting behaviour also widely known as post-repairable approach. Another approach where stimulus induces the diffusion of low surface energy material on the abraded surface to retrieve the bio-inspired wettability. Due to the requirement of external interaction for healing the damage, time-consuming, and expensive synthesis procedure involved in regenerating hierarchal topography/chemistry after each damaged cycle, both of these techniques are less appropriate for practical utility. Additionally, the store of molecules with low surface energy will eventually deplete, making it harder to maintain prolonged unperturbed performance.[94-98] Levkin et al. introduced the idea of "bulk superhydrophobicity" to address the problems with physical durability.[99] Using a single polymeric coating, the creation of a chemically "reactive" durable interface offers a great alternative for adjusting various bio-inspired wettability. The development of chemically "reactive" durable surfaces, however, for adjusting various bio-inspired wettability, remains a very difficult task, and the pace of research in the literature is quite modest.

1.4. Thin and Chemically Reactive Polymeric Interfaces

Earlier, thin and chemically reactive polymeric interfaces were emanated as idiosyncratic phenomena to explore the development of functional materials. For example, the adsorption of two "reactive" co-polymers, poly (vinylpyrrolidene/vinyl chloroformate) and poly(vinylpyrrolidene/vinyl chloroformate modified with N-hydroxysuccinimide), onto silica particles for prospective chromatographic applications was demonstrated by Perrin et al. in 1994 (Figure 1.10A), where the application of "reactive" polymers will enable the eventual association of various chemical functionalities.[100] In 2001, Major et al. showed how di-ester formation between the accessible hydroxyl group and adipoyl chloride could produce the covalent multilayer construction of maleimidevinyl ether (MVE), a thin, smooth "reactive" film having lingering acid chloride groups that can bind more polymer layers (Figure 1.10B).[101] Next, in 2007, Dyer et al. created a thin (1–8 nm) polyallylamine and polyethylene glycol

diacrylate coating over a silicon substrate, and they looked into how this affected the ability of proteins to adhere to the coating as shown in Figure 1.10C.[102] However, Wang et al. motivated the diatom frustules in 2009 by soaking them alternately in solutions of tris(2-aminoethyl) amine and dipentaerythritol penta-acrylate, to create an extremely thin (between 5 and 25 nm) covering with residual 'reactive' acrylate groups on the surface that helped to link hydroxyl-rich tris(hydroxymethyl)aminomethane as the final layer (Figure 1.10D).[103]

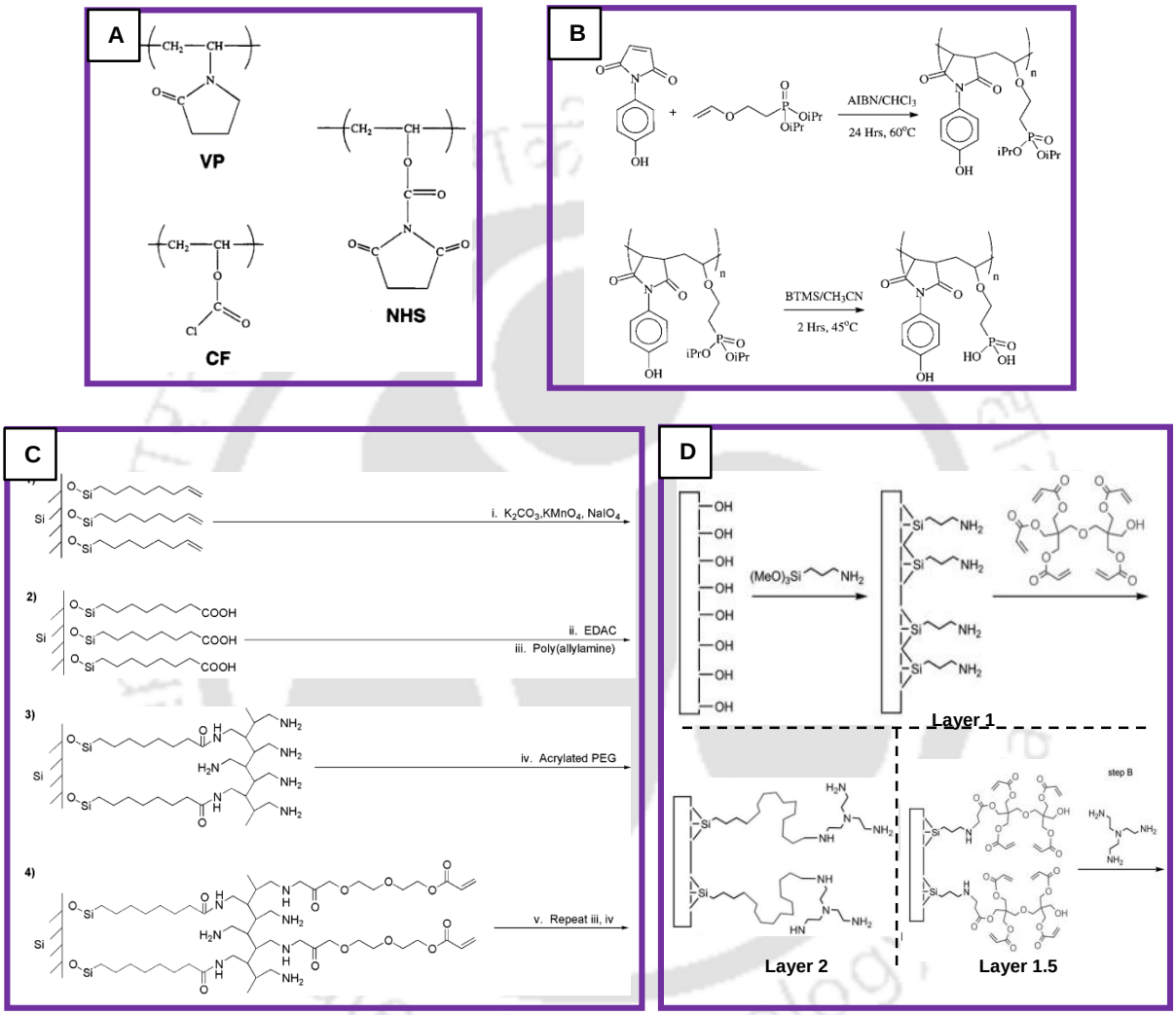

Figure 1.10. (A) The structural formulae of the monomer units that were employed to develop the specific chemically reactive co-polymers. VP, CF, and NHS represent the units of, respectively, poly(l\r-vinylpyrrolidone), poly(viny1 chloroformate), and poly(viny1 chloroformate) modified with N-hydroxysuccinimide. Reprinted with permission from *Langmuir* **1994**, *10*, 3635–3641. Copyright 1994, American Chemical Society. (B) Structutal representation of the monomers used in the synthesis of the MVE (maleimidevinyl ether) alternating copolymer, used for the formation of smooth and reactive thin film. Reprinted with permission from *Langmuir* **2001**, *17*, 1163–1168. Copyright 2001, American Chemical Society. (C) Hyperbranching poly(allylamine) (PAAm) and polyethyleneglycol (PEG) on silicon through covalent interaction of acrylate and amine functionalities, Reprinted with permissionfrom *Langmuir* **2007**, *23*, 7018–7023. Copyright 2007, American Chemical Society. (D) Dendritic growth of hyperbranched polyacrylate monomer (Sartomer SR-399)/ tris(2-aminoethyl)amine (TAEA) thin films on silica-bearing surfaces via Michael addition reaction. Adapted from *Adv. Funct. Mater.* **2009**, *19*, 2768–2776. Copyright 2018, Wiley-VCH Verlag GmbH & Co. KGaA, Weinheim.

In 2010, Chen et al. reported a chemical vapour deposition approach for developing a chemically reactive coating with poly(4-ethynyl-p-xylylene-co-p-xylylene) on variety of substrates.[104] The 'reactive' alkyne groups undergo 1,3-dipolar cycloaddition reaction with an azide based ink to develop patterns using the dip pen lithography technique. Furthermore, this polymer pen technique was adapted to deposit an alkylamine modified DNA ink on epoxy functionalized glass via nucleophilic ring-opening reaction (Figure 1.11).[105-106] In 2018, Atwater et al. utilized a fmoc-protected polyethylene glycol methacrylate-co-methyl methacrylate substrate to pattern with a layer of amino acids in a microcantilever spotting process, followed by heating to allow amidation reaction, and then spotting with another layer of amino acids on top of the existing one to develop a peptide microarray (Figure 1.12).[107] But such strategy fails to provide extreme liquid repellent property as these chemically reactive coating remains relatively smooth and unable to provide adequate hierarchical topography.

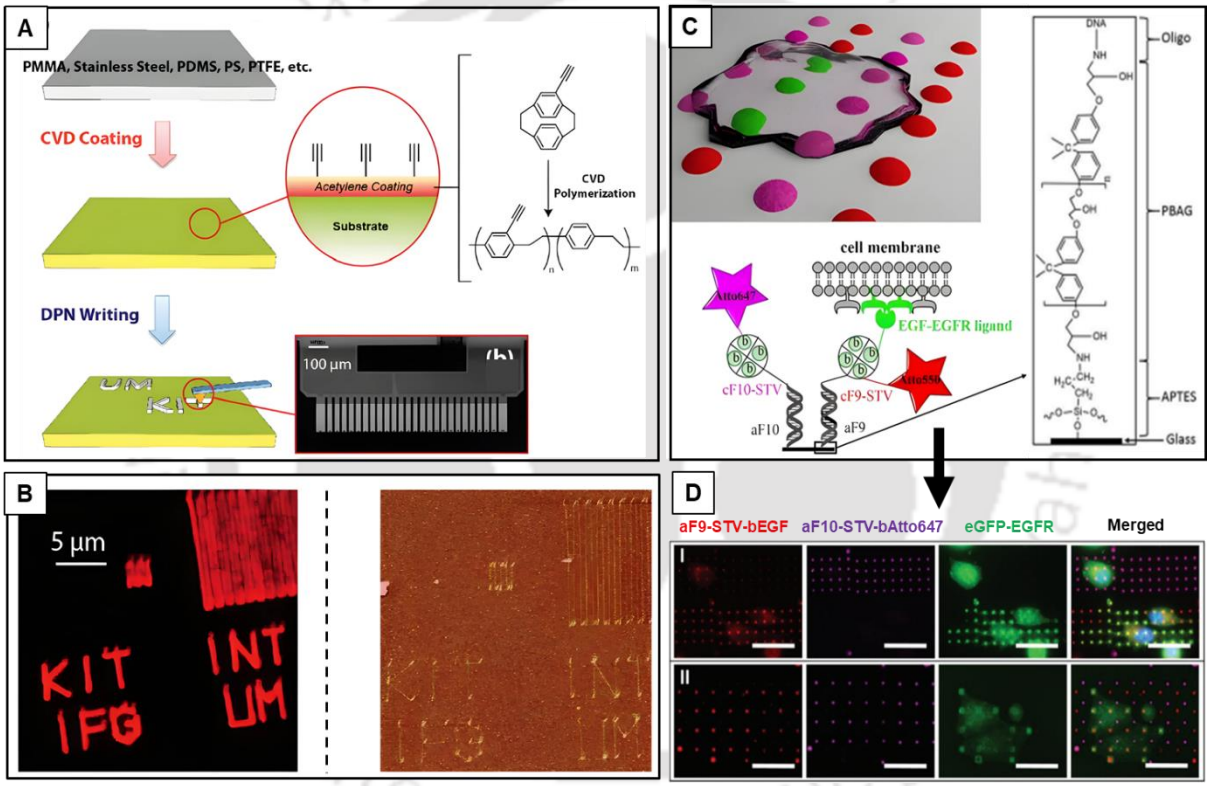

Figure 1.11. (A) Schematic representation of the DPN (dip pen nanolithography) writing technique modified for CVD-coated substrates. The ethynyl-presenting polymer, poly(4-ethynylp-xylylene-co-p-xylylene), is used as an example; inking molecules are covalently attached via click chemistry. Micrograph of a 1D cantilever array with 26 pens. (B) Fluorescence micrograph of a poly(4-ethynyl-pxylylene-co-p-xylylene)-coated gold surface after DPN writing; features consist of 300-nm lines to form texts and rectangular boxes. AFM image (tapping mode topography) showing self-assembled gold-streptavidin particles after DPN-based click reaction. Reprinted with permission from *J. Am. Chem. Soc.* **2010**, *132*, 18023–18025. Copyright 2010, American Chemical Society. (C-D) Schematic illustration of a cell on a hybridized oligonucleotide array presenting EGF features. Chemical structure of the substrate. Recruitment of EGFR (green) on EGF bearing features (red). The neutral features (magenta) do not alter the even EGFR distribution in the cell membrane and act as inherent control. All scale bars equal 50 µm. Reprinted with permission from *Chem. Commun.* **2016**, *52*, 12310-12313. Copyright 2016, The Royal society of Chemistry.

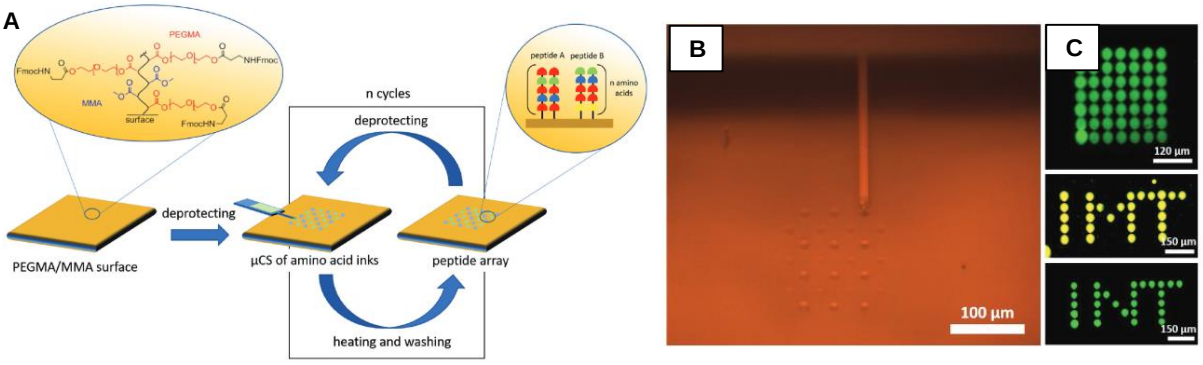

Figure 1.12. (A) Process flow diagram for the synthesis of peptides. In a CS procedure, the corresponding amino acid was identified on the PEGMA/MMA surfaces. Then, the microarray is heated, starting the coupling of the spotted amino acids, and unreacted amino acids are removed. A second layer of amino acids may be observed on top of the current array after an acetylation and deprotection phase. Each location in such a microarray can have a unique peptide of length n amino acids with n of these cycles. Spotting setup. (B) The µCS spotting process as seen in the instrument camera. The microchannel cantilever hovers above the sample. On the sample surface, a spotted array of amino acid ink can be seen. (C) Fluorescently labelled test patterns: a regular array of glycine in a 40 µm pitch (top), IMT logo spotted with lysine (middle), and INT logo spotted with glycine (bottom). Reprinted with permission from *Adv. Mater.* **2018**, *30*, 1801632. Copyright 2018, Wiley-VCH Verlag GmbH & Co. KGaA, Weinheim.

1.5. Approaches for Hierarchically Featured/Porous Chemically Reactive Polymeric coatings

Design of porous and rough chemically reactive interface appeared as a promising approach for bulk optimization of essential chemistry and topography to achieve desired liquid repellent properties.

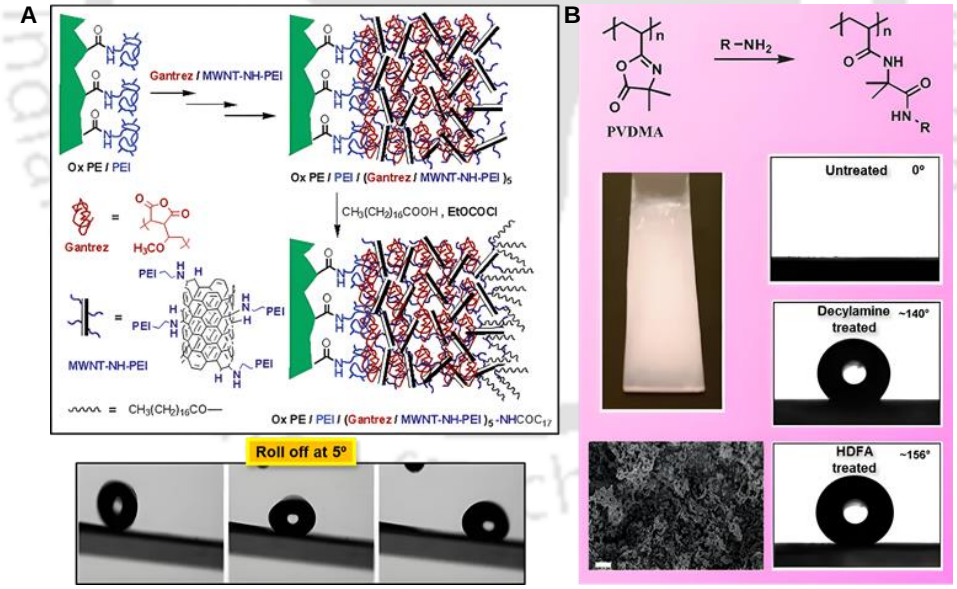

Figure 1.13. (A) Schematic displays covalent layer-by-layer self-assembly of gantrez/MWNT-NH-PEI on PEI grafted oxidized PE films and further acylation with a mixed anhydride prepared from ethyl chloroformate and octadecanoic Acid. Water sliding behavior of a superhydrophobic film prepared by covalent assembly: water droplet rolling off the surface. The stage is tilted 5°, and the interval between each frame is 33 ms. Reprinted with permission from *Langmuir* **2008**, *24*, 4245–4253. Copyright 2008, American Chemical Society. (B) Structural representation of poly(2-vinyl-4,4-dimethylazlactone) and scheme of reaction with amine functionalized nucleophiles. Digital and FESEM images of 100-bilayer PEI/PVDMA film (PEI = Polyethyleneimine). Contact angle images illustrating wettability transition from hydrophilicity to hydrophobicity followed by superhydrophobicity was achieved by post modification with decylamine and heptadecafluoroundecylamine respectively. Figure is adapted from *Chem. Mater.* **2010**, *22*, 6319–6327. Copyright 2010, The Royal society of Chemistry.

For example, in 2008, MWCNT (multi-walled carbon nanotube) surface modified with amine groups and electrophilic polyanhydride containing polymer (Gantrez) were covalently reacted through LBL assembly to obtain a hierarchically featured porous amine reactive coating which further chemically modified via acrylate groups of the mixture prepared by ethyl chloroformate and octadecanoic acid (Figure 1.13A).[108]

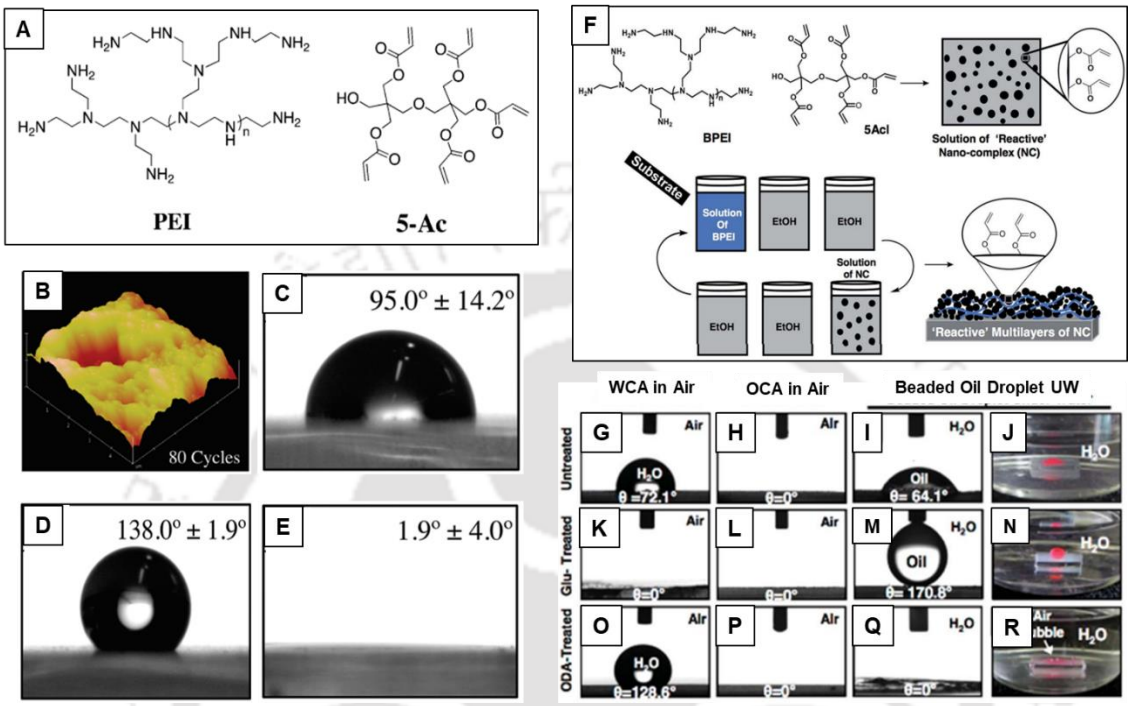

Figure 1.14. (A) Structural representation of branched poly(ethyleneimine) (PEI) and small molecule dipentaerythritol pentaacrylate (5-Ac). (B) AFM images (5 μm × 5 μm) of 80-bilayer PEI/5-Ac films prepared on bare silicon substrates. The scale in the z direction for each image is 1.2 μm. (C-E) Static water contact angles images of 80-bilayer PEI/5-Ac film before chemical modification (C) and after chemical modifications with decylamine (D) and glucamine (E) respectively. Reprinted with permission from *Biomacromolecules* **2012**, *13*, 1523–1532. Copyright 2012, American Chemical society. (F) Chemical structures of poly(ethylenimine) (BPEI) and dipentaerythritol penta-acrylate (5Acl). Formation of amine reactive nanocomplexes upon mixing of the reactant chemicals. LBL deposition of reactive nanocomplex and BPEI multilayer film formation is depicted by schematic illustration. Various wettability property of such films are analysed by contact angle measurements, such as water in air (G, K, O); oil contact angles in air (H, L. P); oil wettability under water (I-J, M-N, Q-R) respectively. Reprinted with permission from *Chem. Sci.* **2017**, *8*, 6092-6102. Copyright 2017, The Royal society of Chemistry.

After these surface functionalizations, coating exhibits anti-wetting properties. Later, Buck et al. acquired an approach of click type chemical reaction to compose a multi layered coating of poly(2-vinyl-4,4-dimethylazlactone) (PVDMA) and branched polyethyleneimine (PEI), where residual amine and azalactone groups covalently interacted to provide reactive superhydrophobicity (Figure 1.13B).[109-113] Moreover, the available azalactone groups at the interfaces allow the further modification with amine containing small molecules to achieve durable superhydrophobicity. In 2009, sequential covalent reactions of PEI and dipentaerythritol penta-acrylate (5-Acl) emanated a durable chemically reactive coating.[114] Next, Beechler et al. in 2012 adapted this facile chemical approaches to prepare a porous and rough coating with residual acrylate groups. Such coating provides hydrophobicity after post-covalent modifications (Figure 1.14A-E).[115]

But on prolonged exposure of water, embedded superhydrophobiccity compromised through hydrolysis of residual acrylate groups. Parbat et al. exploited the covalent chemical interaction between branched poly ethylene imine (BPEI) and dipentaerythritol penta-acrylate (5-Acl) via 1,4-conjugate addition reaction to acquire a chemically reactive nanocomplex (CRNC).[116]

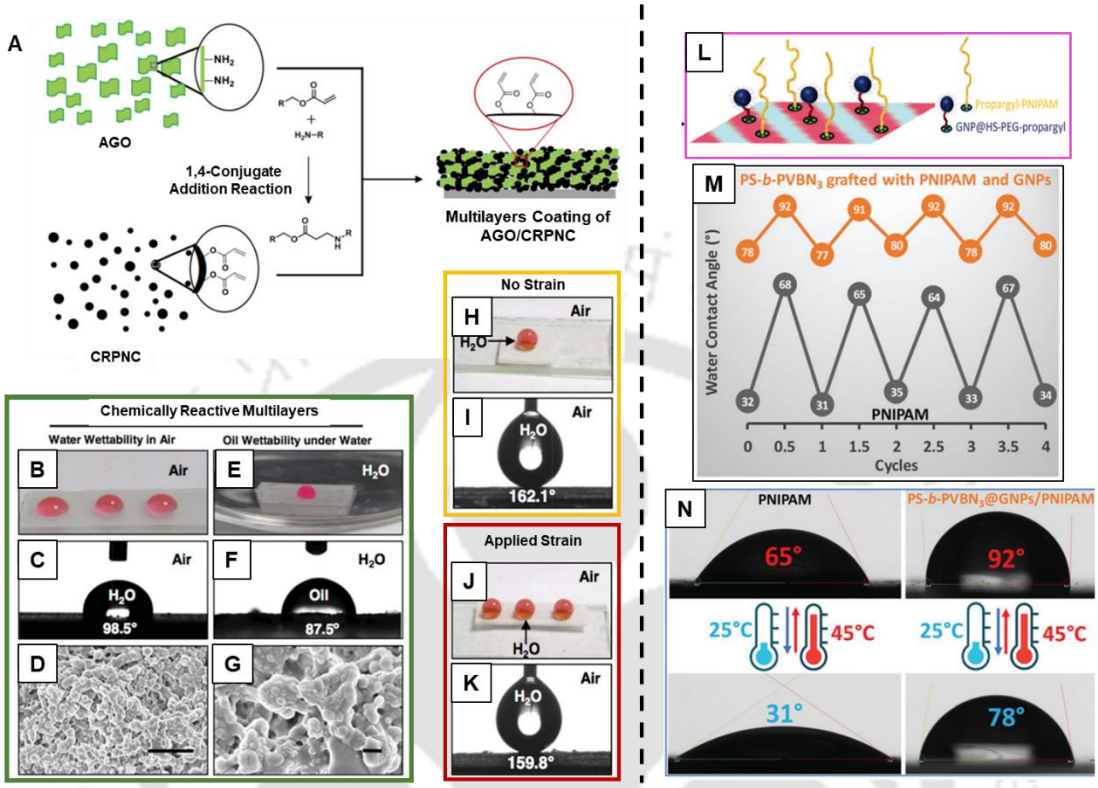

Figure 1.15. (A) Schematic presentation of the covalent integration and LBL (layer by layer) deposition of amine functionalized graphene oxide (A; AGO) and chemically reactive polymeric nano-complex (CRPNC, prepared by mixing branched polyethylenimine (BPEI) and penta-acrylate (5Acl) in methanol) through 1,4 conjugate addition reaction. (B-G) Digital (B, E) and contact angle (C, F) images of beaded water droplets (in air; B, C) and oil droplet (under water; E, F) on the multi-layered film without any chemical modification. FESEM images of multilayers film in low (D; scale: 5µm) and high (G; scale: 1µm) magnifications. (H-K) Digital (A, C, E) and contact angle (B, D, F) images of beaded water droplets (in air) before (H-I) and during (J-K) application of external tensile strain (100%) on the multilayers coatings. Figure is adapted from *J. Mater. Chem. A* **2018**, *6*, 15993-16002. Copyright 2018, The Royal society of Chemistry. (L) Dual grafting of PNIPAM and gold nanoparticles onto PVBN3 domains of a nanopatterned film of PS-b-PVBN3. (M-N) Reversible wettability behaviour of pure PNIPAM film (grey) and PS-b-PVBN3 film grafted with PNIPAM (orange), observed by the measurement of water contact angle at 25 and 45 °C. Reprinted with permission from *Nanoscale* **2020**, *12*, 7532-7537. Copyright 2020, The Royal society of Chemistry.

Further sequential layer-by-layer deposition of CRNC and BPEI resulted a porous multi-layered coating with residual chemical reactivity, that post-chemically functionalized with decylamine and glucamine to achieve various extremes of wettability (Figure 1.14F-R). Next, in 2018 Das et al. extended this idea of reactive multilayers using amine functionalized graphene oxide (AGO) nanosheets with CRNC by alternative dipping in the solutions of AGO and CRNC for 30 seconds each. This leads to the fabrication of hierarchically featured, highly flexible, rough coatings on various substrates, such as PDMS film, polyurethane fabric etc. as shown in Figure 1.15A-K.[117] Thereafter, spin coating of poly(pentafluorophenyl acrylate) and polystyrene has performed on silicon substrate followed by polystyrene removal through vapour induced phase separation method allowed to fabricate an amine

reactive micro/nano-featured coating.[118] In 2020, Loudy et al. developed an "azide" reactive theroresponsive thin film by the self-assembly of polystyrene-b-poly(vinyl benzyl azide), which has been further treated with propargaryl-capped-gold nanoparticles and ethynyl functionalized poly(N-isopropylacrylamide) by 1,3-dipolar cycloaddition reaction (Figure 1.15L-N).[119]

1.6. Approaches for Deriving Patterned Superhydrophobic Interfaces

Dessert beetles have contrast wettability patterns on their backs, and they use them to collect fog water by first nucleating the droplets on hydrophilic peaks until the droplet size reaches the critical point, then rolling them off over the waxy hydrophobic bumps.

Researchers have developed immense interest in nature inspired patterned interfaces with contrast wettability due to its potential applications in various research topics. In 2010, Takai et al. prepared superhydrophobic surfaces by chemical vapour deposition of a trimethoxysilane on glass or silicon substrates, followed by irradiation with UV light of wavelength 172 nm for 30 minutes in presence of a photomask to fabricate a superhydrophobic-superhydrophilic patterned interfaces. The reported average static water contact angles (WCA) on superhydrophobic surface was 155º and on superhydrophilic region, it was 0º respectively.[120] Next, in 2011, phase separation method was adopted by Mano and co-workers to fabricate a rough superhydrophobic polystyrene (PS) surface with WCA ~ 151º and then spatially selectively exposed the surface to UV and ozone to generate superhydrophilic patterns.[121-124] Han et al. and Zahner et al. implemented butyl methacrylate crosslinked with ethylene dimethacrylate to achieve a microporous superhydrophobic film. Further, an UV initiated photografting modification was adapted to achieve superhydrophilic patterns on superhydrophobic background. Later, poly(2-hydroxyethyl methacrylate-co-ethylene dimethacrylate) (HEMA-EDMA) was used for the fabrication of superhydrophilic thin polymer films by UV-initiated free radical reaction, its post-modification with 2,2,3,3,3-pentafluoropropyl methacrylate (PFPMA) through UV initiated photografting process allowed to generate superhydrophobic micropatterns.[125-129]

Next, Patton et al utilized thiol-yne chemistry in association with lithographic technique to fabricate hydrophilic–hydrophobic patterned interfaces. Photopolymerization of poly(propargyl methacrylate) brushes provided the yne reactivity at the interfaces which has further functionalized with thiols adequately.[130] In order to make superhydrophilic-superhydrophobic micropatterns, Feng et al. also demonstrated the utilisation of UV-induced sequential thiol-yne click chemistry, but following faster and initiator-free approach. A thin and porous polymeric coating of poly(2-hydroxyethyl methacrylate-co-ethylene dimethacrylate) (HEMA-EDMA) on a glass substrate has prepared followed by post chemical modification with 4-pentynoic acid to provide a reactive alkyne contained interface. Then the surface was functionalized with hydrophobic or hydrophilic thiols, depending on that surface became either superhydrophobic or superhydrophilic. Such as, 1H, 1H, 2H, 2H-perfluorodecanethiol in acetone was added to the reactive alkyne surface before being exposed to UV light through a photomask to finally generate a wettability pattern (Figure 1.16A-B).[131, 132]

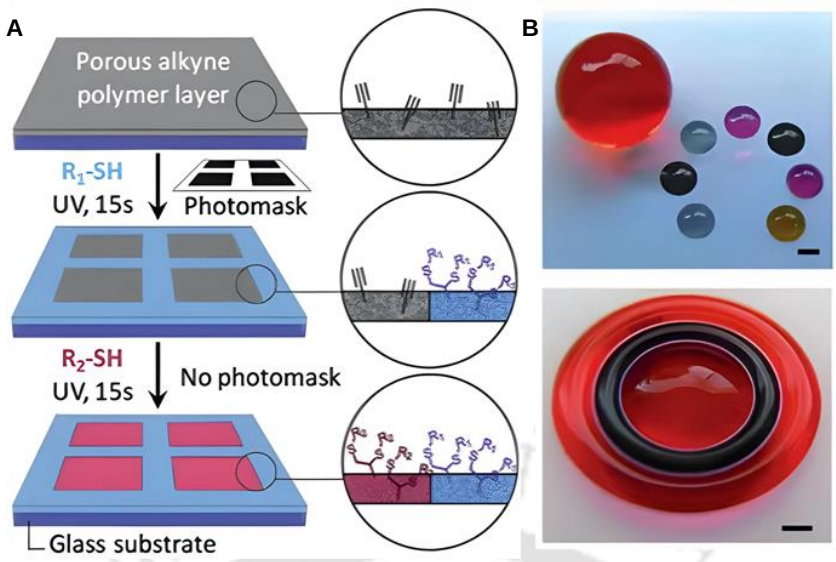

Figure 1.16. (A) Schematic representation of superhydrophobic–superhydrophilic micropatterns using thiol-yne reaction on alkyne-modified porous polymer substrate. (B) Optical images of wettability patterns filled with dye–water solutions; (scale bar = 100 µm). Reprinted with permission from *Adv. Mater. Interfaces* **2014**, *1*, 1400269. Copyright 2014, Wiley-VCH Verlag GmbH & Co. KGaA, Weinheim.

Later, vinyl reactive surface which further undergoes functionalization with either thiol or disulphide molecules via UV initiated thiol-ene reactions, was introduced first by Li et al. as shown in Figure 1.17.[133]

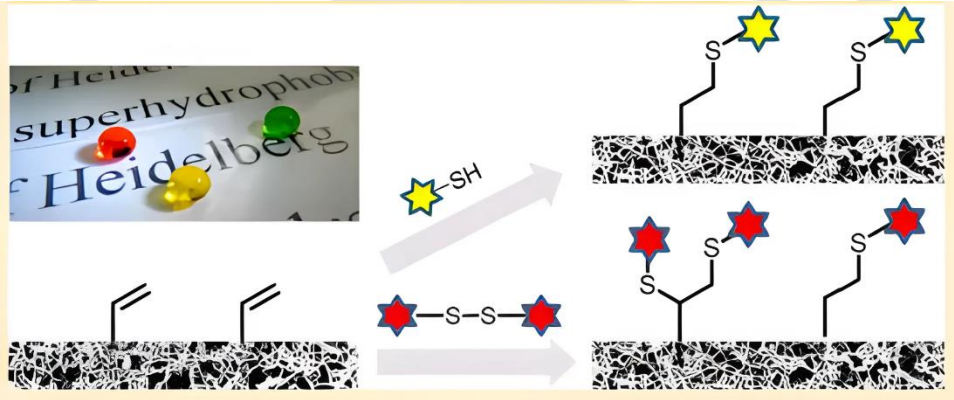

Figure 1.17. Digital image of beaded water droplets on PAINTS (Photoactive, inscribable, non-wettable, and transparent surface) prepared on glass substrate and schematic represents the vinyl reactive surface and thiol-ene reaction with the respective thiols and disulfides. Reprinted with permission from *Nano Lett.* **2015**, *15*, 675–681. Copyright 2014, American Chemical Society.

Photoactive, inscribable, non-wettable, and transparent surface (PAINTS) was first developed by condensation of trichlorovinylsilane on a glass substrate. However, there are no fluorinated functionalities at the surface, the PAINTS are superhydrophobic with static WCA of 166º.

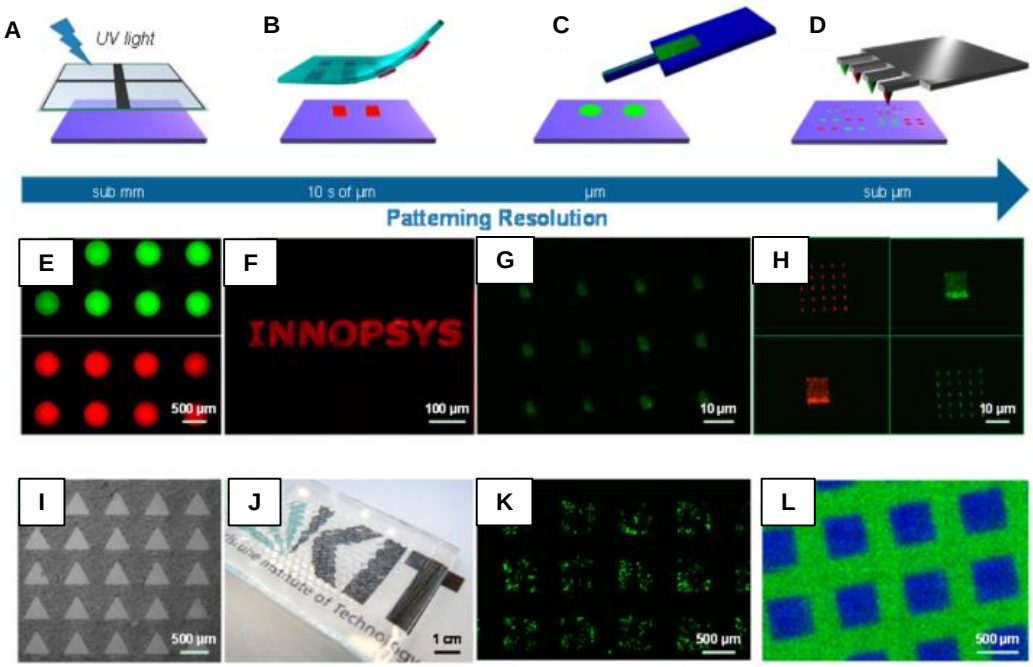

Figure 1.18. (A-D) Schematic illustration of several surface patterning techniques showing details from submillimeters to submicrometers (A) UV exposure using a photomask in combination with (B) microcontact printing, (C) microchannel cantilever spotting, and (D) dip pen nanolithography are the first two. (E) Fluorescence microscopic images of hydrophilic patterned array prepared on the PAINTS by photolithographic technique filled with fluorescein isothiocyanate (FITC) and rhodamine B. (F) Microcontact printing of rhodamine-SH pattern immobilized by UV radiation on the PAINTS. (G) Cantilever spotting of FITC-SH pattern on PAINTS, (H) Multiplexed dip pen lithographic pattern by rhodamine-SH and FITC-SH. (I-L) Superhydrophobic-hydrophilic pattern under water (I) microscopic images representing a visibility contrast due to the higher transpency of hydrophilic patterns. (J) Digital image showing an array of wettability patterned interfaces and (K) seeded HEK 293 cells after 24 hours, (L) A superhydrophobic–hydrophilic micropattern created by two successive photo click alterations, as seen in the ToF-SIMS chemical map. Reprinted with permission from *Nano Lett.* **2015**, *15*, 675–681. Copyright 2014, American Chemical Society.

In presence of a photomask, the disulfide-ene reaction was used to photopattern a superhydrophobic–hydrophilic micropattern. However, a highly hydrophilic micropattern was created on the superhydrophobic PAINTS after UV irradiation through a photomask on PAINTS coated with 3,3-dithiodipropionic acid solution (Figure 1.18). In a separate study, PAINTS was first modified with cysteamine through thiol-ene reaction to generate hydrophilic patterns where, photomask was used to achieve spatially selective modification. Non UV exposed regions were still vinyl reactive, therefore modified further with 1H,1H,2H,2H-perfluorodecanethiol to impart the superhydrophobicity on the remaining parts of the surface. Consequently, a well-defined superhydrophobic-hydrophilic patterned interfaces were prepared. Lee et al. have transformed superhydrophobic surfaces to hydrophilic by the polymerization of dopamine and fabricated patterned interfaces by partly exposing the superhydrophobic surfaces to the dopamine solution through micro-moulded capillaries.

Next, amine-reactive "ink" (i.e., D-glucamine) has used to print superhydrophilic designs on a layer of superhydrophobic polymer, Lynn and colleagues have demonstrated such quick and easy modification process. Superhydrophobic polymer prepared by LBL assembly of PEI (poly[ethyleneimine]) and

PVDMA (poly[2-vinyl-4,4-dimethylazlactone]), contains azalactone functionality at the surface which allows facile covalent modification with the modifiers having primary amine groups.[134]

1.7. Applications of Superhydrophobic and Patterned Interfaces

Various alternative fabrication techniques have been developed during the past 20 years to construct functional interfaces with antiwetting properties for their use in a variety of research area.

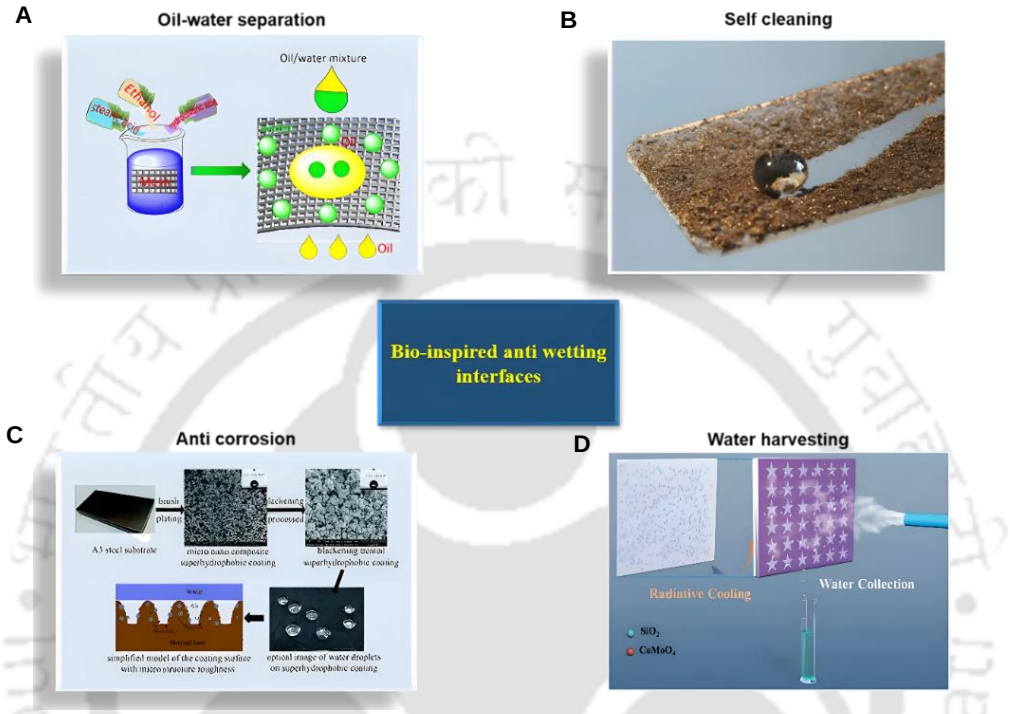

Figure 1.19. (A-D) Applications of bio-inspired anti wetting interfaces in variety of necessary aspects, i.e., oil-water separation (A), self-cleaning (B), anti-corrosion (C) and water harvesting (D) respectively. Figures are adapted from *J. Phys. Chem. A* **2016**, *120*, 5617–5623. Copyright 2016, American Chemical Society; *APPLIED OPTICS* **2011**, *9*, C257. Copyright 2011, Optical Society of America; *RSC Adv.* **2015**, *5*, 103000-103012; Copyright 2020, The Royal society of Chemistry; *Global Challenges* **2020**, *4*, 1900094. Copyright 2020, Wiley-VCH Verlag GmbH & Co. KGaA, Weinheim.

Many different applications at practically relevant scenarios, such as self-cleaning, oil/water separation, drug delivery, anti-corrosion, anti-biofouling, anti-icing, water harvesting, and so on have been demonstrated (Figure 1.19A-D) with a large number of water-repellent interfaces.[135-138] Self-cleaning coatings belong to a class of materials with the capacity to eliminate deposited or tainted dust and dirt on their own. Lotus leaves are a living example of something with this kind of self-cleaning ability because rolling water droplets collect any impurities that have been left on the surface and maintain it clean and dry. Lu et al., for instance, introduced an instant fabrication of an abrasion-tolerant superhydrophobic surface that can function in both oil and air to self-clean contaminated dust particles. Metals can benefit from the same anti-wetting property to shield them from the diverse and severe outside conditions.

One of the most important problems today that costs billions of dollars to fix annually is corrosion of metal. Due to its capacity to shield metal from the outside environments, anti-corrosion coating appears

as a promising approach. Recent studies have shown that treating surfaces with chromium is one of the most effective ways to create anti-corrosion coatings, but one cannot ignore the adverse effects of chromium on human health and the environment. Since anti-wetting surfaces can shield metals from watery environments, it was discovered that superhydrophobic surfaces might be another possibility for anticorrosion coating. Mg alloy surfaces with long-lasting superhydrophobicity were created synthetically by Jiang et al. to increase corrosion resistance. Extreme water repellence provides an alternative to fogging, particularly during the winter. Inconvenient in daily life and in many modern equipment, fogging is prevalent because it frequently happens in mirrors, glasses, and many other substrates. Fog droplets were spotted between the micropapillae of a lotus leaf, hence superhydrophobic surfaces are not the best choice for an antifogging coating. However, using a soft lithography approach and low-surface-energy fluoroalkylsilane post modification, an artificial compound superhydrophobic interface has been developed to achieve with antifogging capabilities. The anti-wetting interfaces inherently absorb oily phases while selectively repelling water, this characteristic is very helpful in the selective separation of oil from oil/water interfaces. Due to the recent increase in industrial oily wastewater discharge into open water resources like rivers and seashores, which will impact the aquatic ecology, and the frequency of oil spill accidents, the separation of oil/water mixtures has become one of the biggest issues in the world. For instance, one of the most severe pollution incidents in recent decades was the oil spill in the Gulf of Mexico. Since surfaces that are superhydrophobic selectively absorb oils while extremely repelling aqueous media. The separation of oil from water using filtration and selective absorption was made possible by the proper coupling of this superhydrophobicity with fibrous or spongy substrates or metal mesh. Insufficient access to drinking water affects around four billion people worldwide. Without the need for a desorption procedure, the right combination of wetting and anti-wetting surfaces can also be used to collect fog from atmospheres. In order to gather artificial water without desorption, a number of patterned superhydrophobic/superhydrophilic interfaces were developed.[139-141]

Moreover, such patterned interfaces remain promising for various bio-relevant applications. Fréchet and colleagues photopatterned a superhydrophilic channel in a superhydrophobic, porous polymer layer.[142] Next, by photocrosslinking prepolymeric solutions in the hydrophilic stripes, Hancock et al. created gradients of solutes, cells, and microspheres enclosed in 3D hydrogels using the hydrophilic-hydrophobic patterns (Figure 1.20).[120] Further, such patterned interfaces have been extended to modulate in cell adhesion and morphology, as well as formation of ECM (extracellular matrix). After seeding of mouse embryonic fibroblast (3T3) cells spontaneously identified and moved toward the superhydrophilic areas, where they quickly adhered and expanded to confluence after 24 hours. On rough versus smooth hydrophobic and hydrophilic interface, Mano and colleagues investigated cell adhesion and proliferation. SaOs-2, a kind of human primary osteosarcoma cell, adhered better to

smooth hydrophilic and rough superhydrophilic PS (polystyrene) surfaces than to smooth hydrophobic or rough superhydrophobic PS surfaces, even after 6 days of growth.

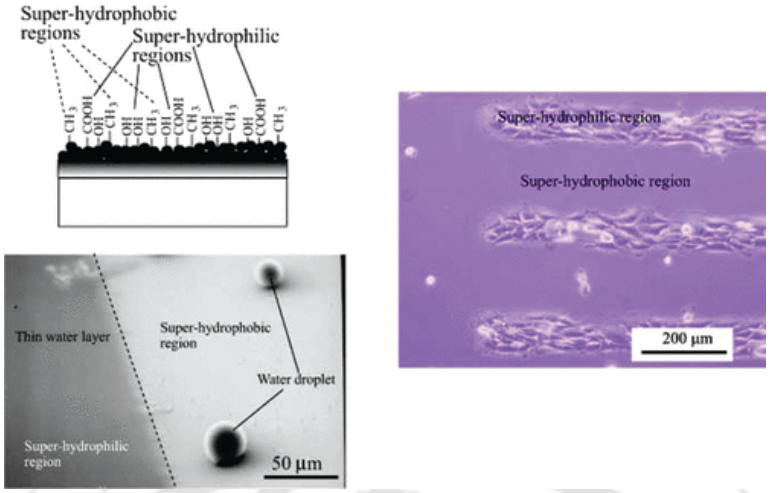

Figure 1.20. Diagram representing fabrication process for the micropatterned superhydrophobic/superhydrophilic surface. After being cultivated for 24 hours, phase-contrast microscopic images of cell adhesion behaviours on the micropatterned surface were shown. Reprinted with permission from *Langmuir* **2010**, *26*, 8147–8154. Copyright 2010, American Chemical Society.

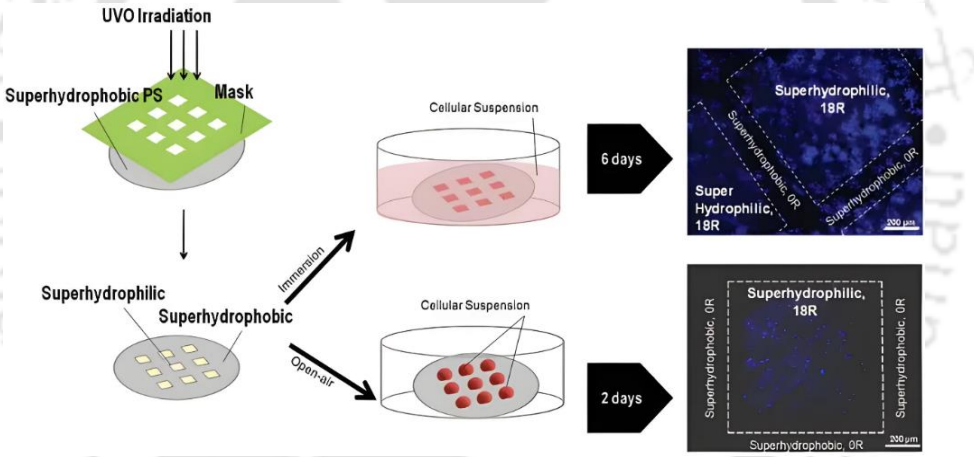

Figure 1.21. Schematic representation of the patterning of superhydrophilic patches on superhydrophobic PS surfaces by UVO (ultraviolet-oxygen) irradiation and employing a hollowed mask; the two cell seedings were performed by immersion and in the open air. SaOs-2 cell nuclei were stained fluorescently with 4′,6-diamidino-2-phenylindole (DAPI) after six days of growth on samples where cells were sown evenly across the surface. Reprinted with permission from *Soft Matter* **2011**, *7*, 8932–8941. Copyright 2011, The Royal Society of Chemistry.

Mano and colleagues grew the cells inside the isolated droplets of cell suspension after depositing the droplets in hydrophilic patterns over a superhydrophobic, rough PS substrate as shown in Figure 1.21.[143] Square superhydrophilic regions confined the aqueous solutions kept into it due to the higher difference in surface tension with the superhydrophobic background. An array of cell solution was manually distributed onto each hydrophilic spot, and the hydrophilic spots were subsequently cultured for 4 hours after being individually coated with various amounts of human serum albumin and human plasma fibronectin. Vermant and colleagues assembled micrometer-sized, sulfate-modified PS particles (2.9 m diameter, 9.7 C cm^2 surface charge density) from an oil-water interface onto a hydrophobic silicon

substrate patterned with hydrophilic patches using the Langmuir-Blodgett deposition method.[144] During such deposition, decane-water was used as the fluid-fluid interface to enhance colloidal dipolar repulsion and create a highly ordered and stable monolayer at the interface, resulting in planar colloidal clusters on the hydrophilic regions where the cluster size depended on the pattern size. Further, Song et al. used hydrophilic-hydrophobic patterned interfaces to generate three dimensional microfeatures. By adjusting the surface energy difference at the boundary between hydrophilic and hydrophobic regions as well as the solution's characteristics, they were able to control the pinning of a droplet containing nanoparticles at the three-phase contact line (TCL) and encouraged asymmetric dewetting to change the droplet's morphology as shown in Figure 1.22.[145]

Jiang and colleagues integrated wettability and shape gradients for more effective water collection compared to straightforward circle-shaped wettability patterns or uniform superhydrophilic or

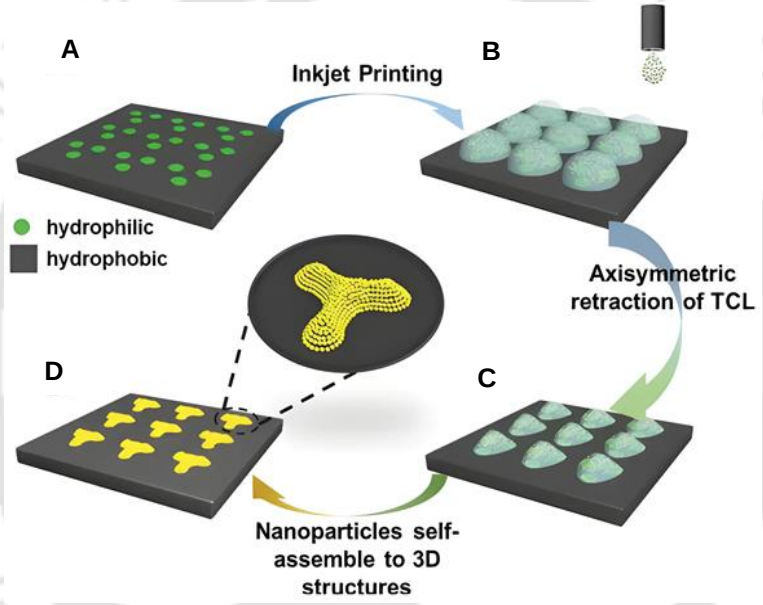

Figure 1.22. Diagram shows three-dimensional microcolloidal crystal formations. (A) The substrate is a hydrophobic silicon wafer with designed hydrophilic pinning areas (green). (B) At predetermined areas, a variety of droplets containing nanoparticles are dispensed via inkjet printing. (C) Hydrophilic pattern-induced asymmetric dewetting results in an array of triangular droplets. (D) It is possible to create arrayed 3D microcolloidal crystals with customizable shape. Reprinted with permission from *Adv. Funct. Mater*. **2015**, *25*, 2237. Copyright 2015, WILEY-VCH Verlag GmbH & Co. KGaA, Weinheim.

superhydrophobic surfaces. Star-shaped wettability patterns were developed to combine surface energy gradients and Laplace pressure gradients in order to swiftly move minute water droplets into more wettable regions as shown in Figure 1.23.[146]

Active research is being done on surfaces that have extreme variances in wettability. Although numerous methods for creating patterned surfaces have already been created, there is still room to enhance their durability, stability, and simplicity in fabrication and modification. However, the development of new and useful applications for patterned surfaces is currently ongoing.

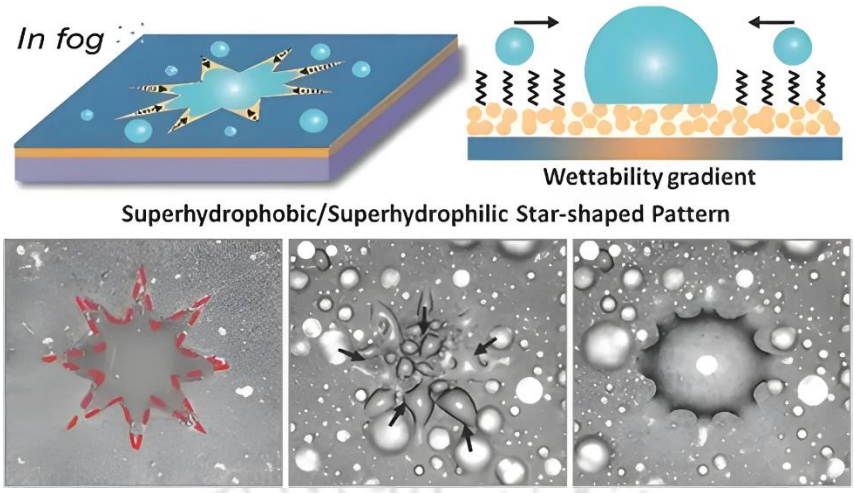

Figure 1.23. Star shaped hydrophilic pattern was prepared by UV light illumination on the heptadecafluorodecyltrimethoxysilane (FAS) modified film through a photomask, creating a bioinspired gradient surface with a star-shaped wettability pattern. The more wettable star-shaped area is where the fog droplets are directionally collected. Reprinted with permission from *Adv. Mater.* **2014**, *26*, 5025. Copyright 2014, WILEY-VCH Verlag GmbH & Co. KGaA, Weinheim.

1.8. Objectives and Motivations

In the last two decades, numerous techniques for creating artificial superhydrophobic interfaces have been reported in the literature, and the most of them involve the use expensive chemicals, sophisticated

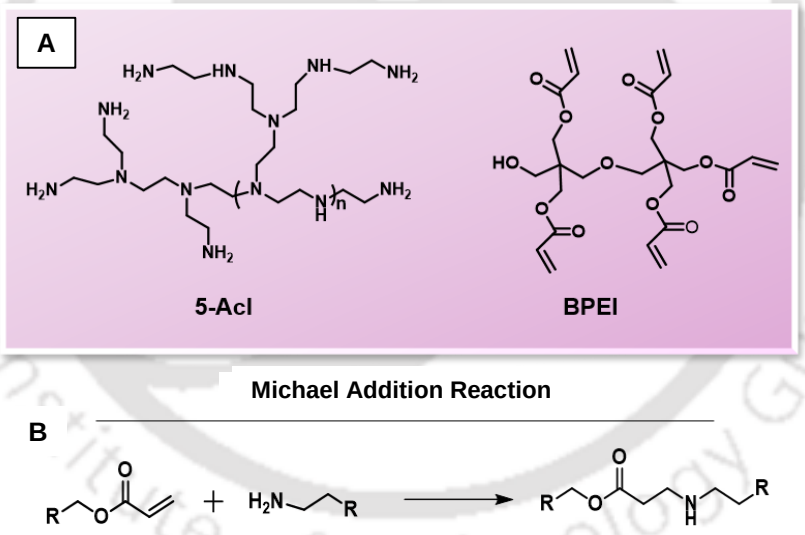

Figure 1.24. (A) Chemical structures of the reactants used for the 1,4-conjugate addition reaction, i.e., BPEI and 5-Acl and (B) Michael addition reaction showing the covalent chemical interaction between acrylate and amine functionalities.

instrumentation, or laborious synthetic processes. A significant obstacle still exists in the synthesis of extremely abrasion-tolerant superhydrophobic coatings that can function in a variety of harsh environments. Several techniques, such as electro spinning deposition, "click-type" ring opening reaction based multilayer coatings, and candle shoot template process are introduced to optimise crucial chemistry and topography both on top and inside the coating and further those synthesised bulk biomimicked coatings were successfully extended for revalidating the inherent tolerance of such designs towards severe physical challenges. Our research team recently introduced a simple Michael

addition reaction between BPEI and 5-Acl for developing bulk superhydrophobic coatings (Figure 1.24).[147]

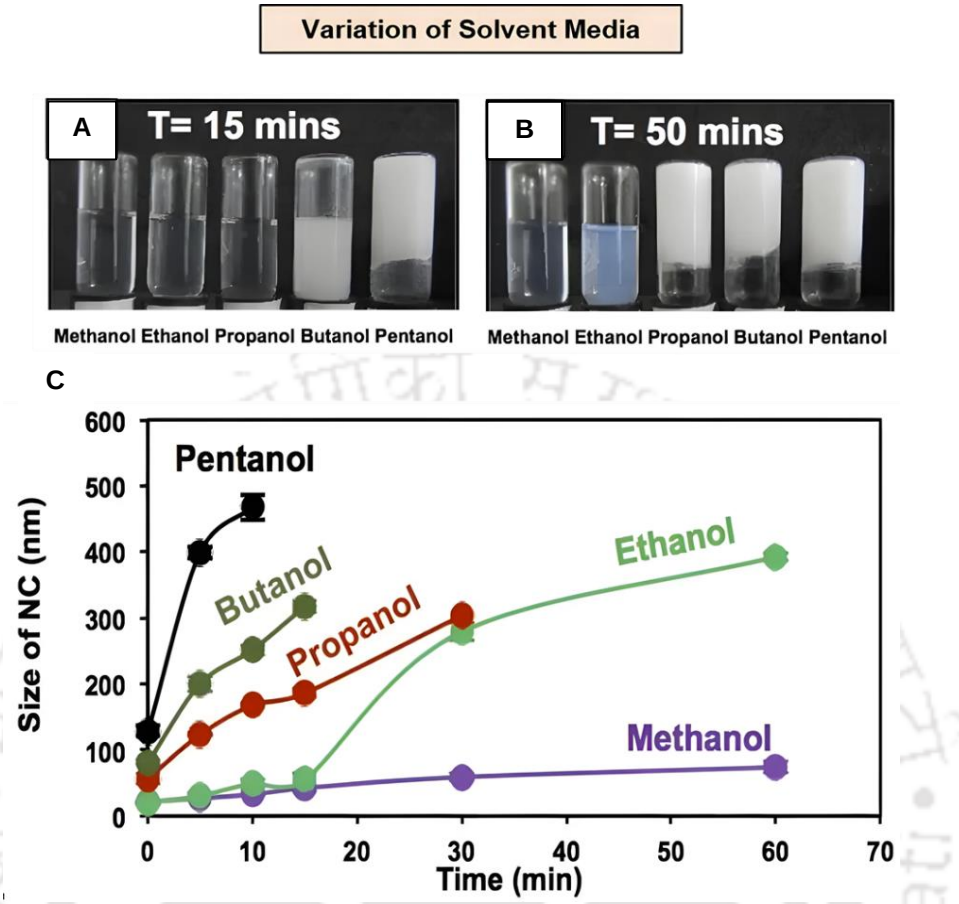

Figure 1.25. (A-B) Digital images of the reaction medium optimization of the acrylate reactive nanocomplex formation at different time intervals. (C) Graphical representation of DLS data which shows the size of nanocomplexes at various higher analogues of methanol. Reprinted with permission from *Green Chem.* **2017**, *19*, 4527-4532. Copyright 2017, The Royal Society of Chemistry.

One of our former lab-mate has developed superhydrophobic monoliths with tailored physical properties—just by changing the reaction medium (alkyl alcohol) for selected reactants. The higher analogues of ethanol led to accelerated sol-gel conversation through formation of chemically reactive polymeric nanocomplex in the reaction mixture (Figure 1.25).[148] Motivated by this investigation, I have developed a primary amine reactive and covalently cross-linked polymeric coating that attempts to rationally address relevant issues connected to biomimetic artificial superhydrophobic coatings. It was convenient to coat a wide variety of substrates using this one-step, in-situ deposition method, including flexible, fibrous, rigid, planar, and geometrically complicated objects with a chemically reactive porous polymeric surface. As a result of the remaining chemical reactivity in the polymeric dip-coating, I have adapted chemically controlled interfacial properties by selecting appropriate chemistry. Further, such polymeric coating approach is used to achieve durable and substrate independent superhydrophobic coating, extremely water repellent conductive pattern interface and abrasion tolerant patterned interfaces of two distinct wettability and fluorescent molecules for anticounterfeiting applications.

1.9. References

1) Parvate, S.; Dixit, P.; Chattopadhyay, S. Superhydrophobic surfaces: insights from theory and experiment. *The Journal of Physical Chemistry B* **2020**, *124*, 1323-1360.
2) Adamson, A. W.; Gast, A. P. Physical chemistry of surfaces. *John willey and sons Inc. New York.* **1990.**
3) Shibuichi, S.; Onda, T.; Satoh, N.; Tsujii, K. Super water-repellent surfaces resulting from fractal structure. *The Journal of Physical Chemistry* **1996**, *100*, 19512-19517.
4) Parkin, I. P.; Palgrave, R. G. Self-cleaning coatings. *Journal of materials chemistry* **2005**, *15*, 1689-1695.
5) Sun, T.; Feng, L.; Gao, X.; Jiang, L. Bioinspired surfaces with special wettability. *Accounts of chemical research* **2005**, *38*, 644-652.
6) De Coninck, J.; de Ruijter, M. J.; Voué, M. Dynamics of wetting. *Current opinion in colloid & interface science* **2001**, *6*, 49-53.
7) Onda, T.; Shibuichi, S.; Satoh, N.; Tsujii, K. Super-water-repellent fractal surfaces. *Langmuir* **1996**, *12*, 2125-2127.
8) Das, S.; Kumar, S.; Samal, S. K.; Mohanty, S.; Nayak, S. K. A Review on Superhydrophobic Polymer Nanocoatings: Recent Development and Applications. *Ind. Eng. Chem. Res.* **2018**, *57*, 2727−2745.
9) Barthlott, W.; Neinhuis, C. Purity of the sacred lotus, or escape from contamination in biological surfaces. *Planta* **1997**, *202*, 1-8.
10) Lafuma, A.; Quéré, D. Superhydrophobic states. *Nature materials* **2003**, *2*, 457-460.
11) Blossey, R. Self-cleaning surfaces—virtual realities. *Nature materials* **2003**, *2*, 301-306.
12) Fürstner, R.; Barthlott, W.; Neinhuis, C.; Walzel, P. Wetting and self-cleaning properties of artificial superhydrophobic surfaces. *Langmuir* **2005**, *21*, 956-961.
13) Miwa, M.; Nakajima, A.; Fujishima, A.; Hashimoto, K.; Watanabe, T. Effects of the surface roughness on sliding angles of water droplets on superhydrophobic surfaces. *Langmuir* **2000**, *16*, 5754-5760.
14) Nakajima, A.; Hashimoto, K.; Watanabe, T.; Takai, K.; Yamauchi, G.; Fujishima, A. Transparent superhydrophobic thin films with self-cleaning properties. *Langmuir* **2000**, *16*, 7044-7047.
15) Otten, A.; Herminghaus, S. How plants keep dry: a physicist's point of view. *Langmuir* **2004**, *20*, 2405-2408.
16) Scardino, A.; De Nys, R.; Ison, O.; O'Connor, W.; Steinberg, P. Microtopography and antifouling properties of the shell surface of the bivalve molluscs Mytilus galloprovincialis and Pinctada imbricata. *Biofouling* **2003**, *19*, 221-230.
17) Schultz, M. P.; Kavanagh, C. J.; Swain, G. W. Hydrodynamic forces on barnacles: Implications on detachment from fouling-release surfaces. *Biofouling* **1999**, *13*, 323-335.

18) Saito, H.; Takai, K. I.; Takazawa, H.; Yamauchi, G. A study on snow sticking weight to water-repellent coatings. *Journal of the Society of Materials Science, Japan* **1997**, *46*, 216-219.

19) Kako, T.; Nakajima, A.; Irie, H.; Kato, Z.; Uematsu, K.; Watanabe, T.; Hashimoto, K. Adhesion and sliding of wet snow on a super-hydrophobic surface with hydrophilic channels. *Journal of Materials Science* **2004**, *39*, 547-555.

20) Quéré, D. Non-sticking drops. *Reports on Progress in Physics* **2005**, *68*, 2495.

21) Han, X.; Guo, Z. Graphene and its derivative composite materials with special wettability: Potential application in oil-water separation. *Carbon* **2021**, *172*, 647-681.

22) Wang, Y.; Guo, Z.; Liu, W. Adhesion behaviors on four special wettable surfaces: natural sources, mechanisms, fabrications and applications. *Soft Matter* **2021**, *17*, 4895-4928.

23) Qiu, L.; Zhang, J.; Guo, Z.; Liu, W. Asymmetric superwetting stainless steel meshes for on-demand and highly effective oil-water emulsion separation. *Separation and Purification Technology* **2021**, *273*, 118994.

24) v Zielecka, M.; Bujnowska, E. Silicone-containing polymer matrices as protective coatings: Properties and applications. *Progress in Organic Coatings* **2006**, *55*, 160-167.

25) Koch, K.; Bhushan, B.; Barthlott, W. Multifunctional surface structures of plants: an inspiration for biomimetics. *Progress in Materials science* **2009**, *54*, 137-178.

26) Gao, X.; Jiang, L. Water-repellent legs of water striders. *nature* **2004**, *432*, 36-36.

27) Li, S.; Huang, J.; Chen, Z.; Chen, G.; Lai, Y. A review on special wettability textiles: theoretical models, fabrication technologies and multifunctional applications. *Journal of Materials Chemistry A* **2017**, *5*, 31-55.

28) Feng, X. J.; Jiang, L. Design and creation of superwetting/antiwetting surfaces. *Advanced Materials* **2006**, *18*, 3063-3078.

29) Yan, Y. Y.; Gao, N.; Barthlott, W. Mimicking natural superhydrophobic surfaces and grasping the wetting process: A review on recent progress in preparing superhydrophobic surfaces. *Advances in colloid and interface science* **2011**, *169*, 80-105.

30) Wang, S.; Liu, K.; Yao, X.; Jiang, L. Bioinspired surfaces with superwettability: new insight on theory, design, and applications. *Chemical reviews* **2015**, *115*, 8230-8293.

31) Liu, M.; Wang, S.; Jiang, L. Nature-inspired superwettability systems. *Nature Reviews Materials* **2017**, *2*, 1-17.

32) Si, Y.; Dong, Z.; Jiang, L. Bioinspired designs of superhydrophobic and superhydrophilic materials. *ACS Central Science* **2018**, *4*, 1102-1112.

33) Archer, R. J.; Becher-Nienhaus, B.; Dunderdale, G. J.; Hozumi, A. Recent progress and future directions of multifunctional (super) wetting smooth/structured surfaces and coatings. *Advanced Functional Materials* **2020**, *30*, 1907772.

34) Sun, Y.; Guo, Z. Recent advances of bioinspired functional materials with specific wettability: from nature and beyond nature. *Nanoscale Horizons* **2019**, *4*, 52-76.

35) Wen, L.; Tian, Y.; Jiang, L. Bioinspired super-wettability from fundamental research to practical applications. *Angewandte Chemie International Edition* **2015**, *54*, 3387-3399.

36) Howell, C.; Grinthal, A.; Sunny, S.; Aizenberg, M.; Aizenberg, J. Designing liquid-infused surfaces for medical applications: a review. *Advanced materials* **2018**, *30*, 1802724.

37) Li, X. M.; Reinhoudt, D.; Crego-Calama, M. What do we need for a superhydrophobic surface? A review on the recent progress in the preparation of superhydrophobic surfaces. *Chemical Society Reviews* **2007**, *36*, 1350-1368.

38) (a) Liu, M.; Zheng, Y.; Zhai, J.; Jiang, L. Bioinspired super-antiwetting interfaces with special liquid−solid adhesion. *Accounts of chemical research* **2010**, *43*, 368-377. (b) Liu, M.; Jiang, L. Switchable adhesion on liquid/solid interfaces. *Advanced Functional Materials* **2010**, *20*, 3753-3764. (c) Liu, K.; Jiang, L. Bio-inspired design of multiscale structures for function integration. *Nano Today* **2011**, *6*, 155-175. (d) Zhang, Y. L.; Xia, H.; Kim, E.; Sun, H. B. Recent developments in superhydrophobic surfaces with unique structural and functional properties. *Soft Matter* **2012**, *8*, 11217-11231. (e) Song, W., Mano, J. F. Interactions between cells or proteins and surfaces exhibiting extreme wettabilities. *Soft Matter* **2013**, *9*, 2985-2999. (f) Sun, T.; Qing, G.; Su, B.; Jiang, L. Functional biointerface materials inspired from nature. *Chemical Society Reviews* **2011**, *40*, 2909-2921.

39) (a) Feng, X. Q.; Gao, X.; Wu, Z.; Jiang, L.; Zheng, Q. S. Superior water repellency of water strider legs with hierarchical structures: experiments and analysis. *Langmuir* **2007**, *23*, 4892-4896. (b) Wei, P. J.; Chen, S. C.; Lin, J. F. Adhesion forces and contact angles of water strider legs. *Langmuir* **2009**, *25*, 1526-1528.

40) Guo, Z.; Liu, W. Biomimic from the superhydrophobic plant leaves in nature: Binary structure and unitary structure. *Plant Science* **2007**, *172*, 1103-1112.

41) Barthlott, W.; Neinhuis, C. Purity of the sacred lotus, or escape from contamination in biological surfaces. *Planta* **1997**, *202*, 1-8.

42) Feng, L.; Li, S.; Li, Y.; Li, H.; Zhang, L.; Zhai, J.; Zhu, D. Super-hydrophobic surfaces: from natural to artificial. *Advanced materials* **2002**, *14*, 1857-1860.

43) (a) Autumn, K.; Liang, Y. A.; Hsieh, S. T.; Zesch, W.; Chan, W. P.; Kenny, T. W.; Full, R. J. Adhesive force of a single gecko foot-hair. *Nature* **2000**, *405*, 681-685. (b) Liu, K., Du, J., Wu, J., & Jiang, L. Superhydrophobic gecko feet with high adhesive forces towards water and their bio-inspired materials. *Nanoscale* **2012**, *4*, 768-772.

44) Autumn, K.; Sitti, M.; Liang, Y. A.; Peattie, A. M.; Hansen, W. R.; Sponberg, S.; Full, R. J. Evidence for van der Waals adhesion in gecko setae. *Proceedings of the National Academy of Sciences* **2002**, *99*, 12252-12256.

45) (a) Feng, L.; Zhang, Y.; Xi, J.; Zhu, Y.; Wang, N.; Xia, F.; Jiang, L. Petal effect: a superhydrophobic state with high adhesive force. *Langmuir* **2008**, *24*, 4114-4119. (b) Bhushan, B.; Nosonovsky, M.

The rose petal effect and the modes of superhydrophobicity. *Philosophical Transactions of the Royal Society A: Mathematical, Physical and Engineering Sciences* **2010**, *368*, 4713-4728.

46) Wenzel, R. N. Resistance of solid surfaces to wetting by water. *Industrial & Engineering Chemistry* **1936**, *28*, 988-994.

47) Cassie, A. B. D.; Baxter, S. Wettability of porous surfaces. *Transactions of the Faraday society* **1944**, *40*, 546-551.

48) Young, T. An essay on the cohesion of fluids. *Philosophical transactions of the royal society of London* **1805**, *95*, 65-87.

49) Shome, A.; Das, A.; Borbora, A.; Dhar, M.; Manna, U. Role of chemistry in bio-inspired liquid wettability. *Chemical Society Reviews*. **2022**, *51*, 5452-5497.

50) Drake, S.; Wisan, W. L. Cause, Experiment, and Science: A Galilean Dialogue Incorporating a New English Translation of Galileo's" Bodies That Stay Atop Water, or Move in It." **1984**.

51) Good, R. J. Contact angle, wetting, and adhesion: a critical review. *Journal of adhesion science and technology* **1992**, *6*, 1269-1302.

52) Young, T. An essay on the cohesion of fluids. *Philosophical transactions of the royal society of London* **1805**, *95*, 65-87.

53) Das, S.; Kumar, S.; Samal, S. K.; Mohanty, S.; Nayak, S. K. A Review on Superhydrophobic Polymer Nanocoatings: Recent Development and Applications. *Ind. Eng. Chem. Res.* **2018**, *57*, 2727−2745.

54) Furmidge, C. G. L. Studies at phase interfaces. I. The sliding of liquid drops on solid surfaces and a theory for spray retention. *Journal of colloid science* **1962**, *17*, 309-324.

55) Cassie, A. B. D. Contact angles. *Discussions of the Faraday society* **1948**, *3*, 11-16.

56) McHale, G.; Shirtcliffe, N. J.; Newton, M. I. Contact-Angle Hysteresis on Super-Hydrophobic Surfaces. *Langmuir* **2004**, *20*, 10146−10149.

57) Queré, D.; Azzopardi, M. J.; Delattre, L. Drops at Rest on a´ Tilted Plane. *Langmuir* **1998**, *14*, 2213−2216.

58) Wenzel, R. N. Resistance of Solid Surfaces to Wetting by Water. *Ind. Eng. Chem.* **1936**, *28*, 988−994.

59) Cassie, A. B. D.; Baxter, S. Wettability of Porous Surfaces. *Trans. Faraday Soc.* **1944**, *40*, 546−551.

60) Plawsky, J. L.; Ojha, M.; Chatterjee, A.; Wayner, P. C. Review of the Effects of Surface Topography, Surface Chemistry, and Fluid Physics on Evaporation at the Contact Line. *Chem. Eng. Commun.* **2008**, *196*, 658−696.

61) Ennaceri, H.; Wang, L.; Erfurt, D.; Riedel, W.; Mangalgiri, G.; Khaldoun, A.; El Kenz, A.; Benyoussef, A.; Ennaoui, A. WaterResistant Surfaces Using Zinc Oxide Structured Nanorod Arrays with Switchable Wetting Property. *Surf. Coat. Technol.* **2016**, *299*, 169− 176.

62) Wang, B.; Zhang, Y.; Shi, L.; Li, J.; Guo, Z. Advances in the Theory of Superhydrophobic Surfaces. *J. Mater. Chem.* **2012**, *22*, 20112−20127.

63) Ishino, C.; Okumura, K. Wetting Transitions on Textured Hydrophilic Surfaces. *Eur. Phys. J. E: Soft Matter Biol. Phys.* **2008**, *25*, 415−424.

64) Bico, J.; Thiele, U.; Quéré, D. Wetting of textured surfaces. *Colloids and Surfaces A: Physicochemical and Engineering Aspects* **2002**, *206*, 41-46.

65) Chu, Z.; Seeger, S. Superamphiphobic surfaces. *Chemical Society Reviews* **2014**, *43*, 2784-2798.

66) Ghasemlou, M.; Daver, F.; Ivanova, E. P.; Adhikari, B. Bio-inspired sustainable and durable superhydrophobic materials: from nature to market. *Journal of Materials Chemistry A* **2019**, *7*, 16643-16670.

67) Jiang, W.; Mao, M.; Qiu, W.; Zhu, Y.; Liang, B. Biomimetic superhydrophobic engineering metal surface with hierarchical structure and tunable adhesion: design of microscale pattern. *Industrial & Engineering Chemistry Research* **2017**, *56*, 907-919.

68) Feng, L.; Zhang, Y.; Xi, J.; Zhu, Y.; Wang, N.; Xia, F.; Jiang, L. Petal effect: a superhydrophobic state with high adhesive force. *Langmuir* **2008**, *24*, 4114-4119.

69) Kostal, E.; Stroj, S.; Kasemann, S.; Matylitsky, V.; Domke, M. Fabrication of biomimetic fog-collecting superhydrophilic–superhydrophobic surface micropatterns using femtosecond lasers. *Langmuir* **2018**, *34*, 2933-2941.

70) Parker, A. R.; Lawrence, C. R. Water capture by a desert beetle. *Nature* **2001**, *414*, 33-34.

71) Li, J.; Ueda, E.; Paulssen, D.; Levkin, P. A. Slippery lubricant-infused surfaces: properties and emerging applications. *Advanced Functional Materials* **2019**, *29*, 1802317.

72) Buck, M. E.; Schwartz, S. C.; Lynn, D. M. Superhydrophobic thin films fabricated by reactive layer-by-layer assembly of azlactone-functionalized polymers. *Chemistry of Materials* **2010**, *22*, 6319-6327.

73) Tian, X.; Verho, T.; Ras, R. H. Moving superhydrophobic surfaces toward real-world applications. *Science* **2016**, *352*, 142-143.

74) Li, Z.; Guo, Z. Bioinspired surfaces with wettability for antifouling application. *Nanoscale* **2019**, *11*, 22636-22663.

75) Ueda, E.; Levkin, P. A. Emerging applications of superhydrophilic-superhydrophobic micropatterns. *Advanced Materials* **2013**, *25*, 1234-1247.

76) Yong, J.; Chen, F.; Yang, Q.; Huo, J.; Hou, X. Superoleophobic surfaces. *Chemical Society Reviews* **2017**, *46*, 4168-4217.

77) Zhang, S.; Huang, J.; Chen, Z.; Yang, S.; Lai, Y. Liquid mobility on superwettable surfaces for applications in energy and the environment. *Journal of Materials Chemistry A* **2019**, *7*, 38-63.

78) Chu, Z.; Feng, Y.; Seeger, S. Oil/water separation with selective superantiwetting/superwetting surface materials. *Angewandte Chemie International Edition* **2015**, *54*, 2328-2338.

79) Cheng, Z.; Zhang, D.; Lv, T.; Lai, H.; Zhang, E.; Kang, H.; Jiang, L. Superhydrophobic shape memory polymer arrays with switchable isotropic/anisotropic wetting. *Advanced Functional Materials* **2018**, *28*, 1705002.

80) Yohe, S. T.; Colson, Y. L.; Grinstaff, M. W. Superhydrophobic materials for tunable drug release: using displacement of air to control delivery rates. *Journal of the American Chemical Society* **2012**, *134*, 2016-2019.

81) Yohe, S. T.; Freedman, J. D.; Falde, E. J.; Colson, Y. L.; Grinstaff, M. W. A mechanistic study of wetting superhydrophobic porous 3D meshes. *Advanced functional materials* **2013**, *23*, 3628-3637.

82) Kratochvil, M. J.; Manna, U.; Lynn, D. M. Superhydrophobic polymer multilayers for the filtration- and absorption-based separation of oil/water mixtures. *Journal of Polymer Science Part A: Polymer Chemistry* **2017**, *55*, 3127-3136.

83) Crick, C. R.; Gibbins, J. A.; Parkin, I. P. Superhydrophobic polymer-coated copper-mesh; membranes for highly efficient oil–water separation. *Journal of Materials Chemistry A* **2013**, *1*, 5943-5948.

84) Zhou, X.; Zhang, Z.; Xu, X.; Guo, F.; Zhu, X.; Men, X.; Ge, B. Robust and durable superhydrophobic cotton fabrics for oil/water separation. *ACS applied materials & interfaces* **2013**, *5*, 7208-7214.

85) Wang, Z.; Wang, Y.; Liu, G. Rapid and efficient separation of oil from oil-in-water emulsions using a Janus cotton fabric. *Angewandte Chemie* **2016**, *128*, 1313-1316.

86) Wang, B.; Guo, Z. pH-responsive bidirectional oil–water separation material. *Chemical Communications* **2013**, *49*, 9416-9418.

87) Osicka, J.; Ilcikova, M.; Popelka, A.; Filip, J.; Bertok, T.; Tkac, J.; Kasak, P. Simple, reversible, and fast modulation in superwettability, gradient, and adsorption by counterion exchange on self-assembled monolayer. *Langmuir* **2016**, *32*, 5491-5499.

88) Han, Z.; Li, B.; Mu, Z.; Niu, S.; Zhang, J.; Ren, L. Energy-efficient oil–water separation of biomimetic copper membrane with multiscale hierarchical dendritic structures. *Small* **2017**, *13*, 1701121.

89) Zhou, C.; Chen, Z.; Yang, H.; Hou, K.; Zeng, X.; Zheng, Y.; Cheng, J. Nature-inspired strategy toward superhydrophobic fabrics for versatile oil/water separation. *ACS applied materials & interfaces* **2017**, *9*, 9184-9194.

90) Kwak, G.; Lee, M.; Yong, K. Chemically modified superhydrophobic WO x nanowire arrays and UV photopatterning. *Langmuir* **2010**, *26*, 9964-9967.

91) Uosaki, K.; Quayum, M. E.; Nihonyanagi, S.; Kondo, T. Decomposition Processes of an Organic Monolayer Formed on Si (111) via a Silicon Carbon Bond Induced by Exposure to UV Irradiation or Ozone. *Langmuir* **2004**, *20*, 1207-1212.

92) Verho, T.; Bower, C.; Andrew, P.; Franssila, S.; Ikkala, O.; Ras, R. H. Mechanically durable superhydrophobic surfaces. *Advanced materials* **2011**, *23*, 673-678.

93) Xue, C. H.; Ma, J. Z. Long-lived superhydrophobic surfaces. *Journal of materials chemistry A* **2013**, *1*, 4146-4161.

94) Zhu, X.; Zhang, Z.; Men, X.; Yang, J.; Wang, K.; Xu, X.; Xue, Q. Robust superhydrophobic surfaces with mechanical durability and easy repairability. *Journal of Materials Chemistry* **2011**, *21*, 15793-15797.

95) Yang, J.; Zhang, Z.; Men, X.; Xu, X.; Zhu, X. A simple approach to fabricate regenerable superhydrophobic coatings. *Colloids and Surfaces A: Physicochemical and Engineering Aspects* **2010**, *367*, 60-64.

96) Li, Y.; Li, L.; Sun, J. Bioinspired self-healing superhydrophobic coatings. *Angewandte Chemie* **2010**, *122*, 6265-6269.

97) (a) Ionov, L.; Synytska, A. Self-healing superhydrophobic materials. *Physical Chemistry Chemical Physics* **2012**, *14*, 10497-10502. (b) Wang, H.; Xue, Y.; Ding, J.; Feng, L.; Wang, X.; Lin, T. Durable, self-healing superhydrophobic and superoleophobic surfaces from fluorinated-decyl polyhedral oligomeric silsesquioxane and hydrolyzed fluorinated alkyl silane. *Angewandte Chemie* **2011**, *123*, 11635-11638.

98) Wang, Z.; Scheres, L.; Xia, H.; Zuilhof, H. Developments and challenges in self-healing antifouling materials. *Advanced functional materials* **2020**, *30*, 1908098.

99) Levkin, P. A.; Svec, F.; Fréchet, J. M. Porous polymer coatings: a versatile approach to superhydrophobic surfaces. *Advanced functional materials* **2009**, *19*, 1993-1998.

100) Vivarat Perrin, M. P.; Amiel, C.; Sebille, B. Preparation of tailorable interfaces: adsorption of reactive copolymers onto silica particles. *Langmuir* **1994**, *10*, 3635-3641.

101) Major, J. S.; Blanchard, G. J. Covalently bound polymer multilayers for efficient metal ion sorption. *Langmuir* **2001**, *17*, 1163-1168.

102) Dyer, M. A.; Ainslie, K. M.; Pishko, M. V. Protein adhesion on silicon-supported hyperbranched poly (ethylene glycol) and poly (allylamine) thin films. *Langmuir* **2007**, *23*, 7018-7023.

103) Wang, G.; Fang, Y.; Kim, P.; Hayek, A.; Weatherspoon, M. R.; Perry, J. W.; Jones, S. C. Layer-By-Layer dendritic growth of hyperbranched thin films for surface Sol–Gel syntheses of conformal, functional, nanocrystalline oxide coatings on complex 3D (Bio) silica templates. *Advanced Functional Materials* **2009**, *19*, 2768-2776.

104) Chen, H. Y.; Hirtz, M.; Deng, X.; Laue, T.; Fuchs, H.; Lahann, J. Substrate-independent dip-pen nanolithography based on reactive coatings. *Journal of the American Chemical Society* **2010**, *132*, 18023-18025.

105) Bog, U.; de los Santos Pereira, A.; Mueller, S. L.; Havenridge, S.; Parrillo, V.; Bruns, M.; Hirtz, M. Clickable antifouling polymer brushes for polymer pen lithography. *ACS Applied Materials & Interfaces* **2017**, *9*, 12109-12117.

106) Kumar, R.; Weigel, S.; Meyer, R.; Niemeyer, C. M.; Fuchs, H.; Hirtz, M. Multi-color polymer pen lithography for oligonucleotide arrays. *Chemical Communications* **2016**, *52*, 12310-12313.

107) Atwater, J.; Mattes, D. S.; Streit, B.; von Bojničić-Kninski, C.; Loeffler, F. F.; Breitling, F.; Hirtz, M. Combinatorial synthesis of macromolecular arrays by microchannel cantilever spotting (μCS). *Advanced Materials* **2018**, *30*, 1801632.

108) Liao, K. S.; Wan, A.; Batteas, J. D.; Bergbreiter, D. E. Superhydrophobic surfaces formed using layer-by-layer self-assembly with aminated multiwall carbon nanotubes. *Langmuir* **2008**, *24*, 4245-4253.

109) Heilmann, S. M.; Rasmussen, J. K.; Krepski, L. R. Chemistry and technology of 2-alkenyl azlactones. *Journal of Polymer Science Part A: Polymer Chemistry* **2001**, *39*, 3655-3677.

110) Messman, J. M.; Lokitz, B. S.; Pickel, J. M.; Kilbey, S. M. Highly tailorable materials based on 2-vinyl-4, 4-dimethyl azlactone:(co) polymerization, synthetic manipulation and characterization. *Macromolecules* **2009**, *42*, 3933-3941.

111) Jones, M. W.; Richards, S. J.; Haddleton, D. M.; Gibson, M. I. Poly (azlactone) s: versatile scaffolds for tandem post-polymerisation modification and glycopolymer synthesis. *Polymer Chemistry* **2013**, *4*, 717-723.

112) Sun, B.; Liu, X.; Buck, M. E.; Lynn, D. M. Azlactone-functionalized polymers as reactive templates for parallel polymer synthesis: synthesis and screening of a small library of cationic polymers in the context of DNA delivery. *Chemical communications* **2010**, *46*, 2016-2018.

113) Buck, M. E.; Zhang, J.; Lynn, D. M. Layer-by-layer assembly of reactive ultrathin films mediated by click-type reactions of poly (2-alkenyl azlactone) s. *Advanced materials* **2007**, *19*, 3951-3955.

114) Ford, J.; Marder, S. R.; Yang, S. Growing "nanofruit" textures on photo-crosslinked SU-8 surfaces through layer-by-layer grafting of hyperbranched poly (ethyleneimine). *Chemistry of Materials* **2009**, *21*, 476-483.

115) Bechler, S. L.; Lynn, D. M. Reactive polymer multilayers fabricated by covalent layer-by-layer assembly: 1, 4-conjugate addition-based approaches to the design of functional biointerfaces. *Biomacromolecules* **2012**, *13*, 1523-1532.

116) Parbat, D.; Manna, U. Synthesis of 'reactive'and covalent polymeric multilayer coatings with durable superoleophobic and superoleophilic properties under water. *Chemical Science* **2017**, *8*, 6092-6102.

117) Das, A.; Sengupta, S.; Deka, J.; Rather, A. M.; Raidongia, K.; Manna, U. Synthesis of fish scale and lotus leaf mimicking, stretchable and durable multilayers. *Journal of Materials Chemistry A* **2018**, *6*, 15993-16002.

118) Das, A.; Sengupta, S.; Deka, J.; Rather, A. M.; Raidongia, K.; Manna, U. Synthesis of fish scale and lotus leaf mimicking, stretchable and durable multilayers. *J. Mater. Chem. A* **2018**, *6*, 15993-16002.

119) Loudy, C. M.; Allouche, J.; Bousquet, A.; Martinez, H.; Billon, L. A nanopatterned dual reactive surface driven by block copolymer self-assembly. *Nanoscale* **2020**, *12*, 7532-7537.

120) Ishizaki, T.; Saito, N.; Takai, O. Correlation of cell adhesive behaviors on superhydrophobic, superhydrophilic, and micropatterned superhydrophobic/superhydrophilic surfaces to their surface chemistry. *Langmuir* **2010**, *26*, 8147-8154.

121) Oliveira, N. M.; Neto, A. I.; Song, W.; Mano, J. F. Two-dimensional open microfluidic devices by tuning the wettability on patterned superhydrophobic polymeric surface. *Applied physics express* **2010**, *3*, 085205.

122) Oliveira, S. M.; Song, W.; Alves, N. M.; Mano, J. F. Chemical modification of bioinspired superhydrophobic polystyrene surfaces to control cell attachment/proliferation. *Soft Matter* **2011**, *7*, 8932-8941.

123) Neto, A. I.; Custódio, C. A.; Song, W.; Mano, J. F. High-throughput evaluation of interactions between biomaterials, proteins and cells using patterned superhydrophobic substrates. *Soft Matter* **2011**, *7*, 4147-4151.

124) Salgado, C. L.; Oliveira, M. B.; Mano, J. F. Combinatorial cell–3D biomaterials cytocompatibility screening for tissue engineering using bioinspired superhydrophobic substrates. *Integrative Biology* **2012**, *4*, 318-327.

125) Han, Y.; Levkin, P.; Abarientos, I.; Liu, H.; Svec, F.; Frechet, J. M. Monolithic superhydrophobic polymer layer with photopatterned virtual channel for the separation of peptides using two-dimensional thin layer chromatography-desorption electrospray ionization mass spectrometry. *Analytical chemistry* **2010**, *82*, 2520-2528.

126) Zahner, D.; Abagat, J.; Svec, F.; Fréchet, J. M.; Levkin, P. A. A facile approach to superhydrophilic–superhydrophobic patterns in porous polymer films. *Advanced Materials* **2011**, *23*, 3030-3034.

127) Geyer, F. L.; Ueda, E.; Liebel, U.; Grau, N.; Levkin, P. A. Superhydrophobic–superhydrophilic micropatterning: towards genome-on-a-chip cell microarrays. *Angewandte Chemie International Edition* **2011**, *50*, 8424-8427.

128) Ueda, E.; Geyer, F. L.; Nedashkivska, V.; Levkin, P. A. DropletMicroarray: facile formation of arrays of microdroplets and hydrogel micropads for cell screening applications. *Lab on a Chip* **2012**, *12*, 5218-5224.

129) Efremov, A. N.; Stanganello, E.; Welle, A.; Scholpp, S.; Levkin, P. A. Micropatterned superhydrophobic structures for the simultaneous culture of multiple cell types and the study of cell–cell communication. *Biomaterials* **2013**, *34*, 1757-1763.

130) Hensarling, R. M.; Doughty, V. A.; Chan, J. W.; Patton, D. L. "Clicking" polymer brushes with thiol-yne chemistry: indoors and out. *Journal of the American Chemical Society* **2009**, *131*, 14673-14675.

131) Feng, W.; Li, L.; Ueda, E.; Li, J.; Heißler, S.; Welle, A.; Levkin, P. A. Surface patterning via thiol-yne click chemistry: an extremely fast and versatile approach to superhydrophilic-superhydrophobic micropatterns. *Advanced Materials Interfaces* **2014**, *1*, 1400269.

132) Geyer, F. L.; Ueda, E.; Liebel, U.; Grau, N.; Levkin, P. A. Superhydrophobic–superhydrophilic micropatterning: towards genome-on-a-chip cell microarrays. *Angewandte Chemie International Edition* **2011**, *50*, 8424-8427.

133) Li, J.; Li, L.; Du, X.; Feng, W.; Welle, A.; Trapp, O.; Levkin, P. A. Reactive superhydrophobic surface and its photoinduced disulfide-ene and thiol-ene (bio) functionalization. *Nano letters* **2015**, *15*, 675-681.

134) Manna, U.; Broderick, A. H.; Lynn, D. M. Chemical patterning and physical refinement of reactive superhydrophobic surfaces. *Advanced Materials* **2012**, *24*, 4291-4295.

135) Zhu, J.; Liu, B.; Li, L.; Zeng, Z.; Zhao, W.; Wang, G.; Guan, X. Simple and green fabrication of a superhydrophobic surface by one-step immersion for continuous oil/water separation. *The Journal of Physical Chemistry A* **2016**, *120*, 5617-5623.

136) Coriand, L.; Mitterhuber, M.; Duparré, A.; Tünnermann, A. Definition of roughness structures for superhydrophobic and hydrophilic optical coatings on glass. *Applied Optics* **2011**, *50*, C257-C263.

137) Wei, Y.; Hongtao, L.; Wei, Z. Preparation of anti-corrosion superhydrophobic coatings by an Fe-based micro/nano composite electro-brush plating and blackening process. *Rsc Advances* **2015**, *5*, 103000-103012.

138) Chen, M.; Yi, Z.; Tao, S.; Wang, S.; Fang, Z.; Lu, C.; Xu, Z. A Pragmatic Device Based on a Double-Sided Functional Structure for Efficient Water Harvesting. *Global Challenges* **2020**, *4*, 1900094.

139) Wang, F.; Pi, J.; Song, F.; Feng, R.; Xu, C.; Wang, X. L.; Wang, Y. Z. A superhydrophobic coating to create multi-functional materials with mechanical/chemical/physical robustness. *Chemical Engineering Journal* **2020**, *381*, 122539.

140) Das, A.; Shome, A.; Manna, U. Porous and reactive polymeric interfaces: an emerging avenue for achieving durable and functional bio-inspired wettability. *Journal of Materials Chemistry A* **2021**, *9*, 824-856.

141) Erbil, H. Y. Practical applications of superhydrophobic materials and coatings: problems and perspectives. *Langmuir* **2020**, *36*, 2493-2509.

142) Han, Y.; Levkin, P.; Abarientos, I.; Liu, H.; Svec, F.; Frechet, J. M. Monolithic superhydrophobic polymer layer with photopatterned virtual channel for the separation of peptides using two-dimensional thin layer chromatography-desorption electrospray ionization mass spectrometry. *Analytical chemistry* **2010**, *82*, 2520-2528.

143) Oliveira, S. M.; Song, W.; Alves, N. M.; Mano, J. F. Chemical modification of bioinspired superhydrophobic polystyrene surfaces to control cell attachment/proliferation. *Soft Matter* **2011**, *7*, 8932-8941.

144) Wirth, C. L.; De Volder, M.; Vermant, J. Fabrication of planar colloidal clusters with template-assisted interfacial assembly. *Langmuir* **2015**, *31*, 1632-1640.

145) Wu, L.; Dong, Z.; Kuang, M.; Li, Y.; Li, F.; Jiang, L.; Song, Y. Printing patterned fine 3D structures by manipulating the three phase contact line. *Advanced Functional Materials* **2015**, *25*, 2237-2242.

146) Bai, H.; Wang, L.; Ju, J.; Sun, R.; Zheng, Y.; Jiang, L. Efficient water collection on integrative bioinspired surfaces with star-shaped wettability patterns. *Advanced Materials* **2014**, *26*, 5025-5030.

147) Rather, A. M.; Manna, U. Facile synthesis of tunable and durable bulk superhydrophobic material from amine “reactive” polymeric gel. *Chemistry of Materials* **2016**, *28*, 8689-8699.

148) Das, A.; Shome, A.; Manna, U. Porous and reactive polymeric interfaces: an emerging avenue for achieving durable and functional bio-inspired wettability. *Journal of Materials Chemistry A* **2021**, *9*, 824-856.

Chapter 2. Rapid and Facile Synthesis of Substrate Independent "Chemically Reactive" and Porous Polymeric Dip Coating

Design of "chemically reactive" coating with a tailored topography is a simple basis for co-optimizing essential physical and chemical parameters, e.g., hierarchical topography and low/high surface energy which are essential for achieving different biomimicked liquid wettability. In general, the essential topography and appropriate chemistry in the superhydrophobic coating is optimized following various top-down and bottom-up approaches, where various hydrophilic building blocks are associated through electrostatic interaction, hydrogen bonding, and other weak bonding (e.g., metal-thiol etc.), for both achieving desired hierarchical features and optimizing the appropriate chemistry on top of this featured interface. Such designs are inappropriate to sustain practically relentlessly harsh settings. So, further development for the synthesis of a durable and substrate-independent superhydrophobic coating is essential for various prospective applications in "real-world" scenarios. However, the design of highly abrasion-tolerant and "absolutely" substrate-independent artificial superhydrophobicity following a simple and scalable synthesis procedure is rare in the literature. In this current work, a catalyst-free and facile chemical approach is adopted for an in situ and rapid deposition of a "chemically reactive" nanocomplex for decorating a wide range of substrates, including water-soluble, water-sensitive, highly flexible, rigid, and fibrous substrates with a highly tolerant biomimicked superhydrophobicity property. Branched poly(ethylenimine) (BPEI) and dipentaerythritol pentaacrylate (5Acl) mutually react through 1,4-conjugate addition reaction in alcoholic solvents to yield chemically reactive nanocomplexes, and a hierarchically featured "chemically reactive" dip coating is fabricated by the appropriate selection of the alcoholic solvent, i.e., 1-heptanol. Furthermore, the choice of small alkylamines for post-covalent modifications of the "chemically reactive" dip coating comprised of residual acrylates provided superhydrophobicity with a tailored water adhesion. A gradual increase in both roll-off angles, and the contact angle hysteresis (from 5° to 30°) was noted with a decrease in the hydrocarbon tail of selected alkylamines. The synthesized biomimicked interfaces are capable of performing under various practically relevant, severe physical and chemical challenges including bending, creasing, twisting, different physical abrasions (i.e., adhesive tape peeling test, abrasive sand paper test, etc.), high compressive strain, highly acidic and alkaline aqueous phases, artificial sea water, river water, etc. Moreover, this current approach was extended for developing various relevant functional materials, including superhydrophilic/superhydrophobic patterns on flexible papers and highly compressible super-oil-absorbent, etc.

* S. Das *et al.*, *ACS Appl. Mater. Interfaces* **2019**, *11*, 34316−34329

2.1. Introduction

The synthesis of extremely water-repellent artificial interfaces, inspired by nature, are recently appearing as a high-potential tool in developing various functional materials for practically relevant widespread applications, where biomimicked water wettability is associated with different strategically selected substrates, adopting different fabrication processes.[1–17] For example, superhydrophobic coating on flat objects (metal, wood, glass, concrete, etc.) are useful for developing self-cleaning interfaces, whereas porous two-dimensional (2D) metal meshes/membranes embedded with extreme water repellence allow a gravity-driven selective filtration of oil/ oily phase from an oil/water mixture.[2,5,9,10] Similarly, compressible and spongy three-dimensional (3D) substrates that are decorated with superhydrophobicity provide a facile basis for an energy-efficient and selective absorption-based oil collection from an oil/water mixture.[7,9,11,12] Thus, the selection of substrates plays an important role in developing different functional materials.[2,5,7,9–12] In this context, in the past, few conventional substrate-independent superhydrophobic coatings are introduced mostly using water-contaminated coating solutions,[18–24] and/or following general deposition processes.[19,20,22–24] These aqueous media-based deposition approaches are inherently inapt for adopting superhydrophobic coatings on water-soluble and water-sensitive substrates. Moreover, spray coatings on complex and three-dimensional objects are challenging. Thus, the design of an "absolutely" substrate-independent superhydrophobic coating that is capable of decorating wide varieties of substrates, including water-soluble (sugar cube), water-sensitive (pH paper), rigid (glass, wood, concrete, and metal), flexible (filter paper), and fibrous (cotton tread) interfaces following a single and scalable deposition process, is highly relevant for various fundamental and applied contexts.

Over the last couple of decades, various methods are introduced in the literature for fabricating artificial superhydrophobic interfaces following various synthetic approaches,[2–24] and most of them are associating with environmentally hazardous chemicals and sophisticated instrumental set-ups or tedious synthetic procedures.[2–24] However, the synthesis of a highly abrasion-tolerant super-hydrophobic coating, which would be capable of performing under various severe settings, remains a challenge. In the past, some special designs including repairable, self-healable, and mechanically durable coatings are introduced which are capable of providing more stable biomimicked interfaces.[18,25–30] Nevertheless, all of these approaches, which are optimized with essential chemistry "only" on top of the hierarchical topography, are completely inappropriate for sustaining severe physical abrasions, as both the essential topography and chemistry that confers extreme water repellency are completely compromised at the top of the coating during practically relevant severe abrasion processes (adhesive tape peeling, sand paper abrasion, scratching etc.).[2–30] In the past, Levkin et al.[31] reported a three-dimensional superhydrophobic coating, which is inherently capable of withstanding severe physical insults,[31] where the freshly exposed interior of the coating, after the

physical removal of top interface, displayed uninterrupted superhydrophobicity.[31] Later on, few other approaches, including electrospinning deposition, "click-type" ring opening-reaction-based layer-by-layer deposition, and candle soot template process are introduced to optimize the essential chemistry and topography, both on top and in the interior of the coating;[32−36] and furthermore, those synthesized bulk biomimicked coatings were successfully extended for revalidating the inherent tolerance of such designs towards severe physical challenges. In the recent past, my labmates also introduced a facile Michael addition reaction for the preparation of bulk superhydrophobic coatings following an again-tedious layer-by-layer deposition process,[37,38] and some of the coating process is only applicable for planar objects.[39] Furthermore, such chemistry is used in preparation of a self-standing superhydrophobic monolith,[40]which is inherently inappropriate for substrate-independent coatings. In comparison to previously reported substrate-specific and tedious deposition processes,[31−40] here, a facile and single-step deposition approach is introduced to synthesize an "absolutely" substrate-independent and highly tolerant superhydrophobic coating, following the same Michael addition reaction between an amine, and acrylate groups at ambient conditions.

In this current report, various important above-mentioned existing challenges related to biommicked artificial superhydrophobic coatings are attempted to be rationally addressed by following a simple and scalable synthetic process, where a primary amine-reactive and covalently cross-linked polymeric coating is introduced by a single step and in situ deposition of a "chemically reactive" nanocomplex following a robust and rapid covalent reaction between the amine and acrylate groups at ambient conditions, without the aid of any catalyst. The choice of reaction medium in the "chemically reactive" reaction solution played a crucial role in controlling the wettability in the dip coated interface. This single-step and in situ deposition process inherently allowed to coat a wide range of substrates, including materials with various chemical compositions (water-insoluble, water-sensitive/soluble), flexible, fibrous, rigid, planar, and geometrically complex objects with "chemically reactive" porous polymeric interface. Moreover, the residual chemical reactivity in the polymeric dip coating allowed us to modulate the chemistry with various primary amine-containing small molecules, which resulted in the facile adaptation of both chemically controlled adhesive (roll-off angle 30°−10°) and nonadhesive (roll-off angle ~ 5°) superhydrophobicity. The synthesized superhydrophobicity was inherently enabled for sustaining practically relevant various physical manipulations/abrasions including bending, creasing, compressive deformation, scratching as well as different forms of physical erosions, etc., and prolonged (30 days) exposures to various harsh chemical settings, those with extremes of pH, sea water, river water, and surfactant contaminated aqueous phase, without compromising the embedded extreme water repellency. The performance of as synthesized superhydrophobic coatings (on flexible and rigid flat objects), which were pre-treated with various

severe abrasive tests (e.g., adhesive tape peel, sand paper abrasion, and scratching) is investigated in detail. Moreover, superhydrophobic coatings developed on water-sensitive and water soluble substrates were strategically exploited for designing hydrophilic/superhydrophobic physical patterns and highly compressible super-oil-absorbents that performs under practically relevant severe settings, and the spongy super- hydrophobic material that derived from the water-soluble template is capable of removing a wide range of oil/oily phases from respective oil/water mixtures with an oil-absorption capacity around 2000 wt%. Thus, our synthetic approach provided a simple basis for developing an "absolutely" substrate-independent and various severe-abrasion-tolerant artificial superhydrophobic coating that is inherently capable of performing in diverse, challenging, and practically relevant scenarios, without perturbations in biomimicked wettability.

2.2. Experimental Section

2.2.1. Materials. Branched poly(ethyleneimine) (BPEI, MW~25000 Da), dipentaerythritol pentaacrylate (5Acl, MW~524.21 g mol^{-1}), octadecylamine, dodecylamine, decylamine, octylamine, heptylamine, hexylamine, pentylamine, butylamine, propylamine, sodium dodecyl sulphate (SDS), and dodecyl trimethylammonium bromide (DTAB) were purchased from Sigma-Aldrich, Bangalore, India. Methanol was purchased from EMPLURA, Mumbai, India. Ethanol was purchased from TEDIA, USA. 1-propanol, 1-butanol, 1-pentanol, 1-hexanol, and 1-heptanol were procured from Alfa Aesar. THF was purchased from RANKEM, Maharashtra, India. Microscopic glass slides were obtained from JSGW (Jain Scientific Glass Works, India) and sand paper (grit no. 400) was acquired from Million International, India. Adhesive tape (Johnson tape Ltd. India) was purchased from local sources. Litmus paper was purchased from Merck Specialities Private Limited, Mumbai, India. Hydrochloric acid (HCl, ~37%) and ammonia solution (NH_3, ~25%) were acquired from Merck Life Science Pvt. Ltd., Mumbai, India. Sugar cubes were obtained from a local shop in IIT Guwahati, India. Rhodamine-6G was acquired from LOBA Chemie (Laboratory Reagents and Fine Chemical) Mumbai, India. Sand was obtained from a construction site at IIT Guwahati, India.

2.2.2. General Considerations. Contact angles and roll-off angles of the beaded water droplets were measured using the KRUSS Drop Shape analyser-DSA25 instrument with an automatic liquid dispenser at ambient temperatures and the dynamic and static water contact angles were measured at different locations on each sample. Roll-off angle was measured with KRUSS Drop Shape Analyzer-DSA25 instrument, where the water droplet was beaded gently on the as synthesized water-repellent coatings, and then the whole stage of the contact angle instrument was tilted using the software of the embedded program in the instrument to find out the actual minimum contact angle for rolling-off the beaded water droplet. Then, to mimic more realistic conditions, we have set the stage with that minimum contact angle and followed by exposure to the water droplet. The

dynamic light scattering (DLS) data was recorded using a Zetasizer Nano ZS90 instrument (model no. ZEN3690). All the samples were coated with a thin layer of gold sputter prior to obtaining scanning electron microscopy images (SEM) of the dip coatings using a Carl Zeiss Field Emission Scanning Electron Microscope (FESEM). Fourier-transform infrared (FTIR) spectra were recorded using a Perkin Elmer Spectrophotometer instrument at an ambient temperature, where the polymeric matrix was mixed properly with KBr (Potassium Bromide) prior to forming the KBr pellet. The digital images were captured by using Canon Power Shot SX420 IS digital camera.

2.2.3. Preparation of the "Chemically Reactive" Polymeric Dip Coating and Post Covalent Modifications. The solutions of 5Acl (132.5 mg mL^{-1}) and BPEI (50 mg mL^{-1}) in various alcoholic solvents (starting from ethanol to 1-heptanol) were separately prepared in glass vials. Then, the solution (1.2 mL) of BPEI was mixed with the solution (4 mL) of 5Acl to prepare a dispersion of growing polymeric nanocomplexes. Selected substrates were submerged in respective dipping solutions for 10 min. After the in situ deposition of the reactive polymeric nanocomplexes, the dip coated substrates with polymeric dip coatings were kept for solvent evaporation in open air prior to washing with THF thoroughly. The residual chemical reactivity of the dip coatings was characterized with FTIR analysis. The water wettability of the dip coatings was altered depending on the selection of appropriate alcoholic solvents (see result & discussion section for more details). Furthermore, the "chemically reactive" dip coatings were covalently post-functionalized with different aliphatic alkylamines including octadecylamine (5 mg mL^{-1}), dodecylamine (2.5 mg mL^{-1}), decylamine (0.2 mL mL^{-1}), octylamine (0.2 mL mL^{-1}), heptylamine (0.2 mL mL^{-1}), hexylamine (0.2 mL mL^{-1}), pentylamine (0.2 mL mL^{-1}), butylamine (0.2 mL mL^{-1}), and propylamine (0.2 mL mL^{-1}). First of all, polymeric dip coatings were exposed to the rationally selected primary amine containing small molecules overnight, then the material was thoroughly washed with THF, and dried under the stream of compressed air prior to further essential characterizations or other relevant proof-of-concept demonstrations.

2.2.4. Physical and Chemical Durability of the Superhydrophobic Dip Coating. To investigate the tolerance of the synthesized superhydrophobic dip coating under various practically relevant and severe settings, different acute physical abrasions were performed on the dip coated material. The details of those standard physical durability tests including adhesive tape peeling test, sand paper abrasion test, sand drop test, and scratch test are provided in the following section;

2.2.4.1. Adhesive Tape Peel test. Double sided adhesive tape (1 × 1 cm) was first attached onto a microscopic glass slide, and then, the superhydrophobic polymeric dip coating (3 × 1 cm) was brought in contact to the freshly exposed adhesive surface with an applied load of 1 kg. The external applied load is likely to facilitate a uniform and homogeneous contact between the polymeric dip

coating and the adhesive surface. After 30 min, the adhesive tape was manually peeled off from the polymeric dip coating. During the removal of the adhesive surface, the top portion of the dip coating was arbitrarily transferred to the adhesive tape and left behind a physically eroded polymeric dip coating with exposed interiors. The test was repeated 5 times and the weight of the materials lost after each and every step of the abrasion was measured (~5 mg after 5 cycles). The water repelling property was examined on such physically abraded interfaces by measuring the water contact angle and visual inspection of the beading of water droplets (dyed with Rhodamine-6G) on the coated substrate before and after performing the test.

2.2.4.2. Sand Paper Abrasion Test. In this physical challenge, an abrasive sand paper (grit no. 400; 3 × 1 cm) and superhydrophobic dip coated glass slide (3 × 1 cm) were immobilized on two separate microscopic glass slides using a double-sided adhesive tape, in a way that both the abrasive sand paper surface and the polymeric dip coating were exposed to air. Next, the abrasive interface of the sand paper was manually rubbed with the speed of 8.45 cm/s on the polymeric dip coating 25 times, with an applied external load of 500 g. During this abrasion process, the top portion of the polymeric dip coating was physically eroded (~86 mg) in the form of a white powder, and the interior of the polymeric coating was exposed. After that, the water wettability was investigated on both the physically damaged polymeric coating and the abraded white powdery material by contact angle measurements and visual inspections.

2.2.4.3. Sand Drop Test. In this standard physical durability test, polymeric dip coating (3 × 1 cm) was tilted at 45° prior to continuously pouring a stream of sand grains (100 g) from a height of 20 cm using a funnel. Any noticeable change in the integrity of the polymeric dip coating was not observed at the end of this durability test. Furthermore, water wettability was examined by acquiring the contact angle of the beaded water droplet.

2.2.4.4. Scratch Test. The ODA-treated substrate was scratched manually using a sharp-edged knife for several times in air, and then the water wettability of the material was examined thoroughly by contact-angle measurements and digital images using coloured water before and after the test.

2.2.4.5. Exposures to UV Light. The as-synthesized polymeric dip coating was continuously kept under UV light for 30 days, where two different UV light sources (8 watts) with a wavelength of absorption maxima at 264 and 365 nm were used in the study. The impact of the prolonged exposure of UV light was monitored by measuring water contact angles at regular intervals.

2.2.4.6. Chemical Durability. The ability of the superhydrophobic dip coating to retain its embedded extreme water repellent property, after exposure to different harsh chemically complex environments, was investigated in detail. The as-synthesized superhydrophobic dip coating was

exposed to various practically relevant and chemically challenging settings including alkaline solution (pH 11), acidic solution (pH 1), anionic surfactant (SDS, 1 mM) solution, cationic surfactant (DTAB, 1 mM) solution, river water (Brahmaputra River, Assam, India), and artificial sea water for a prolonged duration (30 days). The artificial seawater was prepared by mixing $MgCl_2$ (0.226 g), $MgSO_4$ (0.325 g), NaCl (2.673 g), and $CaCl_2$ (0.112 g) in 100 mL of deionized water in a volumetric flask.

2.2.4.7. Investigating Self-Cleaning Performance on Physically Damaged Dip Coatings. The self-cleaning of deposited dust and dirt on the as-synthesized superhydrophobic dip coating was compared before and after incurring severe physical abrasions on the polymeric coating. A freshly prepared superhydrophobic coating was contaminated with dust particles, prior to exposing a few droplets of water on a tilted interface. The beaded water droplets were immediately rolled off, and the deposited dust particles (on the polymeric coating) were collected by the air/water interface of the rolling water droplets. Eventually, all the dust particles were displaced completely from the superhydrophobic coating and left behind a self-cleaned and dried interfaces. To investigate the performance of such self-cleaning on the physically damaged superhydrophobic coatings, the same superhydrophobic dip coating was first exposed to various practically relevant and challenging settings including creasing, adhesive tape peeling test, and sand paper abrasion test. During these processes, the polymeric coating incurred obvious and severe physical insults (see result & discussion for more details). Then, the physically abraded polymeric coating was contaminated with dust particles prior to extending it to demonstrate the self-cleaning of the deposited dust particles.

2.2.5. Preparation of Porous and Spongy Superhydrophobic Material Using Water-Soluble Sugar Cube. The current dip coating approach was successfully extended to achieve super-hydrophobic coatings on highly water-soluble substrates, where a sugar cube (solid, 25 x 15 mm) was selected as the model water-soluble substrate. This material was further exploited for developing a highly and reversibly compressible superhydrophobic sponge through the strategic sacrifice of a water-soluble substrate. First, the dip-coated sugar cube, which is embedded with superhydrophobicity, was soaked with ethanol prior to placing in DI water, and immediately the coated sugar cube was sunk in the aqueous phase and settled on the bottom of the beaker. However, after 1.5 h of this aqueous exposure, the sugar cube buoyed up at the water−air interface and it turned into a supple, soft spongy cubic material. The material was then taken out of water and thoroughly washed with DI water and methanol before air-drying. After that, the spongy and soft sugar cube was transferred to a 5-Acl solution prepared in 1-heptanol for 15 min before proceeding toward the post-modification step using a primary amine containing small molecules, for example, ODA molecules, and then washed with THF

rigorously to remove the excess ODA. After air-drying, the water wettability on the material was characterized.

2.2.6. Selective Absorption-Based Separation of Oil/Water Mixture. The as-synthesized superhydrophobic sponge that derived from the water-soluble substrate (i.e., sugar cube) was extended further for selective absorption-based oil/water separation. The spongy superhydrophobic material was exposed to a floating crude oil on an aqueous phase. The oil phase was rapidly and completely absorbed by the material and the separated oil phase was further recollected in a separate container by a manual squeezing of the spongy material. The material was found to be very efficient (as an adsorbent) toward the selective absorption of various oils including vegetable oil, motor oil, petrol, diesel, and silicone oil.

2.3. Results and Discussions

2.3.1. In Situ Growth of "Chemically Reactive" Interface and Post-Covalent Modifications. In the past, many synthetic approaches are introduced following either an electrostatic interaction or condensation reaction process to develop hierarchically featured interfaces that are chemically inactive toward further covalent reactions at ambient conditions, which demands an additional optimization of low surface energy on top of the hierarchical interface, mostly through weak chemical bonding/interactions.[18,41−50] Thus, as expected, such artificial superhydrophobicity is likely to be delicate towards severe physical/chemical abrasions.[51] In the recent past, a catalyst-free and rapid covalent reaction between amines and acrylate groups at ambient conditions is strategically exploited in developing different nanostructures, amplifications of functional chemical groups, etc.[52−54] This simple chemistry is further extended recently for constructing a covalently cross-linked and "chemically reactive" polymeric multilayers following a multistep layer-by-layer deposition process.[55,56] Inspired by these designs, here, a single-step and facile dip coating is introduced, where the reaction mixture of BPEI/5Acl readily reacted through a 1,4-conjugate addition reaction (Figure 2.1A, B) and a range of selected substrates (including water soluble/water sensitive interfaces) were immersed in the dipping solution to obtain a "chemically reactive" and inherently hydrophobic coating (Figure 2.1C−F). The residual acrylate groups in the polymeric dip coating allowed to post-covalently modify with selected alkylamines (i.e., octadecylamine: ODA), and eventually the post-modified interfaces became extremely water repellent as shown in Figure 2.1F, G. In the recent past, different alkali metal ions doped reaction mixtures of BPEI/5Acl were transformed into a self-standing polymeric gel via the formation of a milky solution of a polymeric nanocomplex, and the rate of gelation was observed to be rapid for smaller alkali metal ions.[57] This approach allowed the tailoring of different physical properties (shrinkage, compressive deformation, etc.) in the superhydrophobic self-standing monolith.[52] Furthermore, the alcoholic solvents also play a pivotal role in controlling

the growth of the reactive nanocomplex (Figure 2.2A), where the composition of the reaction mixture

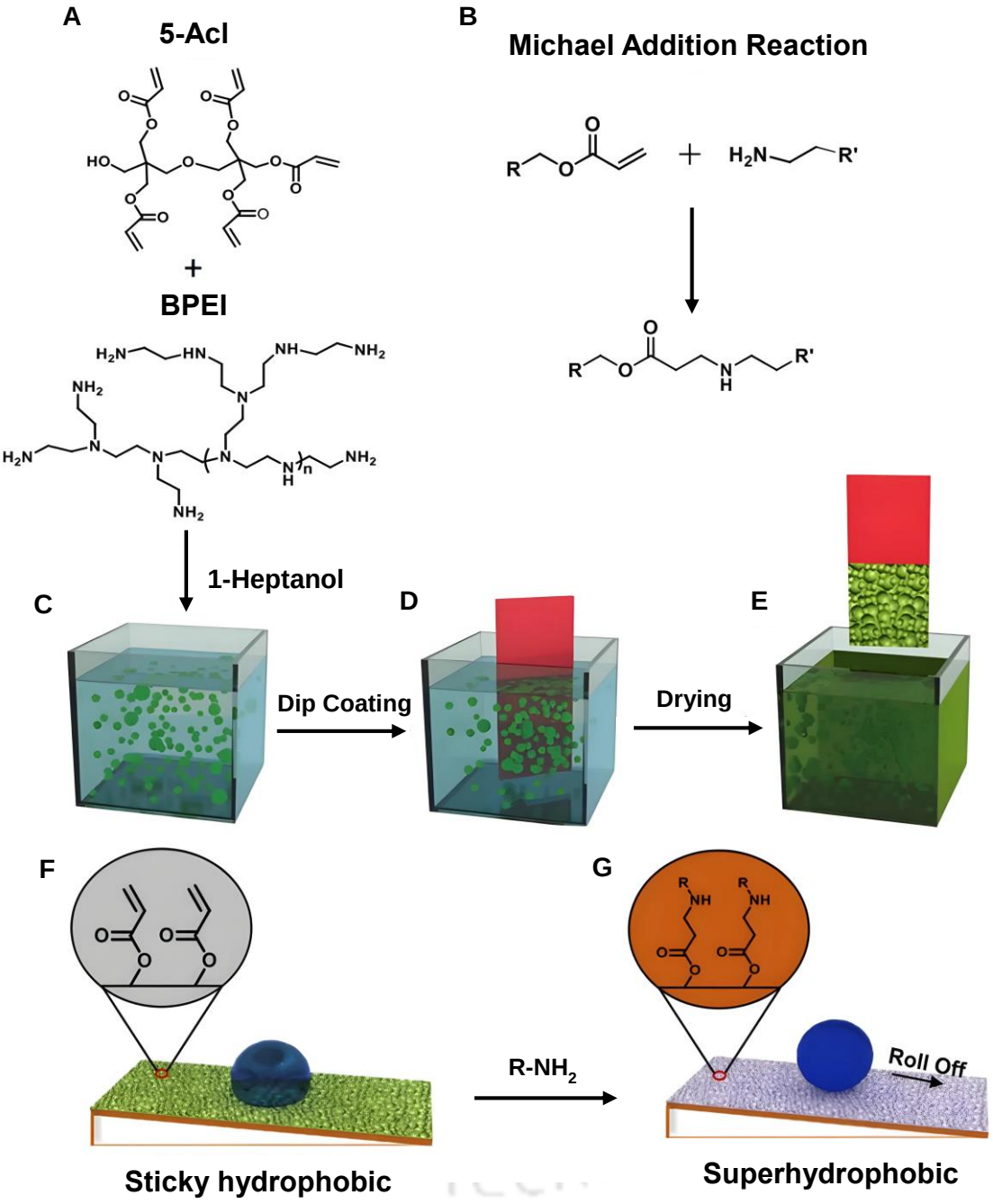

Figure 2.1. (A) Chemical structures of dipentaerythritol pentaacrylate (5Acl) and branched poly(ethyleneimine) (BPEI). (B) The Michael addition reaction between the acrylate and primary amine groups at ambient conditions, without the aid of a catalyst. (C−E) Schematic representation of the in situ deposition of a growing polymeric nanocomplex on a selected substrate following a single dipping process. (F) Representation of the "chemically reactive" and inherently hydrophobic polymeric dip coating. (G) Post-modifications of the dip coating with alkylamine, having a long hydrocarbon tail yielded by either a controlled adhesive or non-adhesive superhydrophobicity.

kept unaltered. The growth of nanocomplex was observed to be faster for higher analogue of ethanol as shown in Figure 2.2A, even the sol gel conversion of the reaction mixture was found to be accelerated for reaction mixture that were prepared in pentanol, hexanol and heptanol as shown in Figure 2.2E-G. The growth of the nanocomplex in heptanol (1130 nm) was noticed to be significantly high in comparison to pentanol (455 nm) and other lower analogues of pentanol as shown in Figure 2.2A.

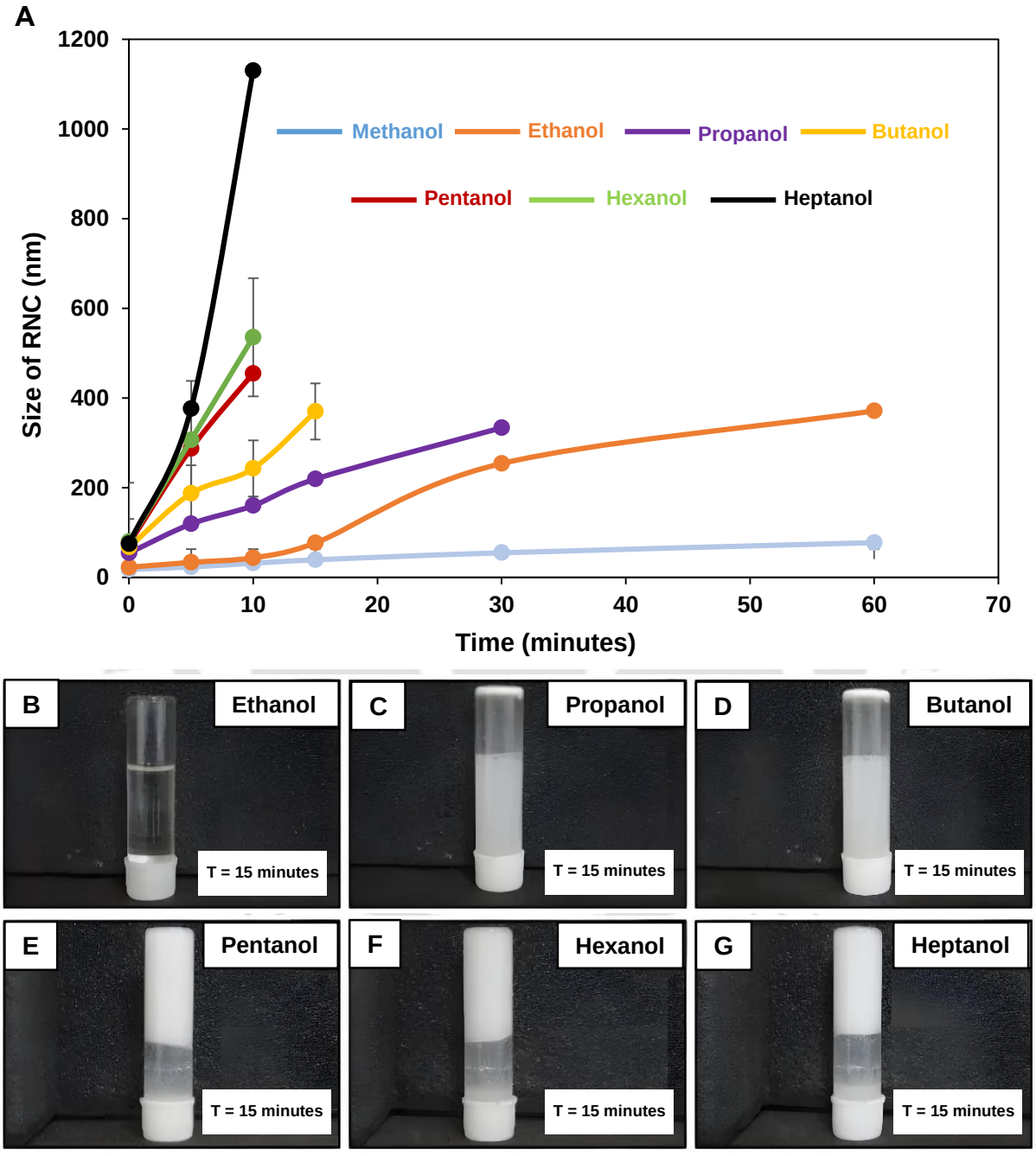

Figure 2.2. (A) Plot comparing the growth of polymeric nanocomplexes (PNC) in different alcoholic reaction media (starting from methanol to 1- heptanol). (B-G) Digital images accounting physical changes in the reaction mixtures of BPEI/5Acl in ethanol (B), 1-propanol (C), 1-butanol (D), 1-pentanol (E), 1-hexanol (F) and 1-heptanol (G) after 15 minutes.

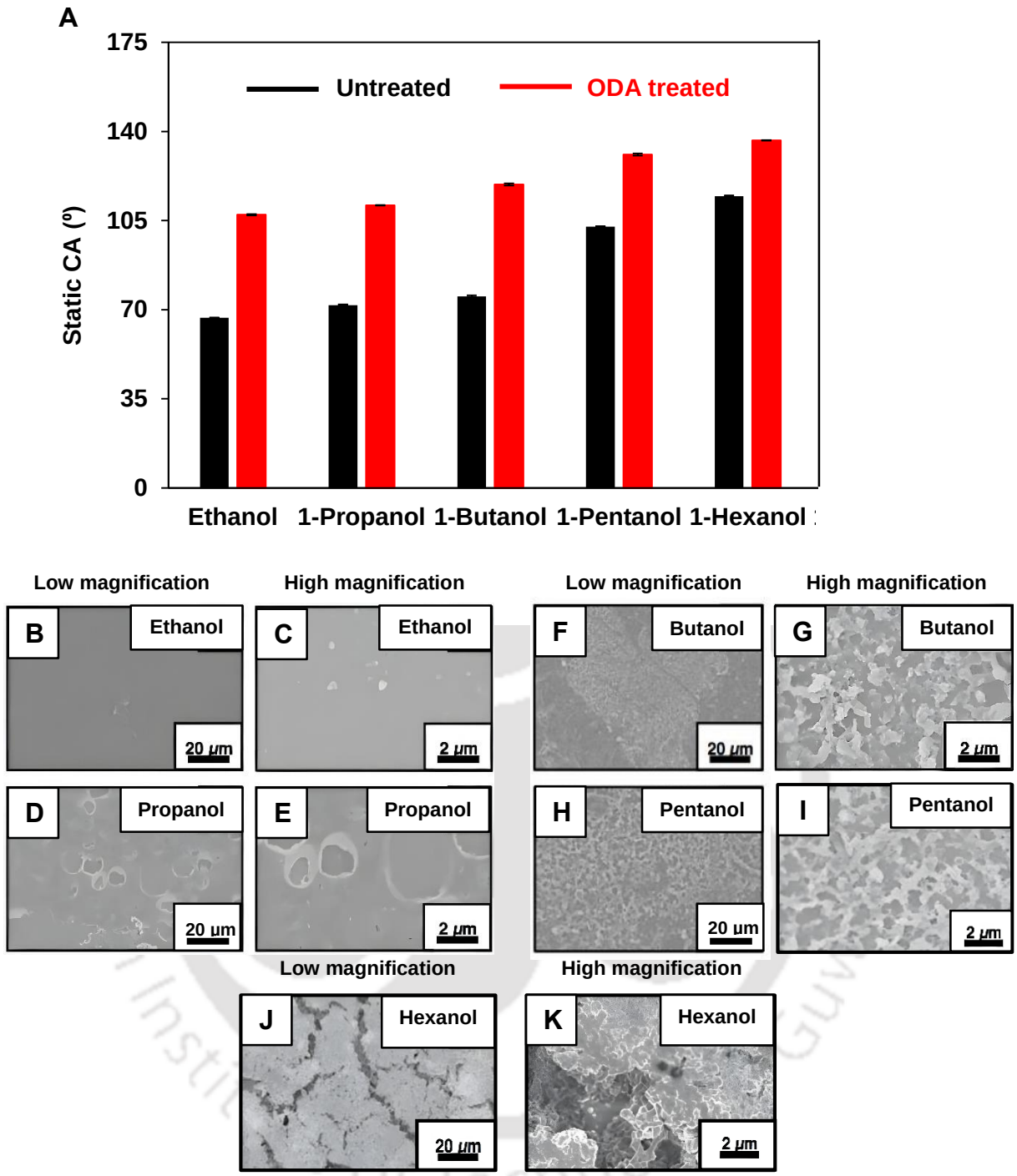

Figure 2.3. (A) Black bars in the graph accounting the gradual change in static contact angles of beaded water droplets on dip coatings on the changing the reaction media with higher analogues of ethanol, whereas, the red bars representing the elevation of hydrophobicity of each polymeric dip coating (that are prepared from different alcoholic solvents) after post functionalization with octadecylamine (ODA) through 1,4-conjugate addition reaction. (B-K) FESEM images of these polymeric dip coatings that are developed from different alcoholic solvents in low (B, D, F, H, J) and high (C, E, G, I, K) magnifications.

This sol-gel conversion of the reaction mixture was further extended here in developing "absolutely" substrate-independent and abrasion-tolerant biomimicked coatings following a simple dipping process. The selected substrates (water-soluble or water-insoluble) were immersed (for 10 min) in the

"chemically reactive" dipping solution of BPEI/5Acl, which were prepared in different alcoholic solvents starting from ethanol to heptanol. The in situ growing nanocomplexes were deposited on the

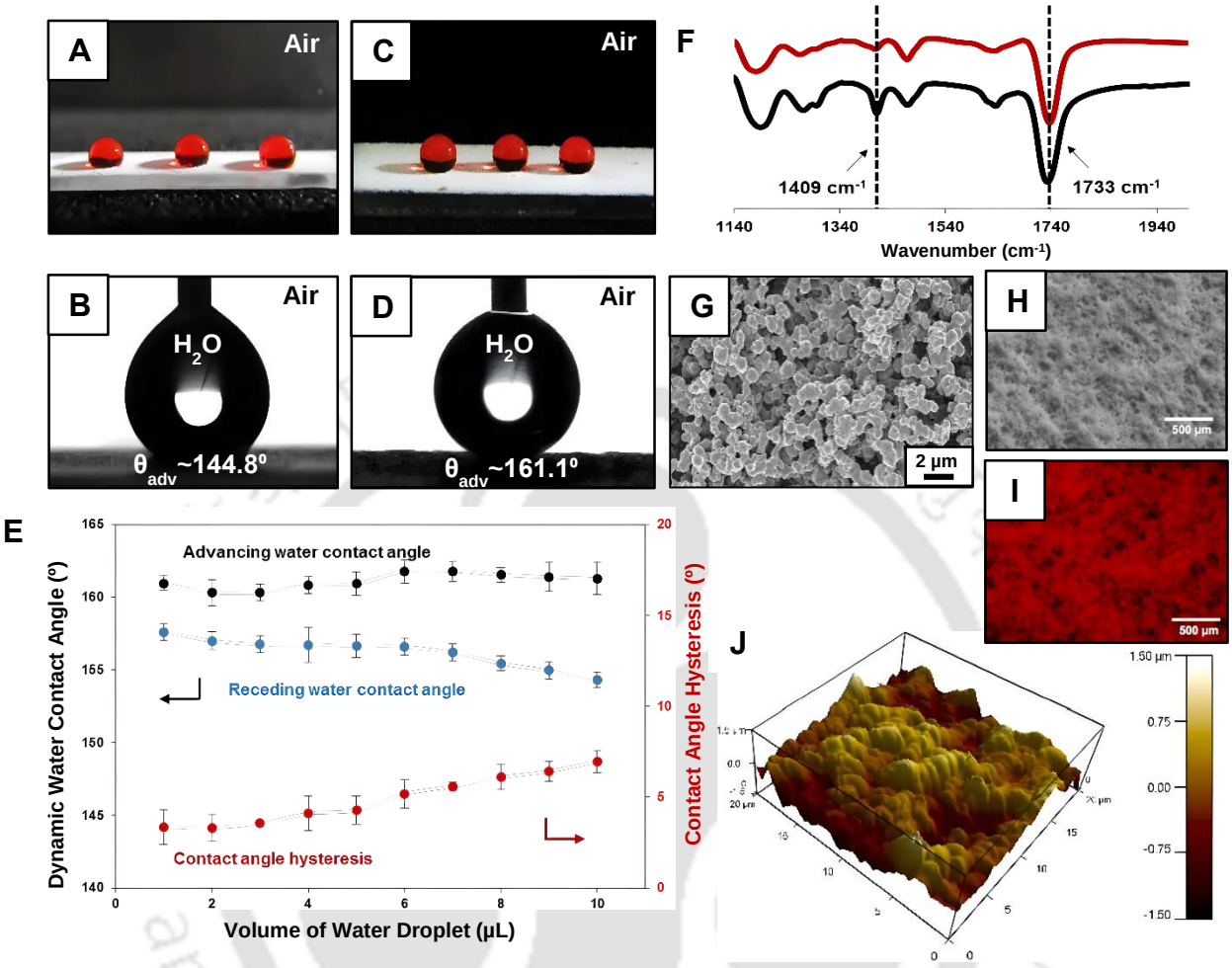

Figure 2.4. (A-D) Digital images (A, C) and advancing contact angle images (B, D) of the beaded water droplet (red color aids visual inspection) on the dip coating (A, B) before and (C, D) after post-modification with ODA. (E) The plot represents the change in advancing water contact angle (black line), receding contact angle (blue line) and contact angle hysteresis (red line) with the change in volume of beaded water droplets on superhydrophobic coating. (F) FTIR spectra of the "chemically reactive" dip coating before (black) and after (red) post-chemical modification with ODA. (G) FESEM image of hierarchically featured porous and "chemically reactive" dip coating. (H, I) Optical microscopic image of as-synthesized superhydrophbic coating, where fluorescence image (I) is aquired after physical deposition of rhodamine dye. (J) Atomic force microscopic image of superhydrophobic coating over 20 µm x 20 µm area. The color scale range is ± 1.5 µm.

selected interface and eventually provided "chemically reactive" and inherently hydrophobic polymer coatings, and the embedded hydrophobicity in the polymeric matrix was found to be increased gradually on replacing ethanol with its higher analogues as a reaction medium, as shown in Figure 2.3A. Moreover, the rate of gelation due to change in reaction medium influenced the morphology of the deposited polymeric coating as shown in Figure 2.3B-K. However, none of the dip coatings were inherently embedded with superhydrophobicity; and the polymeric dip coating, prepared using

heptanol, was found to be the most hydrophobic among all, with an advancing WCA of ~145°, as shown in Figure 2.4A, B. Furthermore, the post-covalent modification of the dip coatings with ODA molecules through the 1,4-conjugate addition reaction allowed the improving of the water repellency significantly, and the same polymeric coating displayed superhydrophobicity with an advancing WCA of ~161°, as shown in Figure 2.4C, D and the beaded water droplets immediately rolled off the tilted synthesized superhydrophobic dip coating with a ≥5° angle. A small change (below 10°) in the receding contact angle and contact angle hysteresis is observed on changing the volume of the beaded water droplet from 1 to 10 μL on superhydrophobic interfaces as shown in Figure 2.4E. The post-covalent modification of the dip coating through 1,4-conjugate addition reaction was investigated with the widely accepted and standard FTIR analysis. The IR signatures at 1409 and 1733 cm^{-1}, which are corresponding to the symmetric deformation of the C–H bond for the β carbon of the vinyl group and carbonyl groups, respectively, revealed the existence of residual acrylate groups in the polymeric dip coating. Furthermore, the IR peak intensity at 1409 cm^{-1} was significantly reduced with respect to the IR peak at 1733 cm^{-1}, after the post-covalent modification of the "chemically reactive" dip coating with ODA molecules. The primary amine groups of ODA molecules readily reacted with residual acrylate groups in the polymeric dip coating through a 1,4-conjugate addition reaction. During this mutual covalent reaction between the amine and the acrylate groups, only the vinyl groups are compromised, whereas the carbonyl group remained intact. Thus, the IR signature for carbonyl stretching at 1733 cm^{-1} provided an internal reference, and the reduction of the IR peak (1409 cm^{-1}) for the β carbon of the vinyl group, with respect to the carbonyl groups (1733 cm^{-1}), unambiguously suggested the covalent modulation of the "chemically reactive" dip coating with the selected alkylamine (i.e., ODA) as shown in Figure 2.4F. Furthermore, the morphology of the polymeric dip coating was examined with the FESEM study, where polymeric granular domains were randomly aggregated and provided a highly porous polymeric coating as shown in Figure 2.4G, and this embedded topography in the polymeric dip coating was appropriate for displaying extreme water repellency as shown in Figure 2.4C, D. The optical microscopic images and atomic force microscopic images in the Figure 2.4H-J also independently revalidated the existence of an appropriate hierarchical topography in the synthesized superhydrophobic coating. The roughness of the polymeric coating was found to be 790.43 ± 28.65 nm. However, the same reaction mixture of BPEI/5Acl, which was prepared in ethanol, provided a featureless (as confirmed with FESEM study, Figure 2.3C, D) "chemically reactive" polymeric coating. Even after post-covalent modification with ODA, the water droplet beaded on the polymeric coating with a static contact angle of ~107°.

2.3.2. Superhydrophobic Coatings with Chemically Tailored Roll-off Angles. In general, the optimization of the essential chemistry that confers superhydrophobicity is adopted following

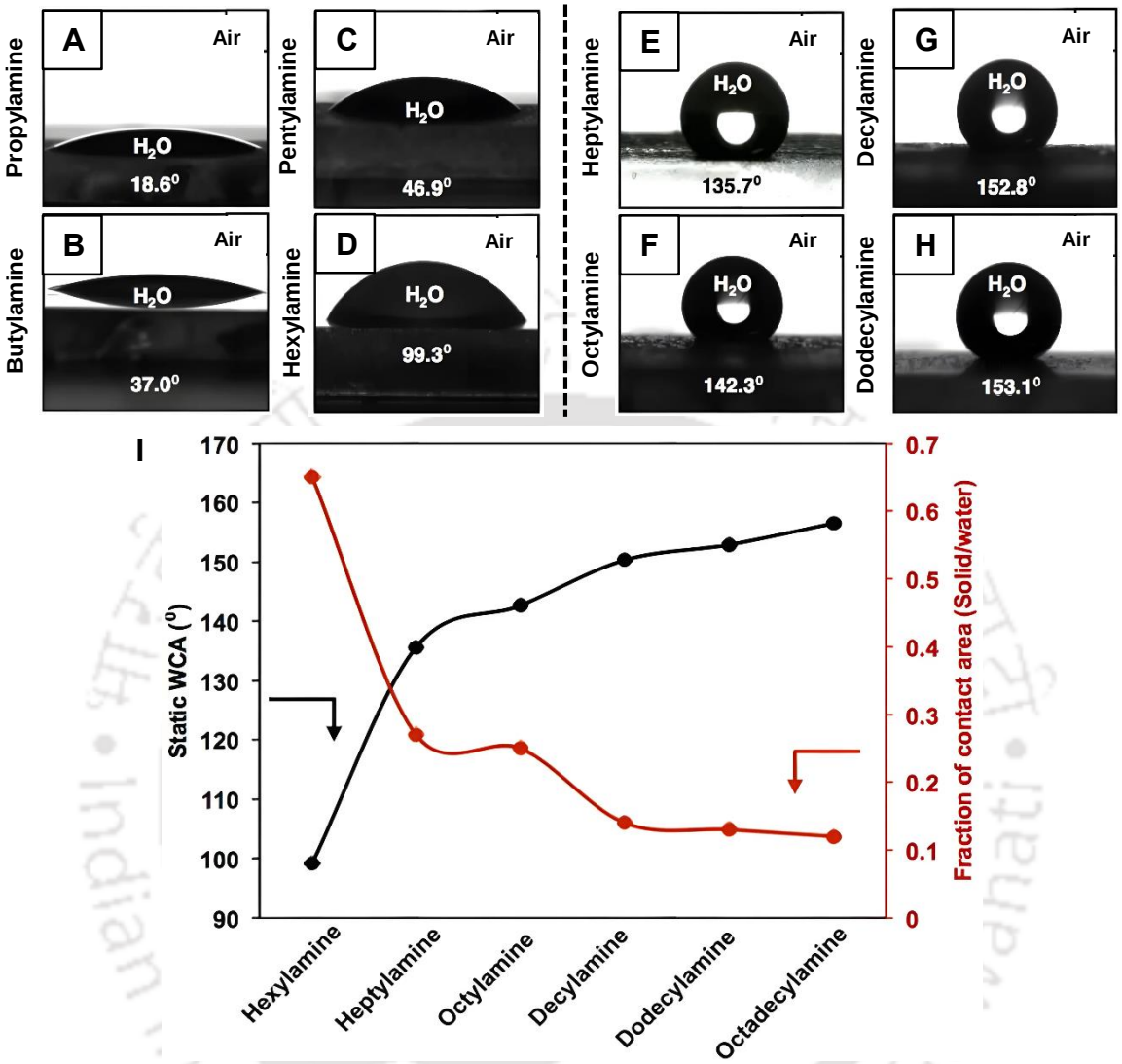

Figure 2.5. (A-H) Contact angles images of beaded water droplet on polymeric dip coatings (which is prepared from heptanol), after post chemical modifications with propylamine (A), butylamine (B), pentylamine (C), hexylamine (D), heptylamine (E), octylamine (F), decylamine (G), dodecylamine (H) through 1,4-conjugate addition reaction. (I) Illustration of the change of static water contact angles (black) and the fraction of contact area (red) between polymeric coating/beaded water droplet after post-modification of the "chemically reactive" polymeric coatings with n-hexyl amine and its higher analogues.

either the chemical vapor deposition of fluorinated molecules or immobilizing hydrocarbons through weak chemical bonding/interactions.[18,41–50] On the other side, the controlled regulation of the roll-off angle in superhydrophobic interfaces are mostly achieved through the modulation of the complex topography in the biomimicked interfaces.[58–63] Here, the "chemically reactive" polymeric dip coatings, which were prepared using heptanol, were post modified with various alkylamines for achieving chemically tailored water wettability, where the length of the hydrocarbon tail was gradually

increased from propylamine to octadecylamine as shown in Figure 2.5A-I. The hydrophobicity was gradually increased with post-modifications of the same polymeric dip coating with alkylamines having longer hydrocarbon tails (from heptylamine to ODA) as shown in Figure 2.6A-K, and the interface displayed extreme water repellency, where the metastable trapped air in the hierarchically same polymeric featured interface minimized the contact between the beaded aqueous phase and the solid interface. Next, the changes in the fraction of the contact area between the beaded water phase and polymeric dip coating have been estimated following the widely accepted equations 1 and 2,

$$\cos\theta_r = f_1 \cos\theta - f_2 \quad (1)$$

$$f_1 + f_2 = 1 \quad (2)$$

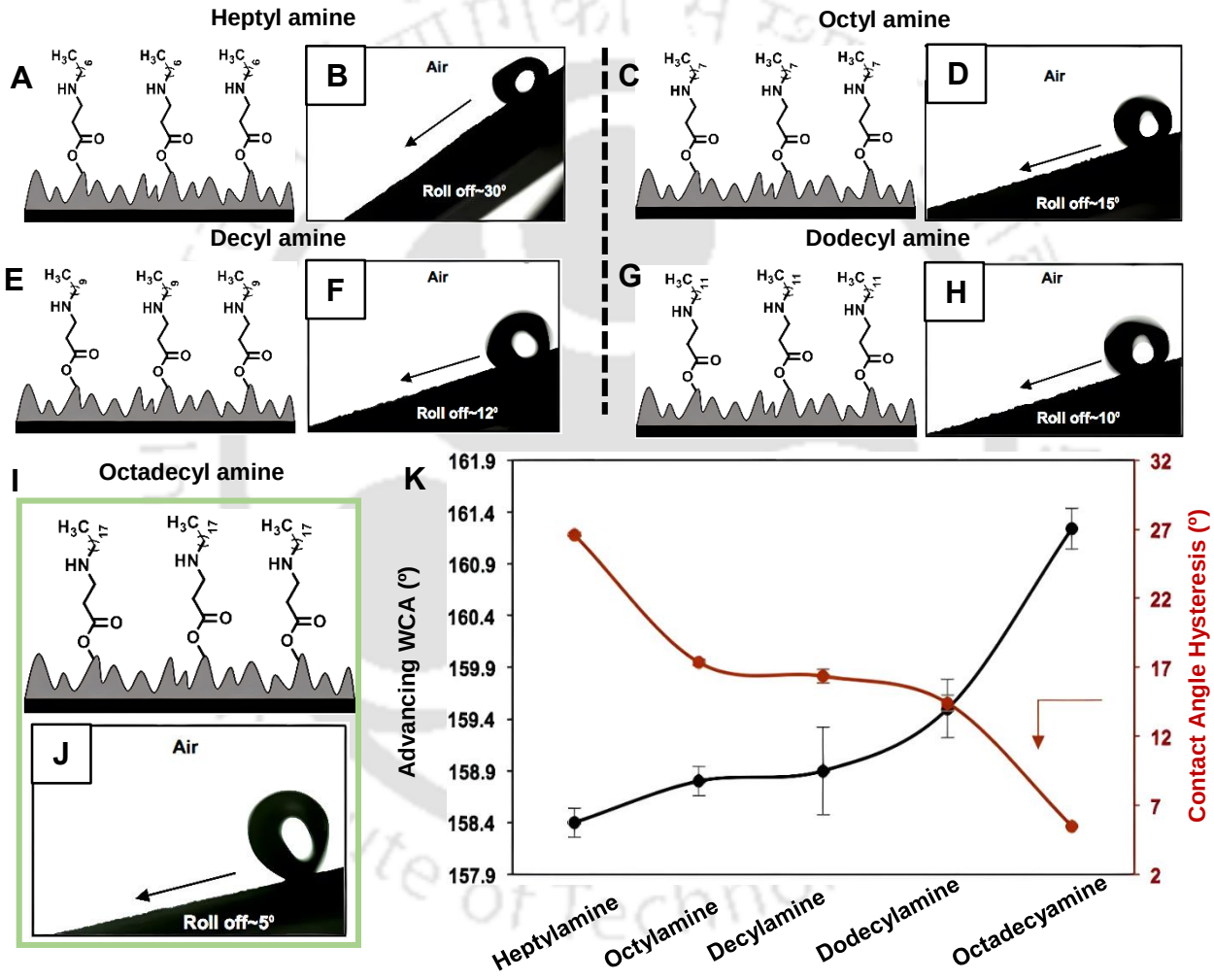

Figure 2.6. (A-J) Schematic representations of post-chemical modifications of "chemically reactive" dip coating with different alkyl-amines through a 1,4-conjugate addition reaction and (B, D, F, H, J) roll-off angle images of the beaded water droplet on polymeric dip coatings that are covalently modified with (A–B) 1-heptylamine, (C–D) 1- octylamine, (E–F) 1-decylamine, (G–H) dodecylamine, and (I–J) octadecylamine. (K) The plot accounting the change in contact angle hysteresis (red line) and advancing water contact angle (back line) with variation of hydrocarbon tail length of alkylamines that are used for post covalent modification of the chemically reactive coating through 1,4 conjugate addition reaction. The contact angle hysteresis is accounting the water adhesion property.

where θ and θ_r are the static water contact angle on smooth (ethanol was reaction medium, Figure 2.3B) and hierarchically (1-heptanol was reaction medium, Figure 2.4G) featured dip coatings, respectively, and both the polymeric coatings were post-modified with same alkylamines (from heptylamine to ODA) for maintaining an equivalent chemical functionality in the respective smooth and featured dip coatings, which are developed from respective alcoholic solvents (reaction media). Furthermore, the fraction of contact area for polymeric dip coating/beaded water droplet and trapped air/beaded water droplet are denoted as f_1 and f_2, respectively.

The gradual increase in the hydrocarbon tail length of the strategically selected alkylamine that are covalently immobilized in the "chemically reactive" dip coating allowed to reduce the fraction of contact area between the beaded water droplet and polymeric dip coating from 0.65 to 0.12, due to more entrapment of metastable trapped air as evident from Figure 2.5I (red curve). This gradual reduction in the contact area between beaded aqueous phase and polymeric coating provided a facile and chemically controlled avenue to design various superhydrophobic interfaces with a tailored receding contact angle and roll-off angles (which is defined as the minimum tilted angle of solid interfaces where beaded water droplets readily started rolling without any loss of the liquid phase) as shown in Figure 2.6. The "chemically reactive" polymeric dip coatings, which is post-modified with different alkylamines (from 1-heptaylamine to 1-ODA), displayed very similar advancing WCA (above 150°), however, the receding WCA was gradually altered. Eventually, the contact angle hysteresis was gradually increased (Figure 2.6) with decreasing the hydrocarbon tail length of selected alkylamines (from octadecylamine to heptylamine). Furthermore, the gradual increase in the roll-off angle of the beaded water droplet on different chemically modified interfaces independently revalidating the existence of tailored water adhesion in the as synthesized superhydrophobic dip coatings.

The porous polymeric dip coating displayed superhydrophobicity with an advancing water contact angle of above 155° and a roll-off angle of 30° after post-covalent modifications with heptylamine, and the same "chemically reactive" coatings were embedded with superhydrophobicity with lower roll-off angles after the post-covalent modulation of the polymeric dip coating with higher analogues of heptylamine as shown in Figure 2.6B, D, F, H, J. The beaded water droplet readily rolled off on the octylamine-treated dip coating at a tilting angle of ≥15°, whereas the interface that was treated with dodecylamine displayed a roll-off angle of ≥10° and a further increase in the hydrocarbon tail length (i.e., ODA) provided a superhydrophobic coating with an even lower roll-off angle that was 5°.

2.3.3. Durability of Superhydrophobic Dip Coatings. Furthermore, ODA-treated, non-adhesive superhydrophobic dip coating was exposed to various physical and chemical challenges to investigate its tolerance under practically relevant various and severe settings. Different standard abrasive

physical challenges like adhesive tape test, abrasive sand paper test, and sand drop test were imposed on the synthesized polymeric dip coating (Figure 2.7A−H). First, a freshly exposed adhesive surface was brought in contact with the superhydrophobic dip coating with an applied external load of 1 kg, where the external applied load facilitated the uniform contact between the adhesive surface and superhydrophobic interface. During the manual peeling of the adhered adhesive surface from the dip coating, the top portion of the superhydrophobic polymeric coating was arbitrarily cleaved and readily transferred to the adhesive surface (Figure 2.7C), and at the end, a physically damaged dip coating

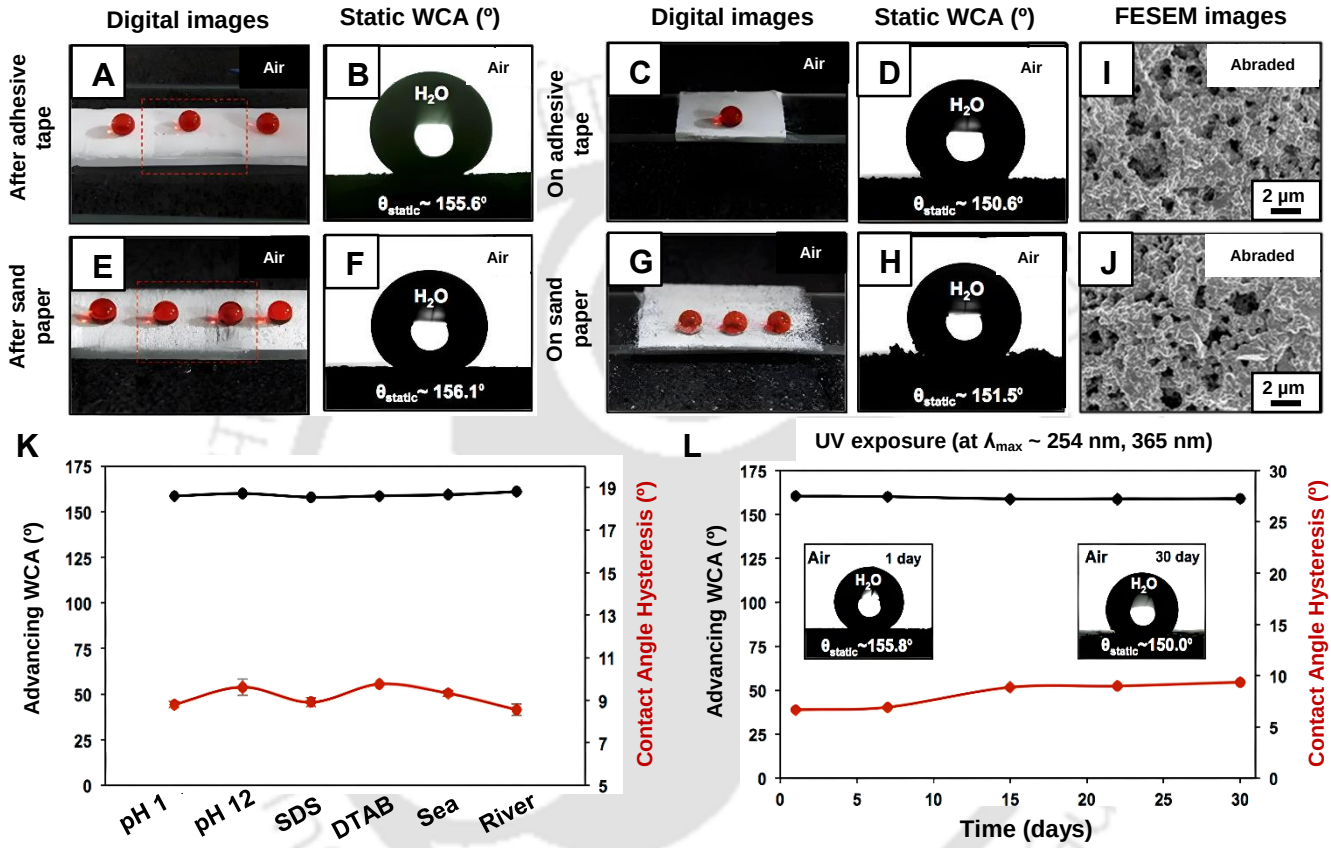

Figure 2.7. (A, C, E, G) Digital images and (B, D, F, H) static water contact angle images of beaded water droplet on the freshly exposed interior of the polymeric dip coating after performing (A−D) severe adhesive tape peeling test and (E−H) sand paper abrasion test, respectively. (A, E) Dotted red box indicating the physically abraded area of the dip coating because of (A) adhesive tape test and (E) sand paper abrasion test. (C) Arbitrarily cleaved and (G) physically eroded top interface of the dip coating, which were immobilized on an (C) adhesive tape and (G) abrasive sand paper, respectively, continued to display (C, D, G, H) extreme water repellency. (I, J) FESEM images of the physically abraded polymeric dipcoatings after performing (I) adhesive tape test and (J) sand paper abrasion test. (K) Plot accounting the advancing water contact angles (WCA, black curve) and WCA hysteresis (red curve) of the beaded droplet on the polymeric dip coating after its prolonged (30 days) immersion in acidic (pH 1) water, alkaline (pH 12) water, SDS (1 mM)/DTAB (1 mM)-contaminated aqueous phases, artificial sea water, and river water. (L) Graph illustrating the change in the advancing WCA (black curve) and WCA hysteresis (red curve) on the beaded droplet on the dip coating after exposure to UV light (λmax = 254 nm and λmax = 365 nm) over 30 days.

with freshly exposed interior (indicated with red dotted box in Figure 2.7A) was observed. However, this physically abraded polymeric dip coating displayed an uninterrupted extreme water repellency

with an advancing WCA of ~159° as shown in Figure 2.7B, moreover, the cleaved interface of dip coating attached on the adhesive surface (Figure 2.7C) also displayed superhydrophobicity (Figure 2.7D). Furthermore, the morphology of the physically abraded interface was examined with an FESEM study (Figure 2.7I, J), where the granular domains were remained arbitrarily aggregated and provided an appropriate topography for adopting superhydrophobicity. Next, the same as synthesized superhydrophobic dip coating on a glass substrate was exposed to an abrasive sand paper (3 × 1 cm) with an applied load of 500 g, where the abrasive interface was manually moved with back and forth motion for 25 times, and during this abrasion process, a top interface of the polymeric dip coating was physically eroded in the form of white powder, which was physically deposited on the abrasive sand paper as shown in Figure 2.7G. However, the water droplet beaded on such physically damaged interface (indicated with a dotted red box in Figure 2.7E) with an advancing WCA of 160° and the eroded powdery material that physically deposited on the abrasive sand paper also appeared to be extremely water repellent as shown in Figure 2.7G, H. After performing the sand paper abrasion test, the topography of physically damaged polymeric dip coating was examined with FESEM imaging, a hierarchically featured interface, which is appropriate for conferring extreme water repellency, is observed as shown in Figure 2.7J.

Furthermore, sand grains (100 g) were allowed to pour on the synthesized superhydrophobic dip coating from a height of 20 cm, where the substrate was tilted with an angle of 45°; however, both the physical integrity and the embedded water wettability remained intact. Thus, the synthesized polymeric dip coating was inherently capable of sustaining severe physical challenges, including different kinds of arbitrary physical abrasions, without compromising the embedded extreme water repellency, which is attributed to the bulk (including the top and interior of the coating) optimization of essential physical/chemical parameters (that confers extreme water repellency) in the "chemically reactive" dip coating. Thereafter, as synthesized superhydrophobic coatings were kept continuously under various harsh chemical settings, including highly acidic aqueous phases (pH ~ 1), highly alkaline aqueous phases (pH ~ 12), surfactant (sodium dodecylsulphate (SDS, 1 mM), dodecyltrimethylammonium bromide (DTAB, 1 mM))-contaminated water, artificial sea water, and river water (Bramhaputra river, Assam) for a prolonged duration (30 days) to investigate the impact of these practically relevant and challenging chemical settings on the embedded superhydrophobicity. However, these polymeric dip coatings continued to display extreme water repellency with an advancing WCA above 155° and a contact angle hysteresis below 10° after washing and air-drying the biomimicked dip coating, as shown in Figure 2.7K. Furthermore, the synthesized dip coating withstood the prolonged (30 days) irradiation of UV (with maximum wavelengths at 254 nm and 365 nm) light, and an aqueous droplet beaded on the UV light-treated superhydrophobic coating with an advancing WCA above 155° and a contact angle hysteresis below 10° as shown in Figure 2.7L. Such exemplary durability of the embedded

superhydrophobicity at severe chemical challenges is achieved through the rational and in situ association of the nanocomplex and followed by the post-covalent modulation of the "chemically reactive" dip coating through robust and rapid 1,4-conjugate addition reaction between amine and acrylate groups.

2.3.4. Substrate-Independent Superhydrophobic Coating and Design of Functional Materials. In the past, generally, the substrate-independent superhydrophobic coatings were referred to the process, which are capable of providing biomimicked coatings on water-insoluble, flexible, and rigid

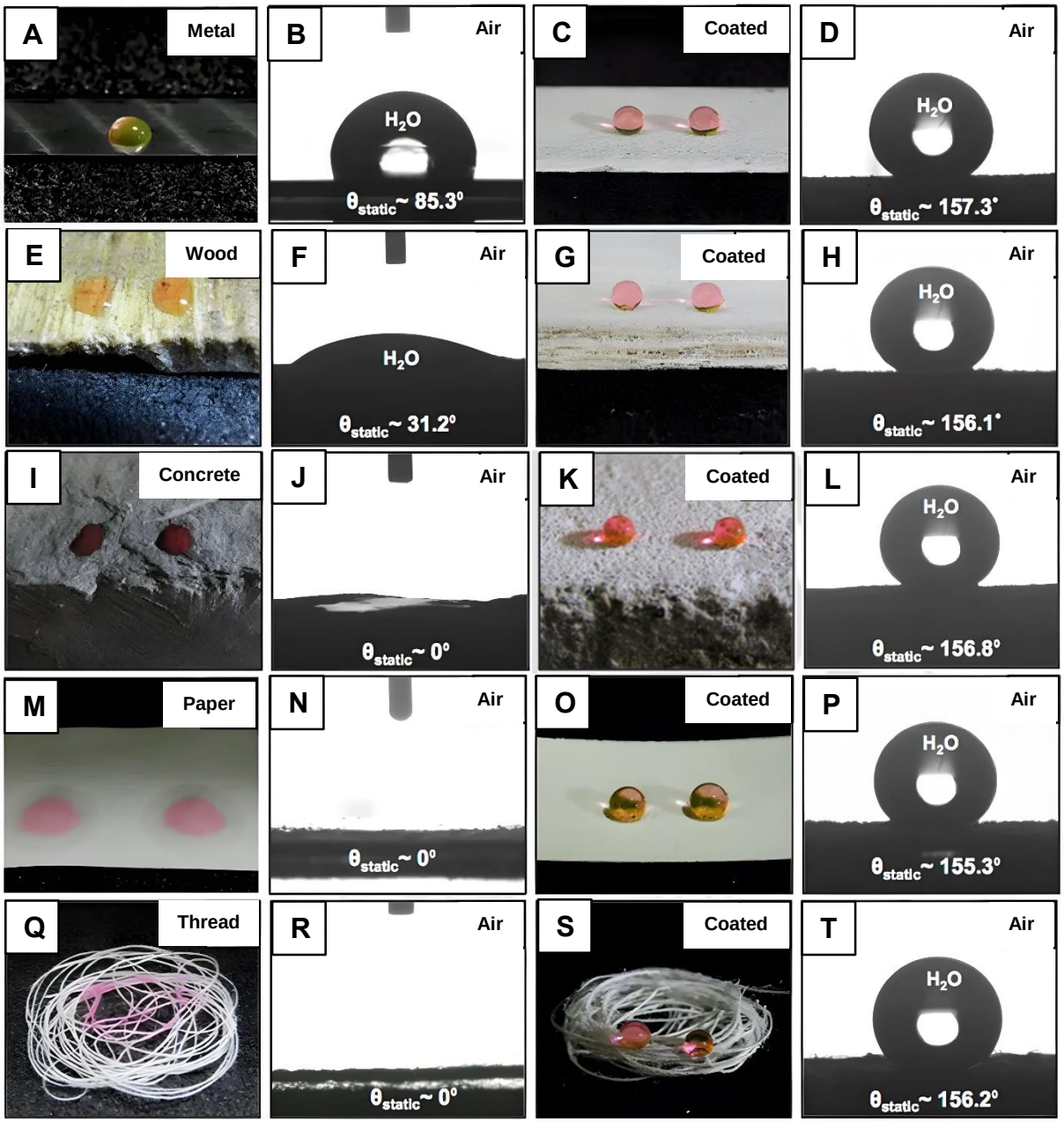

Figure 2.8. (A-T) Digital images (A, C, E, G, I, K, M, O, Q, S) and static contact angle images (B, D, F, H, J, L, N, P, R, T) of the beaded water droplet on uncoated and various superhydrophobic dip-coated objects i.e., (A−D) metal, (E−H) wood, (I−L) concrete, (M−P) filter paper, and (Q−T) cotton threads.

interfaces,[18–24] even though such approaches are inappropriate for achieving superhydrophobic coating on geometrically complex and (or) water-soluble/water-sensitive substrates.

Here, this water-immiscible heptanol medium-based "chemically reactive" and in situ dip coating approach was extended further for the coating of a wide range of substrates including a flexible and rigid planar interface, a geometrically complex fibrous substrate, a water-sensitive substrate, and even a water-soluble substrate. For a proof-of-concept demonstration, metal, wood, concrete, and filter paper were selected as model rigid and flexible planar substrates for depositing polymeric dip coatings, and all the hydrophilic interfaces became extremely water repellent with a static WCA above 155°, as shown in Figure 2.8A−P. Next, a highly flexible and superhydrophilic cotton thread having a more complex geometry was also successfully decorated with biomimicked super water wettability following a "chemically reactive" dip coating process as shown in Figure 2.8Q−T. Next, litmus paper and sugar cubes are selected as model water-sensitive and water-soluble substrates, respectively, for demonstrating successful deposition of the superhydrophobic coating without compromising the integrity of the water-soluble components in the selected substrates. First, litmus paper was taken as a model water-sensitive substrate (Figure 2.9A, B), where the water soluble litmus dye is physically deposited on the fibrous paper and was successfully decorated with biomimicked dip coating, and the dip-coated (post-modified with ODA) litmus paper became extremely water repellent with an advancing WCA of ~159°, as shown in Figure 2.9C, D. The topography of the coated litmus paper was further characterized by an FESEM study, where the polymeric dip coating consisted of randomly aggregated diffuse granular domains, which eventually provided a hierarchically featured porous interface (Figure 2.9E, F) that conferred an extreme water repellency, as shown in Figure 2.9C. Next, the superhydrophobic litmus paper was exposed to various and relevant manual deformations including bending, twisting, and creasing; however, the embedded super-water repellency remained unaffected on the creased area of the coating with an advancing WCA of above 156°, as shown in Figure 2.9G- J. Furthermore, this superhydrophobic litmus paper was extended for the proof-of-concept demonstration of the physical defect-triggered spatially selective rapid infiltration of the aqueous phase. This process is fundamentally interesting for developing smart materials (e.g., hydrophilic/superhydrophobic pattern). First, a water-soluble litmus loaded paper, which was coated with superhydrophobic dip coating, was exposed to acidic (pH 1) water droplets. The acidic water droplet beaded on the coated litmus paper with high WCA (~155°), and no change in color on the coated litmus paper on the area of beading was noted, likely due to the restricted ingression of the acidic aqueous phase to the pH-responsive water-soluble litmus dyes. Next, a few holes were manually introduced to the superhydrophobic litmus paper to expose the underneath hydrophilic substrate that was loaded with water-soluble litmus dye, and acidic water droplets were placed both on the physically damaged interface (manual holes) and the unaffected area of the coating, as shown in Figure 2.9K.

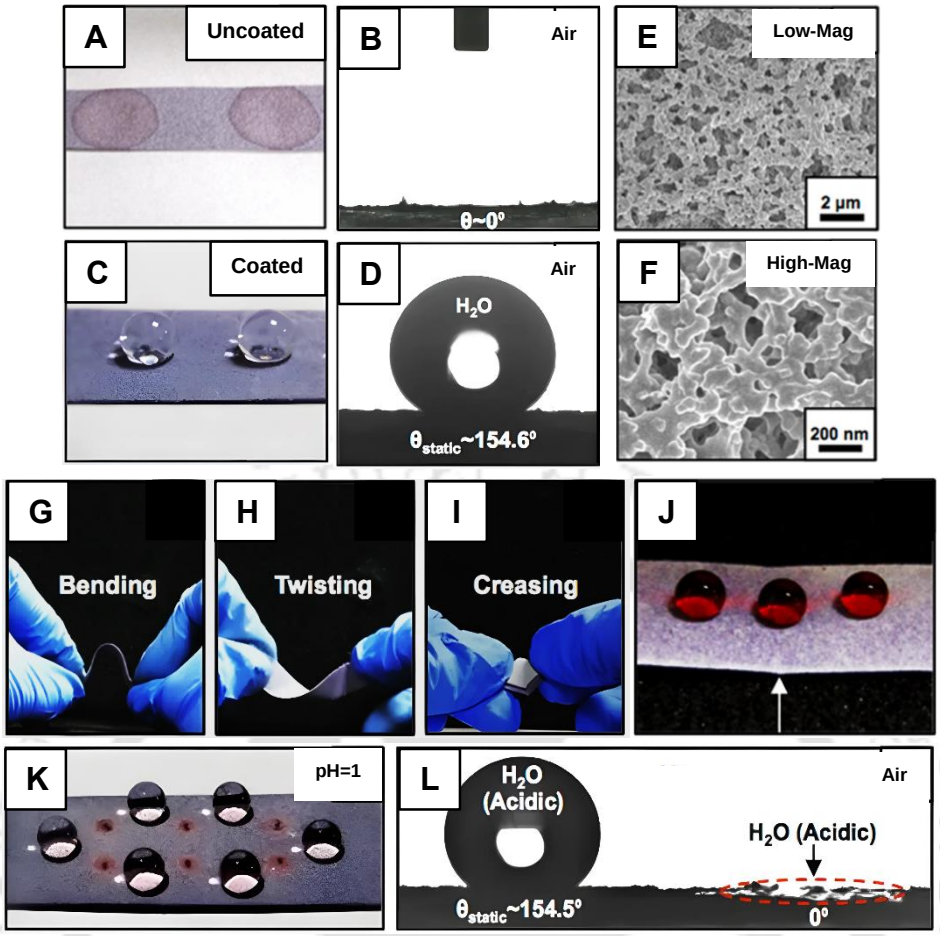

Figure 2.9. (A, C) Digital images and (B, D) contact angle images of the beaded water droplet on both (A, B) uncoated and (C, D) superhydrophobic dip-coated blue litmus paper. (E, F) FESEM images of dip-coated litmus paper at (E) low and (F) high magnifications. (G–I) Digital images depicting various common physical manipulations including (G) bending, (H) twisting, and (I) creasing. (J) Illustration of the beading of the water droplet on the polymeric coating after performing these physical manipulations, the white arrow indicating the creased mark on the superhydrophobic litmus paper. (K) Digital image and (L) contact angle image describing the beading/wetting of acidic (pH 1) water droplets on superhydrophilic/superhydrophobic patterned interface of the dipcoated litmus paper, where the superhydrophilic domain is incurred through introducing of manual holes, and rest of the area remained superhydrophobic. These holes soaked the acidic water and immediately the color of litmus paper changed from blue to red around each hole.

The acidic water droplets, which were placed on the holes are immediately soaked in the litmus paper and turned the color of litmus dye from blue to red. This instant change in the color of the litmus dye revealed that the process of the superhydrophobic coating did not alter the pH-responsive property of the litmus dye. This simple study also provided a basis to develop the physical damage-guided superhydrophobic/superhydrophilic-patterned interface (Figure 2.9L). Furthermore, such an interface would be useful in the physical defect-triggered release of bioactive small molecules, where physical defects would control the rate of infiltration of the aqueous phase in the material and eventually control the release of the loaded cargo. Thereafter, a highly water soluble substrate, which is a sugar cube (can soak the water droplet immediately with WCA = 0°; Figure 2.10A, B) was successfully coated

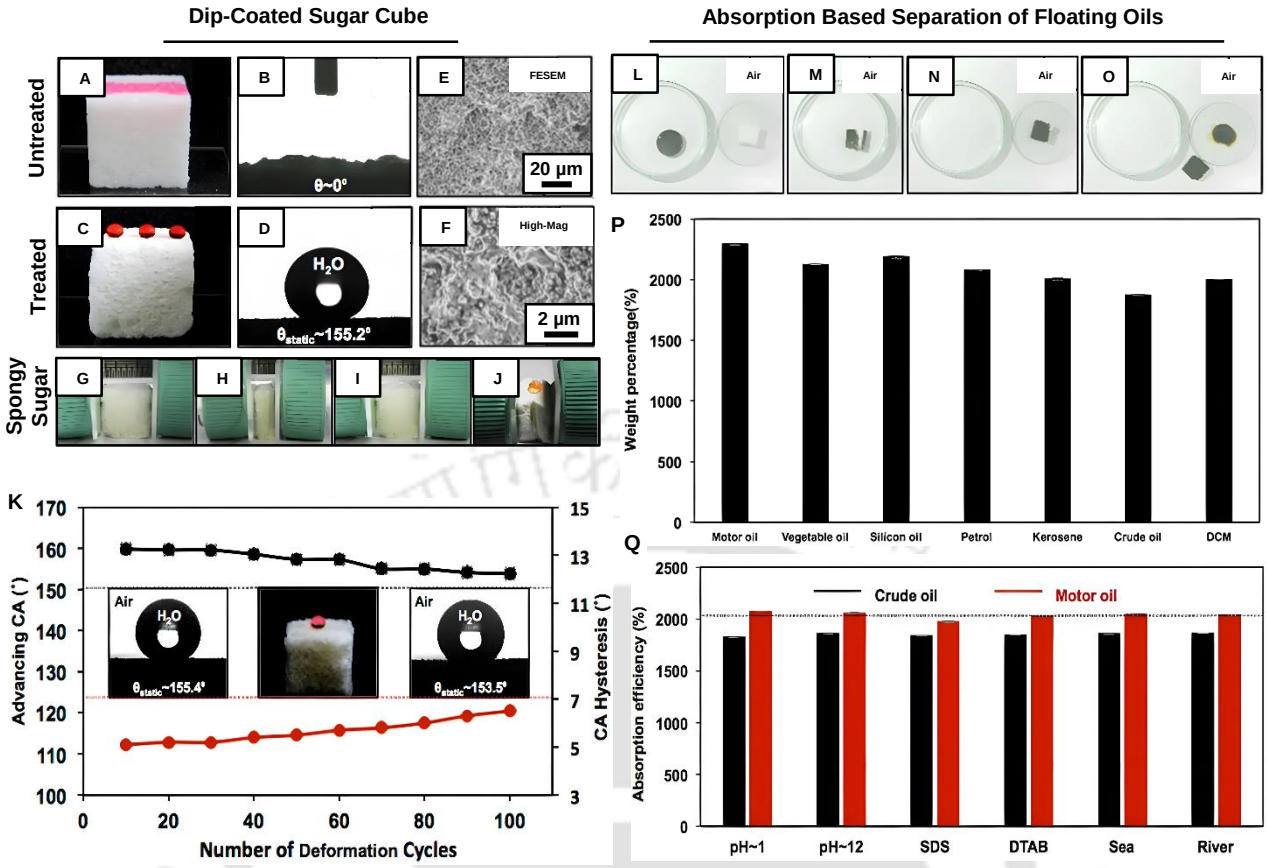

Figure 2.10. (A, C) Digital images and (B, D) contact angle images of beaded water droplet (red color aids visual inspection) on (A, B) uncoated and (C, D) superhydrophobic dip-coated sugar cubes. (E, F) FESEM images accounting the topography of dip-coated sugar cube at both (E) low and (F) high magnifications. (G–I) Digital images depicting the compressive deformation and autorecovery of the sugar cube-derived spongy polymeric material; the superhydrophobic sugar cube became a spongy polymeric material after sacrificing the water-soluble sugar substrate. (J) Digital image of the beaded water droplet on the compressed spongy material. (K) Plot illustrating the variation in advancing WCA (black curve) and WCA hysteresis (red curve) during the manual compressive deformation of the spongy polymeric material 100 times. (L–O) Digital images demonstrating the (L–N) successful separation of the floating (L) crude oil from the aqueous phase using a sugar cube-derived spongy superhydrophobic material, and (O) application of a compressive strain allowed to recollect the absorbed crude oil from the material. (P) Plot accounting the efficiency of absorbing various oils/oily phase (motor oil, vegetable oil, silicon oil, petrol, kerosene, crude oil, and DCM). (Q) Illustration of the selective oil-absorption capacity of the superhydrophobic sponge under different harsh chemical environments.

with the polymeric dip coating and the material became extremely water repellent with an advancing WCA of 158°, as shown in Figure 2.10C, D. The morphology of the polymeric dip coating was analyzed with an FESEM study, and a hierarchically featured interface was characterized with arbitrary arrangements of polymeric granular domains as shown in Figure 2.10E, F. As such, the biomimicked superhydrophobic coating allowed protection of water-soluble substrates from accidental exposure of the aqueous phase. Moreover, this superhydrophobic coating on a water-soluble sugar cube provided a facile basis for developing a spongy superhydrophobic material by the strategic sacrifice of the underneath water-soluble substrate (Figure 2.10G-J). The embedded extreme water repellency of the superhydrophobic sugar cube was likely to restrict the dissolution of the underneath substrate (e.g.,

sugar cube) in water. So, the external trapped air that conferred the extreme water repellency was first tactfully removed from the superhydrophobic sugar cube by exposing the material in ethanol. Then, the ethanol-soaked material was placed in DI (deionized) water for 1 h, followed by a thorough washing of the material with water before air-drying. After this treatment, the water-soluble sugar cube was dissolved out from the material and provided a much lighter (97.3% weight loss) and highly (80%) compressible material, as shown in Figure 2.10G, H. Moreover, the shape and size of the material self-recovered after releasing the applied compressive stress, as shown in Figure 2.10I. Then, the water wettability was examined on the spongy substrate after sacrificing the underneath water-soluble template and followed by post-treatment with 5Acl and ODA, and the material continued to display extreme water repellency with an advancing WCA of 160.3° and this embedded

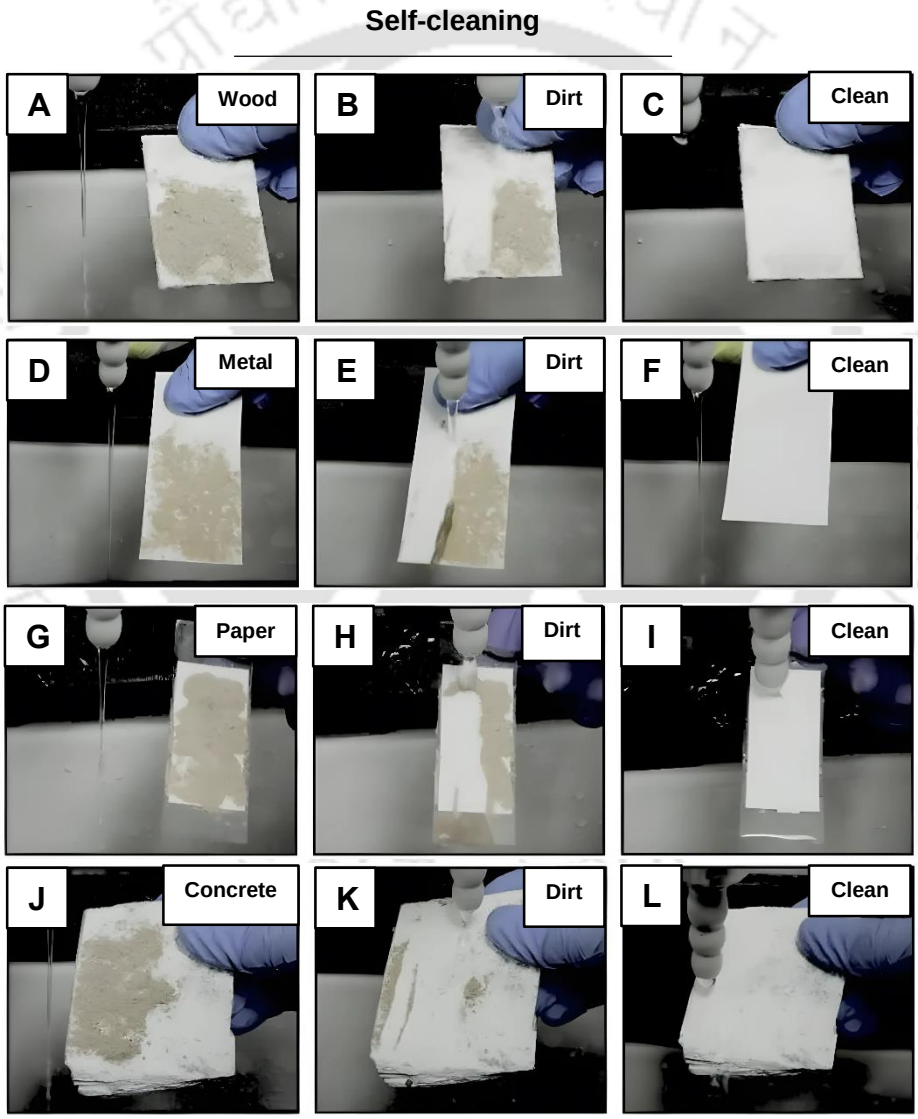

Figure 2.11. (A-L) Digital photographs are illustrating the self-cleaning performance of the superhydrophobic dip coating on wood (A-C); metal (D-F); filter paper (G-I) and concrete (J-L).

superhydrophobicity remained unaffected even after incurring a compressive strain in the material, as shown in Figure 2.10J.

Next, this superhydrophobic spongy material was repetitively deformed for 100 cycles; however, the water repellency was observed to be remained intact with an advancing WCA above 150° and a contact angle hysteresis below 10°, as shown in Figure 2.10K. Such highly compressible and porous superhydrophobic substrate was further extended in environment-friendly remediation of oil spillages following the selective and spontaneous absorption principle. As a proof-of-concept demonstration, a piece of as synthesized superhydrophobic sponge was brought in contact with a droplet of crude oil that was floating on an aqueous phase, as shown in Figure 2.10L; immediately, the crude oil started absorbing in the material, as shown in Figure 2.10M, N, and finally the crude oil was successfully separated with an absorption capacity of above 1850 wt%. Then, the crude oil-absorbing superhydrophobic material was removed from aqueous phase and manually squeezed to redistribute the absorbed oil in a separate container as shown in Figure 2.10O.

This process was successfully repeated with various other oils including motor oil, vegetable oil, silicone oil, petrol, diesel, and kerosene, and the selective oil-absorption capacity was estimated to be ≥2000 wt % as shown in Figure 2.10P. Furthermore, this oil-absorption capacity remained unaffected in various practically relevant and severe chemical settings including extremes of pH, surfactants (DTAB, SDS), contaminated water, river water, and artificial sea water, as shown in Figure 2.10Q. Thus, the embedded superhydrophobic coating is capable of performing under various severe chemically challenging settings.

Furthermore, experiments were designed to demonstrate the performance of the synthesized superhydrophobic coating in presence of practically relevant, different, and extreme physical challenges. The biomimicked dip coatings that were deposited on various rigid and flexible objects were extended for demonstration of the self-cleaning of dust and dirt-contaminated surfaces. First of all, superhydrophobic-dip-coated wood, metal, filter paper, and concrete were contaminated with dust particles, and the biomimicked interfaces were found to be readily self-cleaned under the stream of water as shown in Figure 2.11A−L, where the deposited dust were collected on the air/water interfaces of the beaded water droplet, which was readily rolled-off from the tilted surface of respective coated substrates due to existence of non-adhesive superhydrophobicity. Such a demonstration of self-cleaning on the artificial biomimicked interface, without exposure to any physically abrasive challenges, is commonly demonstrated in literature. However, in the present study, the self-cleaning demonstration was rarely performed with physically abraded superhydrophobic coatings. Superhydrophobic filter paper was selected as the model substrate for such demonstration, where this superhydrophobic flexible substrate was exposed to various severe physical challenges, for example, creasing, sand paper abrasion, and adhesive tape test, prior to examining the rolling of beaded water droplet on the tilted

interface. After incurring these practically relevant physical challenges to the superhydrophobic filter paper, the physical integrity of the biomimicked dip coating was damaged, and some top portions

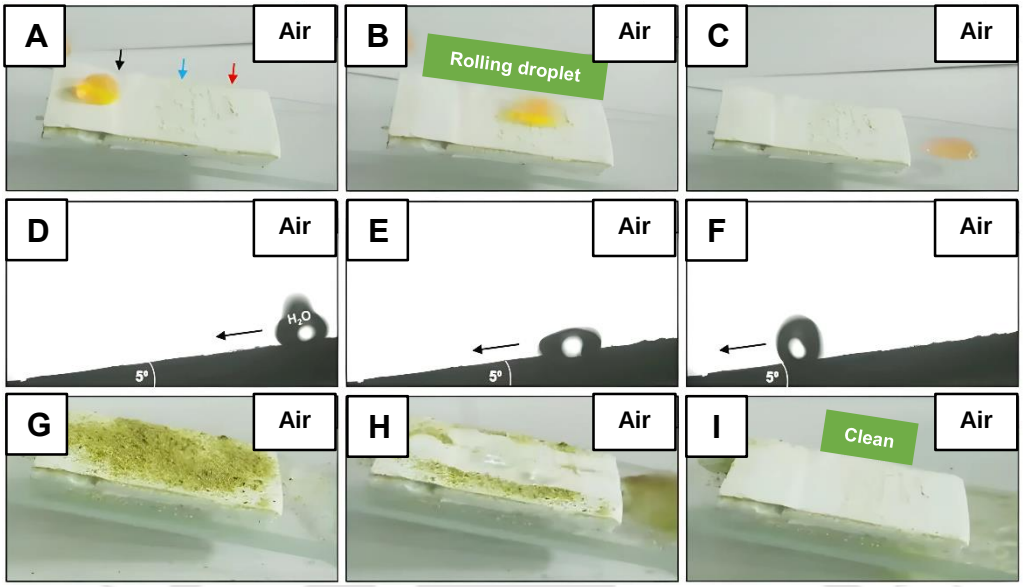

Figure 2.12. (A–C) Digital images and (D–F) contact angle images illustrating the rolling of beaded water droplets on the physically and arbitrarily abraded superhydrophobic interface (that was kept tilted at 5°); the black, blue, and red arrows indicate the areas of dip coating, which were exposed to creasing, adhesive tape peeling test, and sand paper abrasion test, respectively. (G–I) Digital images illustrating the self-cleaning of the deposited dust from the same physically abraded superhydrophobic coating.

(indicated with blue and red arrow, Figure 2.12A) of the coating were physically abraded as noted in Figure 2.12A. However, beaded water droplet readily rolled off on the physically damaged superhydrophobic interface (which was tilted at a 5° angle) as shown in Figure 2.12B–F. This simple study unambiguously revalidated the existence of uninterrupted non-adhesive superhydrophobicity in the physically damaged dip coating. Furthermore, this physically abraded superhydrophobic interface was contaminated with dust particles, and as expected, the physically damaged biomimicked coating remained highly capable of self-cleaning the deposited dust upon aqueous exposure as shown in Figure 2.12G–I. Thus, the current biomimicked dip coating was capable of performing both self-cleaning and environmental remediation of oil spills under practically relevant, severe physical and chemical settings, respectively. Such "absolutely" substrate-independent and highly durable and facile superhydrophobic dip coating would be useful in developing other various relevant functional materials for a wide range of applications at diverse and challenging "real-world" scenarios.

2.4. Conclusions

In this current report, a facile, highly scalable, and "chemically reactive" single-step dip coating approach is unprecedentedly introduced for developing an "absolutely" substrate-independent and severe abrasions-tolerant biomimicked coating. A mutual and catalyst-free 1,4-conjugate addition reaction between the amine and acrylate groups of BPEI and 5Acl, respectively, in selected alcoholic solvent, provided an elegant basis for (a) in situ deposition of a "chemically reactive" polymeric nanocomplex on various selected substrates to develop a porous polymeric coating in a single step, and (b) post-covalent modification of the polymeric dip coating with different alkylamines allowed to achieve the desired water wettability. Thus, both essential topography and appropriate chemistry was optimized through a 1,4-conjugate addition reaction and eventually yielded superhydrophobicity with different roll-off angles. Such superhydrophobic coatings are with a potential for controlled and no-loss transfer of tiny aqueous droplets. Furthermore, the synthesized superhydrophobicity was inherently tolerant toward both severe and diverse chemical and physical challenges, even when the biomimicked dip coating was capable of sustaining physical abrasions, and the exposed interiors of the coating displayed an uninterrupted extreme water wettability. Such biomimicked dip coatings with exemplary durability were successfully applied on various substrates including water-stable, water-sensitive, water-soluble, flexible, rigid, planar, and geometrically complex objects. The superhydrophobic coating on water-sensitive and water-soluble substrates allowed the designing of a highly compressible and durable superhydrophobic sponges. The physical damage on the superhydrophobic litmus paper triggered a spatially selective rapid infiltration of the aqueous phase, whereas highly compressible superhydrophobic sponges allowed the selective absorption-based environmentally friendly remediation of crude oil and other oil/oily spillages at various chemically challenging settings. Furthermore, the synthesized superhydrophobic coating was also capable of performing under harsh physical settings and the self-cleaning performance was successfully demonstrated with physically and arbitrarily abraded superhydrophobic coating on filter paper. Thus, the current report provided a simple chemical approach for synthesizing highly tolerant and "absolutely" substrate-independent superhydrophobic coatings that are capable of performing in various practically relevant and challenging settings.

2.5. References

1) Barthlott, W.; Neinhuis, C. Purity of the Sacred Lotus, or Escape from Contamination in Biological Surfaces. *Planta* **1997**, *202*, 1−8.
2) Feng, L.; Zhang, Z.; Mai, Z.; Ma, Y.; Liu, B.; Jiang, L.; Zhu, D. A Super-Hydrophobic and Super-oleophilic Coating Mesh Film for the Separation of Oil and Water. *Angew. Chem., Int. Ed.* **2004**, *43*, 2012− 2014.

3) Li, X. M.; Reinhoudt, D.; Crego-Calama, M. What do we need for a Superhydrophobic Surface? A Review on the Recent Progress in the Preparation of Superhydrophobic Surfaces. *Chem. Soc. Rev.* **2007**, *36*, 1350−1368.
4) Song, W.; Veiga, D. D.; Custodio, C. A.; Mano, J. F. Bioinspired Degradable Substrates with Extreme Wettability Properties. *Adv. Mater.* **2009**, *21*, 1830−1834.
5) Yao, X.; Song, Y.; Jiang, L. Applications of Bio-Inspired Special Wettable Surfaces. *Adv. Mater.* **2011**, *23*, 719−734.
6) Yohe, S. T.; Colson, Y. L.; Grinstaff, M. W. Superhydrophobic Materials for Tunable Drug Release: Using Displacement of Air to Control Delivery Rates. *J. Am. Chem. Soc.* **2012**, *134*, 2016−2019.
7) Zhu, Q.; Chu, Y.; Wang, Z.; Chen, N.; Lin, L.; Liu, F.; Pan, Q. Robust Superhydrophobic Polyurethane Sponge as a Highly Reusable Oil-Absorption Material. *J. Mater. Chem. A* **2013**, *1*, 5386−5393.
8) Ueda, E.; Levkin, P. A. Emerging Applications of Super- hydrophilic-Superhydrophobic Micropatterns. *Adv. Mater.* **2013**, *25*, 1234−1247.
9) Darmanin, T.; Guittard, F. Recent Advances in the Potential Applications of Bioinspired Superhydrophobic Materials. *J. Mater. Chem. A* **2014**, *2*, 16319−16359.
10) Wen, L.; Tian, Y.; Jiang, L. Bioinspired Super-Wettability from Fundamental Research to Practical Applications. *Angew. Chem., Int. Ed.* **2015**, *54*, 3387−3399.
11) Wang, H.; Wang, E.; Liu, Z.; Gao, D.; Yuan, R.; Sun, L.; Zhu, Y. A Novel Carbon Nanotubes Reinforced Superhydrophobic and Superoleophilic Polyurethane Sponge for Selective Oil−Water Separation through a Chemical Fabrication. *J. Mater. Chem. A* **2015**, *3*, 266−273.
12) Jayaramulu, K.; Datta, K. K. R.; Rösler, C.; Petr, M.; Otyepka, M.; Zboril, R.; Fischer, R. A. Biomimetic Superhydrophobic/ Superoleophilic Highly Fluorinated Graphene Oxide and ZIF-8 Composites for Oil-Water Separation. *Angew. Chem., Int. Ed.* **2016**, *55*, 1178−1182.
13) Su, B.; Tian, Y.; Jiang, L. Bioinspired Interfaces with Superwettability: From Materials to Chemistry. *J. Am. Chem. Soc.* **2016**, *138*, 1727−1748.
14) Gao, A.; Wu, Q.; Wang, D.; Ha, Y.; Chen, Z.; Yang, P. A Superhydrophobic Surface Templated by Protein Self-Assembly and Emerging Application toward Protein Crystallization. *Adv. Mater.* **2016**, *28*, 579−587.
15) Falde, E. J.; Yohe, S. T.; Colson, Y. L.; Grinstaff, M. W. Superhydrophobic Materials for Biomedical Applications. *Biomaterials* **2016**, *104*, 87−103.
16) Wu, Y.; Feng, J.; Gao, H.; Feng, X.; Jiang, L. Superwettability- Based Interfacial Chemical Reactions. *Adv. Mater.* **2019**, *31*, 1800718.
17) Zhang, S.; Huang, J.; Chen, Z.; Yang, S.; Lai, Y. Liquid Mobility on Superwettable Surfaces for

Applications in Energy and the Environment. *J. Mater. Chem. A* **2019**, *7*, 38−63.

18) Li, Y.; Li, L.; Sun, J. Bioinspired Self-Healing Superhydrophobic Coatings. *Angew. Chem., Int. Ed.* **2010**, *49*, 6129−6133.
19) Mates, J. E.; Ibrahim, R.; Vera, A.; Guggenheim, S.; Qin, J.; Calewarts, D.; Waldroupd, D. E.; Megaridis, C. M. Environmentally- safe and Transparent Superhydrophobic Coatings. *Green Chem.* **2016**, *18*, 2185−2192.
20) Schlaich, C.; Camacho, L. C.; Yu, L.; Achazi, K.; Wei, Q.; Haag, R. Surface-Independent Hierarchical Coatings with Superamphipho- bic Properties. *ACS Appl. Mater. Interfaces* **2016**, *8*, 29117−29127.
21) Zhi, D.; Lu, Y.; Sathasivam, S.; Parkin, I. P.; Zhang, X. Large- scale Fabrication of Translucent and Repairable Superhydrophobic Spray Coatings with Remarkable Mechanical, Chemical Durability and UV Resistance. *J. Mater. Chem. A* **2017**, *5*, 10622−10631.
22) Schlaich, C.; Wei, Q.; Haag, R. Mussel-Inspired Polyglycerol Coatings with Controlled Wettability: From Superhydrophilic to Superhydrophobic Surface Coatings. *Langmuir* **2017**, *33*, 9508−9520.
23) Ren, T.; He, J. Substrate-Versatile Approach to Robust Antireflective and Superhydrophobic Coatings with Excellent Self- Cleaning Property in Varied Environments. *ACS Appl. Mater. Interfaces* **2017**, *9*, 34367−34376.
24) Baidya, A.; Ganayee, M. A.; Ravindran, S. J.; Tam, K. C.; Das, S. K.; Ras, R. H. A.; Pradeep, T. Organic Solvent-Free Fabrication of Durable and Multifunctional Superhydrophobic Paper from Water-borne Fluorinated Cellulose Nanofiber Building Blocks. *ACS Nano* **2017**, *11*, 11091−11099.
25) Wang, H.; Xue, Y.; Ding, J.; Feng, L.; Wang, X.; Lin, T. Durable, Self-Healing Superhydrophobic and Superoleophobic Surfaces from Fluorinated-decyl Polyhedral Oligomeric Silsesquioxane and Hydrolyzed Fluorinated Alkyl Silane. *Angew. Chem., Int. Ed.* **2011**, *50*, 11433−11436.
26) Deng, X.; Mammen, L.; Zhao, Y.; Lellig, P.; Müllen, K.; Li, C.; Butt, H. J.; Vollmer, D. Transparent, Thermally Stable and Mechanically Robust Superhydrophobic Surfaces Made from Porous Silica Capsules. *Adv. Mater.* **2011**, *23*, 2962−2965.
27) Zhu, X.; Zhang, Z.; Men, X.; Yang, J.; Wang, K.; Xu, X.; Zhou, X.; Xue, Q. Robust Superhydrophobic Surfaces with Mechanical Durability and Easy Repairability. *J. Mater. Chem.* **2011**, *21*, 15793− 15797.
28) Mates, J. E.; Bayer, I. S.; Palumbo, J. M.; Carroll, P. J.; Megaridis, C. M. Extremely Stretchable and Conductive Water- repellent Coatings for Low-cost Ultraflexible Electronics. *Nat. Commun.* **2015**, *6*, 8874−8881.
29) Wu, M.; Li, Y.; An, N.; Sun, J. Applied Voltage and Near- Infrared Light Enable Healing of Superhydrophobicity Loss Caused by Severe Scratches in Conductive Superhydrophobic Films. *Adv. Funct. Mater.* **2016**, *26*, 6777−6784.

30) Paven, M.; Fuchs, R.; Yakabe, T.; Vollmer, D.; Kappl, M.; Itakura, A. N.; Butt, H. J. Mechanical Properties of Highly Porous Super Liquid-Repellent Surfaces. *Adv. Funct. Mater*. **2016**, *26*, 4914−4922.

31) Levkin, P. A.; Svec, F.; Frećhet, J. M. Porous Polymer Coatings: a Versatile Approach to Superhydrophobic Surfaces. *Adv. Funct. Mater*. **2009**, *19*, 1993−1998.

32) Manna, U.; Broderick, A. H.; Lynn, D. M. Chemical Patterning and Physical Refinement of Reactive Superhydrophobic Surfaces. *Adv. Mater*. **2012**, *24*, 4291−4295.

33) Deng, X.; Mammen, L.; Butt, H. J.; Vollmer, D. Candle Soot as a Template for a Transparent Robust Superamphiphobic Coating. *Science* **2012**, *335*, 67−70.

34) Yohe, S. T.; Grinstaff, M. W. A Facile Approach to Robust Superhydrophobic 3D Coatings via Connective-particle Formation using the Electrospraying Process. *Chem. Commun.* **2013**, *49*, 804−806.

35) Keshtov, M. L.; Marochkin, D. V.; Kochurov, V. S.; Khokhlov, R.; Koukaras, E. N.; Sharma, G. D. New conjugated Alternating Benzodithiophene-containing Copolymers with Different Acceptor Units: Synthesis and Photovoltaic Application. *J. Mater. Chem. A* **2014**, *2*, 155−171.

36) Manna, U.; Lynn, D. M. Restoration of Superhydrophobicity in Crushed Polymer Films by Treatment with Water: Self-Healing and Recovery of Damaged Topographic Features Aided by an Unlikely Source. *Adv. Mater*. **2013**, *25*, 5104−5108.

37) Parbat, D.; Gaffar, S.; Rather, A. M.; Gupta, A.; Manna, U. A General and Facile Chemical Avenue for the Controlled and Extreme Regulation of water wettability in Air and oil wettability Under Water. *Chem. Sci*. **2017**, *8*, 6542−6554.

38) Das, A.; Sengupta, S.; Deka, J.; Rather, A. M.; Raidongia, K; Manna, U. Synthesis of fish scale and lotus leaf mimicking, Stretchable and Durable Multilayers. *J. Mater. Chem. A* **2018**, *6*, 15993−16002.

39) Das, A.; Deka, J.; Raidongia, K.; Manna, U. Robust and Self- Healable Bulk-Superhydrophobic Polymeric Coating. *Chem. Mater*. **2017**, *29*, 8720−8728.

40) Jana, N.; Parbat, D.; Manna, U. Rational Use of Dual Chemical Reactivity in a Single Interface for Optimizing both Super- hydrophobicity and Underwater Superoleophobicity. *Chem. Mater*. **2019**, *31*, 1479−1484.

41) Feng, X. J.; Jiang, L. Design and Creation of Superwetting/ Antiwetting Surfaces. *Adv. Mater*. **2006**, *18*, 3063−3078.

42) Yan, Y. Y.; Gao, N.; Barthlott, W. Mimicking Natural Superhydrophobic Surfaces and Grasping the Wetting Process: a Review on Recent Progress in Preparing Superhydrophobic Surfaces. Adv. *Colloid Interface Sci*. **2011**, *169*, 80−105.

43) Toma, M.; Loget, G.; Corn, R. M. Flexible Teflon Nanocone Array Surfaces with Tunable

Superhydrophobicity for Self-Cleaning and Aqueous Droplet Patterning. *ACS Appl. Mater. Interfaces* **2014**, *6*, 11110−11117.

44) Wang, S.; Liu, K.; Yao, X.; Jiang, L. Bioinspired Surfaces with Superwettability: New Insight on Theory, Design, and Applications. *Chem. Rev.* **2015**, *115*, 8230−8293.

45) Wu, M.; Ma, B.; Pan, T.; Chen, S.; Sun, J. Silver-Nanoparticle- Colored Cotton Fabrics with Tunable Colors and Durable Antibacterial and Self-Healing Superhydrophobic Properties. *Adv. Funct. Mater.* **2016**, *26*, 569−576.

46) Osicka, J.; Ilcǐkova,́M.; Popelka, A.; Filip, J.; Bertok, T.; Tkac, J.; Kasak, P. Simple, Reversible, and Fast Modulation in Super- wettability, Gradient, and Adsorption by Counterion Exchange on Self-Assembled Monolayer. *Langmuir* **2016**, *32*, 5491−5499.

47) Han, Z.; Li, B.; Mu, Z.; Niu, S.; Zhang, J.; Ren, L Energy- Efficient Oil-Water Separation of Biomimetic Copper Membrane with Multiscale Hierarchical Dendritic Structures. *Small* **2017**, *13*, 1701121.

48) Zhou, C.; Chen, Z.; Yang, H.; Hou, K.; Zeng, X.; Zheng, Y.; Cheng, J. Nature-Inspired Strategy toward Superhydrophobic Fabrics for Versatile Oil/Water Separation. *ACS Appl. Mater. Interfaces* **2017**, *9*, 9184−9194.

49) Zang, D.; Zhu, R.; Zhang, W.; Yu, X.; Lin, L.; Guo, X.; Liu, M.; Jiang, L. Corrosion-Resistant Superhydrophobic Coatings on Mg Alloy Surfaces Inspired by Lotus Seedpod. Adv. Funct. Mater. 2017, 27, 1605446.

50) Milionis, A.; Sharma, C. S.; Hopf, R.; Uggowitzer, M.; Bayer, I. S.; Poulikakos, D. Engineering Fully Organic and Biodegradable Superhydrophobic Materials. *Adv. Mater. Interfaces* **2019**, *6*, 1970007.

51) Verho, T.; Bower, C.; Andrew, P.; Franssila, S.; Ikkala, O.; Ras, R. H. A. Mechanically Durable Superhydrophobic Surfaces. *Adv. Mater.* **2011**, *23*, 673−678.

52) Farrer, R. A.; LaFratta, C. N.; Li, L.; Praino, J.; Naughton, M. J.; Saleh, B. E. A.; Teich, M. C.; Fourkas, J. T. Selective Functionalization of 3-D Polymer Microstructures. *J. Am. Chem. Soc.* **2006**, *128*, 1796− 1797.

53) Wang, G.; Fang, Y.; Kim, P.; Hayek, A.; Weatherspoon, M. R.; Perry, J. W.; Sandhage, K. H.; Marder, S. R.; Jones, S. C. Layer-By- Layer Dendritic Growth of Hyperbranched Thin Films for Surface Sol−Gel Syntheses of Conformal, Functional, Nanocrystalline Oxide Coatings on Complex 3D (Bio)silica Templates. *Adv. Funct. Mater.* **2009**, *19*, 2768−2776.

54) Ford, J.; Marder, S. R.; Yang, S. Growing "Nanofruit" Textures on Photo-Crosslinked SU-8 Surfaces through Layer-by-Layer Grafting of Hyperbranched Poly(Ethyleneimine). *Chem. Mater.* **2009**, *21*, 476−483.

55) Bechler, S. L.; Lynn, D. M. Reactive Polymer Multilayers Fabricated by Covalent Layer-by-Layer

Assembly: 1,4-Conjugate Addition-Based Approaches to the Design of Functional Biointerfaces. *Biomacromolecules* **2012**, *13*, 1523−1532.

56) Parbat, D.; Manna, U. Synthesis of 'reactive' and Covalent Polymeric Multilayer Coatings with Durable Superoleophobic and Superoleophilic Properties Under Water. *Chem. Sci.* **2017**, *8*, 6092−6102.

57) Rather, A. M.; Shome, A.; Kumar, S.; Bhunia, B. K.; Mandal, B. B.; Srivastava, H. K.; Manna, U. Alkali Metal-ion Assisted Michael Addition Reaction in Controlled Tailoring of Topography in a Superhydrophobic Polymeric Monolith. *J. Mater. Chem. A* **2018**, *6*, 17019−17031.

58) Cheng, Z.; Feng, L.; Jiang, L. Tunable Adhesive Superhydrophobic Surfaces for Superparamagnetic Microdroplets. *Adv. Funct. Mater.* **2008**, *18*, 3219−3225.

59) Lee, W.; Park, B. G.; Kim, D. H.; Ahn, D. J.; Park, Y.; Lee, S. H.; Lee, K. B. Nanostructure-dependent Water-droplet Adhesiveness Change in Superhydrophobic Anodic Aluminum Oxide Surfaces: from Highly Adhesive to Self-cleanable. *Langmuir* **2010**, *26*, 1412−1415.

60) Zhang, D.; Chen, F.; Yang, Q.; Yong, J.; Bian, H.; Ou, Y.; Si, J.; Meng, X.; Hou, X. A Simple way to Achieve Pattern-dependent Tunable Adhesion in Superhydrophobic Surfaces by a Femtosecond Laser. *ACS Appl. Mater. Interfaces* **2012**, *4*, 4905−4912.

61) Zhang, E.; Wang, Y.; Lv, T.; Li, L.; Cheng, Z.; Liu, Y. Bio- inspired Design of Hierarchical PDMS Microstructures with Tunable Adhesive Superhydrophobicity. *Nanoscale* **2015**, *7*, 6151−6158.

62) Nine, M. J.; Tung, T. T.; Alotaibi, F.; Tran, D. N. H.; Losic, D. Facile Adhesion-Tuning of Superhydrophobic Surfaces between "Lotus" and "Petal" Effect and Their Influence on Icing and Deicing Properties. *ACS Appl. Mater. Interfaces* **2017**, *9*, 8393−8402.

63) Yang, C.; Wu, L.; Li, G. Magnetically Responsive Superhydrophobic Surface: In Situ Reversible Switching of Water Droplet Wettability and Adhesion for Droplet Manipulation. *ACS Appl. Mater. Interfaces* **2018**, *10*, 20150−20158.

Chapter 3. Water Repellent Conductive Pattern Interface for Monitoring Human Motions and Expressions

The conversion of mechanical deformation into electrical signals is a widely used principle for various relevant applications. Facile and scalable fabrication, ultrahigh-sensitivity, low-response time and uninterrupted performance under severe conditions are hallmarks of an efficient strain-sensor that would be suitable for realistic application. In the past, various approaches were introduced to achieve high gauge factor—mainly associated with a large tensile deformation. But, in reality, a flexible strain sensor that displays a high gauge factor at low applied strain and remains efficient under practically relevant diverse and challenging conditions would be more appropriate for unambiguous and effective monitoring of human motions and other relevant applications. But, a low-strain sensor with ultrahigh sensitivity and durability is yet to be introduced in the literature. Here, a metal-free, chemically reactive and conductive ink is unprecedentedly introduced following a 1,4-conjugate addition reaction. Furthermore, a strategic integration of a chemically reactive porous paper with the prepared conductive ink allowed the development of a chemically reactive and conductive interface that allowed desired post covalent modification with selected alkylamines under ambient conditions. Taking advantage of the spatially selective deposition of the prepared ink on chemically reactive paper and the ability of post covalent modification of the prepared ink, an abrasion tolerant superhydrophobic and conductive patterned interface was developed for achieving a low-strain (below 0.2%) based flexible strain sensor with an ultrahigh sensitivity (gauge factor ~ 18300) and low response time (8 ms). The external low-strain induced cracks on the flexible and durable superhydrophobic and conductive patterned interface provided a facile basis for real-time and wireless monitoring of slow, fast, weak and strong human motions and expressions—under diverse conditions, including continuous aqueous exposures, physical abrasions etc.

* S. Das *et al.*, *Mater. Horiz.* **2021**, *8*, 2851–2858

3.1. Introduction

The conversion of mechanical deformation into an electrical signal in the form of voltage, resistance etc. has remained a facile basis for developing different functional materials.[1–5] In this context, different nanomaterials are strategically associated to achieve conductive flexible/stretchable interfaces having organized and complex topography for a wide range of potential applications—including wireless monitoring of human motion, soft robotics, electronic skin, etc.[6–15] The desired requisites of an efficient strain sensor that would be appropriate for practical applications are (a) high sensitivity (means high gauge factor), (b) low response time and (c) ability to perform under practically relevant challenging settings. In the past, various metal and other conductive nanomaterials have been associated following some complex deposition process to achieve strain sensors—but only stretchable strain sensors displayed high gauge factor on incurring a large tensile deformation.[6–15] In reality, the repetitive and large tensile deformation is known to lead unwanted fatigue and failure in polymeric and soft materials.[16] Furthermore, the attachment of a highly stretchable interface with the human skin at different and relevant parts of the body demands special and additional arrangements for achieving desired and unambiguous results.[17] On the other side, the conductive hydrogels are another important class of materials that allowed the development of stretchable strain sensors with high sensitivity and wide detection range. But, the hydrogels can be readily deformed and remained highly sensitive to the relative humidity of the environment. In fact, such materials are inadequate to sustain harsh physical and chemically complex aqueous exposures.[18–20] Hence, the design of a flexible sensor with a high gauge factor that performed at low applied strain (below 0.5%) would be a more appropriate approach for various relevant applications. Nevertheless, in the recent past, a few important designs were introduced to report strain sensors with improved sensitivity, linearity, response time, stability, and detection limits—following a relatively simple fabrication process.[21–26] Unfortunately, the report of extremely water repellent and abrasion tolerant low-strain based sensors with ultrahigh gauge factor is yet to be introduced in the literature. In our current design, a flexible, non-stretchable and environmentally friendly substrate was extended to design a low strain based (below 0.5%) and non-stretchable motion sensor with high sensitivity. Under realistic settings, a strain sensor is likely to face severe abrasive and complex aqueous exposures—but the tolerance of reported strain sensors towards both physical and chemical challenges has barely been examined in the past.[6–15] Recently, the association of extreme water repellency with strain sensors has emerged as an effective approach for preventing unwanted perturbation of the electrical signal during exposure to practically relevant complex and common aqueous conditions.[27–34] In this context, most of the reported conductive superhydrophobic interfaces were derived from environmentally hazardous and fluorinated molecules;[27–30] moreover, barely any reported approach demonstrated the tolerance of the prepared superhydrophobic conductive interface under severe abrasive conditions[27–34] —which is extremely important for its realistic applications. In this paper, we have introduced a simple and roust chemical approach to report (i) a physical abrasion tolerant, (ii) superhydrophobic and (iii) low-strain (0.2%)

based resistive strain sensor with (iv) an ultra-high gauge factor (~18300), (v) low (8 ms) response time and (vi) high stability (15000 cycles) for (vii) real time and wireless monitoring of different human motions/expressions—even in the presence of continuous aqueous exposure.

3.2. Experimental Section

3.2.1. Materials. Dipentaerythritol pentaacrylate (5Acl, MW ~524.21 g mol^{-1}), (3-aminopropyl)trimethoxysilane (APTMS, MW ~179.29 g mol^{-1}) and octadecylamine (ODA) were purchased from Sigma-Aldrich, Bangalore, India. Ethanol was acquired from TEDIA, USA. Glass slides and abrasive (grit no. 400) sand paper were bought from Jain Scientific Glass Works and Million International, India respectively. Adhesive tape (Johnson tape Ltd. India), Fountain Pen (Legend Executive Fountain Pen) and filter paper (Whatman 42) was supplied by local sources. Hydrochloric acid (~37%), Hydrazine Hydrate (~80%) and ammonia solution (~25%) were purchased from Merck Life Science Pvt. Ltd., Mumbai, India. Graphite fine powder and Methylene Blue dye were acquired from LOBA Chemie, Mumbai, India. $MgCl_2$, $MgSO_4$, NaCl, and $CaCl_2$, all of these salts were bought from Emplura, Mumbai, India.

3.2.2. General Considerations. KRUSS Drop Shape analyser-DSA25 instrument was used to measure all of the water contact angles, which actually contained an auto systematic liquid dispenser. Scanning Electron Microscopy images were obtained by using a Carl Zeiss Field Emission Scanning Electron Microscope (FESEM), prior to imaging a gold sputtered thin layer was prepared on all the samples. PerkinElmer UATR instrument was used to record ATR-FTIR spectrum of all the samples at ambient conditions. The digital images of the samples were taken by using Nikon Coolpix b700 digital camera. Thickness of the material was measured by using stylus surface profilometer (Veeco-Dektak 150).

3.2.3. Amino-Graphene Oxide (AGO) Synthesis. A reported procedure was followed to prepare aminographene oxide (AGO),[1] where two consecutive reactions (nitration and reduction) were adopted to synthesize AGO from the freshly prepared GO sheets. In nitration step, 50 mg of air dried GO powder was dispersed in 50% nitric acid (100 mL), and the whole reaction mixture was kept under stirring for 12 hours at ambient condition. After completion of the reaction, obtained product was filtered to be separated and washed thoroughly with acetone followed by vacuum drying. Next, the freshly prepared nitro graphene oxide was dispersed in 50:50 ethanol–water mixture with a concentration of 0.1 mg/mL. Thereafter, adequate amount of ammonium hydroxide (150 µL) and hydrazine hydrate (50 µL) were added into the reaction mixture under continuous agitation—such that the reaction temperature maintained at 70 °C.

3.2.4. Preparation of Chemically Reactive Conductive Ink. A reaction mixture was prepared where 1 ml of 5-Acl (concentration of 132.5 mg/ml), 100 mg of AGO and 100 µL of APTMS were mixed and sonicated for 20 minutes at ambient condition before applying to the selected substrates. The reaction

mixture was remained chemically reactive due to presence of residual acrylate groups. The deposition of the chemically reactive interface provided conductive interface with resistance of 3.2 KΩ. The amount of AGO controlled the resistance of the deposited ink.

3.2.5. Fabrication of Superhydrophobic and Conductive Interface. Firstly, a chemically reactive polymeric coating that loaded with residual acrylate groups was developed on a selected paper (filter paper, A4 Paper, tracing paper) following a previous reported procedure,[2] where the selected papers were individually dip coated in a reaction mixture of 5-Acl/BPEI. Thereafter, the chemically reactive ink was spatially selectively deposited on the chemically reactive paper to develop various pattern interfaces following different printing approaches, such as stamp printing, screen printing etc. Then, the chemically reactive ink deposited interface was thoroughly washed with ethanol and air-dried prior to treat with octadecylamine (ODA) for overnight. The post-chemical modification with ODA allowed to achieve desired water repellency.

3.2.6. Physical Durability of the Superhydrophobic and Conductive Interfaces.

The tolerance of the prepared superhydrophobic and conductive pattern interface under various practically relevant challenging environments was examined by adopting widely accepted and standard physical abrasion tests—including adhesive tape peeling test, random scratch test and sand paper abrasion test etc.

3.2.7. Adhesive Tape Test. First, a freshly exposed adhesive tape (3 × 1 cm) was applied on the superhydrophobic and conductive interface (3 × 1 cm) with an external load to facilitate a uniform contact. Thereafter, the adhesive tape was removed from the superhydrophobic and conductive interface. Both the water-wettability and electrical property of the treated interface were examined in details. All of these properties were observed to be intact even after 25 cycles of such abrasions.

3.2.8. Sand Paper Abrasion Test. An abrasive sand paper (3 × 1 cm) was brought in the contact of the superhydrophobic and conductive interface under an external load of 100 g. Next, the abrasive sand paper was manually rubbed with back-and-forth motion (speed of 7 cm/s) for 25 times. During this abrasion, the underlying interior of the material was exposed in air and the top portion was randomly abraded. Thereafter, the water wettability and electrical properties were investigated for the sand paper treated interface.

3.2.9. Scratch Test. The superhydrophobic and conductive interface was arbitrarily scratched multiple times by using a sharp-edged knife and then the water-repellent property and conductivity of the interface was examined.

3.2.10. Characterization of Electrical Property. The DC characterization of the synthesized superhydrophobic and conductive pattern interface (denoted as strain sensor) was conducted through the Keithley 4200 SCS pulse parametric analyzer. The prepared strain sensor was studied with 10um

Tungsten probes of the Precise's Everbeing BD-6 probe station (generally recognized as Device Under Test, DUT). The connections 4 between the probe station and the pulse parametric analyzer were established through tri-axial cables to obtain low noise and low leakage during the measurements. Moreover, each measurement was done with 4200 SCS (semiconductor characterization system) card combined with a remote preamplifier unit of the analyzer, which on combination have extremely low current measuring capability (~1fA). Different human motions and expressions were monitored in air and under water exposures by employing a tri-axial cable with crocodile clips at the DUT end.

3.2.11. DATA Acquisition System.

The data acquisition system comprises of the following three parts:

3.2.12. Arduino Nano Board. The Arduino Nano board (version 3) which has an AVR architecture ATMEGA 328 microcontroller clocking at 16 MHz with an operating voltage of 5 Volts was employed for acquiring the data from the synthesized strain sensor. This board is compact (18 x 45 mm) and light weight (approximately 7 grams) which makes it suitable for wearable applications. The superhydrophobic and conductive pattern interface was integrated in a simple voltage divider circuit with a tunable resistor (to tune and accommodate different patterned sensor strip with different inherent or base resistances). The output of this voltage divider was proportional to the change in the resistance of the strain sensor on bending the pattern interface. This output voltage read through one of the ADC (analogue to digital converter) pins of the Arduino Nano and mapped to the corresponding resistance. These values were further supplied to the transceiver (Tx/Rx) pins. Moreover, LCD display allowed to display this data.

3.2.13. Bluetooth Module (HC 05). The data acquisition system was interfaced with the Bluetooth module HC-05 to transmit the data from strain sensor to the receiver, i.e. an android mobile phone. This module was again compact (26.9mm x 13mm x 2.2 mm) and light weight to assure wearable aspects. The module requires 5 Volt DC supply. It utilized Bluetooth V2.0+EDR which operated at 2.4 GHz ISM band and has improved data rate of 2Mbps. The obtained values from the transceiver (Tx/Rx) pins of the Arduino microcontroller were transmitted with a baud rate of 9600 over 2.4 GHz ISM bandwidth. The emission power of the module was below 4dBm which 5 provided a working range of 10 meters between the receiver and transmitter with either Android Mobile or Laptop with Bluetooth connectivity.

3.2.14. A Display Device (Smart Phone/ Laptop). Any android mobile or laptop with Bluetooth connectivity can be used to receive the transmitted data over the Bluetooth bandwidth through the proper pairing of the Bluetooth modules and setting up the baud rate of 9600. In our demonstration, an android mobile phone was used to obtain the data through serial data display programs or apps.

3.3. Results and Discussions

3.3.1. Development of Chemically Reactive and Conductive Patterned Interfaces.

In our current design, 1,4-conjugate addition reaction that appeared as an important avenue for developing various functional and smart materials,[35–37] has been extended for achieving a chemically reactive and conductive ink as shown in Figure 3.1A through the strategic association of the selected

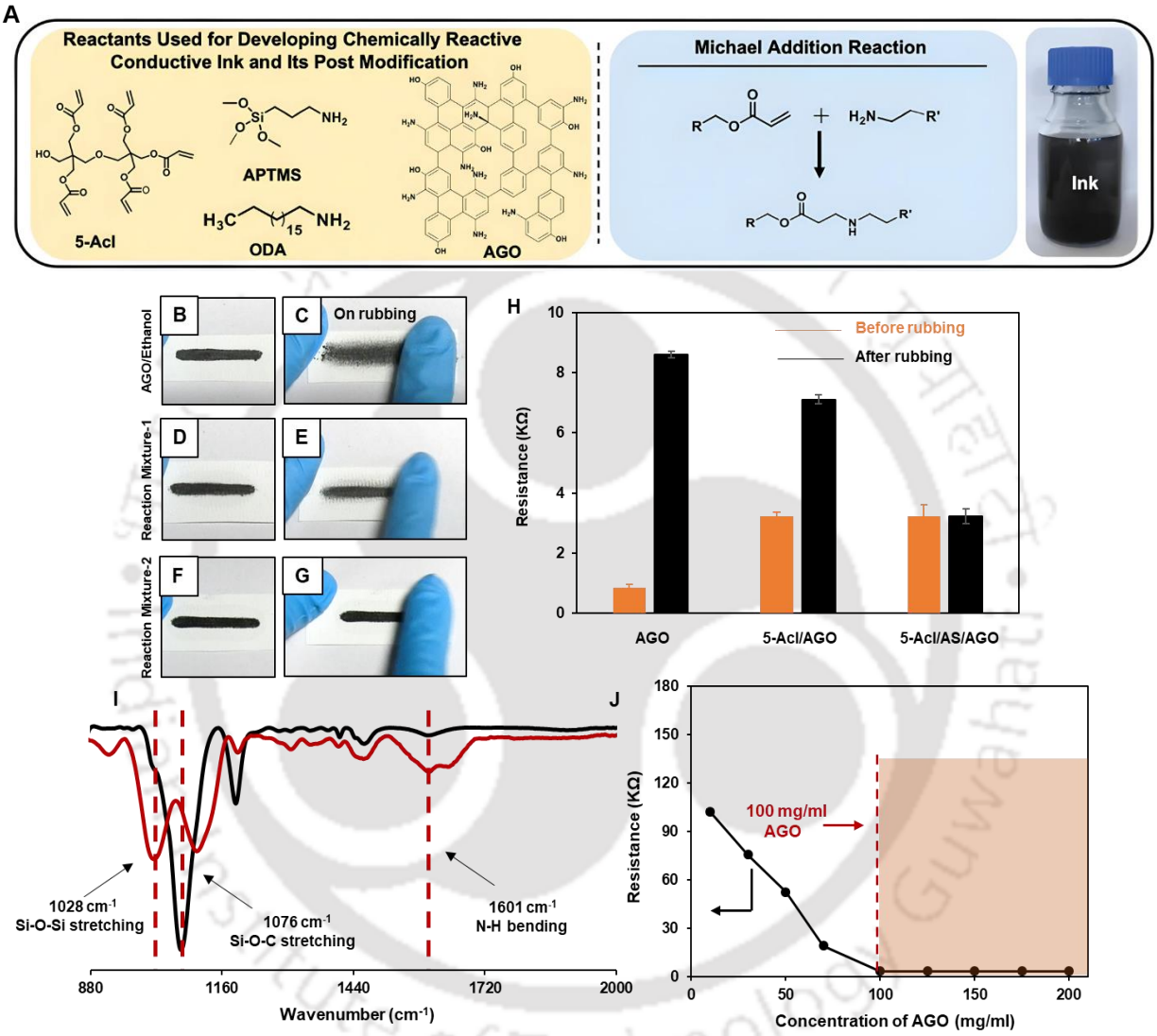

Figure 3.1. (A) Chemical structures of reactants used for the preparation of a chemically reactive and conductive ink, i.e., dipentaerythritol pentaacrylate (5-Acl), 3-aminopropyltrimethoxysilane (APTMS), octadecylamine (ODA) and aminographeneoxide (AGO); schematic of 1,4-conjugate addition reaction between the acrylate and primary amine groups of the reactants under ambient conditions. (B-G) Digital images depicting the impact of simple finger wiping test on different conductive coatings that were derived from AGO (B-C), reaction mixture 1 (5-Acl and AGO; D-E) and reaction mixture 2 (5-Acl, APTMS and AGO; F-G). Only, the coating that prepared from reaction mixture 2 remained efficient to survive the finger wiping test. (H) The bar graph accounting the change in resistance of the above mentioned conductive coatings before and after incurring the finger wiping test. (I) ATR-FTIR spectra of APTMS in solution (black) and after depositing (red, air-dried) on selected substrate. The characteristic IR peaks for Si-O-Si and Si-O-C appeared at 1028 cm^{-1} at 1076 cm^{-1}. After air-drying, an intense IR peak for Si-O-Si at 1028 cm^{-1} revealed the self-polymerization of APTMS on air-drying. (J) The plot accounting the impact of change in the concentration of used AGO in the reaction mixture-2 on lowering the resistance of the deposited ink.

three distinct reactants: dipentaerythritol pentaacrylate (5Acl, multifunctional crosslinker), aminopropyl trimethoxysilane (APTMS; binder) and amino-graphene oxide (AGO (7% of nitrogen), prepared following a previously reported protocol[38]) under ambient conditions. The reaction mixtures (RM-1and2) that were differently formulated with selected reactants allowed to investigate the role of each reactant towards the designing of durable, conductive and superhydrophobic patterns that would be appropriate for designing a low-strain (less than 0.5%) based ultrasensitive sensor for convenient monitoring of different and relevant human motions/expressions—even in the presence of continuous aqueous exposure. The individual physical deposition of the conductive ingredient i.e. AGO and the reaction mixture-1 (RM-1; mixture of AGO/5Acl) on bare paper failed to sustain even the finger wiping

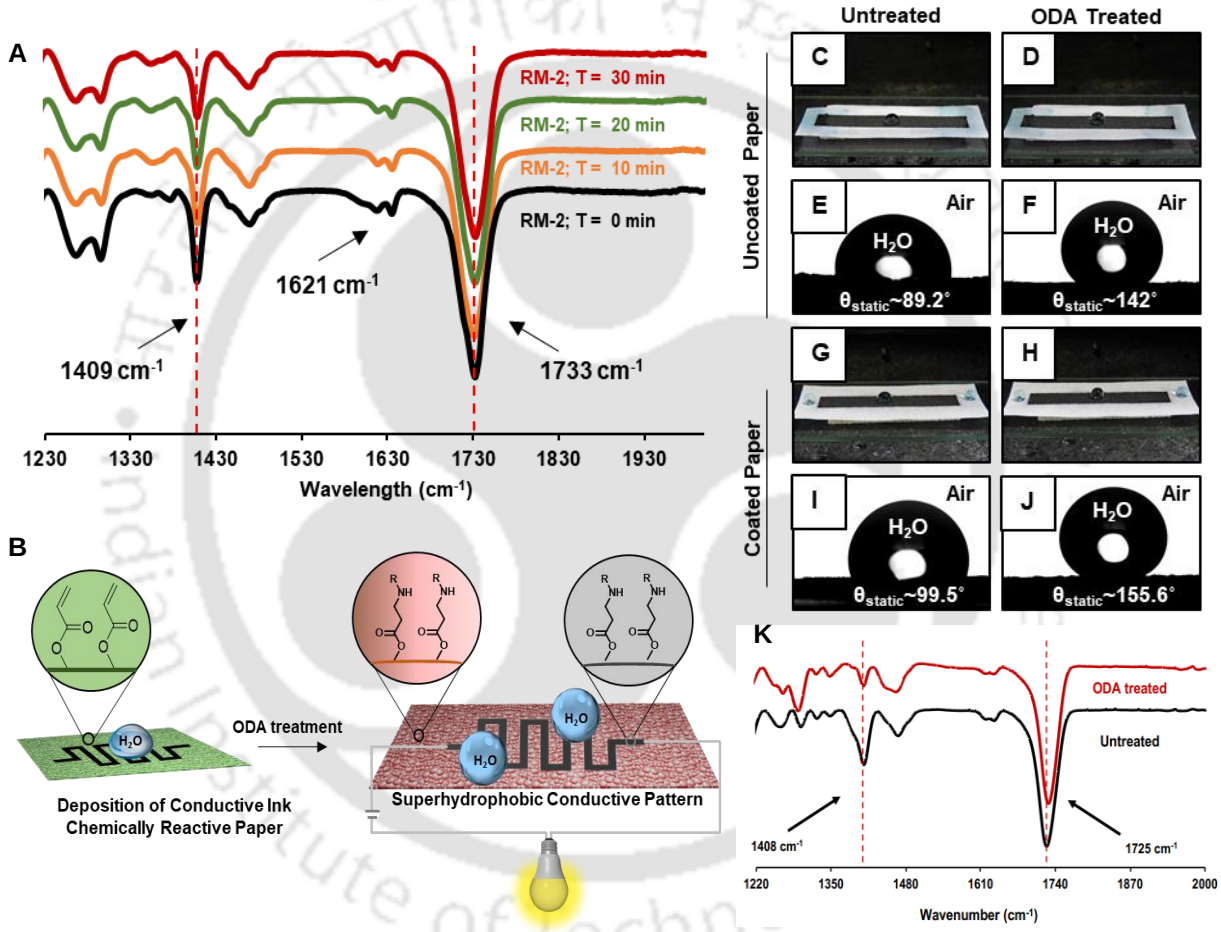

Figure 3.2. (A) ATR-FTIR spectra accounting the 1,4 conjugate addition reaction between amine and acrylate groups in the reaction mixture of 5-Acl, APTMS and AGO, where the IR signature at 1409 cm^{-1} for an acrylate group was recorded at different intervals of time. (B) Schematic depicting the fabrication of an extremely water repellent and conductive pattern interface, where the chemically reactive conductive ink was deposited spatially selectively on the dip coated chemically reactive paper, prior to post-modifying with octadecyl amine (ODA). (C-J) Digital images and static contact angle images of the beaded water droplets on the deposited chemically reactive ink on both bare paper (C-F) and chemically reactive coated paper (G-J), before (C, E; G, I) and after (D, F; H, J) the post covalent modification with ODA. (K) FTIR data demonstrating the successful post-chemical modification of the deposited chemically reactive conductive ink with ODA, where the characteristic acrylate peak at 1408 cm^{-1} was significantly depleted after the post modification with ODA.

test and the resistance significantly changed after the application of such common and mild abrasive exposure as shown in Figure 3.1B–E. Whereas, the reaction mixture-2 (RM-2) that comprised of AGO/ 5Acl/APTMS remained efficient to tolerate the same finger wiping test (Figure 3.1F and G)—and no change in resistance was noted as shown in Figure 3.1H. The physical abrasion tolerance is likely due to the self-polymerization of APTMS (Figure 3.1I). As expected, the association of nonconductive reactants (5Acl/APTMS) with AGO in the RM-2 enhanced the resistance of the deposited ink; however, the gradual increment in the content of AGO (from 10 mg mL^{-1} to 100 mg mL^{-1}) in the reaction mixture helped in lowering the resistance from 102 KΩ to 3.2 KΩ as shown in Figure 3.1J. This particular conductive ink (with resistance of 3.2 KΩ and thickness ~ 30 mm) that derived from reaction RM-2 was selected for the rest of the study. On the other hand, another reactant i.e. 5Acl (a) allowed the covalent integration of the selected conductive material i.e. AGO, and also (b) provided essential residual chemical reactivity enabling the deposited conductive ink to undergo appropriate post covalent modifications—following a facile 1,4-conjugate addition reaction between amine and acrylate under ambient conditions. The existence of residual acrylate groups in the deposited ink was validated through an attenuated total reflection Fourier-transform infrared spectroscopy (ATR-FTIR) study. The characteristic IR peak intensity for the asymmetric C–H stretching of the vinyl moiety of acrylate groups at 1409 cm^{-1} was depleted by ~ 26% in the RM-2 over 30 minutes as shown in Figure 3.2A. No further change in IR peak intensity at 1409 cm^{-1} was noted even after 12 h. The residual acrylate groups in the reaction mixture allowed the post-covalent modification of the deposited and dry ink with selected alkylamine having a long hydrocarbon tail. The subsequent post covalent modification of the deposited ink (that derived from RM-2) on a printer paper with the selected octadecylamine (ODA) altered the water wettability significantly from ~ 89.2º to 142º as shown in Figure 3.2C-F. The post covalent modification of the deposited ink was further characterized through the ATR-FTIR study. The signature for the residual acrylate group at 1409 cm^{-1} was significantly diminished after the post covalent modification of the conductive ink with ODA as shown in Figure 3.2K. Thus, a chemically reactive and conductive interface (with resistance of 3.2 KΩ) is developed through the strategic use of the 1,4-conjugate addition reaction at ambient conditions. During this post covalent modification process, the change in resistance of the deposited ink was not observed. Thereafter, a superhydrophobic and conductive pattern (Figure 3.2B) was developed by strategic association of this amine-reactive and conductive ink (CRCI) with a chemically reactive paper—which was prepared by dip coating a selected paper into a dispersion of chemically reactive polymeric nanocomplex following the earlier reported protocol.[39] The post covalent modification of deposited CRCI (WCA ~ 99º, Figure 3.2G and I) on the chemically reactive paper with octadecylamine provided an extremely water repellent (WCA of 155º, Figure 3.2H and J) and conductive (with resistance of 3.2 KΩ) interface, where a stream of water can easily bounce on the extremely water repellent conductive interface as shown in Figure 3.3A. Such an interface remained efficient to tolerate different and severe abrasive exposures—including twisting,

creasing, scratching, adhesive tape test, sandpaper abrasion test, and sand drop test as shown in Figure 3.3B.

Both the water wettability and the resistance remained mostly unaffected after exposing the superhydrophobic and conductive interface to such practically relevant and challenging conditions as superhydrophobic and conductive interface to such practically relevant and challenging conditions as

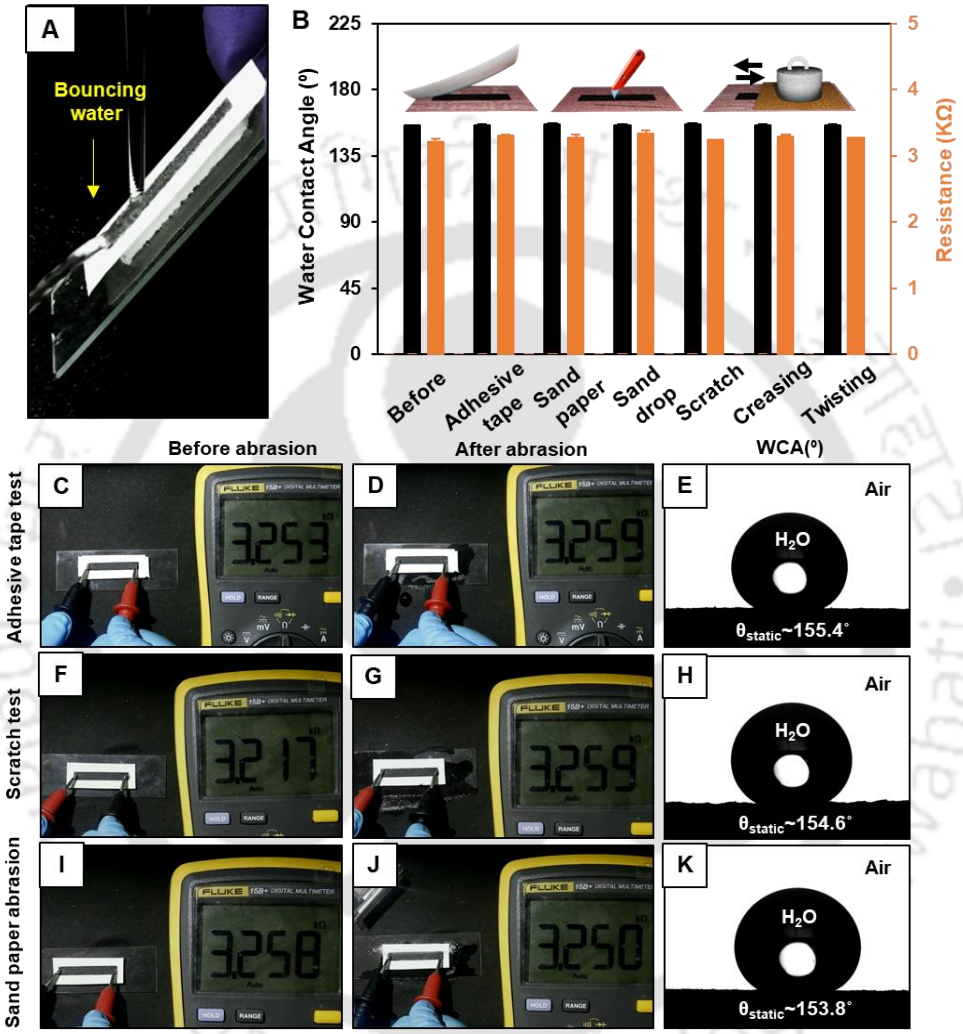

Figure 3.3. (A-B) Digital image of the bouncing of liquid water after hitting the superhydrophobic and conductive interface (A). (B) Graph accounting the tolerance of both the embedded water wettability and resistance under various harsh and abrasive physical settings. (C-D, F-G, I-J) Digital images showing the change electrical resistance of the superhydrophobic and conductive interface before and after performing physical abrasions including adhesive tape tests (C-D); scratch tests (F-G); and sand paper abrasions test (I-J) respectively. (E, H, K) Water contact angle images illustrated the existence of superhydrophobicity after exposing the prepared superhydrophobic and conductive interface to different physical abrasions including adhesive tape tests (E); scratch tests (H); and sand paper abrasions test (K) respectively.

shown in Figure 3.3B and Figure 3.3C-K. Thereafter, the deposited chemically reactive ink before and after post covalent modifications with ODA were separately exposed to different aqueous phases to examine the impact of the embedded superhydrophobicity on the resistance of the conductive interface. While, different aqueous phases easily infiltrated into the chemically reactive ink and altered the

resistance of the conductive interface, the embedded superhydrophobicity prevented infiltration of the aqueous phase—and the resistance of the same conductive interface after ODA modification remained unaffected as shown in Figure 3.4.

Moreover, a negligible change in the electrical performance (resistance) was observed on the exposure of the prepared conductive interface to a broad range of temperatures (from 0º C to 70º C) and relative humidities (from 1% to 90%) as shown in Figure 3.4A, B. The flexible, conductive (with resistance of 3.2 KΩ and thickness ~ 30 mm) and superhydrophobic (static WCA ~ 155º) interface (denoted as FCSI) was further extended to examine its ability towards strain sensing performance.

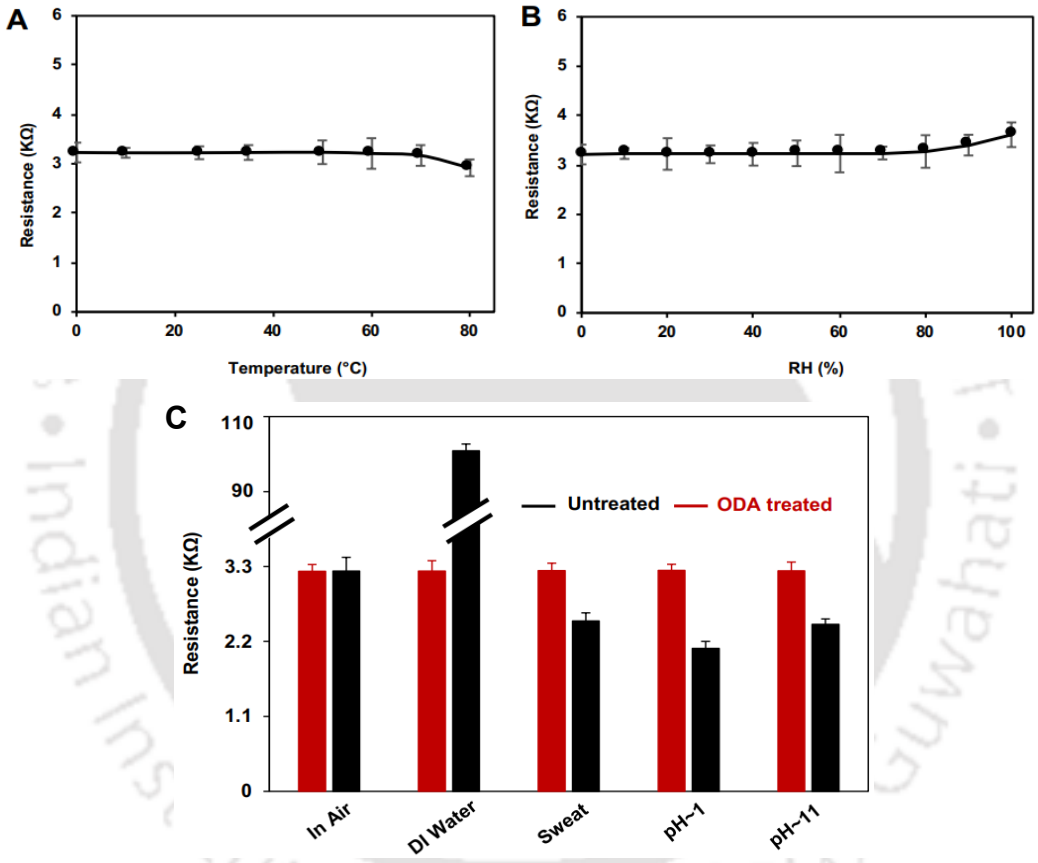

Figure 3.4. (A-B) Illustrating the impact of changes in the temperature (°C; A) and relative humidity (RH%; B) on the resistance of the conductive interface. (C) The bar plot comparing the change in the resistance of deposited chemically reactive ink with (red bars) and without (black bars) ODA modification after exposing to air, DI water, artificial sweat, pH~1 and pH~11.

The resistance of the superhydrophobic and conductive interface readily and reversibly changed from 3.2 KΩ to 25.6 KΩ on bending the selected substrate to 30º as shown in Figure 3.5A–C. After releasing the applied bending, the substrate returned to its initial shape and the resistance of the conductive interface was restored back to 3.2 KΩ (Figure 3.5C).

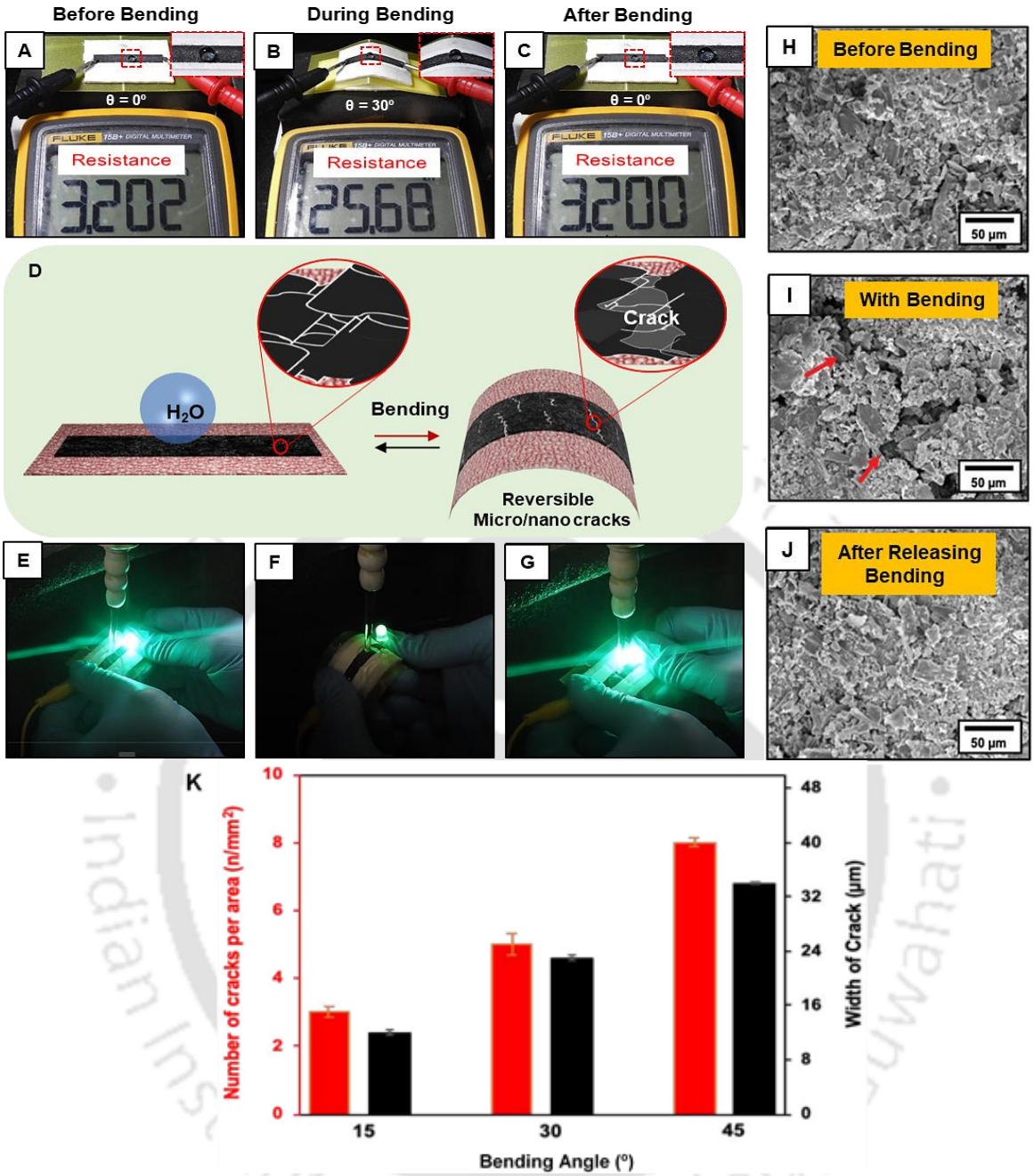

Figure 3.5. (A–C) Digital images depicting the reversible changes (from 3.2 KΩ to 25.6 KΩ) in the resistance of the superhydrophobic and conductive interface on incurring bending from 0º to 30º. (D) Schematic showing the appearance of reversible cracks during bending of the superhydrophobic and conductive interface. The change in resistance is attributed to this crack on the conductive interface. (E–G) FESEM images revealed the existence of reversible cracks during the bending of the conductive and superhydrophobic interface. (H–J) Demonstrating the reversible change in the resistance under continuous exposure of aqueous phase, where the brightness of the LED light varied with bending the conductive and superhydrophobic interface under the continuous exposure of an aqueous phase. (K) The resistance of superhydrophobic and conductive interface enhanced with increasing the bending angle both in air (black) and under submerged (red) conditions.

On bending, the change in the resistance of the deposited ink on the flexible substrate is likely due to the generation of physical cracks and defects as depicted in Figure 3.5D. In the past, the induction of cracks and defects in a well-organized conductive interface remained a widely used principle to develop strain sensors.[12] However, the deposition of RM-2 provided a hierarchically featured interface where

AGO was randomly oriented as examined with the FESEM study in Figure 3.5H. On bending the ink deposited flexible substrate, some microcracks appeared in the same interface (Figure 3.5I), however, on releasing the applied strain, the microcracks disappeared (Figure 3.5J). This reversible appearance of cracks supports the switchable change in the resistance of the flexible, conductive and superhydrophobic interface (FCSI). The elevated bending angles influenced both the number of cracks and width of the cracks on the prepared conductive interfaces as shown in Figure 3.5K. Eventually, the resistance of the interface changed with increasing the bending angle. Furthermore, an experiment was designed to examine the bending assisted change in resistance of the superhydrophobic and conductive interface—in the presence of continuous exposure to the tap water. First, the superhydrophobic ink was connected to a commercially available light-emitting diode (LED) using a battery input of 9 V.

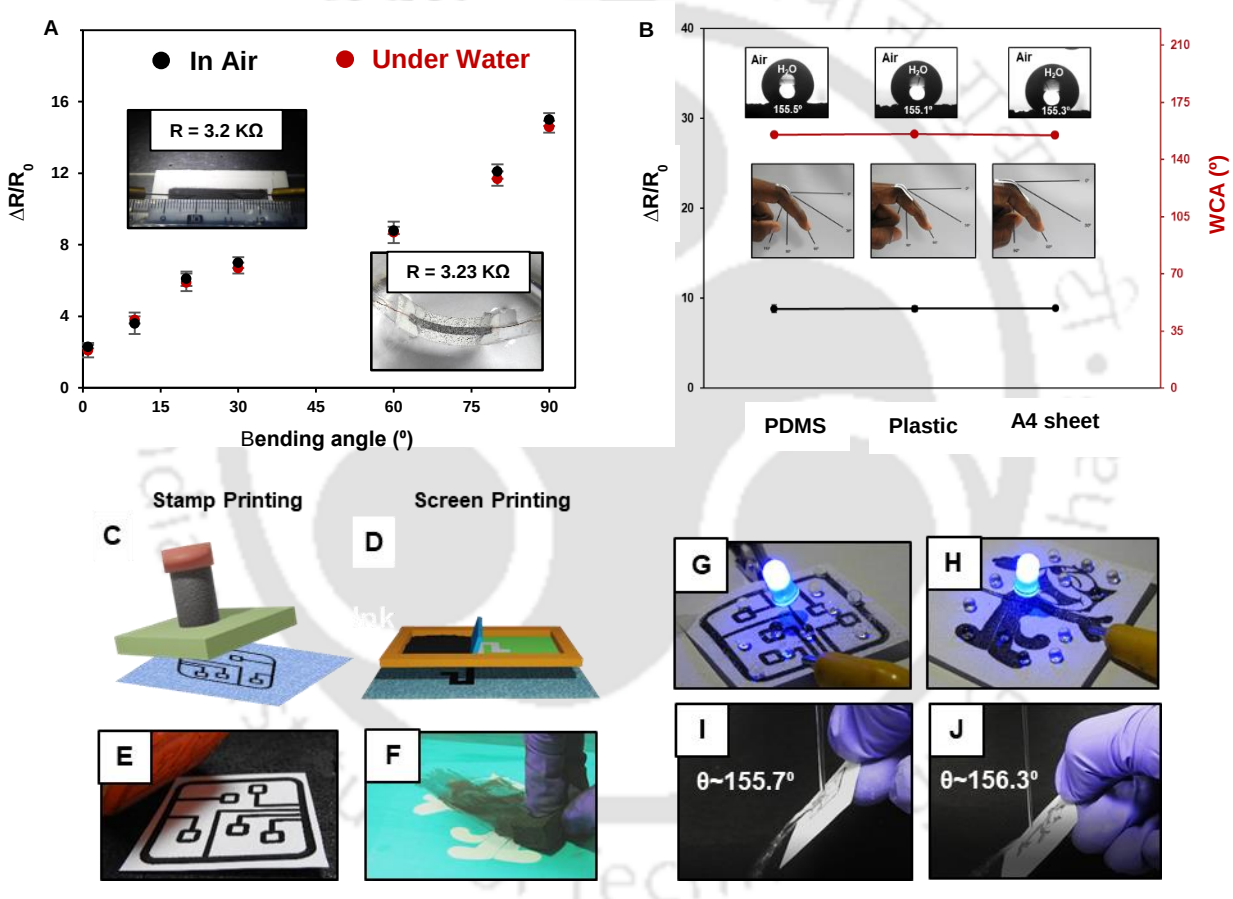

Figure 3.6. (A) The resistance of superhydrophobic and conductive interface enhanced with increasing the bending angle both in air (black) and under submerged (red) conditions. (B) Demonstrating the successful deposition of superhydrophobic and conductive coating on various flexible interfaces—including PDMS film, plastic film and paper. The change in resistance remained same on incurring bending of 60°. The water contact angle (WCA) of beaded droplet on the coated substrates remained well above 150°. (C-D, E-F) Schematic (C, D) and digital images (E, F) illustrating different patterning methods, i.e., stamp printing (C-E) and screen printing (D-F) for developing pattern conductive interfaces. (G, H) External circuit that connected to LED was integrated with the prepared patterns to depict the conductive behaviour. (I, J) Digital images accounting the presence of superhydrophobicity of the pattern interface, where the jet of tap water immediately bounced off from the pattern interface that post modified with ODA.

Thereafter, the superhydrophobic ink that was kept in contact with the stream of water was gradually bent as shown in Figure 3.5E and F. The light intensity of the LED significantly depleted on the application of the manual bending to the FCSI; however, after releasing the applied strain, the light intensity of the LED recovered back as shown in Figure 3.5G. This simple demonstration confirmed that the developed conductive interface remained efficient—in the presence of continuous water exposure. Furthermore, the change in the resistance of FCSI was examined by increasing the bending angle (from 0º to 90º) both in air and under water. The change in resistance of the FCSI gradually increased from 3.2 KΩ to 15 KΩ as shown in Figure 3.6A (black), and a very similar result was obtained on repeating the same experiment under water as shown in Figure 3.6B (red). Thus, the embedded superhydrophobicity allowed FCSI to perform—even under water. The current coating approach can be successfully extended to other flexible substrates—with ability to display similar water repellency (above 150º) and change in resistance as shown in Figure 3.6B. The prepared conductive ink can be deposited with spatial selectivity on the hydrophobic and chemically reactive paper following different standard processes—including stamp printing and screen printing (Figure 3.6C, D).

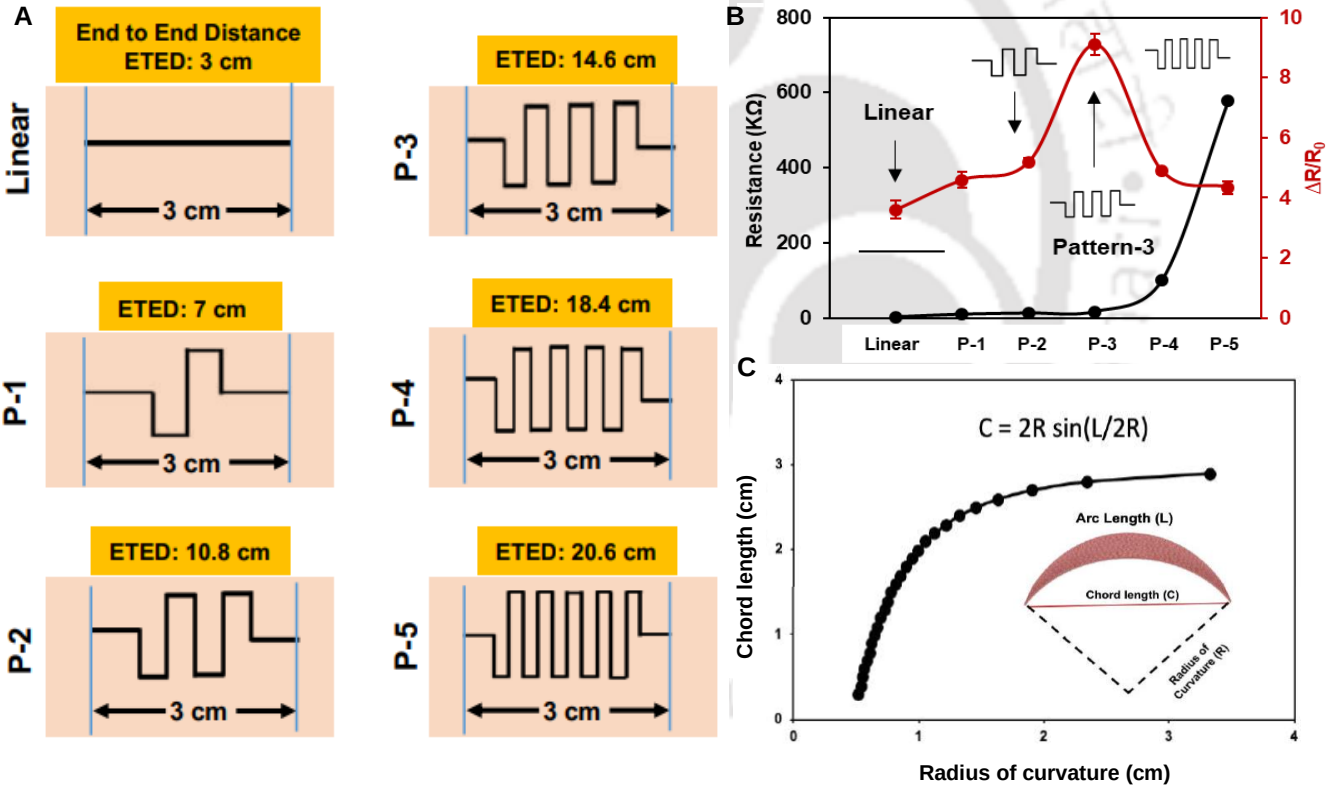

Figure 3.7. (A) Schematic representation of various conductive patterns—including, linear, pattern-1 (P1), pattern-2 (P-2), pattern-3 (P-3), pattern-4 (P-4) and pattern-5 (P-5); maintaining the end to end distance (ETED) of the deposited ink was gradually changed from 3 cm (linear) to 20.6 cm (P5). The apparent length of each pattern remained 3 cm. Illustrating the essential parameters that involved in calculation of gauge factor (GF) of the patterned interface., where the thickness of the sensor (i.e. coated tracing paper; h) is 30 µm. (B) The plot accounting the absolute resistance and the change in resistance of different water repellent and conductive pattern interfaces (linear, P-1, P-2, P-3, P-4, and P-5. (C) The change of chord length, (C) with radius of curvature, (R) for a fixed arc length (L) of 3 cm.

By taking advantage of this spatially selective deposition of the conductive ink, different patterned conductive and superhydrophobic interfaces with variable resistance were prepared for developing a

strain sensor with high gauge factor—that accounts for the sensitivity of the prepared sensor. The spatially selective deposition of chemically reactive and conductive ink on a chemically reactive paper allowed the preparation of patterned interfaces (denoted as P-1, P-2, P-3, P-4 and P-5, Figure 3.7A, B) with variable end to end distance (3 cm to 20.6 cm) of the conductive region—keeping the overall dimension of all the patterns identical, i.e. 3 cm with increasing the end to end distance (from 3 cm to 20.6 cm) of the deposited conductive ink, the absolute resistance of the patterned interfaces gradually enhanced from 3.2 KΩ to 578.3 KΩ. Interestingly, the change in the resistance was observed to be maximum (9.1 times) for P-3 (Figure 3.7B, red line) under identical conditions, where each and every patterned interface was bent at 10º. Thereafter, the sensitivity of P-3 was examined on application of

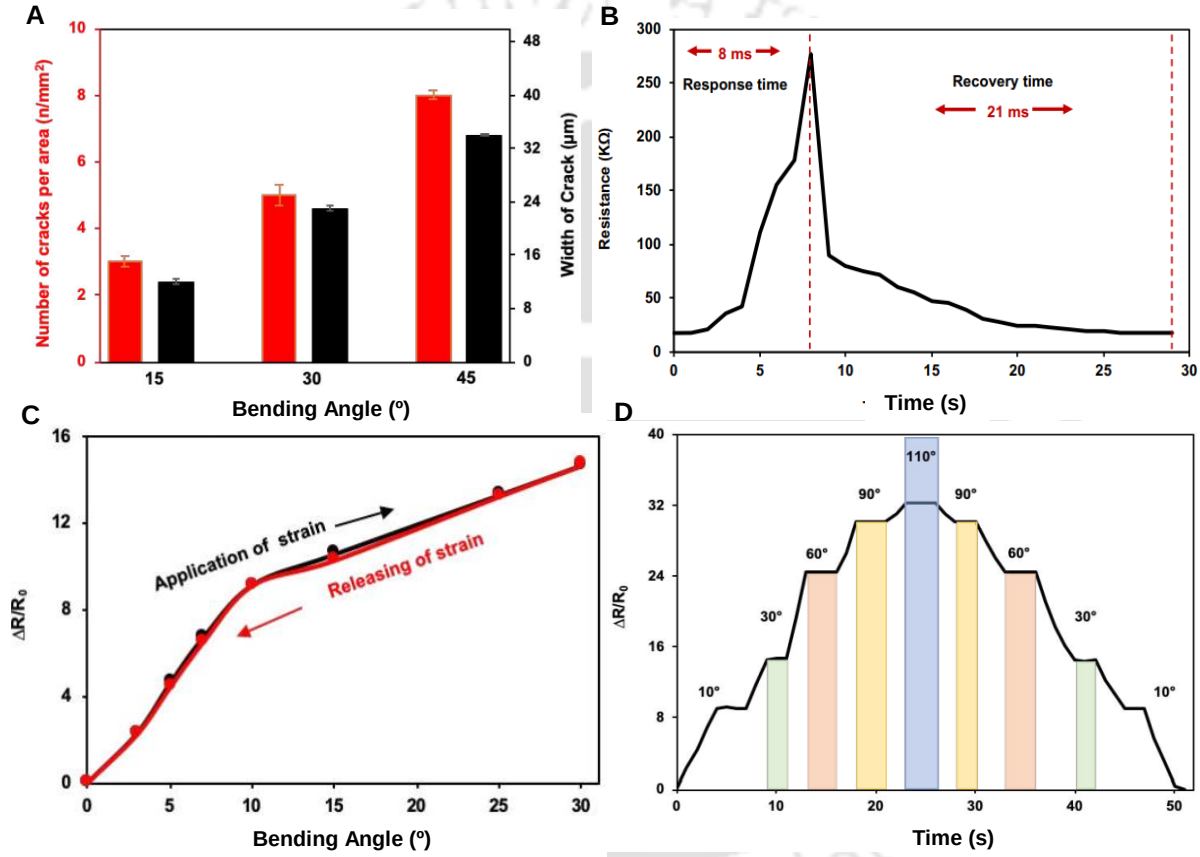

Figure 3.8. (A) Accounting the changes in the number of cracks (per mm^2) and their width on the conductive and superhydrophobic interfaces with increasing the bending angle. (B) The plot accounting the response and recovery time of the prepared sensor (P-3) in response on bending the pattern interface at 30°. (C) Accounting the hysteresis of the change of resistance of the prepared interface on application and releasing of external strain—i.e. bending. (D) Depicting the changes of resistance of the prepared coating with dynamic changes (forwards/backwards) of bending.

low strain (less than 0.5%). The gauge factor that accounts for sensitivity of the P-3 against the applied strain was calculated following the widely used and standard equation:[6]

$$\text{Gauge Factor (GF)} = (\Delta R/R_0)/\varepsilon \qquad (1)$$

where, R_0 and ΔR are absolute resistance and the change in the resistance of the patterned interface (P-3) after incurring the applied strain (denoted as e). The applied e on the patterned (P-3) interface was calculated using eqn (2) and eqn (3).

$$\varepsilon = (\pm)\ h/2R \quad (2)$$

$$C = 2R \sin(L/2R) \quad (3)$$

where, h, L, C and R represent the thickness of the sensor (30 mm), the arc length (3 cm), the chord length and the radius of curvature of the synthesized strain sensor. A schematic diagram to illustrate the above mentioned parameters and the change of chord length (L) with radius of curvature (R) are provided in Figure 3.7C. The change of the applied strain on the prepared interface influenced the gauge factor of the sensor—likely due to the difference in the number and width of the generated cracks (Figure 3.8A). The gauge factor of P-3 was observed to be ~ 15800 at very low (0.15%, equivalent to bending at 60º) applied strain. In the past, mostly strain sensors with high GF values were obtained by application of very large tensile strain, however the report of low strain-based sensors with GF value above 1000 is extremely rare to achieve. Thus, the current approach of chemically reactive and conductive ink that derived through 1,4 conjugate addition reactions provided a unique solution to achieve a flexible, paper-based and extremely water-repellent conductive pattern with unprecedented gauge factor at low applied strain. Such a principle would be appropriate for monitoring various human motions/expressions and other relevant biomedical and robotic applications. Apart from the gauge factor, a rapid response of the conductive interface towards applied strain and fast recovery of the change in resistance after releasing the applied strain are other key characteristics of an efficient strain sensor. The superhydrophobic and conductive pattern (P-3) interface was bent at 30º and monitored both the change and recovery of the resistance with time. Interestingly, the currently developed interface provided a rapid response (8 ms) to the applied strain and a very fast recovery (21 ms) was noted after releasing the applied strain as shown in Figure 3.8B. Such rapid response to applied strain is rare in the reported sensors. The change in the resistance of the prepared sensor was noticed to be gradually altered with the association of dynamic change in the applied strain (i.e. increment/decrement of bending deformations) as shown in Figure 3.8D. Moreover, the change in the resistance due to the bending of the interface was observed to be completely reversible as confirmed from the hysteresis curve in Figure 3.8 C. Furthermore, the pattern interface was repetitively bent at 30º using an automated mechanical device for 15000 times, and the change in the resistance of the same interface was measured with a bending angle of 30º at a regular interval as presented in Figure 3.9A. Furthermore, the change in the resistance at each and every step during the process of incurring the bending of 30º for 1000 times is also provided in Figure 3.9B. But, the change reversible and rapid change in the resistance with fast recovery time.

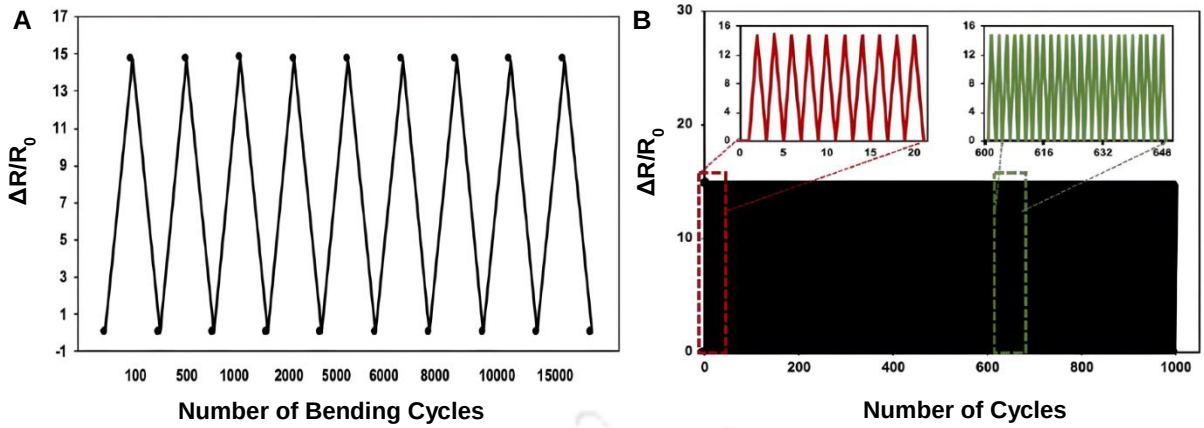

Figure 3.9. (A) The plot accounting the durability of the flexible superhydrophobic and conductive interface (FSCI) after incurring repetitive bending (at 30°) for 15000 cycles, where the changes in resistance were recorded at regular interval. The change in resistance remained unaltered even after 15,000 cycles of bending the FSCI. (B) Illustrating the change in resistance at each and every step during the repetitive bending of the same interface for 1000 cycles, and insets displayed some subsets of them.

Such repetitive performance, rapid response and fast recovery of the synthesized strain sensor (P-3) was attributed to the design of the unique chemically reactive and conductive ink, where the covalently crosslinked and hierarchically featured network of AGO remained chemically reactive for associating desired superhydrophobicity. The random hierarchical feature is likely to contribute towards the crack induced in the resistance remained unaltered after successive bending of the flexible interfaces. Thereafter, the extremely water repellent and conductive pattern (P-3) was associated with both the Arduino Nano board (version 3) and the Bluetooth module HC-05 for wireless monitoring of different human motions and expressions as illustrated in Figure 3.10A. The adequate attachment of the patterned interface (P-3) at an appropriate location is essential to achieve characteristic signal (i.e. change in resistance) during both soft and strong movement of different parts (elbow, knee, finger, throat, neck, eyes etc.) of the human body as depicted in Figure 3.10B and C. As a proof of concept demonstration of wireless detection of different soft and strong human motions, the patterned interface (P-3) was first attached on a finger prior to bending at different angles, and the change in the resistance was noted to be gradually elevated with increasing the bending angle—from 30º to 110º in air as depicted in Figure 3.10D. A real-time and wireless change in the resistance during the bending of the prepared patterned interface in air was demonstrated with the help of the display of a smartphone as illustrated. Next, the same pattern interface was gradually bent underwater as depicted in Figure 3.10E—and a very similar change in resistance was noted as shown in Figure 3.10D (right side: green shaded area). As expected, the embedded superhydrophobicity allowed the successful underwater performance of the conductive pattern interface. Later, the same conductive pattern interface was attached to the knee of an adult volunteer from our lab for monitoring both slow (~5 steps per minute) and fast (~ 30 steps per minute) walking, where the nature of resistance changes was noticed to be very different depending on the speed of the walking.

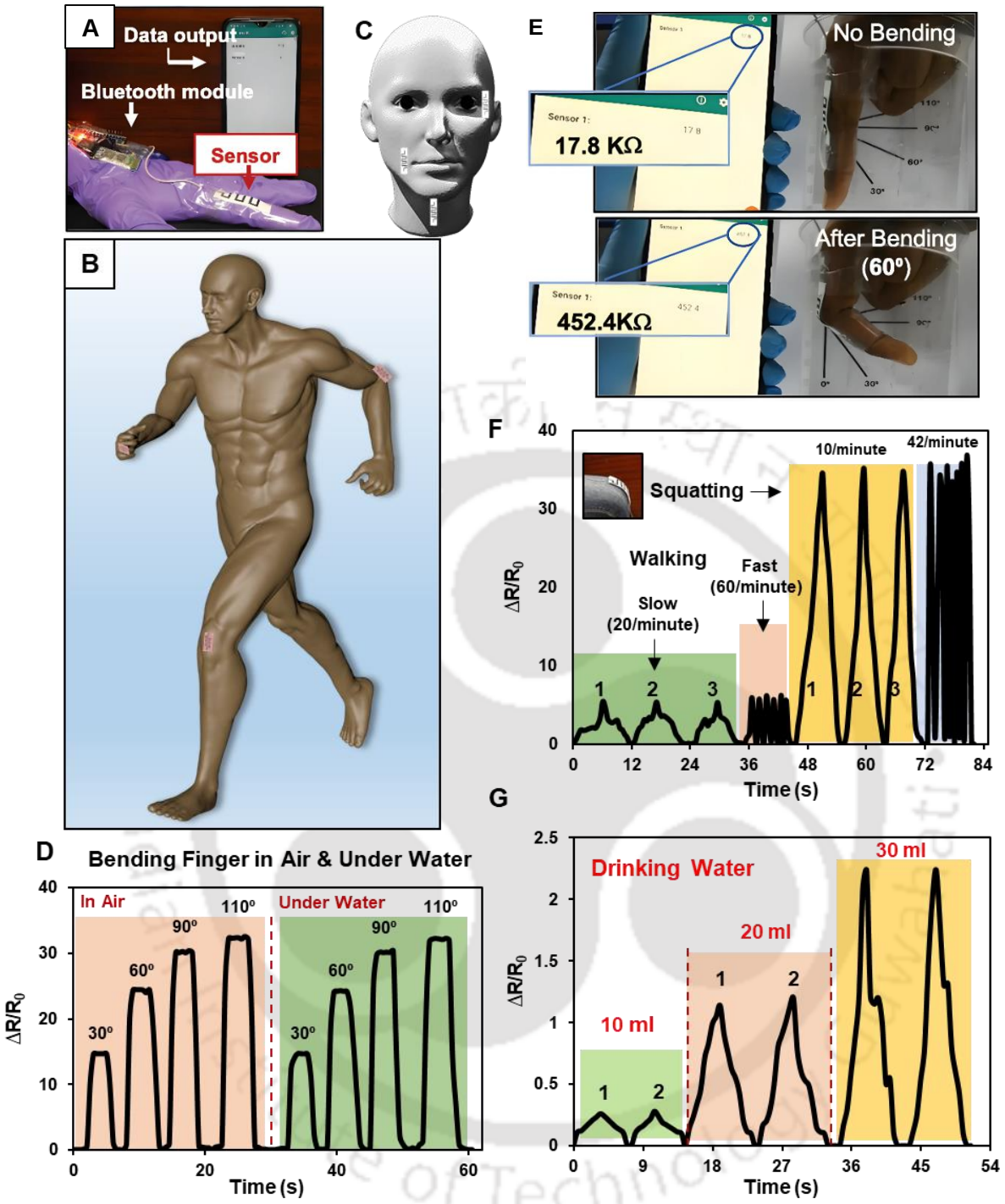

Figure 3.10. (A) Digital image showing the set-up consisting of sensor, Bluetooth module and data output device (e.g. smart phone) for wireless detection of different motions (B) and expressions (C) of humans, where the superhydrophobic and conductive pattern (P-3) interface was used as a sensor and appropriate attachment of this pattern interface allowed the monitoring of different motions and expressions, with the red circle pointing out the position of the sensor (pattern interface: P-3). (D) The plot accounting the gradual change in resistance of the pattern interface that attached to a finger of a volunteer on bending the finger at different angles (from 30° to 110°) both in air (left side) and under water (right side). (E) Digital images displaying the instant change of resistance (from 17.8 KΩ to 452.4 KΩ) after incurring the bending of 60° of the superhydrophobic and conductive patterned interface underwater. (F–G) Plots illustrated the electrical response (in form of change in resistance) of the superhydrophobic and conductive pattern (P-3) interface that attached to different parts of a volunteers' body (C and D) for monitor walking and squatting (F), swallowing of drinking water with different volumes (G).

Due to the slower bending of the knee, the base width of the signal (change in resistance vs time) was noticed to be large, in comparison to fast walking. As expected, the amplitude of the change in resistance remained very similar as the extent of bending of the knee kept merely the same for both the occasions as shown in Figure 3.10F.

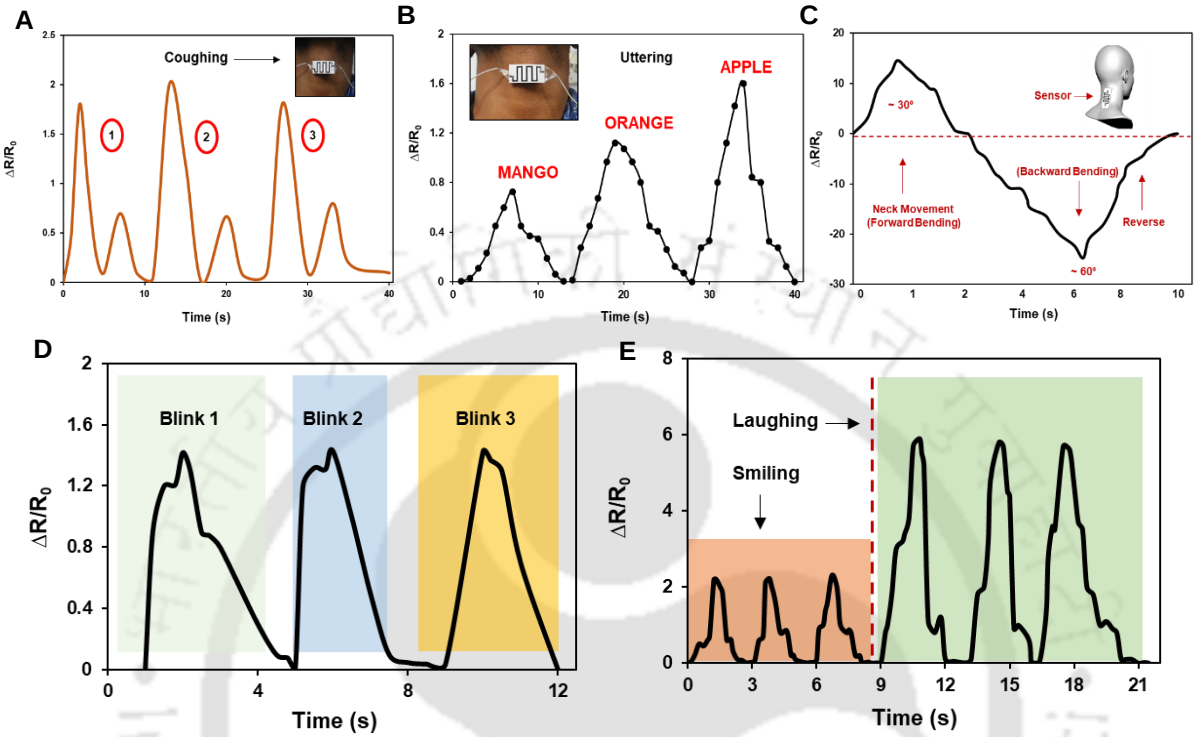

Figure 3.11. (A-B) Graph demonstrates the detection of coughing (A) and uttering of different words (B). (C) Forward and reverse bending of neck was successfully monitored using the flexible superhydrophobic and conductive interface (FSCI), the inset image revealed the position of FSCI on the neck of a volunteer. During forward bending a positive change in resistance was noted and a negative change of resistance appeared due to backward bending of the FSCI (sensor). The backward bending makes the interface more conductive. (D-E) Plots illustrated the electrical response (in form of change in resistance) of the superhydrophobic and conductive pattern (P-3) interface that attached to different parts of a volunteers' body to monitor blinking of eyes, (D) smiling and laughing (E).

Furthermore, this conductive pattern interface remained efficient to differentiate the walking and squatting movements. A significantly higher (~7 fold more) change in resistance was noted during the squatting as it caused more bending of the pattern interface. Again, a completely distinct pattern of the signal (change in resistance vs time) was noted for fast (6 per minute) and slow (36 per minute) squatting as depicted in Figure 3.10F. Thereafter, the conductive pattern interface was attached at the throat of a lab volunteer to monitor coughing (Figure 3.11A), uttering different words (Figure 3.11B) and swallowing of different volumes of water (Figure 3.10G). As expected, on increasing the volume (from 10 mL to 30 mL) of the drinking water, the amplitude for the change in the resistance is enhanced as shown in Figure 3.10G. Interestingly, the attached conductive patterned interface on the neck allowed it to detect even forward and backward movement of the neck as shown in Figure 3.11C. The concave (~ 30º) and convex (~ 60º) bending of the neck provided two distinct forms of the signal during both forward and backward movements, respectively. Furthermore, the same paper-based superhydrophobic and conductive pattern, i.e. P-3 was attached at the appropriate parts of the face for

detecting different facial expressions—including blinking of eyes, smiling and laughing as shown in Figure 3.11D and E. The blinking of eyes led to a very minute change in the facial deformation—but the prepared ultrasensitive conductive patterned interface remained efficient to detect such facial expressions. On the other side, laughing caused more deformation of the face in comparison to smiling resulting in a distinct signal (change in resistance with time) as shown in Figure 3.11E. During the course of the study, we noticed that a localized pressure on such pattern interfaces can lead to a

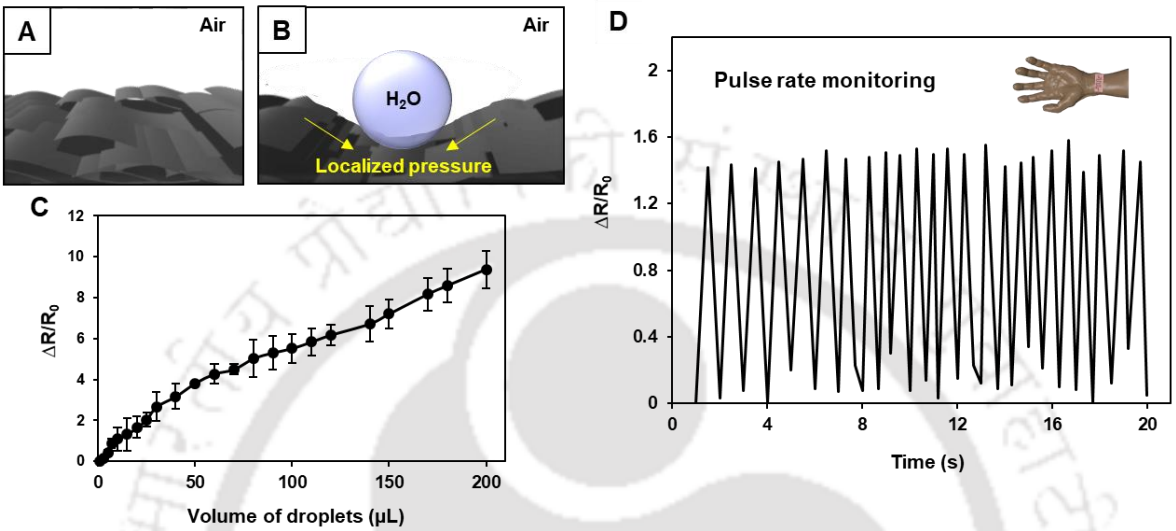

Figure 3.12. (A-B) Schematic demonstrating localized deformation of FSCI against the applied pressure, where the beaded water droplet on the FSCI is responsible for elevating the resistance of the pattern interface. (C) Graph accounting the change in resistance on increasing the volumes of beaded water droplets. (D) Plot illustrated the electrical response (in form of change in resistance) of the superhydrophobic and conductive pattern (P-3) interface that attached to the wrist of a volunteers' body to monitor wrist pulse rate.

significant change in resistance. Most likely, the localized load on such flexible interface led to some local deformation—which remained sufficient to perturb the resistance of the patterned interface as depicted in Figure 3.12A and B. To validate this hypothesis, we have placed water droplets with different volumes on the superhydrophobic and conductive interface, prior to measuring the change in resistance. With increasing the volume of beaded water droplets, an increase of the change in the resistance was noted as shown in Figure 3.12C. This simple study provided a facile basis to monitor events that are associated with localized pressure. For example, the currently developed pattern interface was extended to monitor pulse rate that is associated with a weak and localized muscle movement. Interestingly, the attachment of the pattern interface (P-3) at the wrist of an adult male, allowed the successful monitoring of the wrist pulses as shown in Figure 3.12D, where 24 significant spikes appeared within 20 seconds—due to the successive change of resistance.

3.4. Conclusions

In conclusion, an extremely water-repellent and abrasion tolerant conductive pattern interface is unprecedentedly and successfully introduced for low-strain based ultra-sensitive detection of both strong and weak movements of body parts during walking, squatting, coughing, uttering, swallowing, blinking, wrist pulses etc. Thus, such an approach could be extremely useful in studying the interaction of human/machine and monitoring patients during the rehabilitation process. Furthermore, the embedded water repellency and ability to sustain severe abrasive exposure allowed it to perform under water and under various practically relevant extremes of conditions. Thus, the current and simple design of superhydrophobic and conductive pattern interface has immense potential for different and more realistic applications.

3.5. References

1) Wang, C.; Hwang, D.; Yu, Z.; Takei, K.; Park, J.; Chen, T.; Ma, B.; Javey, A. User-interactive electronic skin for instantaneous pressure visualization. *Nat. Mater.***2013**, *12*, 899-904.

2) Amjadi, M.; Kyung, K. U.; Park, I.; Sitti, M. Stretchable, Skin-Mountable, and Wearable Strain Sensors and Their Potential Applications: A Review. *Adv. Funct. Mater.* **2016**, *26*, 1678-1698.

3) Liu, W.; Song, M.-S.; Kong, B.; Cui, Y. Flexible and Stretchable Energy Storage: Recent Advances and Future Perspectives. *Adv. Mater.* **2017**, *29*, 1603436.

4) Amit, M.; Chukoskie, L.; Skalsky, A.J.; Garudadri, H.; Ng, T. N. Flexible Pressure Sensors for Objective Assessment of Motor Disorders. *Adv. Funct. Mater.* **2020**, *30*, 1905241.

5) Liu, D.; Qi, P.; Guo, Y.; Liu, B.; Zhu, H.; Yang, Y.; Liu, B.; Li, C.; Zhang, J.; Yu, B. Liedberg and X. Chen, Thickness-Gradient Films for High Gauge Factor Stretchable Strain Sensors. *Adv. Mater.* **2015**, *27*, 6230-6237.

6) Chen, S.; Song, Y.; Ding, D.; Ling, Z.; Xu, F. Flexible and Anisotropic Strain Sensor Based on Carbonized Crepe Paper with Aligned Cellulose Fibers. *Adv. Funct. Mater.* **2018**, *28*, 1802547.

7) Sun, F.; Tian, M.; Sun, X.; Xu, T.; Liu, X.; Zhu, S.; Zhang, X.; Qu, L. Stretchable Conductive Fibers of Ultrahigh Tensile Strain and Stable Conductance Enabled by a Worm-Shaped Graphene Microlayer. *Nano Lett.* **2019**, *19*, 6592-6599.

8) Shi, X.; Liu, S.; Sun, Y.; Liang, L.; Chen, Y. Lowering Internal Friction of 0D–1D–2D Ternary Nanocomposite-Based Strain Sensor by Fullerene to Boost the Sensing Performance. *Adv. Funct. Mater.* **2018**, *28*, 1800850.

9) Qiao, Y.; Wang, Y.; Tian, H.; Li, M.; Jian, J.; Wei, Y.; Tian, Y.; Wang, D.-Y.; Pang, Y.; Geng, X.; Wang, X.; Zhao, Y.; Wang, H.; Deng, N.; Jian, M.; Zhang, Y.; Liang, R.; Yang, Y.; Ren, T.-L. Multilayer Graphene Epidermal Electronic Skin. *ACS Nano* **2018**, *12*, 8839-8846.

10) Kim, K.-H.; Jang, N.-S.; Ha, S.-H.; Cho, J. H.; Kim, J.-M. Highly Sensitive and Stretchable Resistive Strain Sensors Based on Microstructured Metal Nanowire/Elastomer Composite Films. *Small* **2018**, *14*, 1704232.

11) Miao, W.; Yao, Y.; Zhang, Z.; Ma, C.; Li, S.; Tang, J.; Liu, H.; Liu, Z.; Wang, D.; Camburn, M. A.; Fang, J.-C.; Hao, R.; Fang, X.; Zheng, S.; Hu, N.; Wang, X. Micro-/nano-voids guided two-stage film cracking on bioinspired assemblies for high-performance electronics. *Nat. Commun*, **2019**, *10*, 3862.

12) Yanga, Y.; Caoa, Z.; Hed, P.; Shia, L.; Dingd, G.; Wanga, R.; Sun, J. $Ti_3C_2T_x$ MXene-graphene composite films for wearable strain sensors featured with high sensitivity and large range of linear response. *Nano Energy* **2019**, *66*, 104134.

13) Tan, C.; Dong, Z.; Li, Y.; Zhao, H.; Huang, X.; Zhou, Z.; Jiang, J.-W.; Long, Y.-Z.; Jiang, P.; Zhang, T.-Y.; Sun, B. A high performance wearable strain sensor with advanced thermal management for motion monitoring. *Nat. Commun.* **2020**, *11*, 3530.

14) Hang, C.-Z.; Zhao, X.-F.; Xi, S.-Y.; Shang, Y.-H.; Yuan, K.-P.; Yang, F.; Wang, Q.-G.; Wang, J.-C.; Zhang, D. W.; Lu, H.-L. Highly stretchable and self-healing strain sensors for motion detection in wireless human-machine interface. *Nano Energy* **2020**, *76*, 105064.

15) Wang, Z.; Xianga, C.; Yaoa, X.; Flocha, F.L.; Mendeza, J.; Suo, Z. Stretchable materials of high toughness and low hysteresis. *Proc. Natl. Acad. Sci. U. S. A.* **2019**, *116*, 5967-5972.

16) S. Wang, Y. Fang, H. He, L. Zhang, C. Li and J. Ouyang, Wearable Stretchable Dry and Self-Adhesive Strain Sensors with Conformal Contact to Skin for High-Quality Motion Monitoring. *Adv. Funct. Mater.* **2021**, *31*, 2007495.

17) Wu, Z.; Yang, X.; Wu, J. Conductive Hydrogel- and Organohydrogel-Based Stretchable Sensors. *ACS Appl. Mater. Interfaces* **2021**, *13*, 2128-2144.

18) Wu, J.; Wu, Z.; Lu, X.; Han, S.; Yang, B.-R.; Gui, X.; Tao, K.; Miao, J.; Liu, C. Ultrastretchable and Stable Strain Sensors Based on Antifreezing and Self-Healing Ionic Organohydrogels for Human Motion Monitoring. *ACS Appl. Mater. Interfaces* **2019**, *11*, 9405-9414.

19) Wu, Z.; Shi, W.; Ding, H.; Zhong, B.; Huang, W.; Zhou, Y.; Gui, X.; Xie, X.; Wu, J. Ultrastable, stretchable, highly conductive and transparent hydrogels enabled by salt-percolation for high-performance temperature and strain sensing. *J. Mater. Chem. C* **2021**, ***9***, 13668-13679.

20) Amjadi, M.; Turan, M.; Clementson, M. P. C.; Metin, S. Parallel Microcracks-based Ultrasensitive and Highly Stretchable Strain Sensors. *ACS Appl. Mater. Interfaces* **2016**, *8*, 5618-5626.

21) Fang, X.; Tan, J.; Gao, Y.; Lu, Y.; Xuan, F. High-performance wearable strain sensors based on

fragmented carbonized melamine sponges for human motion detection. *Nanoscale* **2017**, *9*, 17948-17956.

22) J. Lee, S. Shin, S. Lee, J. Song, S. Kang, H. Han, S. G. Kim, S. Kim, J. Seo, D. E. Kim and T. Lee, Highly Sensitive Multifilament Fiber Strain Sensors with Ultrabroad Sensing Range for Textile Electronics. *ACS Nano* **2018**, *12*, 4259-4268.

23) Gupta, N.; Rao, K. D. M.; Srivastava, K.; Gupta, R.; Kumar, A.; Marconnet, A.; Fisher, T. S.; Kulkarni, G. U. Cosmetically Adaptable Transparent Strain Sensor for Sensitively Delineating Patterns in Small Movements of Vital Human Organs. *ACS Appl. Mater. Interfaces* **2018**, *10*, 44126–44133.

24) Yin, F.; Yang, J.; Ji, P.; Peng, H.; Tang, Y.; Yuan, W. Bioinspired Pretextured Reduced Graphene Oxide Patterns with Multiscale Topographies for High-Performance Mechanosensors. *ACS Appl. Mater. Interfaces* **2019**, *11*, 18645–18653.

25) Gao, Y.; Li, Q.; Wu, R.; Sha, J.; Lu, Y.; Xuan, F. Laser Direct Writing of Ultrahigh Sensitive SiC-Based Strain Sensor Arrays on Elastomer towards Electronic Skins. *Adv. Funct. Mater.* **2019**, *29*, 1806786–1806795.

26) Lin, J.; Cai, X.; Liu, Z.; Liu, N.; Xie, M.; Zhou, B.; Wang, H.; Guo, Z. Anti-liquid-Interfering and Bacterially Antiadhesive Strategy for Highly Stretchable and Ultrasensitive Strain Sensors Based on Cassie-Baxter Wetting State. *Adv. Funct. Mater.* **2020**, *30*, 2000398.

27) Gao, J.; Wu, L.; Guo, Z.; Li, J.; Xua, C.; Xuea, H. A hierarchical carbon nanotube/SiO_2 nanoparticle network induced superhydrophobic and conductive coating for wearable strain sensors with superior sensitivity and ultra-low detection limit. *J. Mater. Chem. C* **2019**, *7*, 4199-4209.

28) Gaoa, J.; Wanga, L.; Guoa, Z.; Lia, B.; Wanga, H.; Luoa, J.; Huanga, X.; Xuea, H. Flexible, superhydrophobic, and electrically conductive polymer nanofiber composite for multifunctional sensing applications. *Chem. Eng. J.* **2020**, *381*, 122778.

29) Wang, P.; Wei, W.; Li, Z.; Duan, W.; Han, H.; Xie, Q. A superhydrophobic fluorinated PDMS composite as a wearable strain sensor with excellent mechanical robustness and liquid impalement resistance. *J. Mater. Chem. A* **2020**, *8*, 3509-3516.

30) Li, Q.; Liu, H.; Zhang, S.; Zhang, D.; Liu, X.; He, Y.; Mi, L.; Zhang, J.; Liu, C.; Shen, C. Superhydrophobic Electrically Conductive Paper for Ultrasensitive Strain Sensor with Excellent Anticorrosion and Self-Cleaning Property. *ACS Appl. Mater. Interfaces*, **2019**, *11*, 21904-25914.

31) Shuang, W.; Xiaosheng, D.; Yaofa, L.; Shiyu, L.; Mi, Z.; Zongliang, Du.; Xu, C.; Haibo, W. Hierarchical design of waterproof, highly sensitive, and wearable sensing electronics based on

MXene-reinforced durable cotton fabrics. *Chem Engineering Journal* **2021**, *408*, 127363.

32) Chu, Z.; Jiao, W.; Huang, Y.; Zheng, Y.; Wang, R.; He, X. Superhydrophobic gradient wrinkle strain sensor with ultra-high sensitivity and broad strain range for motion monitoring. *J. Mater. Chem. A* **2021**, *9*, 9634-9643.

33) Liu, L.; Jiao, Z.; Zhang, J.; Wang, Y.; Zhang, C.; Meng, X.; Jiang, X.; Niu, S.; Han, Z.; Ren, L. Bioinspired, Superhydrophobic, and Paper-Based Strain Sensors for Wearable and Underwater Applications. *ACS Appl. Mater. Interfaces* **2021**, *13*, 1967-1978.

34) Baruah, U.; Manna, U. The synthesis of a chemically reactive and polymeric luminescent gel. *Chem. Sci.* **2021**, *12*, 2097-2107.

35) Liu, C.; Bai, H.; He, B.; He, X.; Zhang, J.; Chen, C.; Qiu, Y.; Hu, R.; Zhao, F.; Zhang, Y.; He, W.; Chau, J. H. C.; Chen, S.; Lam, J. W. Y.; Tang, B. Z. Mn−O Covalency Governs the Intrinsic Activity of Co-Mn Spinel Oxides for Boosted Peroxymonosulfate Activation. *Angew. Chem., Int. Ed.* **2021**, *60*, 2-2.

36) Baruah, U.; Manna, U. The synthesis of a chemically reactive and polymeric luminescent gel. *Chem. Sci.* **2021,** *12*, 2097-2107.

37) Das, A.; Deka, J.; Raidongia, K.; Manna, U. Robust and Self-Healable Bulk-Superhydrophobic Polymeric Coating. *Chem. Mater.* **2017,** *29*, 8720-8728.

38) Das, S.; Das, A.; Parbat, D.; Manna, U. Catalyst-Free and Rapid Chemical Approach for in Situ Growth of “Chemically Reactive” and Porous Polymeric Coating. *ACS Appl. Mater. Interfaces* **2019**, *11*, 34316-34329.

Chapter 4. Covalently Modulated and Transiently Visible Writing: Rational Association of Two Extremes of Water Wettabilities

Anti-counterfeit measures are of ever increasing importance for society, e.g. for securing the authenticity and the proof of origin for medical drugs. Here, an arms race of counterfeiters and valid manufacturers is taking place, resulting in the need of hard to forge, yet easy to read-out marks. Anti-counterfeiting measures based on micro-patterns, while being attractive for their need in not widely available printing methods while still being easily read out with fairly common basic optical equipment are often limited by being too easily destroyed by wear or handling. Here, nature-inspired wettability is rationally exploited for developing an unprecedented anti-counterfeiting method, where hidden information can be only identified under direct exposures to an aqueous phase or mist and disappears again on air-drying the interface. A chemically reactive and hierarchically featured dip coating, capable of spatially selective covalent modification with primary amine containing small molecules, is developed for abrasion tolerant patterning interfaces with two extremes of water wettabilities, i.e. superhydrophilicity and superoleophobicity. Arbitrary hand writing with glucamine, followed by chemical modification with octadecylamine, provided 'invisible' text on the synthesized interface. The glucamine treated region selectively become optically transparent and superhydrophilic due to rapid infiltration of the aqueous phase on exposure to liquid water or mist. The remaining interface remains opaque and superhydrophobic due to metastable entrapment of air. The hidden text became transiently and reversibly visible by naked eye under exposure to liquid-water/mist. Furthermore, microchannel cantilever spotting (μCS) is adopted for demonstrating well defined chemical patterning on the microscale. These patterns remained capable of sustaining severe physical abrasions because of the bulk functionalization, retaining the wetting properties (and thus pattern read-out). Such simple synthesis of spatially controlled, direct and covalently modulated wettability could be useful for various applied and fundamental contexts.

* S. Das *et al.*, *ACS Appl. Mater. Interfaces* **2020**, *12*, 2935-2943

4.1. Introduction

Hiding secret information is the general basis for defying the severe challenges related to counterfeiting.[1-8] Mostly, the luminescence dependent approaches including thermoplasmonic nanoparticle, metal-organic frameworks, lanthanide-based inks, complex wrinkling etc.,[2-7] were adopted for this purpose. Moreover, hydrochromic dyes are strategically used in switching colors from invisible to visible depending on dry and wet conditions, where a change in molecular structure of the dye leads to a color change.[8] However, the inherent optical instability and uncontrolled quenching of the reported materials under repetitive exposures to day light and requirement of special equipment for identifying the hidden information are obvious existing challenges in the reported approaches. Therefore, further progress is essential for developing simple, but effective anti-counterfeiting techniques. Here, a covalent and spatially selective chemical modulation approach is unprecedentedly adopted for developing a luminescence-free, transient and reversible visualization of hidden information. This is achieved through strategic use of two extreme water wettability properties: 1) superhydrophobicity[9-10] and 2) superhydrophilicity.[11-12] In the past, different biomimicked interfaces[9-12] were successfully exploited in demonstration of various practically relevant potential applications—including oil/water separation, self-cleaning, drug delivery, corrosion resistance and so on.[13-25] In addition to this, different non-contact (UV light and laser-assisted patterns) of physical surface deposition[26-32] processes have been adopted for developing superhydrophobic and hydrophilic patterned interfaces, where the low surface chemistry of superhydrophobic coating is selectively compromised on top of the hierarchical interface.[26-32] Such synthetic designs are fundamentally inappropriate to sustain any practically relevant severe abrasive insults, and as expected, physically abraded interfaces completely failed to display any patterns. Moreover, examples of direct and contact-based writing on superhydrophobic interface through strategic use of chemical ink is rare in the literature.

In the past, the concept of a hydrophobic/hydrophilic surface that can display a pattern through vapour condensation as a method to make counterfeiting is achieved with ultra-thin self-assembled monolayers (SAMs).[33] However, such interfaces are less likely to sustain under practically relevant physical abrasions. Here, in this current approach, a highly abrasion tolerant and chemically reactive porous polymeric coating is introduced for transiently visible writing. Such demonstration is unprecedented in literature, and such an approach could be useful for anti-counterfeiting applications. The metastable trapped air in the superhydrophobic material inhibits the infiltration of the aqueous phase in the hierarchically featured interface and provided heterogeneous and extreme aqueous repellency.[34] In contrast, superhydrophilic interfaces are highly water compatible and allowed rapid infiltration of aqueous phase.[11] These distinct and extremes water wettabilities are associated with separate chemical requirements. There are very few reported approaches, which are capable of modulating the chemistry

in the hierarchically featured interfaces with a) low surface energy and b) high surface energy moieties. Earlier our lab introduced chemically reactive multilayers (9 bilayers, each bi-layers associated with 6 steps) of a polymeric nanocomplex for developing both superhydrophobicity in air and superoleophobicity under water from a single polymeric coating,[35] where the chemistry of the chemically reactive multilayers coatings is covalently modulated with appropriately selected small molecules. However, the synthesized polymeric coating was found to be inappropriate for spatially selective chemical modification as both organic and aqueous solution of selected small molecules (glucamine) rapidly spread and spilled all over the interface, thus developing a contact based, permanent pattern of two extreme liquid wettabilities was challenging.[35] Here, a single step dip coating approach is introduced, making strategic use of the Michael addition reaction between branched polyethylenimine (BPEI) and dipentaerythritol penta-acrylate (5Acl) as shown in Figure 4.1A-C.[36] The as-synthesized amine reactive polymeric coating allowed i) spatially selective post-covalent modification with glucamine, directly from aqueous medium as shown in Figure1E, where a fountain pen filled with aqueous ink of glucamine was used to manually write 'IITG'. Furthermore, the post chemical modification with ii) hydrophobic small molecules (octadecylamine, ODA, Figure 4.1F) yielded both invisible and permanent text. This hidden information was transiently and reversibly revealed on exposing the interface to either liquid water or even simply mouth's mist. We demonstrate the feasibility of micro-patterning of these coatings by spotting microscale arrays showing the same wetting behaviour on a much smaller scale.

4.2. Experimental Section.

4.2.1. Preparation of the Reactive Thin Layer by Dip Coating. The solutions of dipentaerythritol pentaacrylate (5Acl, 132.5 mg mL^{-1}) and Branched poly(ethyleneimine) (BPEI, 50 mg mL^{-1}) in 1-heptanol were prepared first in two separate glass vials. Then 1.2 ml of BPEI was mixed with 4 ml of 5Acl solution in 1-Heptanol to prepare reaction solution, and then a clean glass slide (5.5 cm × 1 cm) was taken as a model substrate and immersed into the solution immediately and kept the substrate into the solution for different durations (e.g; 1 minute, 3 minutes, 5 minutes, 7 minutes, 10 minutes). Next, the glass substrate was brought out from the reaction mixture, and kept in air for drying. These polymeric dip coatings were thoroughly washed with THF, prior to the post chemical modifications.

4.2.2. Post-Modification with Desired Amine Containing Small Molecules. The chemically reactive polymeric coating was covalently post-functionalized with primary amine containing selected small molecules including octadecylamine (5 mg mL^{-1}, in THF) and Glucamine (2.5 mg mL^{-1}, in DMSO) following procedures described in chapter 2. This chemically reactive polymeric dip coating was exposed to amine containing small molecules solution. Next, the material was thoroughly washed with

THF and dried under the stream of compressed air, prior to further essential characterization or other relevant proof-of-concept experimental demonstrations.

4.2.3. Patterning on the 'Reactive' Hydrophobic Thin Layer. For droplet based chemically modulated patterns, aqueous (alkaline, 10 µL) droplets of glucamine were gently placed on the inherently hydrophobic 'reactive' polymeric coating for 5 minutes. Next, the beaded aqueous droplet was soaked with tissue paper, and the whole substrate was kept in air for drying before exposure to a solution of octadecylamine (ODA, in THF). This spatially selective distinct chemical modulations allowed to develop patterned interfaces with two distinct liquid wettability. Next, manually text was written with fountain pen (PARKER), where the ink was replaced with an aqueous solution of glucamine. After completion of manual writing the selectively wetted interface was kept under humid environment for 5 minutes, the humid environment helped in reducing the rate of evaporation of the aqueous phase. Next, the air dried interface was post-modified with ODA (in THF). This simple process provided invisible hand writing, which was only visible in presence of mist or in contact with liquid water, and became completely invisible again after air-drying the patterned interface.

4.2.4. Patterning Procedure. All patterning by µCS was done on the NLP 2000 instrument (Nanoink Inc.). The microchannel cantilever[40,41] (SPT-S-C10S) were purchased from Bioforce Nanosciences. Prior to use microchannel-cantilever were plasma cleaned by oxygen (0.2 mbar, 100W, 20 sscm O_2, 2 min) on a Diener plasma cleaning system Atto. The microchannel-cantilever reservoir was then filled with 0.5 µl of ink and the ink was pushed into the pen by blowing with a nitrogen stream. All patterning was done at room temperature, with different humidity ranging from 50-70 % RH. The STV_cy3 and glycerol for producing the ink mixture were obtained from Sigma-Aldrich (Germany). STV_cy3 was used as received with concentration of 1 µg/µL. After printing and resting time, the samples were washed with DI water (18.2 MΩ cm, Arium water system, Sartorius, Germany) to make sure to remove unbound ink. Samples were then dried with nitrogen before further analysis. All imaging was done on an upright fluorescence microscope (Eclipse 80i with DS-Qi2 camera, Nikon Germany).

4.3. Results and Discussions

4.3.1. Preparation and General Characterization of Coating. As discussed in chapter 2, a transparent reaction solution of BPEI and 5Acl in heptanol rapidly transformed into an opaque solution due to formation of the polymeric nanocomplex and eventually formed a semisolid polymeric gel within 15 min (Figure 4.2A). The size of the polymeric nanocomplex increases exponentially in the reaction mixture over time (Figure 4.2B).

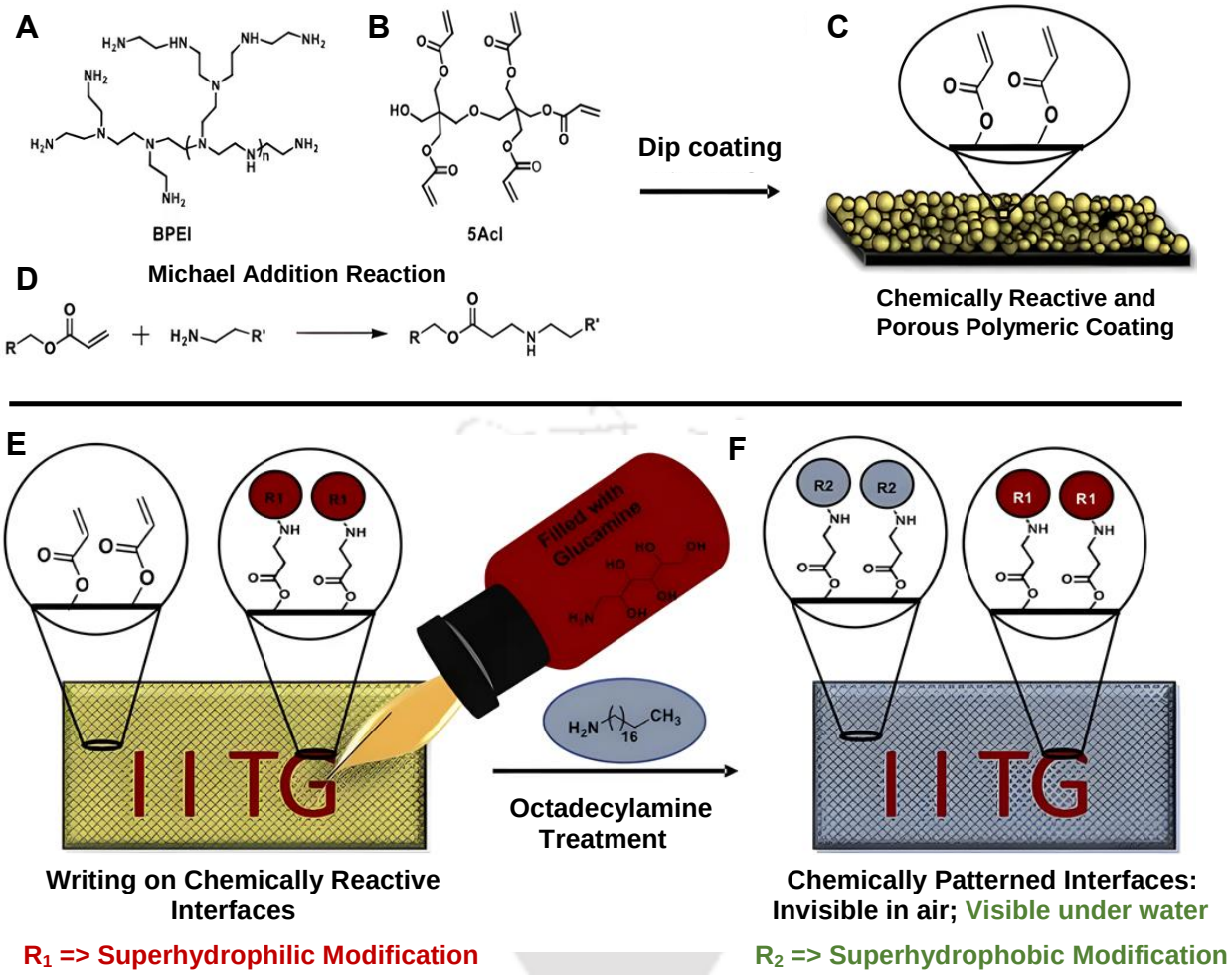

Figure 4.1. (A-B) Chemical structures of branched polyethylenimine (BPEI, A) and dipentaerythritol penta-acrylate (5Acl, B). (C) Schematic presentation of chemically reactive polymeric dip coating that was directly prepared from the reaction mixture of BPEI/5Acl. (D) Illustrating Michael addition reaction between amine and acrylate. (E-F) Spatially selective chemical modulation of the amine reactive polymeric dip coating with aqueous ink of glucamine (E), followed by octadecylamine (F) for synthesis of invisible patterns.

A cleaned glass slide was placed in this reaction mixture for a controlled time, and removed from the reaction mixture followed by air-drying. At the end, a polymeric coating is visible on the glass substrate; the thickness of the coating increases with longer immersion time (from 1 minute to 10 minutes) of the glass slide in the reaction mixture of BPEI/5Acl (Figure 4.3A). Further, water wettability was examined on the polymeric coatings that were prepared by varying the immersion time of the substrates in the reaction solution. The static water contact angle was gradually increased from ~94° to ~132° with increasing immersion time (from 1 minute to 10 minutes) of the respective substrate in the reaction solution as noted in Figure 4.3A. This inherently high hydrophobicity helped in developing chemically modulated and spatially selective patterned interfaces that display a contrast in water (in air) or oil (under water) wettability, such interfacial property is characterized in details.

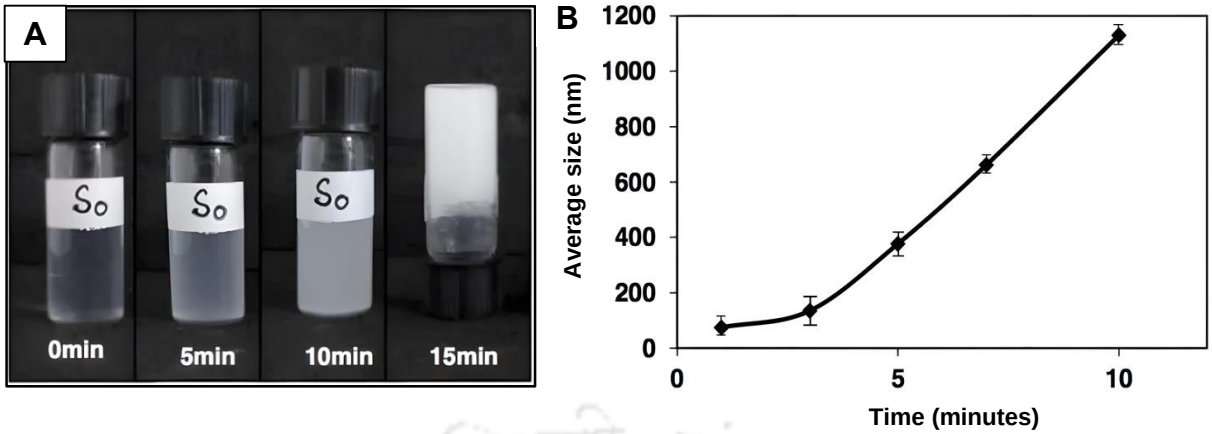

Figure 4.2. (A) Digital image accounts change in appearance of the reaction mixture of BPEI/5Acl in heptanol over the time. (B) DLS study accounting the change in size of the polymeric nanocomplex in the reaction mixtures over different time (e.g.; 1 minute, 3 minutes, 5 minutes, 7 minutes, 10 minutes).

Examining the topography of the synthesized polymeric coatings found that the morphology of the polymeric coatings significantly changed with increasing the substrate immersion times in the reaction solution as shown in Figure 4.4.

A porous and hierarchical topography was noted in the polymeric coating that was prepared by immersing in the reaction solution for 10 minutes, where granular polymeric nanocomplexes were randomly aggregated and formed arbitrary microstructures as shown in Figure 4.4C, F. Next, the available chemical functionality in the synthesized polymeric dip coating was examined by FTIR analysis. The appearance of IR peaks at 1410 cm^{-1} and 1734 cm^{-1}, which were characteristic of a) C-H stretching of β carbon of the vinyl groups and b) carbonyl stretching respectively,[36] revealed the existence of residual acrylate groups as shown in Figure 4.3D. These unreacted acrylate groups were responsible for the reactivity of this polymeric dip coating towards amine molecules and provide a facile avenue for modulating chemistry in the Figure 4.3B-C.

Next, samples of the chemically reactive polymeric dip coating were individually treated with glucamine and ODA, and re-investigated post-chemical modification. The IR peak intensity at 1410 cm^{-1} that corresponded to the C-H stretching of β carbon of the vinyl group, was reduced significantly compared to the carbonyl stretching at 1734 cm^{-1} as internal reference shown in Figure 4.3D. During the Michael addition reaction, the carbonyl moiety in the residual acrylate groups were remained unaffected, and the vinyl groups were converted from sp^2 hybridization to sp^3 hybridization on reaction with primary amine groups as shown in Figure 4.3B-C. Thus, the IR peak intensity for C-H stretching of β carbon of the vinyl groups at 1410 cm^{-1} was reduced, which strongly suggests the successful covalent modulation of the chemically reactive polymeric dip coating with the primary amine containing small molecules.

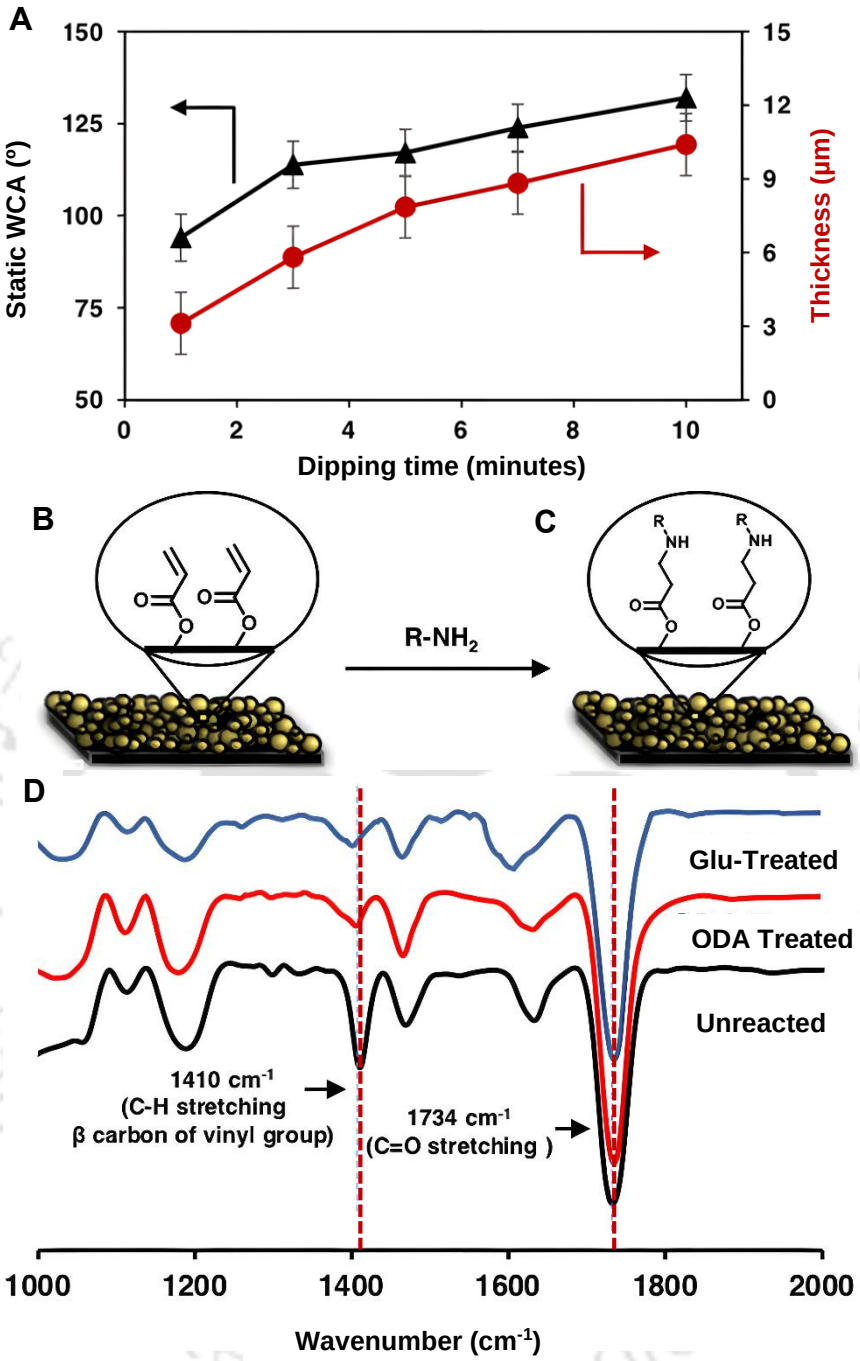

Figure 4.3. (A) The plot accounting the change in the thickness and static water wettability of the polymeric dip coating—with the dipping time of the substrate in the reaction mixture of BPEI/5Acl. (B-C) Schematic representation of postcovalent modulation of the as-synthesized polymeric dip coating with primary amine containing small molecules through Michael-addition reaction. (D) FTIR spectra of chemically reactive dip coating before (black) and after post covalent modulation with glucamine (blue) and octadecylamine (red).

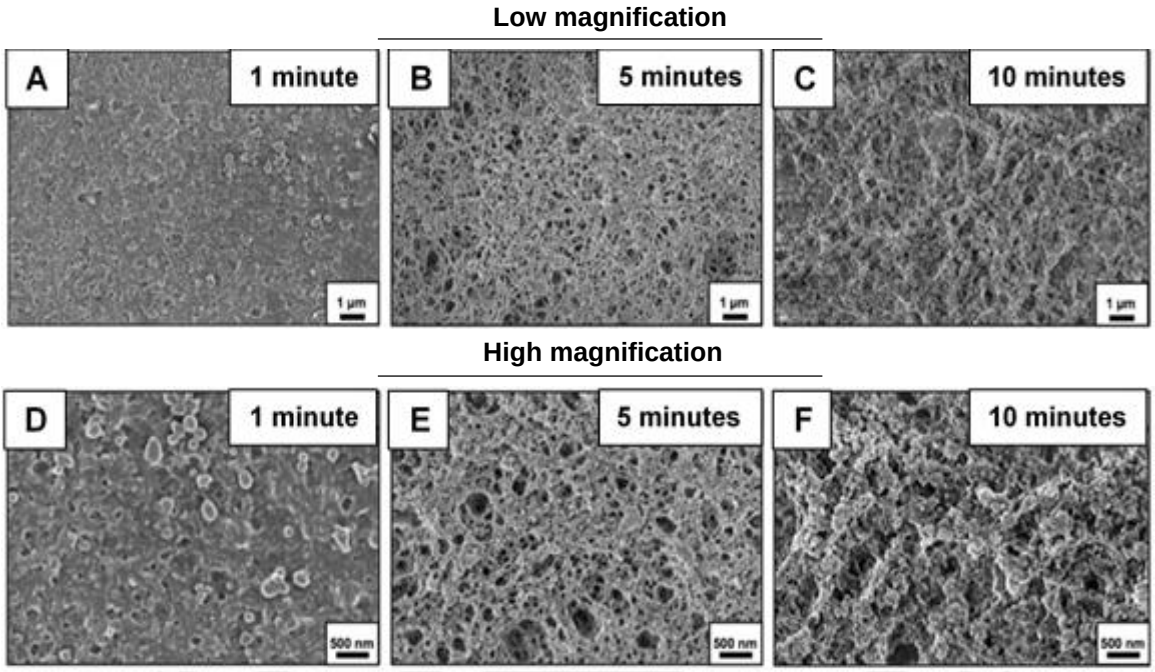

Figure 4.4. (A-F) FESEM images of the polymeric dip coatings that are prepared by immerging the selected substrate in reaction mixture for 1 minute (A, D), 5 minutes (B, E) and10 minutes (C-F), in both low (A, B, C scale bar = 1 µm) and high (D, E, F scale bar = 500 nm) magnifications.

4.3.2. Chemical Modulation of Wettability. Both the water (in air) and oil (under water) wettabilities were individually examined on chemically reactive polymeric coatings formed by dipping glass slides in the reaction mixture of BPEI/5Acl for different durations (1 min, 5 min, and 10 min), after the chemical modification with ODA and glucamine, respectively. The inherently hydrophobic (static water contact angle ~136°) polymeric dip coating (prepared by 10 minutes of immersion in the reaction solution) became non-adhesive superhydrophobic with a static water contact angle of above 155° (Figure 4.5A-D) and a roll of angle of 5°. Water droplets instantly roll off on the ODA-treated polymeric interfaces, and a jet of water immediately bounces away after hitting the interface. These simple demonstrations further revealed the non-adhesive superhydrophobicity. Moreover, this interface was found to be highly opaque (with transparency below 6% as shown in Figure 4.6) and shiny under water, due to the presence of metastable trapped air. This trapped external phase (air) is the primary element for minimizing the effective contact area between the water droplets and the synthesized superhydrophobic interface.

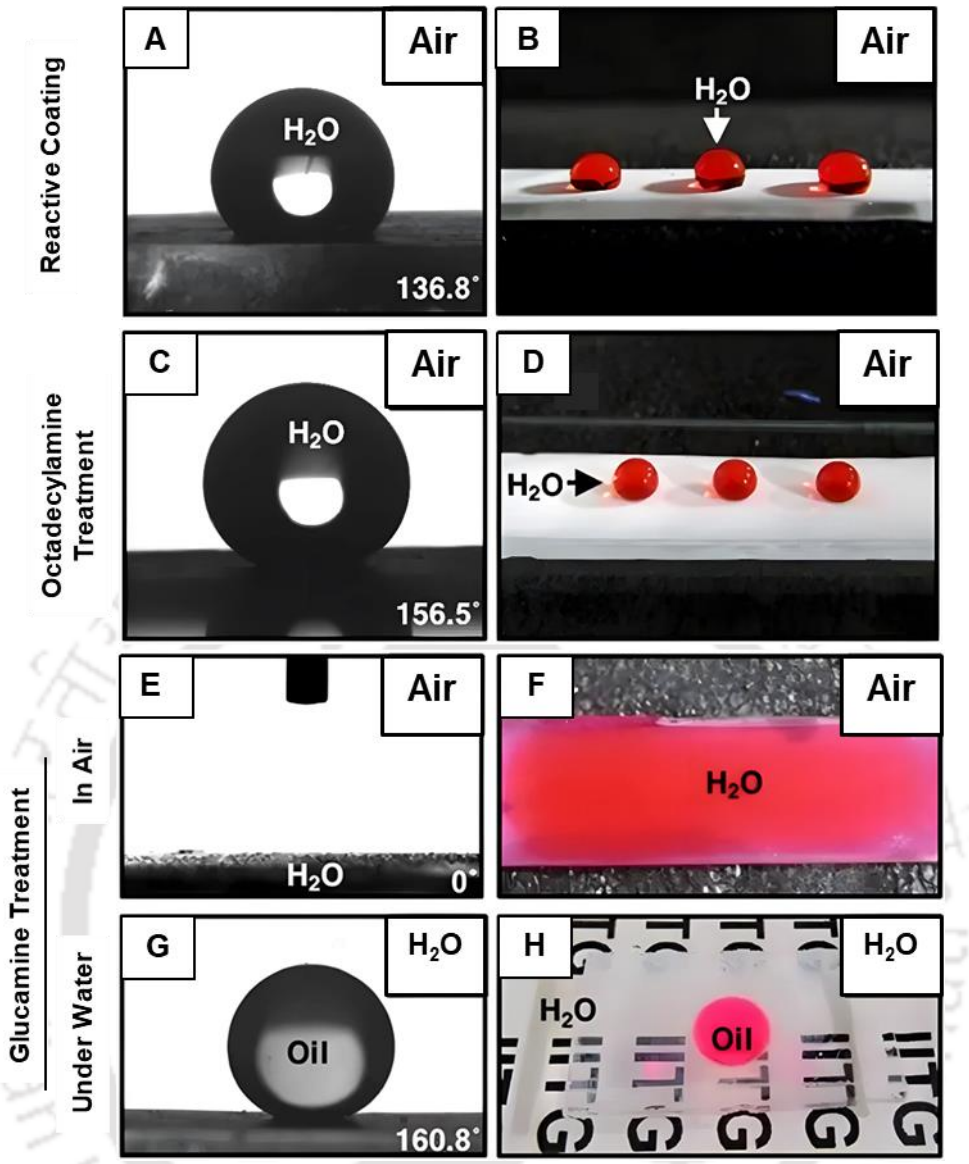

Figure 4.5. (A-H) Contact angle (A, C, E, G) and digital (B, D, F, H) images of beaded water (in air; A-F) and oil (under water; G-H) droplets on the chemically reactive polymeric dip coating before and after treatments with octadecylamine (A-D) and glucamine (E-H).

The fraction of solid contact area with a liquid droplet can be estimated following the general equations 1 and 2,

$$cos\theta_r = f_1 cos\theta — f_2 \quad \text{(eq1)}$$

$$f_1 + f_2 = 1 \quad \text{(eq2)}$$

Where, θ and θ_r are respective liquid (either water in air or oil phase under water) contact angles on both the smooth and featured interfaces, whereas f_1 and f_2 are defining the fraction of contact area between beaded liquid phase (water in air or oil under water) with solid interface and trapped external

phase (air for superhydrophobic interface and aqueous phase for underwater superoleophobicity), respectively.

For the estimation of fraction of contact area, a smooth and featureless (as confirmed from FESEM imaging) polymeric coating was further developed using same chemicals (multilayer (9 bilayers) of BPEI/5Acl) but following reported layer-by-layer deposition procedure.[27- 28] The glucamine treated smooth coating display static oil contact angle (SOCA) of 106.5° under water, whereas the ODA-treated multilayers was with static water contact angle (SWCA) of 56.5° in air. Further, static water (in air) contact angles (Figure 4.3A) on the ODA treated interfaces were used in the eqn 1 and 2 for measuring the fraction of contact area between beaded water with metastable trapped air. Beaded water droplets (SWCA of 155.6°) remain mostly in contact with the metastable trapped air and the fraction contact area was 0.943. Polymeric coatings formed with shorter immersion time (1 minutes and 5 minutes) show adhesive superhydrophobicity after ODA treatment, where water droplets on such interfaces have an advancing water contact angle above 150° and contact angle hysteresis above 10° as shown in Figure 4.3A. The fraction of contact area between the metastable trapped air and the beaded water droplet was reduced to 0.87 (for 5 minutes) and 0.79 (for 1 minute), respectively, allowing more interaction with the beaded liquid phase. On the other side, the same chemically reactive and inherently hydrophobic polymeric coating readily transformed to superhydrophilic in air with a water contact angle of 0°, after chemical modification with glucamine as shown in Figure 4.5E-F

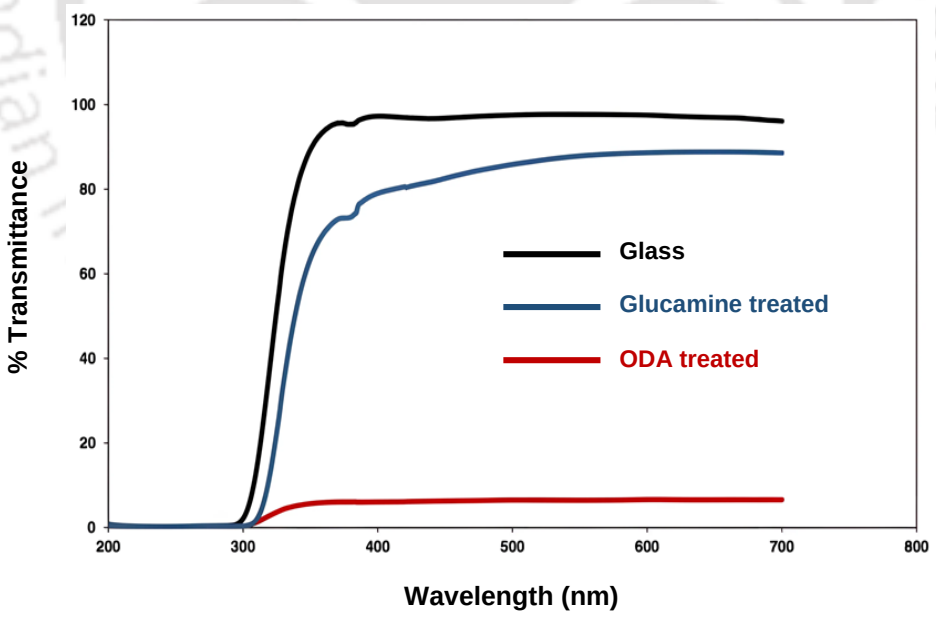

Figure 4.6. The plot comparing the underwater optical transparency of the bare glass (black curve) with polymeric dip coated glass substrates that are post modified with octadecylamine (red curve) and D-glucamine (blue curve) treated.

The hierarchically featured polymeric dip coating, being highly water compatible after glucamine treatment, was presumed to display fish-scale inspired underwater superoleophobicity. As expected, the glucamine treated polymeric coating repelled the widely used model heavy oil (dichloroethane, DCE, colored with red dye) under water with a static oil contact angle of ~161.2° and a contact angle hysteresis below 10° as shown in Figure 4.5G-H. The infused aqueous phase in the hierarchically featured polymeric dip coating (treated with glucamine) contributes to the extreme heterogeneous oil wettability under water by minimizing the contact area between the oil droplet and the polymeric dip coating. The fraction of solid interface that was exposed to the oil phase under water was calculated to be only 0.07, following the same eqn 1 and eqn 2 as mentioned earlier. Moreover, this aqueous phase impregnated, extreme oil repellent polymeric dip coating (modified with glucamine) was found to be highly optically transparent (more than 80 % under visible light (380 nm to 700 nm)) under water as shown in Figure 4.5H and Figure 4.6.

4.3.3. Patterning of Coating and Abrasion Tests. The inherently hydrophobic and chemically reactive dip coating, capable of providing both superhydrophobicity and underwater superoleophobicity, depending on the selection of appropriate chemical modifications, was further

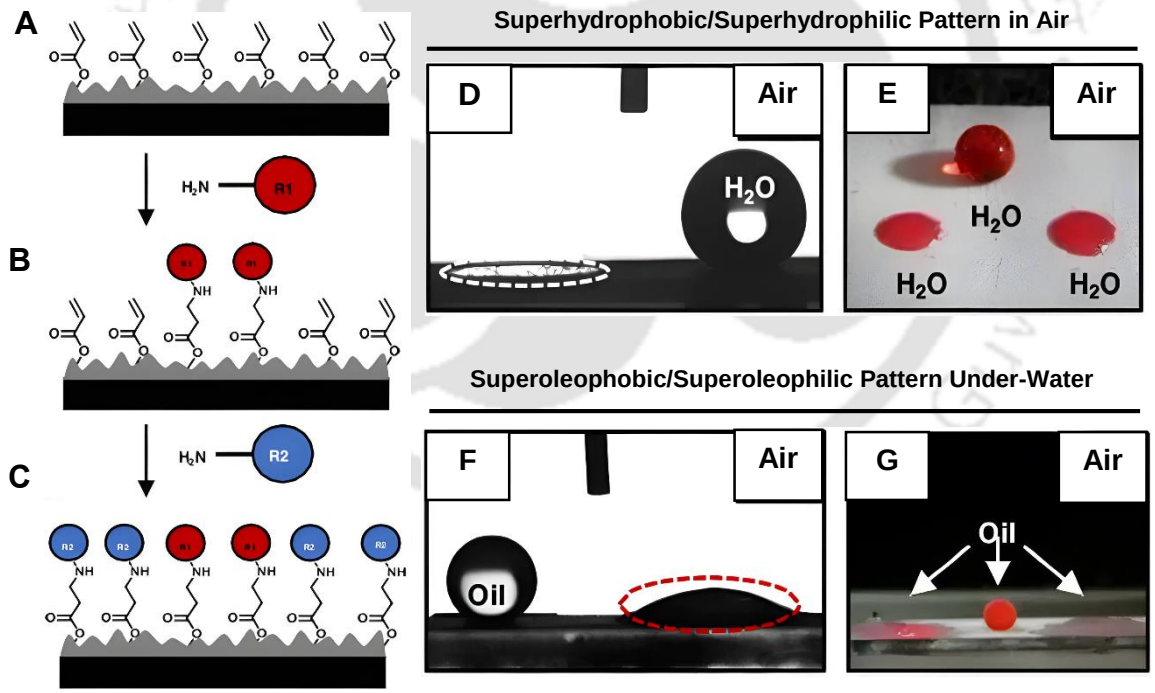

Figure 4.7. (A-C) Schematic representation of location specific modulation of chemistry on the polymeric dip coatings with selected small molecules (B-C). (D-G) Contact angle (D, F) and digital (E, G) images of location specific chemically modulated patterned interface that display superhydrophobic/superhydrophilicity (D-E; in air) and superoleophobicity/superoleophilicity (F-G; under water), where the beading/spreading of water (in air) and oil (underwater) on glucamine and ODA treated area is demonstrated. The glucamine treated area in the patterned interfaces is indicated with dotted white circles and rest of the region is treated with ODA.

exploited in fabricating spatially selective and chemically controlled pattern as shown in Figure 4.7A-C. Here, one type of chemical functionality was selectively applied in the desired location of the reactive dip coating before quenching the rest of the chemical functionality with another type of primary amine containing small molecules through 1,4 conjugate addition reaction. This covalent bonding based back filing approach allows to fabricate arbitrary permanent patterns of two extreme and opposite liquid wettabilities, depending on the appropriate modification of the reactive dip coating with selected primary amine containing small molecules (glucamine, octylamine, octadecylamine, dopamine etc.) or macromolecules (i.e. proteins).

As a proof of concept demonstration, an alkaline (pH~ 9) aqueous droplet of glucamine solution was placed on the chemically reactive and highly hydrophobic polymeric dip coating for spatially selective chemical modification of the coating with glucamine molecules. The rest of the residual acrylate groups in the polymeric coating were scavenged by reaction with a hydrophobic small molecule (ODA). This strategy yielded a superhydrophobic and superoleophobic patterned interface, where the glucamine treated regions were superoleophilic, while the rest of the area was superhydrophobic as shown in Figure 4.7D-E. Furthermore, oil wettability was examined on such chemically modulated patterned interfaces. Oil droplets instantly spread on ODA treated interfaces with a contact angle of 0°, while glucamine treated circular areas on the patterned interface repel oil under water extremely with a static oil contact angle of above 160° as shown in Figure 4.7F-G. Thus, the described chemical modulation approach provides a single basis to create interfaces with patterned wettability within air (superhydrophobicity/superhydrophilicity) and under water (superoleophilicity/superoleophobicity). Furthermore, the synthesized chemically patterned superhydrophobic/superhydrophilic interface was exposed to an adhesive tape peeling test, which involves severe physical abrasion of the polymeric interfaces (Figure 4.8A-C). A freshly exposed adhesive tape was brought in contact with the chemically modulated patterned interface, and the top portion of the polymeric coating was arbitrarily cleaved and transferred to the adhesive surface during the peeling process as shown in Figure 4.8C. However, the embedded patterned wettability remained unperturbed even after incurring such severe physical abrasion to the polymeric coating, and a freshly exposed interior that transferred onto the adhesive tape is also capable of displaying contrast water wettability as shown in Figure 4.8C. Further, experiment was conducted to characterized post-covalent modification at the interior of the polymeric coating with glucamine through 1,4 conjugate addition reaction. First, a large portion of the polymeric coating is modified with glucamine, and ATR spectra was recorded before and after incurring adhesive tape peeling taste on the same polymeric coating. The IR spectra are compared with chemically reactive polymeric coating for monitoring the covalent modification. Very similar depletion of IR peaks at 1410

cm^{-1} with respect to normalized IR peak for carbonyl stretching was noted before and after physical abrasion of the coating as shown in Figure 4.8D.

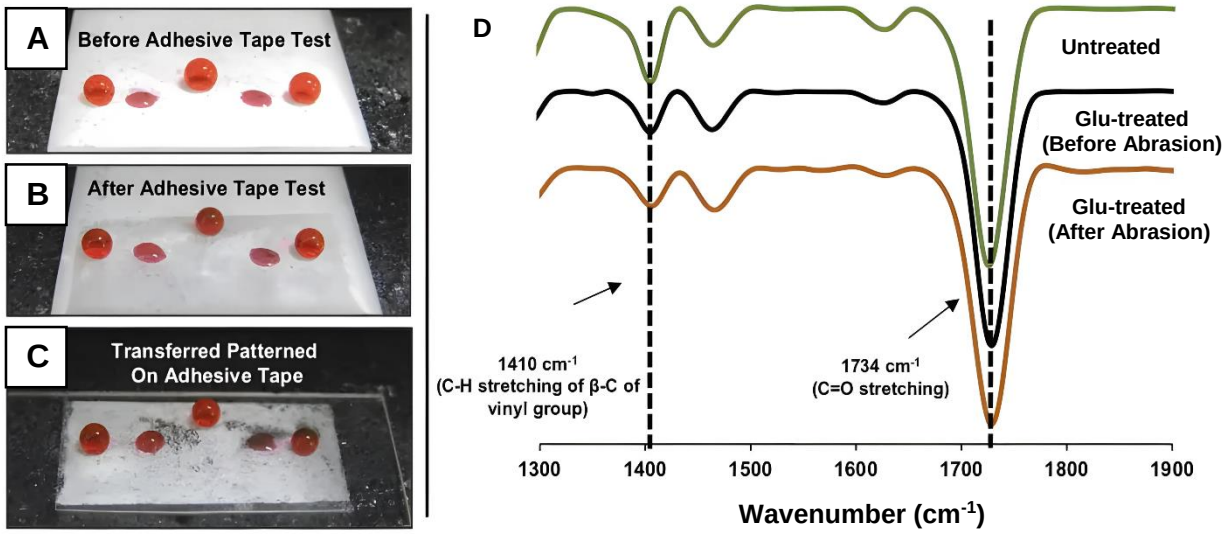

Figure 4.8. (A-C) Digital images showing the retention of the circular hydrophilic pattern (glucamine treated) prepared on the superhydrophobic (post-treated with ODA) dip coated glass substrates (A), after performing the adhesive tape test on the chemically modulated pattern interface (B). During the course of adhesive tape peeling test, the top portion of the polymeric coating is randomly cleaved, and was transferred onto the adhesive tape (C), which resulted in exposure to the interiors of the polymeric coating. However, the patterned water wettability (glucamine treated spots are hydrophilic, other parts treated with ODA superhydrophobic) remained intact in the freshly exposed interiors of the polymeric coating, revealing the three dimensional and inherently durable nature of the patterned interface. (D) Representing IR spectra of polymeric coating before (black line) and after (and orange line) physical abrasion of the glucamine-treated polymeric coating, where both the IR spectra were compared with IR spectrum of untreated polymeric coating (green line).

This IR analysis unambiguously revealed three dimensional post-covalent modification of porous polymeric coating with glucamine. Thus, this simple demonstration validated the existence of three dimensional natures of the chemically modulated patterned/writing, which is capable of withstanding severe physical challenge, and examples of such designs are rare in the literature. Such material could be useful in various potential applications. Here, this approach was extended further for covalently modulated apparently invisible hand writing with contrast liquid wettability for the first time, where the spatially selective displacement of trapped air allowed to control the transparency of the chemically modulated patterned interface depending on dry and wet conditions. The inherently hydrophobic and as-synthesized highly chemically reactive hierarchical interfaces allowed to write text directly, without spreading or spilling, using a fountain pen loaded with an aqueous glucamine ink. Further post chemical modification with ODA provided permanent, invisible and well defined text on such interfaces, with conceivable use for preventing counterfeiting. The apparently hidden (Figure 4.9) information can be visualized by exposure to an aqueous phase as shown in Figure 4.9I.

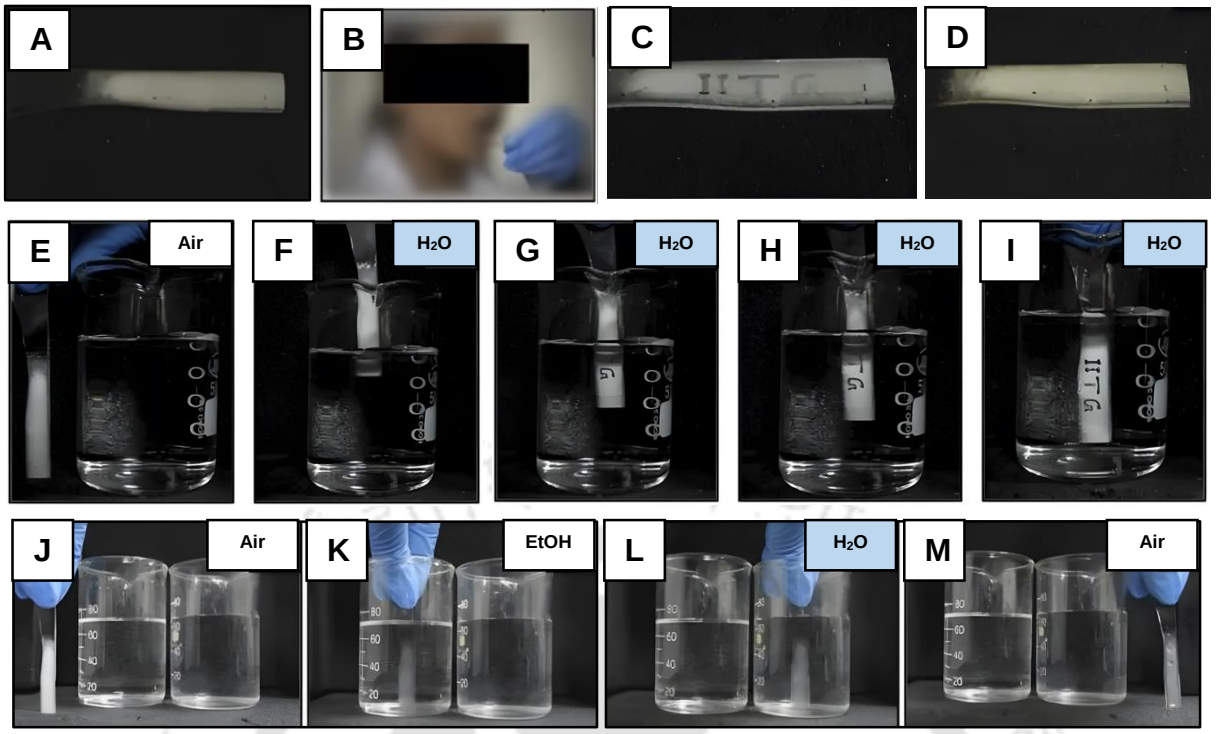

Figure 4.9. (A-D) Digital images illustrating the appearance of invisible hand-writing (A) on exposure to mouth's mist (B-C), and this pattern was disappeared on air drying of condensed aqueous phase (D). (E-I) Digital images illustrating the appearance of visible hand writing (in air, E), once the patterned interface is exposed to liquid water. Whereas no such visibility is observed if the patterned interface is exposed to ethanol (J-K), prior to submerging in water (L-M), the exposure of ethanol removes the metastable trapped air. The selective entrapment of metastable trapped air is crucial for the appearance of invisible pattern.

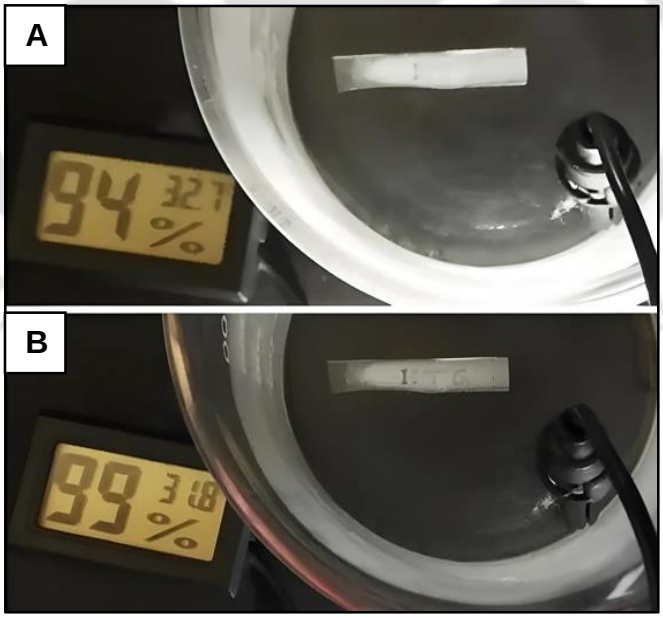

Figure 4.10. (A-B) Digital images accounting the change in visibility of the chemically modulated patterned interface in humid air. The visibility of the pattern is clear (B) with 99% humid air, whereas the appearance of the pattern is faint in 94% humid air (A).

As expected, this text disappeared again on the interface after air-drying. Furthermore, this transient and reversible identification of the hidden information was also successfully achieved by exposing these patterned interfaces under mouth's mist (instead of direct exposure to liquid aqueous phase) for multiple (100) times as shown in Figure 4.9A-D. In the past, the principle of breathing is widely and mostly used in developing different ordered porous films.[37] The invisible pattern on the polymeric

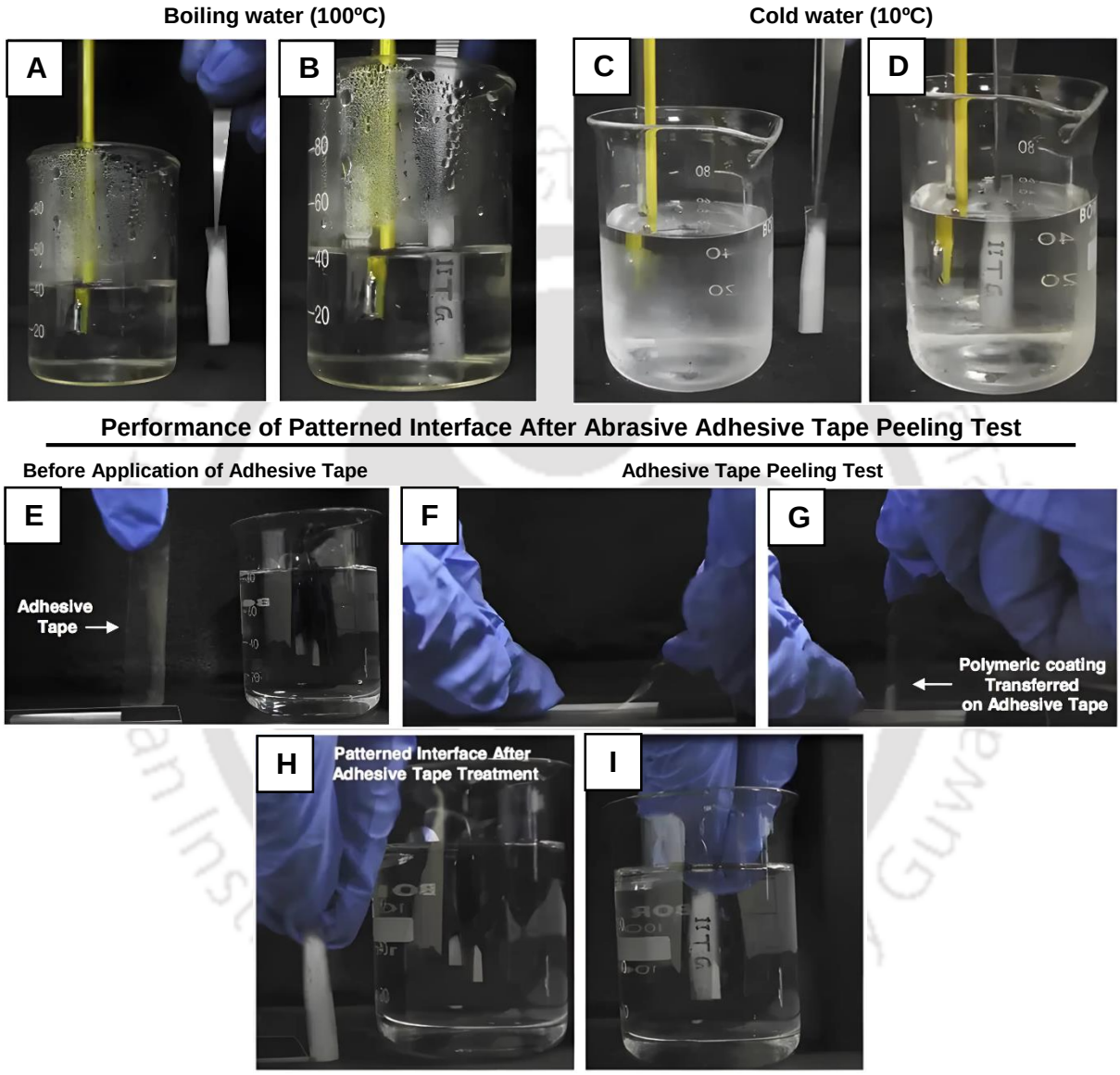

Figure 4.11. (A-D) Demonstrating the performance of an invisible chemically patterned interface at high (100°C; A-B) and low (10°C; C-D) temperatures. (E-I) Digital images illustrating both adhesive tape tests (E-G) and the performance (H-I) of the physically abraded polymeric patterned interfaces under water. During the adhesive tape peeling process, the top portion of the polymeric coating is physically abraded (G). However, the invisible chemically modulated pattern remains intact and the physically abraded pattern is visible under water (I). This impeccable durability of the invisible patterned is attributed to the existence of three dimensional patterned wettability in the polymeric coating.

coating became clearly visible in 99% humid air (Figure 4.10A-B). Moreover, the performance of the chemically patterned polymeric coating remained unaltered at both high (100°C, Figure 4.11A-B) and low (10°C, Figure 4.11C-D) temperatures. The same polymeric interface was contacted to a freshly exposed adhesive tape (Figure 4.11E), and during the peeling process some top portion was physically abraded (Figure 4.11G). Nonetheless, the invisible pattern in the damaged interface was found to still be visible on exposure to water as shown in Figure 4.11H-I. This impeccable durability of the chemically patterned interface is mostly due to the existence of three-dimensional super-liquid-wettability in the polymeric coating as evident from Figure 4.8. Thus, the strategic combination of contrast wettability and transparency provided a facile and completely different approach for easy and repetitive (100 times) identifications of invisible information, where the selective entrapment of metastable trapped air plays a crucial role. The same interface treated with ethanol, prior to exposure to water, is incapable in displaying hidden information as shown in Figure 4.9J-M.

As a further trial, this approach was extended to a model optically opaque substrate, i.e. filter paper. The same synthetic strategy was followed for creating a chemically modulated invisible patterned interface on the filter paper. The hidden information (in air) was revealed after transferring the coated filter paper in DI water (Figure 4.12A-B). Thus, the current approach is likely to be successfully generalized to various substrates.

4.3.4. Development of Micro-patterns. Generation of micro-patterns Anti-counterfeiting can greatly benefit from miniaturization by the ability to hide a marking pattern to keep it secret until an authority

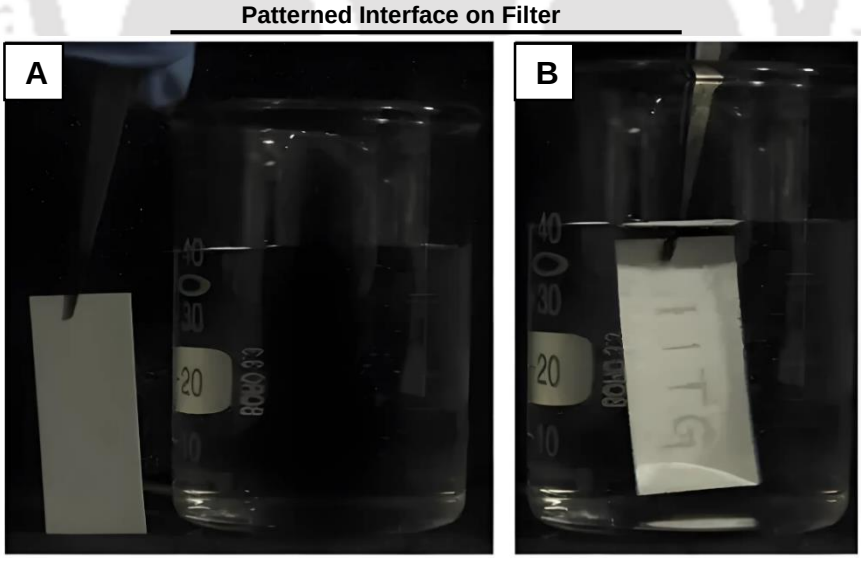

Figure 4.12. (A-B) Digital images accounting the performance of the invisible chemically modulated patterned interface on a filter paper. The pattern is invisible in air (A) on the polymeric coating on an opaque substrate but becomes visible under water (B), likely due to selective displacement of external metastable trapped air from glucamine treated regions.

needs to check authenticity and by making a marking pattern more difficult to reproduce by counterfeiters with usually limited access to specialized micro-patterning tools due to prohibitive investment costs and/or restriction in sale such machines.

To elucidate the feasibility of miniaturizing the patterns on the coating and to show the effect of superhydrophobicity on the microscale, the microchannel cantilever spotting (µCS) technique was used to pattern dot microarrays under controlled environment and parameters.[38,39] First, for determining the pattern quality and establish writing parameters, streptavidin covalently bound with cyanine3 dye (STVCy3) was spotted (Figure 4.13). The amine group in STV covalently binds to the amine reactive group on the surface and the cy3 dye can then be used to check the quality of the written pattern with fluorescence microscopy. The ink was admixed with 20 Vol% glycerol for better flow of ink to the

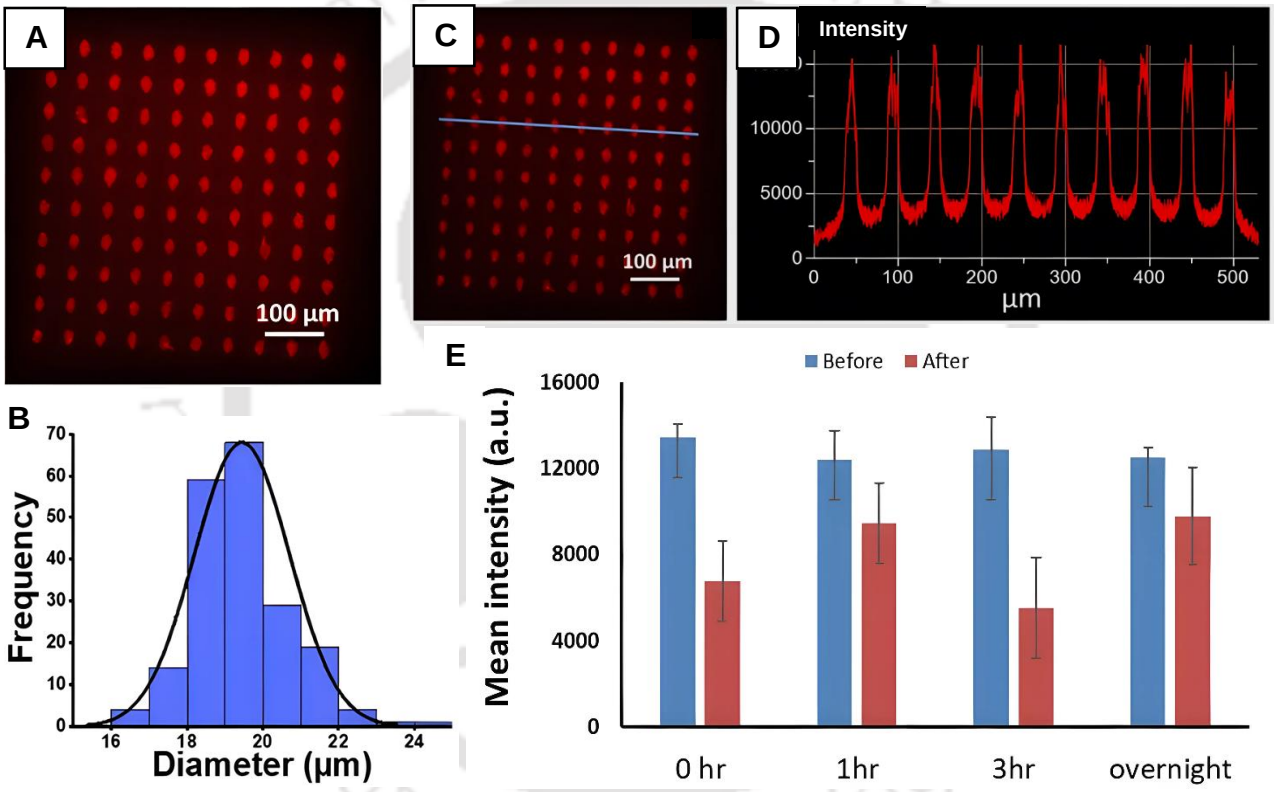

Figure 4.13. (A) Florescence microscopy image of a 10 × 10 dot microarray of a fluorescently labelled protein on amine reactive polymeric dip coating substrate after washing. The dots appear slightly elongated in respect to the cantilever orientation during µCS due to attachment of droplets to the cantilever by capillary forces. (B) Histogram derived from 200 features (two 10 × 10 dot microarrays as seen in (A) showing the homogeneity of obtained patterns. Fluorescence intensity comparison with different resting time. (C) typical 10x10 pattern (D) the intensity graph of the blue line on image (C). (E) comparison graph of the mean intensity with different resting time before and after washing. For each measurement, 100 dot features were evaluated, one standard deviation is given as error bars. The "0 hr" data point refers to immediate washing after lithography takes place, so including printing and sample transfer the protein solution would have around 5 to 10 minutes of reaction time in these cases before the ink is removed by washing.

surface from cantilever and to prevent premature drying. A 10 × 10 dot array was patterned with a dwell time of 5 secs at 60% relative humidity (Figure 4.13A). To complete the reaction samples were let at rest at room temperature overnight. Then, the samples were washed to remove excess ink and inspected (before and after washing) with bright field and fluorescent microscopy. The BF images show that no visible ink droplets remain on the surface after washing, but in fluorescence the patterns are clearly visible after washing, which confirms successful immobilization of a thin film of protein.

The feature size distribution measured over 200 features (from two 10 × 10 microarrays) gives an average diameter of (19.4 ± 1.3) µm (Figure 4.12B).

Influence of reaction time was tested by washing the samples after different resting times and comparing the resulting florescence intensity (Figure 4.13). The binding reaction is obviously rather fast, as samples washed only minutes after patterning show no significant difference in fluorescence intensity after washing to samples allowed to rest for 1h and longer. In order to establish further control over the patterning, a 5 x 5 matrix was patterned with different dwell time (1 to 9 sec).

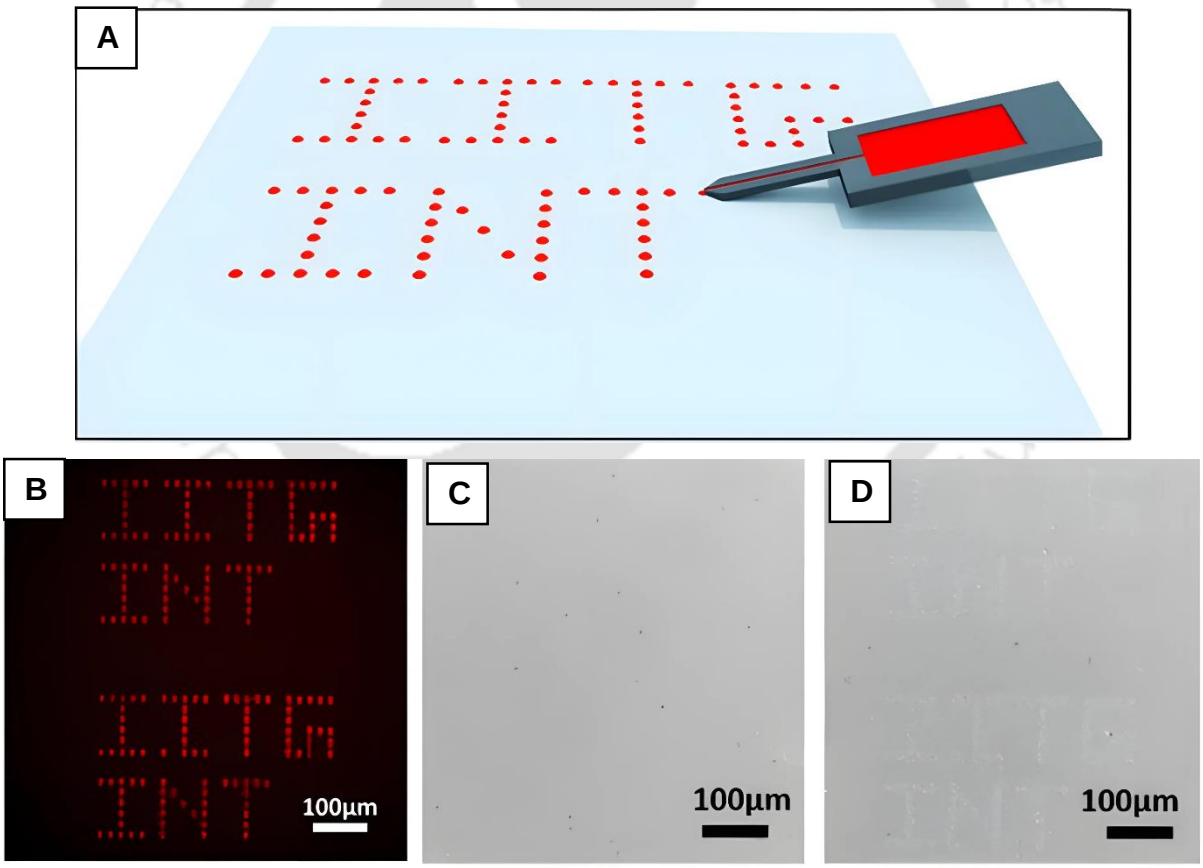

Figure 4.14. (A) The scheme of µCS for IITG and INT microscale logos, spotted with a fluorescently labelled protein (B). (C-D) Bright field images of a wettability pattern before (C) and during (D) exposure to humid air by breathing over the pattern.

The obtained graph shows a linear dependence of average feature diameter with dwell time. In addition to patterning dot features, also lines can be written with the cantilevers. Here, lines of 300 µm length were written with different speeds (1 µm/s to 50 µm/s), resulting in different line thicknesses, as more time is allowed for ink to transfer when the cantilever is moved slowly. As example for arbitrary pattern shape, the "IITG" and "INT" logos were written (Scheme shown in Figure 4.14A) with varying parameters (dwell time 0.1-0.5 sec, 45-60% RH), Figure 4.14B shows a typical fluorescence image after washing. The average feature diameter here is (13.5 ± 0.5) µm. Like before, the logos are not visible in BF after washing (Figure 4.14C).

However, after exposure to humid air by breathing over the sample, the mist or vapour condensed on the pattern makes it visible for a few seconds (Figure 4.14D) before vanishing again when the humidity evaporates. This is especially obvious when dynamically observing the experiment during breathing over the pattern. Here, the effect of the streptavidin is similar to the cysteamine for the macroscopic patterns, raising the local hydrophilicity of the surface in the patterned region and therefore enabling more condensation. Finally, to demonstrate one route for implementation of anti-counterfeiting measures, a 2D barcode encoding the acronym

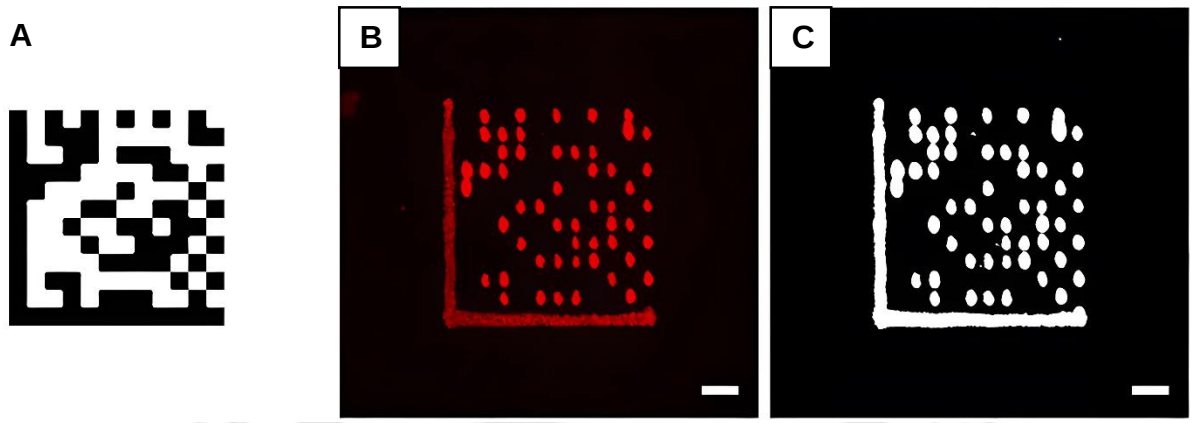

Figure 4.15. (A) Design pattern for a Data Matrix barcode encoding the acronym "KNMF". (B) Fluorescence microscopy image of the 2D code printed via µCS. (C) Threshold version of the image in (B) for better recognition by mobile phones. Scale bars equal 20 µm.

"KNMF" based on the Data Matrix standard[42] was printed as fluorescent micro-pattern (Figure 4.15). In this way, serial numbers or other information can be encoded directly onto an item in a robust way.

4.4. Conclusions

In conclusion, we demonstrated a facile and chemically reactive dip coating allowing for tailoring surface liquid wettability through selection of appropriate chemical modulations. The inherently hydrophobic and chemically reactive interfaces provided a facile basis for spatially selective covalent

modification with utterly distinct functional molecules, yielding invisible chemical patterns. The hand writing with an aqueous ink of glucamine on the amine reactive interfaces, followed by octadecylamine treatment of the entire polymeric coating, provided invisible write-up embedded within two distinct liquid wettabilities. The invisible write-up became visible under direct exposure to liquid water or mouth mist. Furthermore, this coating allows for patterning in the microscale as we demonstrated by spotting experiments with μCS. Here, microarrays showing the same wetting and condensation behavior were demonstrated, showing the potential of the approach for miniaturized, invisible but easy to reveal patterns. Such simple and covalent modulation approach would be of potential interest for addressing issues related to anti-counterfeiting and many other relevant challenges.

4.5. References

1) Auslander, J. D.; Berson, W. Bar Codes Using Luminescent Invisible Inks. Pitney Bowes, *US Patent* **1996**, 5542971.

2) Braeckmans, K.; De Smedt, S. C.; Roelant, C.; Leblans, M.; Pauwels, R.; Demeester, J. Encoding Microcarriers by Spatial Selective Photobleaching. *Nat. Mater.* **2003**, *2*, 169-173.

3) Andres, J.; Hersch, R. D.; Moser, J.-E.; Chauvin, A.-S. A New Anti-Counterfeiting Feature Relying on Invisible Luminescent Full Color Images Printed with Lanthanide-Based Inks. *Adv. Funct. Mater.* **2014**, *24*, 5029–5036.

4) Lee, J.; Bisso, P. W.; Srinivas, R. L.; Kim, J. J.; Swiston, A. J.; Doyle, P. S. Universal Process-inert Encoding Architecture for Polymer Microparticles. *Nat. Mater.* **2014**, *13*, 524-529.

5) Bae, H. J.; Bae, S.; Park, C.; Han, S.; Kim, J.; Kim, L. N.; Kim, K.; Song, S.-H.; Park, W.; Kwon, S. Biomimetic Microfingerprints for Anti-Counterfeiting Strategies. *Adv. Mater.* **2015**, *27*, 2083–2089.

6) Jiang, Y.; Li, G.; Che, W.; Liu, Y.; Xu, B.; Shan, G.; Zhu, D.; Su, Z.; Bryce, M. R. A Neutral Dinuclear Ir(III) Complex for Anti-Counterfeiting and Data Encryption. *Chem. Commun.* **2017**, *53*, 3022-3025.

7) Kalytchuk, S.; Wang, Y.; Poláková, K.; Zbořil, R. Carbon Dot Fluorescence-Lifetime-Encoded Anti-Counterfeiting. *ACS Appl. Mater. Interfaces* **2018**, *10*, 29902–29908.

8) Sheng, L.; Li, M.; Zhu, S.; Li, H.; Xi, G.; Li, Y.-G.; Wang, Y.; Li, Q.; Liang, S.; Zhong, K.; Zhang, S. X.-A. Hydrochromic Molecular Switches for Water-jet Rewritable Paper. *Nat. Commun.* **2014**, *5*, 3044-3052.

9) Feng, L.; Li, S. H.; Li, Y. S.; Li, H. J.; Zhang, L. J.; Zhai, J.; Song, Y. L.; Liu, B. Q.; Jiang, L.;

Zhu, D. B. Super-Hydrophobic Surfaces: From Natural to Artificial. *Adv. Mater.* **2002**, *14*, 1857-1860.

10) Li, X. M.; Reinhoudt, D.; Crego-Calama, M. What Do We Need for a Superhydrophobic Surface? A Review on the Recent Progress in the Preparation of Superhydrophobic Surfaces. *Chem. Soc. Rev.* **2007**, *36*, 1350-1368.

11) Liu, M. J.; Wang, S. T.; Wei, Z. X.; Song, Y. L.; Jiang, L. Superoleophobic Surfaces: Bioinspired Design of a Superoleophobic and Low Adhesive Water/Solid Interface. *Adv. Mater.* **2009**, *21*, 665-669.

12) Su, B.; Tian, Y.; Jiang, L. Bioinspired Interfaces with Superwettability: From Materials to Chemistry. *J. Am. Chem. Soc.* **2016**, *138*, 1727-1748.

13) Chu, Z.; Feng, Y.; Seeger, S. Oil/Water Separation with Selective Superantiwetting/Superwetting Surface Materials. *Angew. Chem. Int. Ed.* **2015**, *54*, 2328-2338.

14) Yao, X.; Gao, J.; Song, Y.; Jiang, L. Superoleophobic Surfaces with Controllable Oil Adhesion and Their Application in Oil Transportation. *Adv. Funct. Mater.* **2011**, *21*, 4270-4276.

15) Kota, A. K.; Kwon, G.; Choi, W.; Mabry, J. M.; Tuteja, A. Hygo responsive Membranes for Effective Oil–water Separation. *Nat. Commun.* **2012**, *3*, 1-9.

16) Ueda, E.; Levkin, P. A. Emerging Applications of Superhyrophilic-Superhydrophobic Micropatterns. *Adv. Mater.* **2013**, *25*, 1234-1247.

17) To, M.; Xue, L.; Liu, F.; Jiang, L. An Intelligent Superetting PVDF Membrane Showing Switchable TransportPerformance for Oil/Water Separation. *Adv. Mater.* **2014**, *26*, 2943-2948.

18) Wen, L.; Tian, Y.; Jiang, L. Bioinspired Super-wettability from Fundamental Research to Practical Applications. *Angew. Chem. Int. Ed.* **2015**, *54*, 3387-3399.

19) Cai, Y.; Lu, Q.; Guo, X.; Wang, S.; Qiao, J.; Jiang, L. Ultrasensitive and Broadband MoS_2 Photodetector Driven by Ferroelectrics. *Adv. Mater.* **2015**, *27*, 4162-4168.

20) Gao, A.; Wu, Q.; Wang, D.; Ha, Y.; Chen, Z.; Yang, P. A Superhydrophobic Surface Templated by Protein Self-Assembly and Emerging Application toward Protein Crystallization. *Adv. Mater.* **2016**, *28*, 579-587.

21) Yu, C.; Cao, M.; Dong, Z.; Wang, J.; Li, K.; Jiang, L. Spontaneous and Directional Transportation of Gas Bubbles on Superhydrophobic Cones. *Adv. Funct. Mater.* **2016**, *26*, 3236-3243.

22) Chen, K.; Zhou, S.; Wu, L. Self-Healing Underwater Superoleophobic and Antibiofouling

Coatings Based on the Assembly of Hierarchical Microgel Spheres. *ACS Nano* **2016**, *10*, 1386-1394.

23) Wu, M.; Ma, B.; Pan, T.; Chen, S.; Sun, J. Silver-Nanoparticle-Colored Cotton Fabrics with Tunable Colors and Durable Antibacterial and Self-Healing Superhydrophobic Properties. *Adv. Funct. Mater.* **2016**, *26*, 569-576.

24) Yohe, S. T.; Freedman, J. D.; Falde, E. J.; Colson, Y. L.; Grinstaff, M. W. A Mechanistic Study of Wetting Superhydrophobic Porous 3D Meshes. *Adv. Funct. Mater*. **2013**, *23*, 3628-3637.

25) Wang, J.; Kaplan, J. A.; Colson, Y. L.; Grinstaff, M. W. Stretch-Induced Drug Delivery from Superhydrophobic Polymer Composites: Use of Crack Propagation Failure Modes for Controlling Release Rates. *Angew. Chem. Int. Ed.* **2016**, *55*, 2796 –2800.

26) Tadanaga, K.; Morinaga, J.; Matsuda, A.; Minami, T. Superhydrophobic−Superhydrophilic Micropatterning on Flowerlike Alumina Coating Film by the Sol−Gel Method, *Chem. Mater*. **2000**, *12*, 590-592.

27) Geyer, F. L.; Ueda, E.; Liebel, U.; Grau, N.; Levkin, P. A.; Superhydrophobic-Superhydrophilic Micropatterning: Towards Genome-on-a-Chip Cell Microarrays. *Angew. Chem. Int. Ed.* **2011**, *50*, 8424-8427.

28) Ueda, E.; Levkin, P. A. Emerging Applications of Superhydrophilic-Superhydrophobic Micropatterns. *Adv. Mater.* **2013**, *25*, 1234-1247.

29) Geng, H.; Bai, H.; Fan, Y.; Wang, S.; Ba, T.; Yu, C.; Cao, M.; Jiang, L. Unidirectional Water Delivery on a Superhydrophilic Surface with Two-dimensional Asymmetrical Wettability Barriers. *Mater. Horiz.* **2018**, *5*, 303-308.

30) Cao, M.; Li, Z.; Ma, H.; Geng, H.; Yu, C.; Jiang, L. Is Superhydrophobicity Equal to Underwater Superaerophilicity: Regulating the Gas Behavior on Superaerophilic Surface via Hydrophilic Defects. *ACS Appl. Mater. Interfaces* **2018**, *10*, 20995-21000.

31) Kostal, E.; Stroj, S.; Kasemann, S.; Matylitsky, V.; Domke, M. Fabrication of Biomimetic Fog-Collecting Superhydrophilic–Superhydrophobic Surface Micropatterns Using Femtosecond Lasers. *Langmuir* **2018**, *34*, 2933-2941.

32) Si, Y.; Dong, Z.; Jiang, L. Bioinspired Designs of Superhydrophobic and Superhydrophilic Materials. *ACS Cent. Sci.* **2018**, *4*, 1102–1112.

33) Du, X.; Wang, J.; Cui, H.; Tang, T.; Tianzhun Wu, Vapor Condensation-Assisted Reverse Display for Anti-counterfeiting Applications. *Proceedings of IEEE*, **2016**, 316-319.

34) Cassie, A. B. D.; Baxter, S. Wettability of Porous Surfaces. *Trans. Faraday Soc.* **1944**, *40*, 546-551.

35) Parbat, D.; Gaffar, S.; Rather, A. M.; Gupta, A.; Manna, U. A General and Facile Chemical Avenue for the Controlled and Extreme Regulation of Water Wettability in Air and Oil Wettability Under Water. *Chem. Sci.* **2017**, *8*, 6542- 6554.

36) Bechler, S. L.; Lynn, D. M. Reactive Polymer Multilayers Fabricated by Covalent Layer-by-layer Assembly: 1,4- Conjugate Addition-based Approaches to the Design of Functional Biointerfaces. *Biomacromolecules* **2012**, *13*, 1523-1532.

37) Zhang, A.; Bai, H.; Li, L. Breath Figure: A Nature-Inspired Preparation Method for Ordered Porous Films. *Chem. Rev.* **2015**, *115*, 9801–9868.

38) Hirtz, M.; Greiner, A. M.; Landmann, T.; Bastmeyer, M.; Fuchs, H. Click-Chemistry Based Multi-Component Microarrays by Quill-Like Pens. *Adv. Mater. Interfaces* **2014**, *1*, 1300129-1300136.

39) Atwater, J.; Mattes, D. S.; Streit, B.; von Bojničić-Kninski, C.; Loeffler, F. F.; Breitling, F.; Fuchs, H.; Hirtz, M. Combinatorial Synthesis of Macromolecular Arrays by Microchannel Cantilever Spotting (µCS). *Adv. Mater.* **2018**, *30*, 1801632-1801638.

40) Xu, J.; Lynch, M.; Huff, J. L.; Mosher, C.; Vengasandra, S.; Ding, G.; Henderson, E. Label-Free Protein and Pathogen Detection Using the Atomic Force Microscope. *Biomed. Microdevices* **2004**, *6*, 117–123.

41) Xu, J.; Lynch, M.; Nettikadan, S.; Mosher, C.; Vegasandra, S.; Henderson, E. Microfabricated "Biomolecular Ink Cartridges"—Surface Patterning Tools (SPTs) for the Printing of Multiplexed Biomolecular Arrays. *Sensors Actuators B Chem.* **2006**, *113*, 1034–1041.

42) GS1 DataMatrix Guideline, Release 2.5.1, Ratified, Jan **2018**, https://www.gs1.org/docs/barcodes/GS1_DataMatrix_Gui deline.pdf, accessed 19.11.2019.

Chapter 5. Multiplexed Covalent Patterns on Double-Reactive Porous Dip Coating

In this chapter, I have conceptualized and demonstrated an approach based on the combination of hydrophobicity, a substrate-independent dip coating as porous material with double residual chemical reactivities for implementing multiplexed, miniaturized and unclonable bulk-infused patterns of different fluorophores following distinct reaction pathways. The embedded hydrophobicity (~102°) restricted the unwanted spreading of beaded aqueous ink on the coating. The constructions of micropatterns on porous dip coating via inkjet printing or microchannel cantilever spotting offered orthogonal read-out and remained readable even after removal of the exterior of the coating. Such interfaces would be useful in developing efficient anticounterfeiting interface.

* S. Das *et al.*, *Chem Asian J.* **2022**, *17*, e202200157

5.1. Introduction

Spatially selective covalent modulation of ultrathin and chemically reactive coatings provide a simple basis to derive various functional patterned interfaces.[1–5] In the earlier reported patterned interfaces, mostly one type of residual reactivity was extended for spatially selective chemical modulation, which was restricted to few nanometres across the used ultrathin coatings.[1–5] While the earlier reported patterns on ultrathin coatings remained inappropriate to sustain physical abrasion, the spatially selective integration of two distinct functional groups in the bulk of the coating following two independent chemical pathways would be interesting in both fundamental and applied contexts. For example, the dual modulation with desired chemistries at same location and orthogonal reading of complex pattern would be useful for high-throughput and parallel screening of biomarkers, developing an effective anti-counterfeiting interface, etc.[6–10] In addition to orthogonal chemical reactivity, the association of adequate water repellency is essential to prevent spillage of aqueous solution during spatially selective hydrophilic modification using aqueous solution of appropriately selected small molecules. However, the utilization of a porous, inherently hydrophobic and dually chemically reactive interfaces for developing complex, bulk, unclonable and miniaturized patterned interfaces are rare in the literature.[11,12] Here, I have utilized a dual chemically reactive porous dip coating (DCRPDC) inherently embedded with two distinct residual chemically reactive groups (acrylate and amine) for developing an orthogonally readable, abrasion tolerant and miniaturized bulk-patterns through the 1,4 conjugate addition reaction of the DCRPDC with selected fluorescent molecules at ambient conditions as shown in Scheme 1. The bulk chemical reactivity in the porous polymeric dip coating provided a basis to develop abrasion tolerant bulk-pattern of selected small molecules.

Moreover, the patterned interface remained washable with water and organic solvents due to the strategic association of robust covalent modifications. Further, the principle was successfully extended to develop QR codes using both microchannel cantilever spotting (μCS),[6,13,14] and ink-jet printing process. Addition to the abilities of providing bulk-modification, the dual chemical reactivity also allowed to associate two distinct florescent molecules following two independent chemical modulation processes.

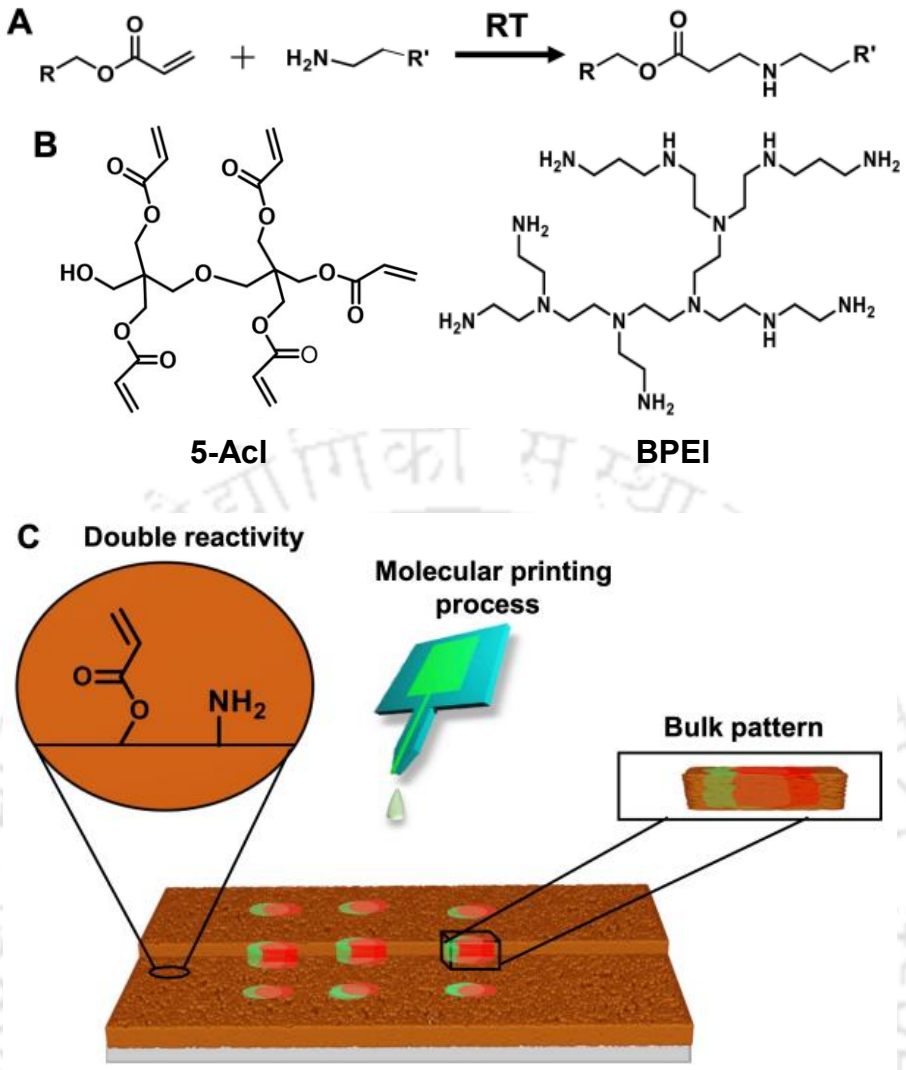

Figure 5.1. (A) Depicting Michael addition reaction between representative acrylate and amine groups. (B) Chemical structures of dipentaerythritol penta-acrylate (5-Acl) and branched polyethylenimine (BPEI). (C) Schematic representing a dual chemically reactive polymeric dip coating provided the spatially selective and bulk orthogonal-covalent-modification through molecular printing process.

5.2. Experimental Section

5.2.1. Preparation of the Dual Reactive Thin Polymeric Coating. Dipentaerythritol pentaacrylate (5Acl, 132.5 mg mL^{-1}) and branched polyethylenimine (BPEI, 50 mg mL^{-1}) solutions in 1-heptanol were first prepared in two separate glass vials. Then, 1.2 mL of BPEI solution was mixed with 4 mL of 5Acl solution to prepare reaction mixture, and thereafter selected substrates a clean glass slide or paper was dipped into the reaction mixture. The substrate was kept into the solution for 1 min. After that, the coated substrate was taken out of the reaction mixture and dried in air, followed by thoroughly washing with THF.

5.2.2. Surface Characterizations.

5.2.2.1 Contact Angle Measurements. Contact angles of beaded water droplets (5 µL) were measured using a KRUSS Drop Shape analyser-DSA25 instrument with an automatic liquid dispenser at ambient temperatures. The static water contact angles were measured at four different locations on the prepared coating to calculate standard deviation as a measure of error. We have applied sessile drop method to acquire the contact angle.

5.2.2.2 Scanning Electron Microscopy (SEM). All the samples were coated with a thin layer of gold sputter prior to obtaining SEM images of the dip coatings using a Carl Zeiss field emission scanning electron microscope (FESEM). The images were acquired in InLens mode. ImageJ software was used to measure surface pore-size from FESEM images.

5.2.2.3 Infrared Spectroscopy. ATR-FTIR spectra were recorded using Spectrum Two UATR, PerkinElmer at an ambient temperature with single reflection mode, Spectrum 10 software was used to process the data. The instrument pressure arm was used to achieve improved contact between the modified and unmodified coatings and the crystal, prior to record the data. The associated software (Spectrum 10 software) of the equipment was used for smoothening the data with smoothening factor of 25.

5.2.2.4 Atomic Force Microscopy (AFM). AFM images was acquired on an Oxford Instrument, MFP-3D Origin system in tapping mode with silicon tip (AC160TS-R3, nominal frequency 325 kHz, nominal force constant 40 N/m). Three different regions of the prepared dip coating were analyzed.

5.2.2.5 Optical Imaging. The digital images were captured by using Nikon Coolpix b700 digital camera. Thickness of the material was measured using stylus surface profilometer (Veeco-Dektak 150). Bright field, fluorescence microscopic images and z-stacking images were captured by using a ZEISS Axio Vert.A1 inverted microscope and Zeiss LSM 880 Laser Scanning Confocal Microscope. Additional fluorescence microscopy for the micropatterns was performed on a Nikon Eclipse 80i upright fluorescence microscope (Nikon, Germany) equipped with an Intensilight illumination (Nikon, Germany), a Nikon DS Qi2 camera, and Cy5 and FITC filters (Nikon Y2E/C). The spot diameters were measured by the built-in NIS-element software (Nikon, Germany) on the microscope for the images presented in ESI Fig. S6. The S.D. from these diameters was reported as error.

5.2.2.6 X-ray Photoelectron Spectroscopy (XPS) Measurements. The X-ray photoelectron spectroscopy (XPS) measurements were carried out under an ultra-high vacuum conditions with a base pressure of 1×10^{-9} mbar. Core-level spectra were recorded under normal emission with a Scienta R4000 hemispherical electron analyzer using Al-Kα radiation (1486.6 eV). Firstly, for every sample the survey XPS spectrum was measured and no unexpected contaminations were observed in these spectra. For a precise determination of the N 1s lines position and necessary correction the XPS Peak 41 software was used.

5.2.3. Fabrication of Spatially Selective Pattern Interfaces. Chemically reactive porous and moderately rough interfaces were separately and manually exposed to aqueous droplet of tetramethylrhodamine cadaverine (TMRC) as well as fluorescein isothiocyanate (FITC) respectively to develop luminescent circular spot on the dipcoating. The substrate was thoroughly washed with ethanol and DI-water to remove loosely bound and unreacted TMRC and FITC. The larger QR-Codes were obtained by printing an aqueous solution of FITC (concentration of 0.1 mg/ml) with a commercial consumer grade inkjet printer (Canon PIXMA G2021) with printing resolution of 4800 × 1200 dpi onto dip-coated paper. The other micropatterns were spotted via μCS on a Nano eNabler System (Bioforce Nanosciences). Firstly, the microchannel-cantilever was cleaned by ozone treatment for 5 minutes. Then, the selected ink, i.e., aqueous solution of TMRC (0.1mg/ml) was loaded to microchannel cantilever (SPT-S-30, Bioforce Nanosciences), and the cantilever was adjusted systematically to touch only the upper periphery of the substrate (to avoid spillages of the ink) for delivering the ink solution to the prepared dip coating. The written pattern using TMRC was developed on the dip-coated hydrophobic polymeric substrate which was previously manually marked with a marker to maintain the design of the pattern along a fixed line and position and used as a reference for the next superimposed pattern prepared by FITC (0.1 mg/ml) on that substrate after the air drying of the previously prepared micro-patterns. Then the whole patterned substrate was placed under laser scanning confocal microscope to capture the fluorescence images. The miniaturized DataMatrix Codes and spot size trials were spotted by μCS on a NLP 2000 instrument (Nanoink, Inc.). The microchannel-cantilever (SPT-S-C10S) was purchased from Bioforce Nanosciences. Prior to use, the microchannel-cantilever was plasma-cleaned by oxygen plasma (0.2 mbar, 100 W, 20 sscm O_2, 2 min) on a Diener plasma system Atto. Streptavidin_alexa 647 (ThermoFisher Scientific, Germany, 1 μg μL^{-1} in DMSO, magenta channel) and FITC (Sigma-Aldrich, Germany, 1 μg μL^{-1} in DMSO, green channel) were used as fluorescent dyes. The microchannel-cantilever reservoir was then filled with 0.5 μL of ink, and the ink was pushed into the pen by blowing with a nitrogen stream. All patterning was done at room temperature, with control humidity and dwell time. All DataMatrix patterns were printed at 30% RH and 0.5 S of dwell time. The dot arrays were printed at different humidity (20%, 45%, 70% RH) and dwell time (0.1, 0.5, 1, 2, 5 sec). The DataMatrix and dot arrays were designed by in-built software in NLP 2000 instrument. After printing, the samples were washed immediately with DI water (18.2 MΩ cm, Arium water system, Sartorius, Germany) to make sure to remove unbound and excess ink. The samples were then dried with nitrogen before further analysis by optical microscopy.

5.2.4. Abrasion Test. For abrasion tests, a double-sided adhesive tape (1 × 1 cm) was first attached onto a microscopic glass slide, and then, the patterned dip coated substrate (3 × 1 cm) was brought in contact to the adhesive tape with an applied load of 500 g. The external load is applied to facilitate a uniform and homogeneous contact between the substrate and the tape. After 20 min, the adhesive tape

was peeled off of the substrate. After removal of the adhesive surface, it was found that top portion of the coating was transferred to that adhesive surface partially, and the interiors of the coating was arbitrarily exposed. Fluorescent patterns were observed to be readable even after 25 cycles of adhesive tape peeling test. To perform sand paper abrasion test, an abrasive sand paper with 4 cm length and 2.5 cm width was exposed to freshly prepared coating with external load of 100 g and applied a back and forth motion for 25 times.

5.3. Results and Discussions

In the recent past, our lab has utilized the 1,4 conjugate addition reaction between selected reactants- i.e. BPEI and 5Acl to develop chemically reactive coating following different fabrication processes- including layer-by-layer deposition technique, spray deposition etc. for associating the durable bio-inspired liquid wettability.[15–17]

In the chapter 1, I have demonstrated that the modulation of the single residual reactivity (i. e. acrylate group) that present in the highly rough (RMS roughness ~ 790±28 nm) and hydrophobic (with water contact angle, WCA of ~132°) dip coating (obtained with an immersion time of 10 minutes) allowed to embed bio-inspired superhydrophobicity through rational post modification with primary amine containing selected hydrophobic (octadecylamine) small molecules.[17] In this chapter, I have introduced the chemically reactive dip coating that was prepared by immersing the selected substrates (glass or paper) in the strategically selective reaction mixture of BPEI and 5Acl in 1-heptanol for only 1 minute to depict orthogonal post-chemical modifications. The prepared dip coating (thickness ~3.2 μm) displayed moderate hydrophobicity with a WCA of ~102° (Figure 5.2A). Moreover, the prepared dip coating was found to be significantly less rough (RMS roughness ~ 72±15 nm). The random deposition of the polymeric nanocomplex provided a porous morphology with aggregated granular microdomains (Figure 5.2B–D). The size and shape of the pores in the prepared coating is irregular with a wide range of distribution from ~150 nm to ~1 μm. Another advantage of the current coating is the existence of two distinct residual chemical reactivity, i.e., amine and acrylate (Figure 5.1C). The XPS signature of N 1s at ~400 eV revealed the presence of residual amine (Figure 5.2E) in the prepared dip coating. Thereafter the existence of residual acrylate group was validated through FTIR analysis as shown in Figure 5.3A.

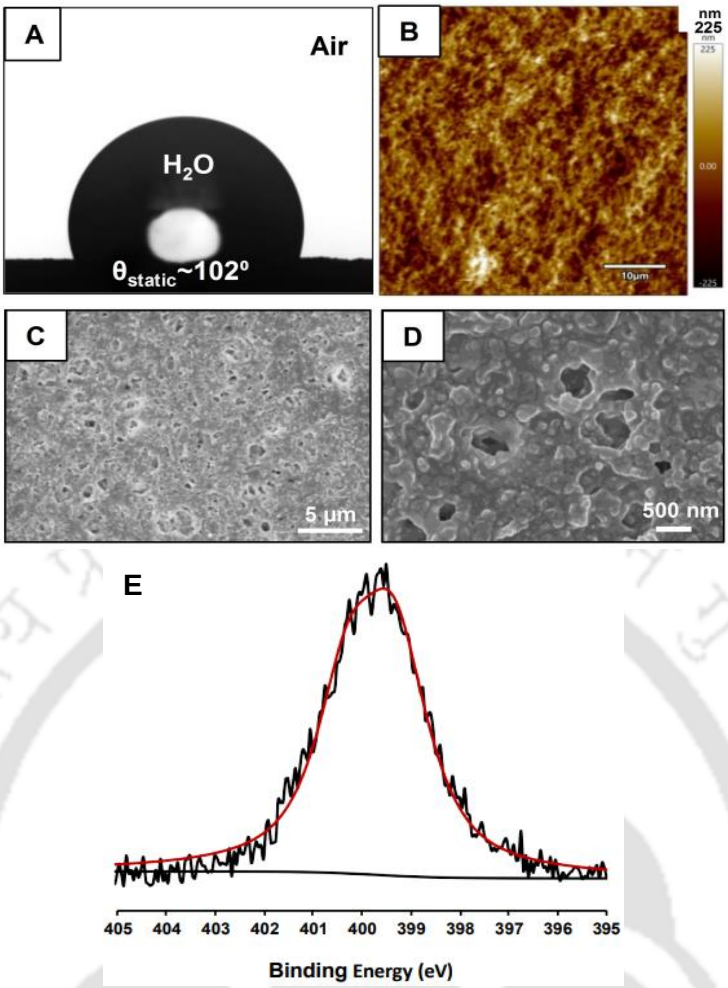

Figure 5.2. (A) The contact angle image of beaded water droplet on the polymeric dip coating. (B) AFM and (C–D) FESEM image of the polymeric dip coating in (C) low and (D) high magnifications. (E) XPS spectra of N 1s of the polymeric dip coating, the XPS signature of dip coating at ~ 400 eV revealed the presence of presence of residual amine.

Even the freshly exposed interior of the physically abraded coating revealed the presence of porous features (Figure 5.3B, C). The ATR-FTIR analysis of the dip coating confirmed the presence of residual acrylate groups where the characteristic IR peaks for C-H deformation of vinyl groups and ester carbonyl stretching appeared at 1408 cm^{-1} and 1733 cm^{-1}, respectively, as shown in Figure 5.3A (black). An additional experiment was designed to examine the existence of residual acrylate groups in both the surface and bulk of the prepared dip coating. The coating was physically abraded by applying adhesive tape peeling process and the successive application of adhesive tape gradually lowered its thickness (from 3.2 µm to 1.6 µm) and randomly exposed the interior of the dip coating.

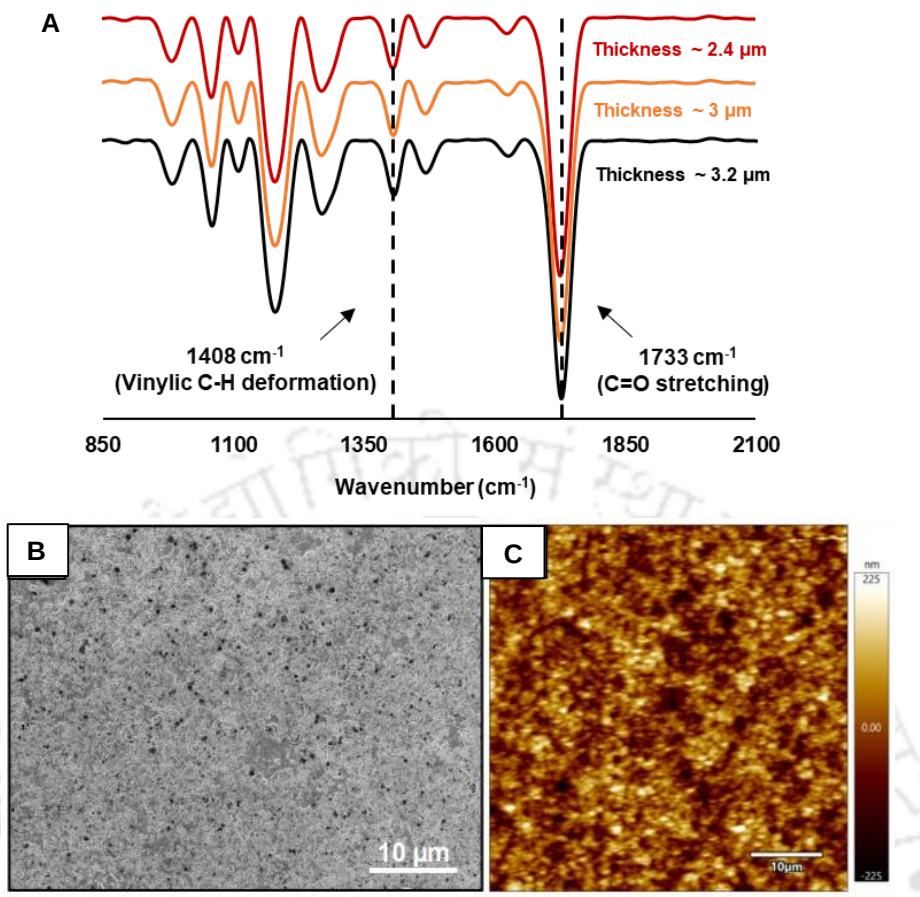

Figure 5.3. (A) ATR-FTIR spectra accounting the presence of residual acrylate group in the synthesized dip coating before (black) and after (orange and red) exposure of the interiors. (B-C) FESEM and AFM images of physically abraded dip coating. The successive application of adhesive tape peeling process exposed the interior of the coating.

Hardly any change in FTIR signature of residual acrylate groups was noted in the dip coating before and after incurring the physical abrasion process as shown in Figure 5.3A. The intensity of the normalized (with respect to ester carbonyl stretching at 1733 cm^{-1}) and the characteristic IR signature for C-H deformation of the β carbon of the vinyl moiety remained unaltered before and after the random exposure of the interior of the coating. Thereafter another physical abrasion process, i.e., sand-paper abrasion was applied to remove the top of coating and the remaining coating on the substrate also to exhibit residual acrylate groups (Figure 5.4).

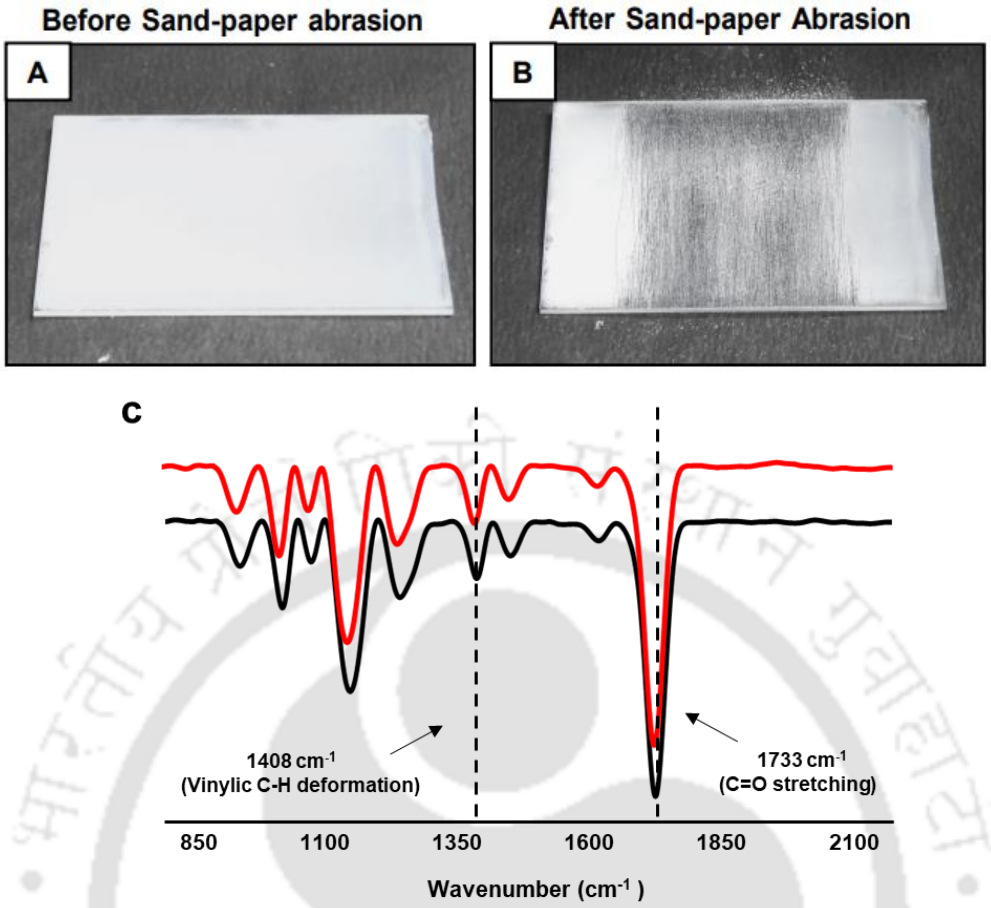

Figure 5.4. (A-B) Digital images of the chemically dip coating before (A) and after (B) sand paper abrasion for 25 times with back and forth motion under 100 g load. (C) ATR-FTIR spectra of the chemically reactive coating before (black) and after (red) sand paper abrasion. ATR-FTIR signatures at 1733 cm^{-1} and 1408 cm^{-1} for carbonyl and vinylic C-H deformation respectively, revealed the presence of residual acrylate group.

Next, I have studied the spatially selective modification with microscopic imaging and FTIR spectral analysis. First of all, two aqueous droplets of two distinct fluorophores, i.e. tetramethylrhodamine (TMR; nonreactive, Figure 5.5B) and tetramethylrhodamine cadaverine (TMRC; readily reactive due to the presence of primary amine moiety, Figure 5.5A) were manually beaded on the prepared dip coating. As expected, two circular spots were observed in the red channel in fluorescence microscopy (Figure 5.5C). After the DI water and followed by ethanol washing, the circular spot made of TMRC remained unaffected. However, the other spot formed out of TMR disappeared (Figure 5.5D).

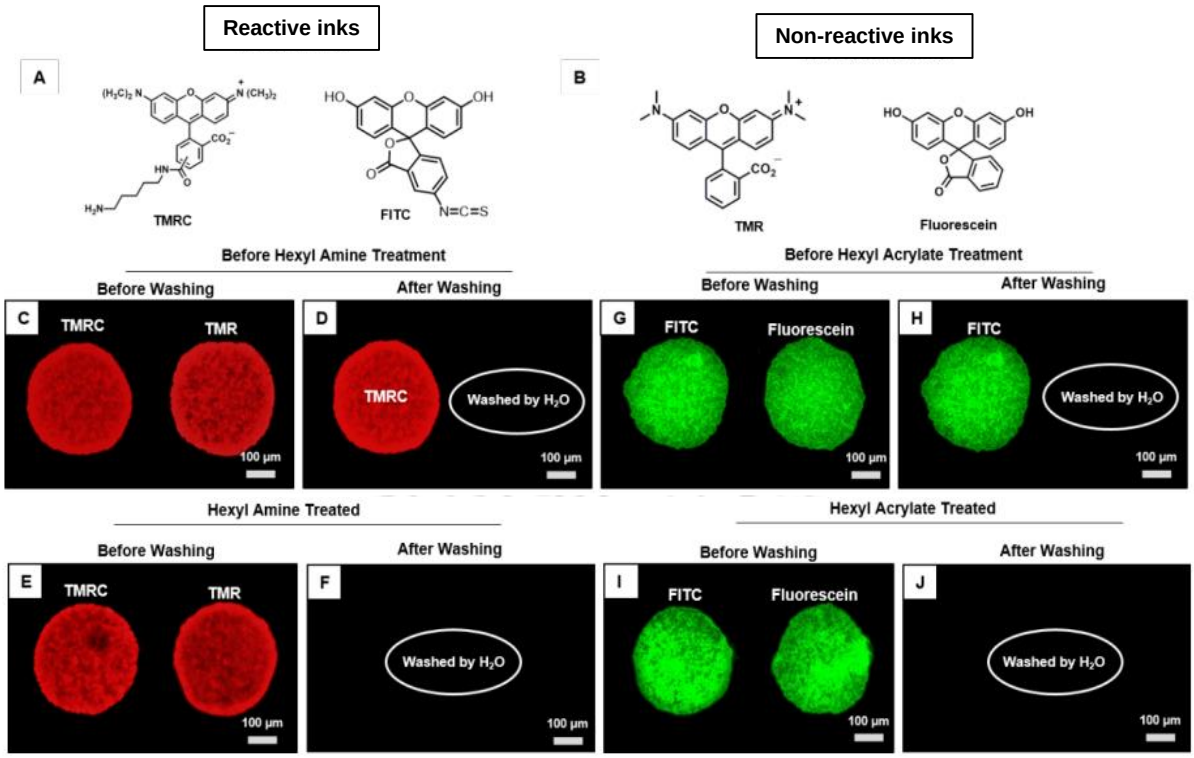

Figure 5.5. Chemical structures of various (A) readily reactive (TMRC, FITC) and (B) non-reactive (TMR, fluorescein) fluorescent inks respectively. (C, D, G, H) Fluorescence microscopy images of dip coating having the physically deposited spots of readily reactive (TMRC, FITC) and non-reactive (TMR, fluorescein) inks (G-J) before (C), (G) and after (D), (H) deionized water washing. After water washing nonreactive dyes disappeared (D), (H). (E), (F), (I), (J) Fluorescence images accounting the disappearance (F), (J) of both reactive and nonreactive inks after water washing from hexyl amine (E), (F) and hexyl acrylate (I), (J) treated dip coatings.

While the 1,4 conjugate addition reaction between the primary amine and residual acrylate of the dip coating allowed a covalent immobilization of TMRC, the lack of such available primary amine in TMR failed as expected to provide covalent association with the dip coating. Rather the physically deposited TMR readily washed away after the application of the DI water and ethanol washing process. In another experiment aqueous droplet of same TMRC beaded on the hexylamine modified dip coating failed to survive such washing treatment as shown in Figure 5.5E–F. This simple demonstration validated that the residual acrylate groups remained highly reactive to primary amine containing small molecules and provide a facile basis for covalent immobilization of selected molecules at ambient condition. On the other side, the same dip coating after manual deposition of two distinct aqueous droplets of fluorescein isothiocyanate (FITC, Figure 5.5A) and fluorescein (Figure 5.5B) displayed two distinct circular and fluorescent spots under the fluorescence microscope as shown in Figure 5.5G. However, the regular washing of the dip coating with DI water and ethanol resulted in the disappearance of the fluorescein based circular spot, while the FITC derived spot remained unaffected under same treatment (Figure 5.5H), due to the covalent attachment of FITC with residual amine of the dip coating (Figure 5.6A). In contrast, the dip coating pre-modified with butyl-acrylate failed to provide such covalent attachment to

the FITC due to lack of residual amine, and thus the deposited FITC readily washed off on DI water exposure as shown in Figure 5.5I–J. Thereafter, the post-modifications of the dip coating with FITC and TMRC were also characterized with ATR-FTIR spectral analysis as shown in Figure 5.6B. The post modification of the dip coating with TMRC resulted in the depletion of normalized IR peak

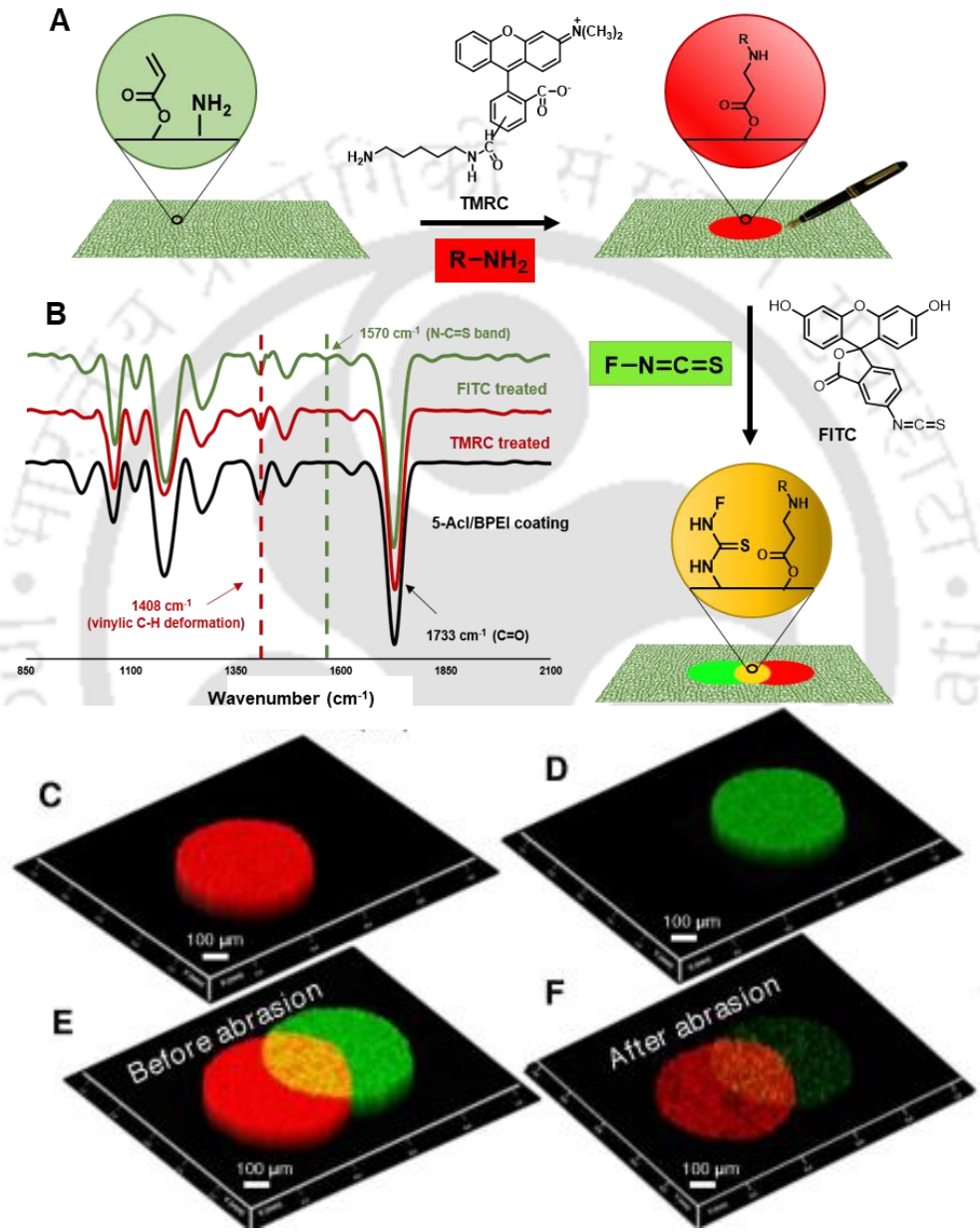

Figure 5.6. (A) Schematic illustrating the covalent and spatially selective modifications of dual chemically reactive dip coating with two distinct fluorescent inks tetramethylrhodamine cadaverine (TMRC) and fluorescein isothiocyanate (FITC), where TMRC and FITC mutually reacted with residual acrylate and amine, respectively at ambient condition. (B) ATR-FTIR spectra accounting the dual chemical modification of dip coating with TMRC and FITC. (C–D) The confocal microscopic images revealed the presence of bulk patterns of TMRC (C) and FITC (D), respectively. (E–F) Merged confocal images of the patterned interface before (E) and after (F) physical abrasion.

intensity for C-H deformation of the vinyl group at 1408 cm^{-1} with respect to the carbonyl stretching at 1733 cm^{-1}. The depletion of the IR peak intensity unambiguously supported the 1,4-conjugate addition reaction between the primary amine of the TMRC and the residual acrylate of the dip coating, where the vinyl moiety of the acrylate is compromised while the carbonyl group remained intact. On the other hand, the residual amine of the dip coating remained highly reactive towards thiocyanide groups. The same coating that was exposed to FITC provided a characteristic IR signature for the N C=S band at 1570 cm^{-1} as shown in Figure 5.6B (green). Thus, both the residual groups-acrylate and amine-remained chemically reactive towards both the amine of TMRC and the thiocyanide of FITC, respectively. Furthermore, the confocal microscopy imaging confirmed the bulk immobilization of both TMRC and FITC on the chemically reactive dip coating as shown in Figure 5.6C–D. The merged (both green and red channel) confocal image in Figure 5.6E revealed the existence of a common section (indicated by yellow color) that is modified with both, TMRC and FITC. Such strategic dual modifications of the chemically reactive interface with two distinct representative fluorophores following two independent reaction pathways allowed to develop a complex luminescent pattern. On the other side, the bulk chemical modifications of the dip coating with selective fluorophores provided an abrasion tolerant patterned interface (Figure 5.6E–F), where the same patterned interface continued to display the desired

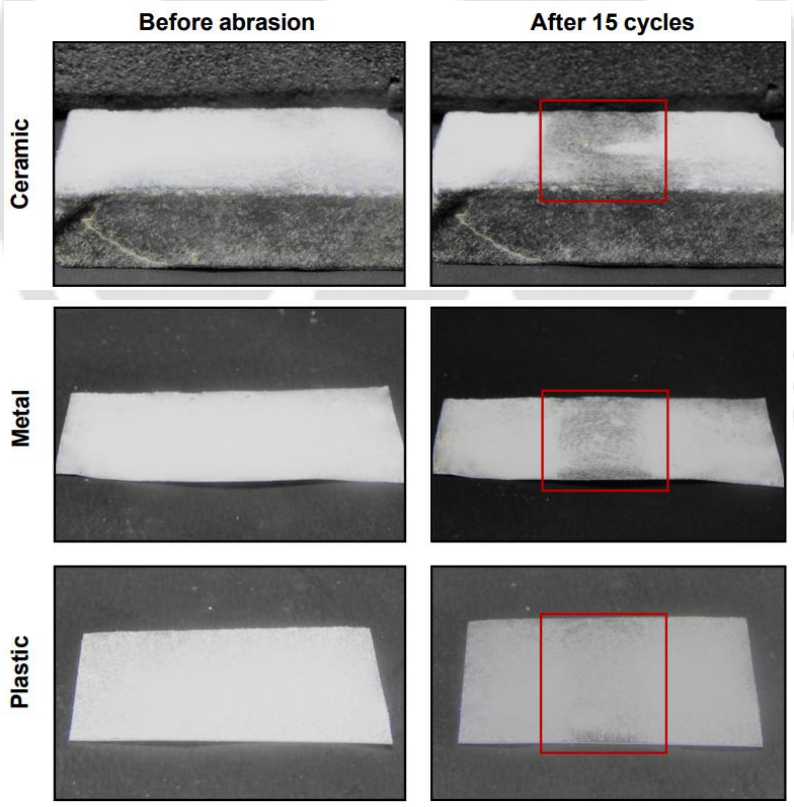

Figure 5.7. Digital Images of coated ceramic, metal and plastic before and after performing adhesive tape peeling test for 15 times. The red box indicated the physically abraded area. Even after repetitive application of adhesive tape peeling test, a complete peeling of the deposited coating is not noted.

fluorescence signal-even after the physical abrasion due to the bulk modification. Such prepared dip coating can be successfully applied on plastic, metal, ceramic and wood (See Figure 5.7). The prepared polymeric coating on other substrate also remained efficient to sustain repetitive adhesive tape peeling test as shown in Figure 5.7.

Encouraged by the multi-functional and abrasive resistant chemical modifications on the dip coating, trials for miniaturized and functional patterns were implemented. For this task, inkjet printing and microchannel cantilever spotting (µCS) were employed. In µCS, inks are spotted in an atomic force microscopy (AFM) by a cantilever with a microchannel connected to an on-chip reservoir for microliter volumes of ink, allowing for chemical reactions in such "micro-reactors"[4,18,19] When the cantilever is brought into contact with a surface, ink can transfer by capillary force from the reservoir to the surface. On porous and moderately hydrophobic substrates, this allows for delivery of sufficient volume of ink for imbibition and bulk functionalization of the substrate interior.[20–22] With the highly precise and

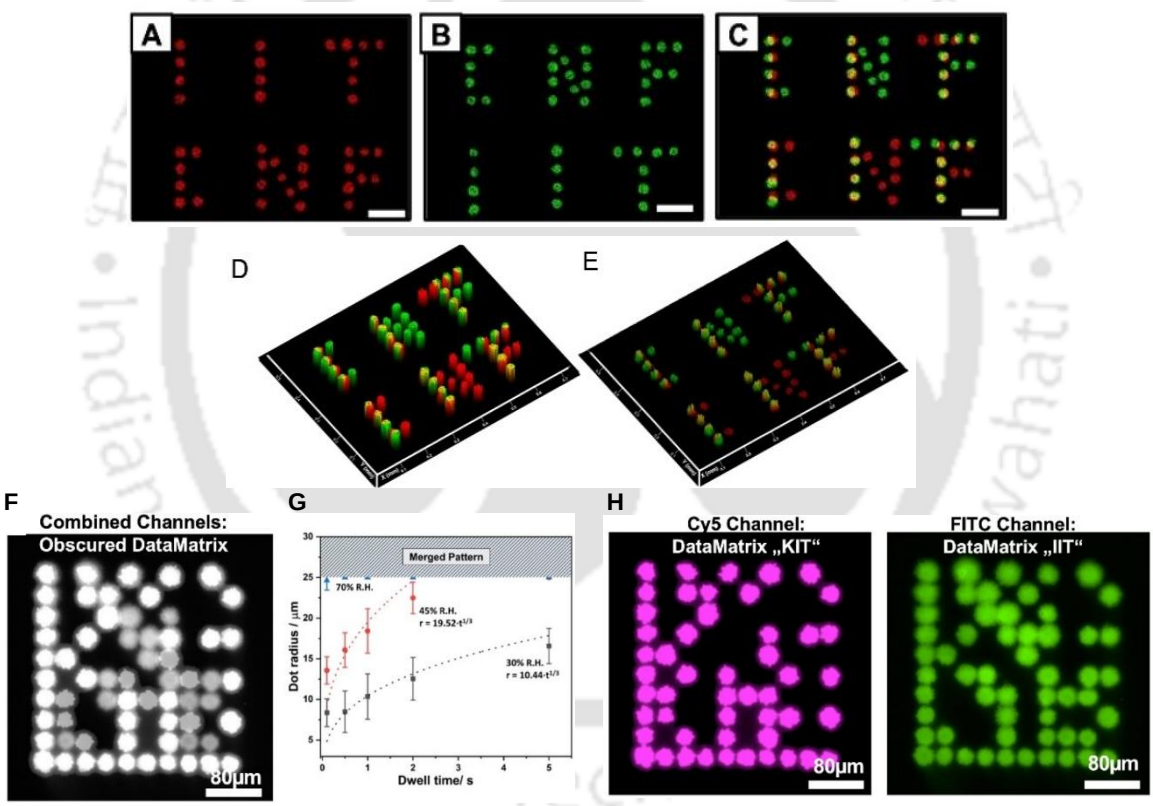

Figure 5.8. Functional and abrasive resistant micropatterns. Confocal microscopy images (scale bar 100 µm) of (A) TMRC and (B) FITC fluorescence channel of µCS spotted letters. A combined image of the fluorescence channels in (C) shows the overlap between the patterns (D) before and (E) after abrasion. (F-H) Combined and single channel fluorescent microscopy images of two different DataMatrix codes printed one over the other with different fluorophore inks. While the combined channel obscures the information, the single channels reveal readable codes. The images are intentionally slightly overexposed for easier readout of the code. The graph shows the radius of features spotted with different dwell times and at different relative humidity (R.H.) during the patterning process.

reproducible position control over the cantilever, arbitrary patterns can be formed and even subsequent deposition of different inks onto the same spot can be achieved.[6] First, as example of arbitrary micropatterns, letters "IIT" and "CNF" were spotted with TMRC and FITC inks via μCS (Figure 5.8). Figure 5.8A and B show the single channel fluorescence microscopy images for each ink, which – when combined – reveal an overlap of both patterns demonstrating the dual functionalization of the surface also on the micro scale (Figure 5.8C). This multiplexing of inks also allows for selective readout of information by selection of the matching filter channel to reveal different information from the same pattern.

Importantly, the micropatterns even stay legible after abrasion (Figure 5.8D–E), enabling a robust information storage. Further, a QR code pattern was printed by inkjet printing FITC ink onto a dip-coated paper. The fluorescence imaging confirmed the development of a QR code capable of sustaining physical abrasion. The interface was physically abraded through adhesive tape peeling as evident from the confocal image of the QR code before and after abrasion. To clearly show the impact of the abrasion treatment to the QR code pattern, fluorescence images were obtained under same exposure conditions and also at an exposure time allowing for the full dynamic range to be covered. Though a slight overexposure would actually benefit direct read-out of the barcode from such an image e.g. by mobile phone, a simple contrast enhancement allows even the abraded QR code to be reliably readout directly (Figure 5.9).

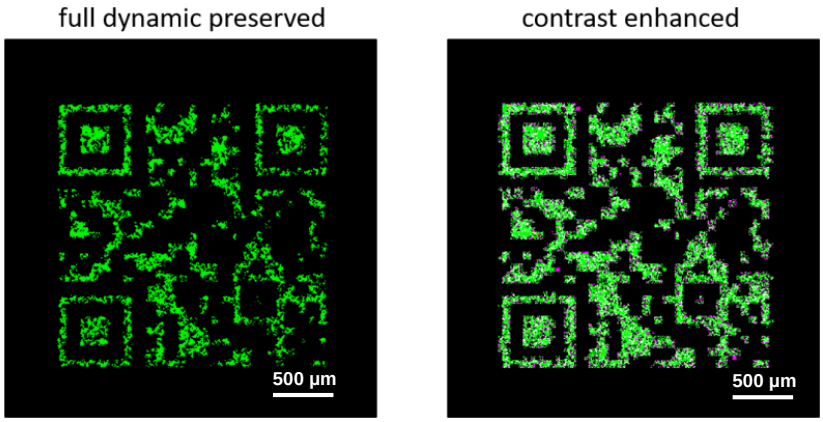

Figure 5.9. Fluorescence microscopy images of QR code pattern after abrasion. Left in exposure conditions optimal for preserving full dynamic range in image and right a simply contrast enhanced version that allows direct readout of the code.

Another important aspect of the current approach is the association of unclonable features in the miniaturized patterns which is important for anticounterfeiting applications.[7] Here, the random fluctuation caused uncontrollable during the patterning could act as an unclonable fingerprint – which cannot be achieved on smooth interface and uncoated paper (Figure 5.10). The presented porous and dip coating allows for a realization of such unclonable features, in particular for the smaller sized features within micropatterns. While bigger spot features e.g., the manually spotted features in the size

range of several hundred show a rather well-defined delineation, the smaller features from μCS approach offer more rugged borders as of the intrinsic randomness of the pores in the substrate becoming visible on this scale of patterning (Figure 5.11). For a demonstration, two different DataMatrix patterns were spotted via μCS (Figure 5.8F). When both channels are overlayed (implying readout without proper fluorescence filtering), the DataMatrix is obfuscated and cannot be read. The single channels as orthogonal readout enabled proper recognition.

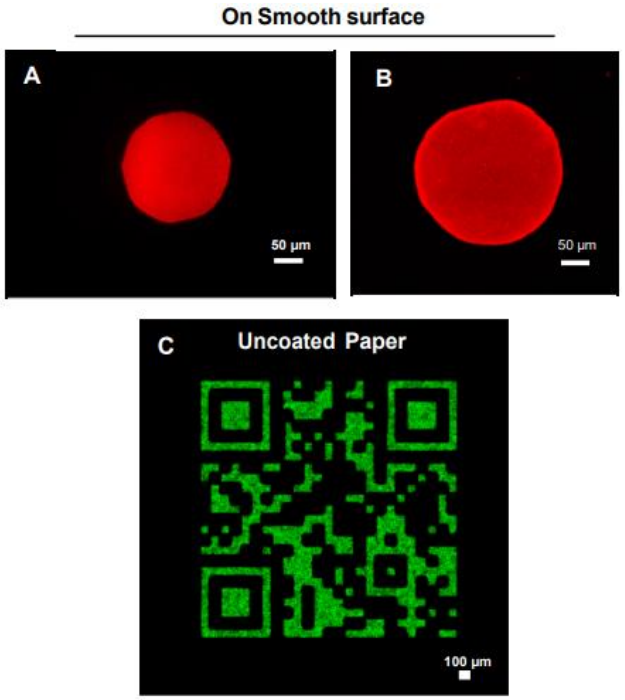

Figure 5.10. Fluorescence microscopy images depicting the featureless edges of the same inks on smooth interfaces (A, B) and on bare paper (C).

As mentioned above, a proper unclonable feature border is in particular obvious in smaller features, which fortunately are readily available via μCS and can be even tuned via dwell time (tip/surface contact time) and relative humidity under which the spotting takes place (Figure 5.8G). Theory predicts, imbibition of a fluid into a porous substrate should follow a dependency on time proportional to t 1/3.[26] This was also shown to be the case for other porous coatings in μCS and our current results are in line with this mode of diffusive imbibition of ink into porous substrates.[20–21] The imbibition rate becomes higher with higher humidities during spotting reflecting the more hydrated state of substrate and ink at raised humidity enabling a faster flow. As the centre distance between features in the test array was arbitrarily set to 50 μm, the dots features start to merge after reaching a feature radius of 25 μm, indicated by the hatched area in the top of the graph. Below this restraint, feature radius size could be tuned down to (7.8±1.7) μm by lowering humidity and dwell time (Figure 5.8G). Generally, for lowest dwell time (0.1 s) the radius is a bit larger than what is expected from the theoretical description.

This can be understood as a small additional amount of ink that will snap off from a meniscus that builds on retraction of the μCS tip and continue to be adsorbed into the substrate. This snap off volume will be similar for each dwell time, therefore affecting feature size in particular for the smallest dwell times where the imbibed volume directly from the tip is also smallest. The granularity of the coating is on the length scale of about 500 nm, as seen in Figure 5.2B–D.

On the one hand, this limits the maximal accuracy in patterning to about 1 to 2 μm (as seen in the standard deviation of the smallest obtained features being ∼1.7 μm), but on the other hand enables an intrinsic anti-counterfeiting approach based on the borders of the spots.

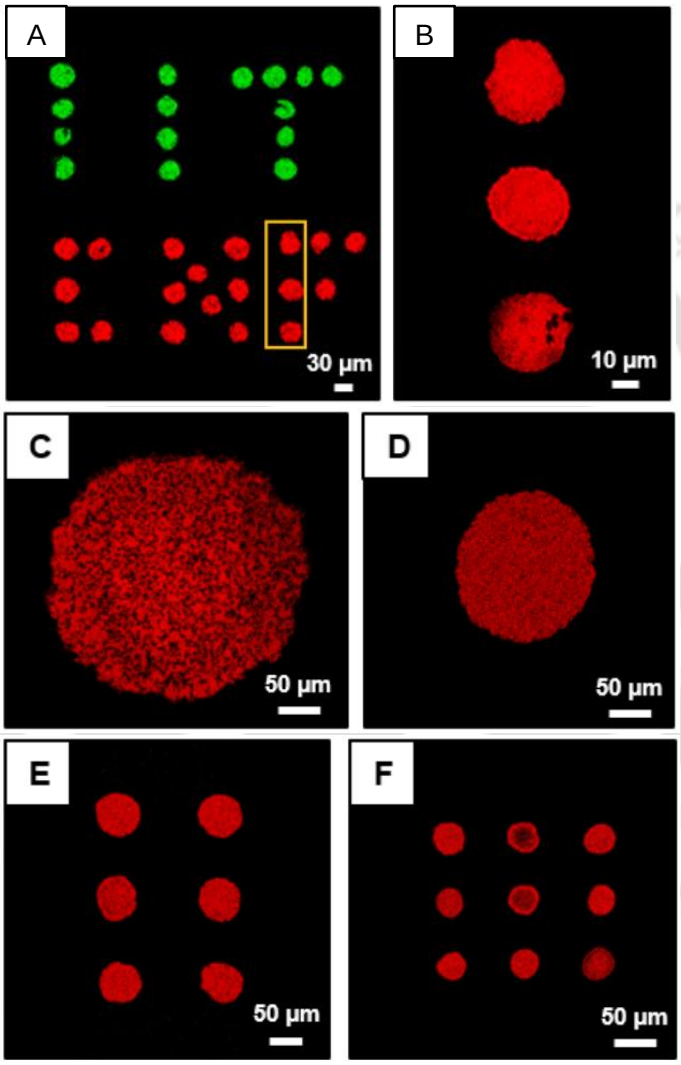

Figure 5.11. (A) Fluorescence microscopy images of the dip coating showing microscopic features of FITC and TMRC inks obtained by microchannel cantilever spotting (μCS). (B) Magnified florescence image of the three spots of TMRC that indicated with yellow box in (A). (C-F) Florescence images accounting the edge effect of the spotted ink (TMRC) on the chemically reactive dip coating.

While the general readout of the DataMatrix micropattern is facilitated by a slight overexposure of the fluorescence images, images preserving the fully dynamic range of the fluorescence signal are in particular well suited for observing the unclonable features of the spot delineation (Figure 5.12).

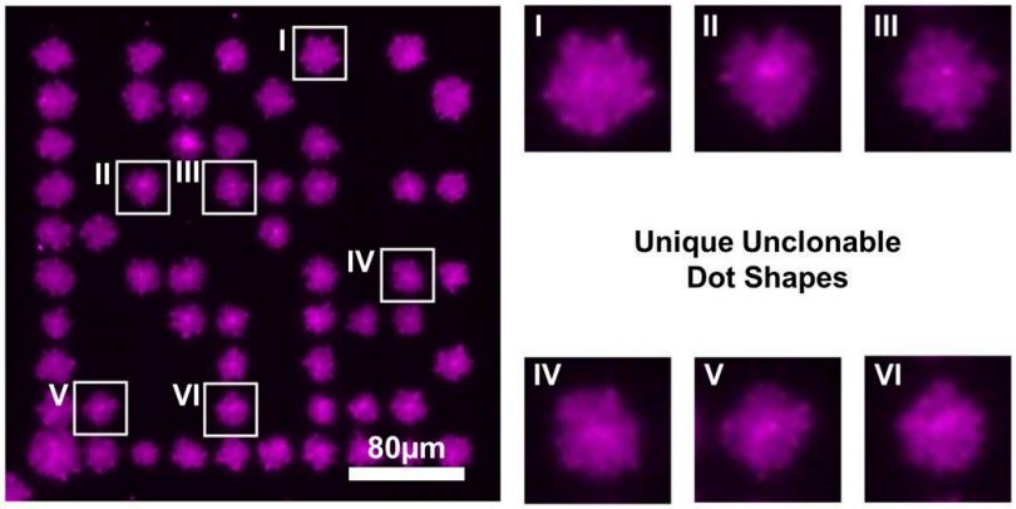

Figure 5.12. A fluorescence image of a DataMatrix code exposed for optimal visibility of the feature borders. 6 selected features of the DataMatrix are enlarged on the right, to exemplify the unclonable dot shapes.

Even by inspecting with naked eye, the borders of the dots already reveal obviously distinct and highly recognizable shapes. The use of machine vision and artificial intelligence could readily enable automated recognition and identification of such features for regular applications [23–25] while the intrinsic randomness of the porous substrate ensures uniqueness and prohibits cloning. The patterns remain stable also under water with no observable swelling or deterioration of the coating or pattern, thus providing a reliable non-clonable feature (Figure 5.13).

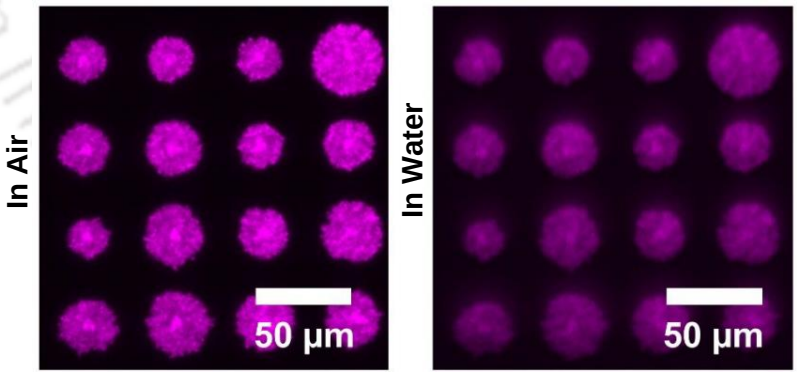

Figure 5.13. Fluorescence images of a 4×4 dot array in air (left) and in water (right). While the intensity and sharpness of the optical images is slightly reduced due to observing through the water film, no substantial change besides this optical effect is noticeable, implying the stability of the printed pattern as well the coating itself under humidity and liquid water.

5.4. Conclusions

In summary, we report a dual chemically reactive and porous dip coating for depicting bulk and complex pattern that enabled orthogonal read out of two distinct patterns in parallel. Further, the strategic post covalent modification with various types of selected and appropriate molecules, proteins, DNA or nanoparticles would allow to develop a different functional material for practically relevant applications including sensing, anticounterfeiting, etc. In future, we will explore such chemically reactive porous polymeric coating in developing rewritable patterns.

5.5. References

1) Bally, F.; Gall, L.; Hussal, C.; Kramer, J.; Cheng, K.; Kumar, R.; Eyster, T.; Baek, A.; Trouillet, V.; Nieger, M.; Bräse, S.; Lahann, J. Polylutidines: Multifunctional Surfaces through Vapor-Based Polymerization of Substituted Pyridinophanes. *Chem. A Eur. J.* **2017**, *23*, 13342-13350.

2) Bally, F.; Cheng, K.; Nandivada, H.; Deng, X.; Ross, A. M.; Panades, A.; Lahann, J. Co-immobilization of Biomolecules on Ultrathin Reactive Chemical Vapor Deposition Coatings Using Multiple Click Chemistry Strategies. *ACS Appl. Mater. Interfaces* **2013**, *5*, 9262-9268.

3) Mawélé Loudy, C.; Allouche, J.; Bousquet, A.; Martinez, H.; Billon, L. A nanopatterned dual reactive surface driven by block copolymer self-assembly. *Nanoscale* **2020**, *12*, 7532-7537.

4) Dadfar, S. M. M.; Sekula-Neuner, S.; Bog, U.; Trouillet, V.; Hirtz, M. Site-Specific Surface Functionalization via Microchannel Cantilever Spotting (µCS): Comparison between Azide–Alkyne and Thiol–Alkyne Click Chemistry Reactions. *Small* **2018**, *14*, 1800131.

5) Behboodi-Sadabad, F.; Zhang, H.; Trouillet, V.; Welle, A.; Plumeré, N.; Levkin, P. A. UV-Triggered Polymerization, Deposition, and Patterning of Plant Phenolic Compounds. *Adv. Funct. Mater.* **2017**, *27*, 1700127.

6) Atwater, J.; Mattes, D. S.; Streit, B.; von Bojničić-Kninski, C.; Loeffler, F. F.; Breitling, F.; Fuchs, H.; Hirtz, M. Combinatorial Synthesis of Macromolecular Arrays by Microchannel Cantilever Spotting (µCS). *Adv. Mater.* **2018**, *30*, 1801632.

7) Ma, T.; Li, T.; Zhou, L.; Ma, X.; Yin, J.; Jiang, X. Dynamic wrinkling pattern exhibiting tunable fluorescence for anticounterfeiting applications. *Nat. Commun.* **2020**, *11*, 1811.

8) Ramalho, J. F. C. B.; Correia, S. F. H.; Fu, L.; António, L. L. F.; Brites, C. D. S.; André, P. S.; Ferreira, R. A. S.; Carlos, L. D. Luminescence Thermometry on the Route of the Mobile-Based Internet of Things (IoT): How Smart QR Codes Make It Real. *Adv. Sci.* **2019**, *6*, 1900950.

9) Khlyustova, A.; Y. Cheng, Y.; Yang, R. Vapor-deposited functional polymer thin films in biological

applications. *J. Mater. Chem. B* **2020**, *8*, 6588-6609.

10) Benz, M.; Asperger, A.; Hamester, M.; Welle, A.; Heissler, S.; Levkin, P.A. A combined high-throughput and high-content platform for unified on-chip synthesis, characterization and biological screening. *Nat. Commun.* **2020**, *11*, 5391.

11) Arppe, R.; Sørensen, T. J. Physical unclonable functions generated through chemical methods for anti-counterfeiting. *Nat. Chem. Rev.* **2017**, *1*, 0031.

12) Canossa, S.; Wuttke, S. Functionalization Chemistry of Porous Materials. *Adv. Funct. Mater.* **2020**, *30*, 2003875.

13) Xu, J.; Lynch, M.; Huff, J. L.; Mosher, C.; Vengasandra, S.; Ding, G.; Henderson, E. Microfabricated Quill-Type Surface Patterning Tools for the Creation of Biological Micro/Nano Arrays. *Biomed. Microdevices* **2004**, *6*, 117-123.

14) Xu, J.; Lynch, M.; Nettikadan, S.; Mosher, C.; Vegasandra, S.; Henderson, E. Microfabricated "Biomolecular Ink Cartridges"—Surface patterning tools (SPTs) for the printing of multiplexed biomolecular arrays. *Sens. Actuators B* **2006**, *113*, 1034-1041.

15) Parbat, D.; Manna, U. Synthesis of 'reactive' and covalent polymeric multilayer coatings with durable superoleophobic and superoleophilic properties under water. *Chem. Sci.* **2017**, *8*, 6092-6102.

16) Maji, K.; Manna, U. Hierarchically featured and substrate independent bulk-deposition of 'reactive' polymeric nanocomplexes for controlled and strategic manipulation of durable biomimicking wettability. *J. Mater. Chem. A* **2018**, *6*, 6642-6653.

17) Das, S.; Das, A.; Parbat, D.; Manna, U. Catalyst-Free and Rapid Chemical Approach for in Situ Growth of "Chemically Reactive" and Porous Polymeric Coating. ACS Appl. Mater. Interfaces **2019**, *11*, 34316-34329.

18) Dadfar, S. M. M.; Sekula-Neuner, S.; Trouillet, V.; Hirtz, M. A Comparative Study of Thiol-Terminated Surface Modification by Click Reactions: Thiol-yne Coupling versus Thiol-ene Michael Addition. *Adv. Mater. Interfaces* **2018**, *5*, 1801343.

19) Dadfar, S. M. M.; Sekula-Neuner, S.; Trouillet, V.; Hirtz, M. Protein Microarray Immobilization via Epoxide Ring-Opening by Thiol, Amine, and Azide. *Adv. Mater. Interfaces* **2021**, *8*, 2002117.

20) Hirtz, M.; Lyon, M.; Feng, W.; Holmes, A. E.; Fuchs, H.; Levkin, P. A. Porous polymer coatings as substrates for the formation of high-fidelity micropatterns by quill-like pens. *Beilstein J. Nanotechnol.* **2013**, *4*, 377-384.

21) Hirtz, M.; Feng, W.; Fuchs, H.; Levkin, P. A. Click-Chemistry Immobilized 3D-Infused Microarrays in Nanoporous Polymer Substrates. *Adv. Mater. Interfaces* **2016**, *3*, 1500469.

22) Arrabito, G.; Ferrara, V.; Ottaviani, A.; Cavaleri, F.; Cubisino, S.; Cancemi, P.; Ho, Y. P.; Knudsen, B. R.; Hede, M. S.; Pellerito, C.; Desideri, A.; Feo, S.; Pignataro, B. Imbibition of Femtoliter-Scale DNA-Rich Aqueous Droplets into Porous Nylon Substrates by Molecular Printing. *Langmuir* **2019**, *35*, 17156-17165.

23) He, X.; Gu, Y.; Yu, B.; Liu, Z.; Zhu, K.; Wu, N.; Zhao, X.; Wei, Y.; Zhou, J.; Song, Y. Multi-mode structural-color anti-counterfeiting labels based on physically unclonable amorphous photonic structures with convenient artificial intelligence authentication. *J. Mater. Chem. C* **2019**, *7*, 14069-14074.

24) Liu, Y.; Han, F.; Li, F.; Zhao, Y.; Chen, M.; Xu, Z.; Zheng, X.; Hu, H.; Yao, J.; Guo, T.; Lin, W.; Zheng, Y.; You, B.; Liu, P.; Li, Y.; Qian, L. Inkjet-printed unclonable quantum dot fluorescent anti-counterfeiting labels with artificial intelligence authentication. *Nat. Commun.* **2019**, *10*, 2409.

25) Im, H.; Yoon, J.; Choi, J.; Kim, J.; Baek, S.; Park, D. H.; Park, W.; Kim, S. Chaotic Organic Crystal Phosphorescent Patterns for Physical Unclonable Functions. *Adv. Mater.* **2021**, *33*, 2102542.

26) Xiao, J.; Stone, H. A.; Attinger, D. Source-like Solution for Radial Imbibition into a Homogeneous Semi-infinite Porous Medium. *Langmuir* **2012**, *28*, 4208-4212.

Chapter 6: Conclusions and Future Directions

This chapter provides a summary of the various works presented in the earlier chapters. In this thesis, chemical requirements are strategically co-optimized with hierarchical topography, which finally results in controllable liquid wettability. Facile 1,4-conjugate addition reaction between chosen reactants using the one step dip-coating technique provide micro/nano- featured interfaces via in-situ deposition of chemically reactive nanocomplexes. The surface chemical functionalities that are related to this coating's chemical reactivity eventually make it appropriate for covalently modifying the interfaces to associate multifunctional characteristics. In chapter 1, I have accounted the fundamental understanding related to superhydrophobicity and pattened interfaces. Further, their prospective applications are illustrated in details. I have presented the relevant challenges associated with the bio-inspired wettability. In chapter 2, I have developed a "completely" substrate-independent and severely abrasion-tolerant biomimicked coating by an easy, highly scalable, and "chemically reactive" single-step dip-coating technique. The selected reactants, e.g., BPEI and 5Acl, are mutually reacted following catalyst-free 1,4-conjugate addition reaction which eventually leads to the formation of “chemically reactive” polymeric nanocomplex. Consequently, by such 1,4-conjugate addition process, both necessary topography and appropriate chemistry were tuned, ultimately leading to superhydrophobicity with modulated water adhesion property. These superhydrophobic coatings have the potential to transport tiny aqueous droplets in a regulated manner without causing any mass-loss. Additionally, this biomimetic dip-coating was able to withstand physical abrasions, even the exposed interiors of the coating consistently displayed an extreme water wettability, indicating that the synthetic superhydrophobicity was inherently resilient to severe and varied chemical and physical challenges. For practical applicability of superhydrophobic interfaces, such tolerance in severe conditions are necessary. Such bioinspired dip-coatings with exceptional durability have been successfully applied to a variety of substrates, including water-stable, water-sensitive, and water-soluble, flexible, rigid, planar, and geometrically complicated structures. The design of functional materials, such as hydrophilic/superhydrophobic patterns and extremely compressible and long-lasting superhydrophobic sponges, was made possible by the superhydrophobic coating on water-sensitive and water-soluble substrates. While highly compressible superhydrophobic sponges enabled the selective absorption-based environmentally friendly remediation of crude oil and other oil/oily spillages at various chemically challenging settings, physical damage to the superhydrophobic litmus paper caused a spatially selective rapid infiltration of the aqueous phase. Next, in chapter 3, a conductive pattern interface that is extremely water-repellent and abrasion-tolerant have successfully developed for low-strain, ultra-sensitive detection of both strong and weak movements of body parts during activities like walking, squatting, coughing, uttering, swallowing, blinking, wrist pulses, etc. In order to monitor patients during the rehabilitation process and investigate the interaction of human/machine, such an

approach could be very helpful. Furthermore, it could function underwater and in a variety of practically important extreme conditions due to its integrated water repellency and capacity to withstand intense abrasive exposure. The prepared superhydrophobic and conductive pattern interface has therefore enormous potential for a variety of more practical applications. In chapter 4, by choosing the spatially selective modifications chemical modulations, contrasting liquid wettability have been achieved. The inherently hydrophobic and chemically reactive surfaces served as an easy foundation for spatially selective covalent modifications with completely different functional molecules. The amine reactive surfaces were manually marked with glucamine using an aqueous ink, and the entire polymeric coating was then treated with octadecylamine to produce an invisible write-up embedded within two different liquid wettabilities. If the invisible writing was exposed directly to liquid water or mouth mist, it became visible. Moreover, as I have showed through spotting tests with CS (cantilever spotting technique), this coating permits patterning at the microscale. In this case, microarrays were used to display the same wetting and condensation behaviour, demonstrating the method's potential for tiny, undetectable, but simple to develop patterns. In order to address problems with anti-counterfeiting and many other pertinent obstacles, such a straightforward and covalent modulation technique would be of relevance. By utilizing the dual chemical reactivity of the porous polymeric dip coating interface, a large-scale, complicated design have prepared that allowed for the parallel reading out of two different fluorescent patterns in an orthogonal fashion as described in chapter 5. Additionally, selective post-covalent modification using various kinds of chosen and appropriate molecules, proteins, DNA, or nanoparticles would enable the development of a new functional material for use in applications like sensing and anti-counterfeiting, among others. We will investigate such chemically reactive porous polymeric coating can be further extended in the future to create rewritable patterns.

The research work illustrated in this thesis possess the potential for providing safety to the various pharmacological sector, economy of the society as well as bio-medical devices in terms of anticounterfeiting applications as well as sensing purposes. The growth of the information society has led to an increase in counterfeit goods, endangering people's lives and health.[1,2] For example, fake pharmaceutical products threat patient safety and public health, causing severe social and economic losses in both developed and less developed countries.[3] Engraving printing, bar code, and two-dimensional code technologies have all been created to combat counterfeiting, although these solutions are not always effective.[4-6] From the initial development of watermarking technology to the current high technology techniques of holography, stimuli-chromic effects (photochromic, hydrochromic and thermochromic) and photoluminescence (fluorescence and phosphorescence), the difficulty of anti-counterfeiting is gradually increasing owing to the enhanced requirements of information security and various limitations of the existing methods.[7-9] Such as, depending on dry and wet conditions, hydrochromic dyes are employed strategically to shift colours from invisible to visible. This happens

because a change in the dye's molecular structure causes a change in colour. However, there are clear difficulties with the reported methodologies, including the need for specialised equipment to find the buried information and the reported materials intrinsic optical instability and uncontrolled quenching upon repeated exposure to daylight. Thereafter, a novel, transitory, and reversible visualisation of hidden information is required to develop via a covalent and spatially specific chemical modulation technique. The method that is the subject of this thesis was developed using chemical patterning to produce contrasting water wettability, which eventually enabled the concealment of sensitive information. Such chemical patterning has been possible to prepare after developing a covalently cross-linked chemically reactive polymeric dip-coating as illustrated in the chapter 4 of this thesis. Covalent modulation provided the durability and prevention from leach out issues and keep the information safe and readable even at various harsh conditions. Polymeric reactants as used in this thesis work chapter 2 covalently cross-linked to provide chemically reactive coating interfaces via random aggregation of reactive polymeric nanocomplex. Therefore, such random features would be useful to develop completely non-forgeable physical tags such as QR code, bar code etc. These type of phenomenon also known as physically unclonable function (PUF). Due to their unpredictable nature and lack of replication, labels based on physical unclonable functions (PUFs, also known as physical one-way functions) allow for a more significant impact on optical encryption and decryption.[10,11] The unique physical characteristic is usually a random 2D or 3D pattern, giving rise to different optical readouts. For instance, some nanomaterial-based PUFs have been recently reported, such as glass micro-bead random speckle patterns, gold nanoparticle or silver nanowire random patterns, and inkjet-printed unclonable quantum dot fluorescent labels.[12, 13-18]

Apart from this, such chemically modulated functional interfaces have the ability to develop specific biologically relevant interfaces via covalent immobilization of proteins, aptamers etc. For example, extreme wettability patterns such as superhydrophilic–superhydrophobic interfaces promote micropatterning of polymer substrates due to the ability of the superhydrophobic barriers to confine both the printed transfection mixtures and the seeded cells within each superhydrophilic spot. These patterned substrates can have an ultrahigh-density of spots while still allowing a statistically significant number of cells per spot, which is not as easily achieved when using uncoated glass slides that are often used for cell microarrays.[19,20,21,22-25] In addition to that, these patterned interfaces are suitable for separation of peptides, e.g., Han et al. employed two-dimensional thin layer chromatography to separate peptides with various hydrophobicities and isoelectric points using a superhydrophilic channel photopatterned in a superhydrophobic porous polymer layer (2D TLC).[26] It further shows the potential of open surface microfluidic systems based on superhydrophilic-superhydrophobic patterns to be paired with a variety of detector systems in the field of miniaturized separation and diagnostic applications.

Another probable applicability is in bioadhesion, e,g., controlled adhesion of proteins, cells or bacteria.[27,28] Ishizaki et al. demonstrated the efficiency of superhydrophilic-superhydrophobic patterns on cell adhesion and morphology, and ECM production.[29]

Moreover, the association of reactive chemical functionalities with the conductive materials is likely to provide basis for Joule heating, sweat sensors etc. In addition to that, such coatings and interfaces have potential ability to be utilized as toxic volatile gas or volatile organic solvent senor for diagnosing various diseases in a non-invasive way.

6.1. References

1) Xie, Y.; Song, Y.; Sun, G.; Hu, P.; Bednarkiewicz, A.; Sun, L. Lanthanide-doped heterostructured nanocomposites toward advanced optical anti-counterfeiting and information storage. *Light: Sci. Appl.* **2022**, *11*, 1–10.
2) Yuan, W.; Pang, R.; Wu, H.; Wang, S.; Su, J.; Wang, J.; Jiao, S.; Li, C.; Zhang, G. Tuningemission color and improving the warm-white persistent luminescence of phosphor BaLu2Al2Ga2SiO12:Pr3+ via Zn2+ co-doping. *Dalton Trans.* **2021**, *50*, 12137–12146.
3) Aldhous, P. Murder by medicine. *Nature* **2005**, *434*, 132– 134.
4) Gao, D.; Gao, J.; Gao, F.; Kuang, Q.; Pan, Y.; Chen, Y.; Pan, Z. Quintuple-mode dynamic anti-counterfeiting using multi-mode persistent phosphors. *J. Mater. Chem. C* **2021**, *9*, 16634–16644.
5) Bai, X.; Yang, Z.; Zhan, Y.; Hu, Z.; Ren, Y.; Li, M.; Xu, Z.; Ullah, A.; Khan, I.; Qiu, J.; Song, Z.; Liu, B.; Wang, Y. Novel Strategy for Designing Photochromic Ceramic: Reversible Upconversion Luminescence Modification and Optical Information Storage Application in the PbWO4:Yb3+, Er3+ Photochromic Ceramic. *ACS Appl. Mater. Interfaces* **2020**, *12*, 21936–21943.
6) Wang, Z.; Li, X.; Li, M.; Zhao, J.; Liu, Z.; Wang, D.; Guan, L.; Wang, F. Two-site occupancy induced the broad-band emission in the Ba4−x−ySryLa6O(SiO4)6:x Eu2+ phosphor for white LEDs and anti-counterfeiting. *Dalton Trans.* **2022**, *51*, 4414–4422.
7) Xuan, Z.; Li, J.; Liu, Q.; Yi, F.; Wang, S.; Lu, W. Artificial Structural Colors and Applications. *Innovation* **2021**, *2*, 100081.
8) Man, Z.; Lv, Z.; Xu, Z.; Liao, Q.; Liu, J.; Liu, Y.; Fu, L.; Liu, M.; Bai, S.; Fu, H. Highly Sensitive and Easily Recoverable Excitonic Piezochromic Fluorescent Materials for Haptic Sensors and Anti-Counterfeiting Applications. *Adv. Funct. Mater.* **2020**, *30*, 2000105.
9) Ding, M.; Dong, B.; Lu, Y.; Yang, X.; Yuan, Y.; Bai, W.; Wu, S.; Ji, Z.; Lu, C.; Zhang, K.; Zeng, H. Energy Manipulation in Lanthanide-Doped Core-Shell Nanoparticles for Tunable Dual-Mode Luminescence towards Advanced Anti-Counterfeiting. *Adv. Mater.* **2020**, *32*, e2002121.
10) Arppe, R.; Sørensen, T. J. Physical unclonable functions generated through chemical methods for anti-counterfeiting. *Nat. Rev. Chem.* **2017**, *1*, 0031.

11) Pappu, R.; Recht, B.; Taylor, J.; Gershenfeld, N. Physical one-way functions. *Science* **2002**, *297*, 2026– 2030.

12) Shi, Y.; Lyu, Z.; Zhao, M.; Chen, R.; Nguyen, Q. N.; Xia, Y. Noble-Metal Nanocrystals with Controlled Shapes for Catalytic and Electrocatalytic Applications. *Chem. Rev.* **2021**, *121*, 649– 735.

13) Alharbi, A.; Armstrong, D.; Alharbi, S.; Shahrjerdi, D. Physically Unclonable Cryptographic Primitives by Chemical Vapor Deposition of Layered MoS2. *ACS Nano* **2017**, *11*, 12772– 12779.

14) Smith, A. F.; Skrabalak, S. E. Metal nanomaterials for optical anti-counterfeit labels. *J. Mater. Chem. C* **2017**, *5*, 3207– 3215.

15) Kim, J.; Yun, J. M.; Jung, J.; Song, H.; Kim, J.-B.; Ihee, H. Anti-counterfeit nanoscale fingerprints based on randomly distributed nanowires. *Nanotechnology* **2014**, *25*, 155303

16) Li, R.; Zhang, Y.; Tan, J.; Wan, J.; Guo, J.; Wang, C. Dual-Mode Encoded Magnetic Composite Microsphere Based on Fluorescence Reporters and Raman Probes as Covert Tag for Anticounterfeiting Applications. *ACS Appl. Mater. Interfaces* **2016**, *8*, 9384– 9394.

17) Kim, J.; Yun, J. M.; Jung, J.; Song, H.; Kim, J.-B.; Ihee, H. Anti-counterfeit nanoscale fingerprints based on randomly distributed nanowires. *Nanotechnology* **2014**, *25*, 155303.

18) Liu, Y.; Han, F.; Li, F.; Zhao, Y.; Chen, M.; Xu, Z.; Zheng, X.; Hu, H.; Yao, J.; Guo, T.; Lin, W.; Zheng, Y.; You, B.; Liu, P.; Li, Y.; Qian, L. Inkjet-printed unclonable quantum dot fluorescent anti-counterfeiting labels with artificial intelligence authentication. *Nat. Commun.* **2019**, *10*, 2409.

19) Stürzl, M.; Konrad, A.; Sander, G.; Wies, E.; Neipel, F.; Naschberger, E.; eipschläger, S.; Gonin-Laurent, N.; Horch, R. E.; Kneser, U.; Hohenberger, W.; Erfle, H.; Thurau, M. High throughput screening of gene functions in mammalian cells using reversely transfected cell arrays: review and protocol. *Comb. Chem. High Throughput Screen.* **2008**, *11*, 159-172.

20) Erfle, H.; Neumann, B.; Liebel, U.; Rogers, P.; Held, M.; Walter, T.; Ellenberg, J.; Pepperkok, R. Reverse transfection on cell arrays for high content screening microscopy. *Nat. Protoc.* **2007**, 2, 392.

21) Wheeler, D. B.; Carpenter, A. E.; Sabatini, D. M. Cell microarrays and RNA interference chip away at gene function. *Nat. Genet.* **2005**, *37*, S25-30.

22) Ziauddin, J.; Sabatini, D. M. Microarrays of cells expressing defined cDNAs. *Nature* **2001**, *411*, 107-110.

23) Simpson, J. C.; Cetin, C.; Erfle, H.; Joggerst, B.; Liebel, U.; Ellenberg, J.; Pepperkok, R. An RNAi screening platform to identify secretion machinery in mammalian cells. *J. Biotechnol.* **2007**, *129*, 352-365.

24) Yarmush, M. L.; King, K. R. Living-Cell Microarrays. *Annu. Rev. Biomed. Eng.* **2009**, *11*, 235-257.

25) Feng, W.; Li, L.; Ueda, E.; Li, J.; Heißler, S.; Welle, A.; Trapp, O.; Levkin, P. A. Surface Patterning via Thiol-Yne Click Chemistry: An Extremely Fast and Versatile Approach to Superhydrophilic-Superhydrophobic Micropatterns. *Adv. Mater. Interfaces* **2014**, *1*, 1.

26) Han, Y.; Levkin, P.; Abarientos, I.; Liu, H.; Svec, F.; Fréchet, J. M. J. Monolithic Superhydrophobic Polymer Layer with Photopatterned Virtual Channel for the Separation of Peptides Using Two-Dimensional Thin Layer Chromatography-Desorption Electrospray Ionization Mass Spectrometry. *Anal. Chem.* **2010**, *82*, 2520 – 2528.

27) Hook, A. L.; Voelcker, N. H.; Thissen, H. Patterned and switchable surfaces for biomolecular manipulation. *Acta Biomater*. **2009**, *5*, 2350 – 2370.

28) Yuan, L.; Yu, Q.; Li, D.; Chen, H. Surface Modification to Control Protein/Surface Interactions. *Macromol. Biosci.* **2011**, *11*, 1031 – 1040.

29) Ishizaki, T.; Saito, N.; Takai, O. Correlation of cell adhesive behaviors on superhydrophobic, superhydrophilic, and micropatterned superhydrophobic/superhydrophilic surfaces to their surface chemistry. *Langmuir* **2010**, *26*, 8147 – 8154.

Publications Related to Thesis Work

1. **Das, S**.; Das, A.; Parbat, D.; Manna, U. Catalyst-free and rapid chemical approach for in situ growth of "chemically reactive" and porous polymeric coating. *ACS applied materials & interfaces* **2019**, *11*, 34316-34329.

2. **Das, S**.; Kumar, R.; Parbat, D.; Sekula-Neuner, S.; Hirtz, M.; Manna, U. Covalently Modulated and Transiently Visible Writing: Rational Association of Two Extremes of Water Wettabilities. *ACS applied materials & interfaces* **2019**, *12*, 2935-2943.

3. **Das, S**.; Singh, R.; Das, A.; Bag, S.; Paily, R. P.; Manna, U. Abrasion tolerant, non-stretchable and super-water-repellent conductive & ultrasensitive pattern for identifying slow, fast, weak and strong human motions under diverse conditions. *Materials Horizons* **2021**, *8*, 2851-2858.

4. **Das, S**.; Kumar, R.; Yang, B.; Bag, S.; Sauter, E.; Hussain, N.; Hirtz, M.; Manna, U. (2022). Multiplexed Covalent Patterns on Double-Reactive Porous Coating. *Chemistry–An Asian Journal* **2022**, *17*, e202200157.

Other Publications

1. Jana, N., Parbat, D., Mondal, B., **Das, S**., & Manna, U. A biodegradable polymer-based common chemical avenue for optimizing switchable, chemically reactive and tunable adhesive superhydrophobicity. *Journal of Materials Chemistry A* **2019**, *7*, 9120-9129.

2. Dhar, M.; Kara, U.; **Das, S**.; Xu, Y.; Mandal, S.; L. Dupont, R.; C. Boerner, E.; Chen, B.; Yao, Y.; Wang, X.; Manna, U. Design of self-cleanable multilevel anticounterfeiting interface through covalent chemical modulation. *Materials Horizons* **2023**, In Press.

Patent

1. Uttam Manna, Roy P. Paily, **Supriya Das**, Rajan Singh, Avijit Das, Sudipta Bag, Low Strain Based, Water Repellent and Highly Sensitive Human Motion Sensor, Indian Patent: 202131028045, Filling date: June 22, **2021.**

Conferences Attended

1. FICS IIT Guwahati 2018 (Department of Chemistry). (International)
2. RAC (Recent Advances in Chemistry) NIT Meghalaya 2019 (Department of Chemistry) (Participated and **Best poster presentation awarded**). (National)
3. ICANN, IIT Guwahati 2019 (Centre for Nanotechnology). (International)
4. Advances in Polymeric Materials, CIPET, Bangalore, India 2020. (International)